

**OPTICAL AND INFRARED SPECTRA
OF SOME UNSTABLE MOLECULES**

by

JUDITH ANNE BARRY

B.S. (Hon.), San Francisco State University, 1981
M.S., San Francisco State University, 1983

A THESIS SUBMITTED IN PARTIAL FULFILMENT OF
THE REQUIREMENT FOR THE DEGREE OF
DOCTOR OF PHILOSOPHY

in

THE FACULTY OF GRADUATE STUDIES
Department of Chemistry

We accept this thesis as conforming
to the required standard

THE UNIVERSITY OF BRITISH COLUMBIA

9 November 1987

© Judith Anne Barry, 1987

In presenting this thesis in partial fulfilment of the requirements for an advanced degree at the University of British Columbia, I agree that the Library shall make it freely available for reference and study. I further agree that permission for extensive copying of this thesis for scholarly purposes may be granted by the head of my department or by his or her representatives. It is understood that copying or publication of this thesis for financial gain shall not be allowed without my written permission.

Department of CHEMISTRY

The University of British Columbia
1956 Main Mall
Vancouver, Canada
V6T 1Y3

Date 9 November 1987

ABSTRACT

Some unstable gaseous molecules, cobalt oxide (CoO), niobium nitride (NbN) and aminoborane (NH₂BH₂), were studied by high resolution optical spectroscopy. A portion of the "red" system of CoO, from 7000 Å to 5800 Å, was measured using laser induced fluorescence techniques. Three bands of the system, with origins at 6338 Å, 6411 Å and 6436 Å, were rotationally analyzed. The lower levels of these parallel bands are the $\Omega = 7/2$ and $5/2$ spin-orbit components of a $^4\Delta_i$ electronic state. Available evidence indicates that this is the ground state of the molecule; its bond length is 1.631 Å. This work completes the determination of the ground state symmetries for the entire series of first row diatomic transition metal oxides. The hyperfine structure in the ground state is very small, supporting a $\sigma^2\delta^3\pi^2$ electron configuration. The upper state, assigned as $\sigma\delta^3\pi^2\sigma^*$, has large positive hyperfine splittings that follow a case (a_β) pattern; it is heavily perturbed, both rotationally and vibrationally.

The sub-Doppler spectrum of the $^3\Phi-^3\Delta$ system of NbN was measured by intermodulated fluorescence techniques, and the hyperfine structure analyzed. Second order spin-orbit interactions have shifted the $^3\Phi_3-^3\Delta_2$ subband 40 cm⁻¹ to the blue of its central first order position. The perturbations to the spin-orbit components were so extensive that five hyperfine constants, rather than three, were required to fit the data to the case (a) Hamiltonian. The $^3\Delta-^3\Phi$ system of NbN is the first instance where this has been observed. The magnetic hyperfine constants indicate that all components of

the ${}^3\Delta$ and ${}^3\Phi$ spin orbit manifolds may be affected, though the ${}^3\Delta$ state interacts most strongly, presumably by the coupling of the ${}^3\Delta_2$ component with the ${}^1\Delta$ state having the same configuration. The Fermi contact interactions in the ${}^3\Delta$ substates are large and positive, consistent with a $\sigma^1\delta^1$ configuration. In the ${}^3\Phi$ state the (b + c) hyperfine constants are negative, as expected from a $\pi^1\delta^1$ configuration. The ${}^3\Delta$ and ${}^3\Phi$ bond lengths are 1.6618 Å and 1.6712 Å, respectively, which are intermediate between those of ZrN and MoN.

The Fourier transform infrared spectrum of the ν_7 BH₂ wagging fundamental of NH₂BH₂ was rotationally analyzed. A set of effective rotational and centrifugal distortion constants was determined, but the band shows extensive perturbations by Coriolis interactions with the nearby ν_5 and ν_{11} fundamentals. A complete analysis could not be made without an analysis of the ν_5 - ν_7 - ν_{11} Coriolis interactions, which is currently not possible because the very small dipole derivative of the ν_5 vibration has prevented its analysis.

TABLE OF CONTENTS

ABSTRACT.....	ii
TABLE OF CONTENTS.....	iv
LIST OF TABLES.....	vii
LIST OF FIGURES.....	viii
CHAPTER I. ELECTRONIC TRANSITIONS IN HETERONUCLEAR	
DIATOMICS.....	1
I.A. Some Properties of Angular Momenta.....	1
I.B. Spherical Harmonics and Spherical Tensor Operators.....	4
I.C. Selection Rules and Hund's Coupling Cases.....	11
I.D. The Hamiltonian.....	21
I.D.1. Nuclear rotational Hamiltonian.....	21
I.D.2. Spin Hamiltonian.....	22
I.D.3. Magnetic hyperfine interactions.....	25
I.D.3.a. The sign of nuclear coupling constants in transition metal complexes	27
I.D.3.a.i. The sign of the Fermi contact interaction.....	27
I.D.3.a.ii. The sign of the dipolar nuclear hyperfine interaction.....	30
I.D.4. The nuclear electric quadrupole interaction.....	31
I.D.5. Λ -Doubling.....	37
CHAPTER II. THE COMPUTERIZED LASER-INDUCED FLUORESCENCE	
EXPERIMENTS.....	40
II.A. Experimental Details.....	40
II.B. Intermodulated Fluorescence.....	43
II.C. Computerization.....	49

CHAPTER III. ROTATIONAL ANALYSIS OF THE RED SYSTEM OF COBALT OXIDE.....	52
III.A. Introduction.....	52
III.B. Experimental.....	56
III.B.1. Synthesis of gaseous cobalt oxide.....	56
III.B.2. The spectrum.....	57
III.C. Analysis.....	60
III.C.1. Rotational analysis of the 6338 Å subband.....	60
III.C.1.a. Rotational constants and hyperfine structure....	60
III.C.1.b. Perturbations.....	67
III.C.2. Rotational analysis of the 6436 Å subband.....	70
III.C.3. Rotational analysis of the 6411 Å subband.....	72
III.D. Discussion.....	78
CHAPTER IV. HYPERFINE ANALYSIS OF NIOBIUM NITRIDE.....	84
IV.A. Introduction.....	84
IV.B. Experimental.....	86
IV.B.1. Synthesis.....	86
IV.B.2. Description of the $^3\Phi - ^3\Delta$ spectrum.....	86
IV.C. Non-Linear Least Squares Fitting of Spectroscopic Data....	97
IV.D. Results and Discussion.....	102
CHAPTER V. ROTATIONAL ANALYSIS OF THE ν_7 BAND OF AMINOBORANE.....	113
V.A. Background.....	113
V.B. The Michelson Interferometer and Fourier Transform Spectroscopy.....	117
V.C. Experimental.....	126
V.D. The Asymmetric Rotor.....	127

V.E. The Rotational Hamiltonian.....	134
V.E.1. The Hamiltonian without vibration interaction.....	134
V.E.2. Coriolis interaction.....	137
V.F. Band Analysis and Discussion.....	138
Appendix I. NbN $^3\Phi$ - $^3\Delta$ Correlation Matrix.....	145
Appendix II. Transitions of the $^3\Phi$ - $^3\Delta$ System of NbN.....	147
Appendix II.A. $^3\Phi_2$ - $^3\Delta_1$	147
Appendix II.B. $^3\Phi_3$ - $^3\Delta_2$	152
Appendix II.C. $^3\Phi_4$ - $^3\Delta_3$	155
Appendix III. Transitions of the ν_7 band of $\text{NH}_2^{11}\text{BH}_2$	160
REFERENCES.....	170

LIST OF TABLES

3.I.	The most prominent bandheads in the 7000 to 5800 Å broadband emission spectrum of gaseous CoO.....	58
3.II.	Assigned lines for the 6338 Å band of CoO ($^4\Delta_{7/2}$ - $^4\Delta_{7/2}$) with the lower state combination differences, Δ_2F'' , in cm^{-1}	63
3.III.	Rotational constants for the analyzed bands of the red system of CoO.....	66
3.IV.	Assigned lines from the 6436 Å ($^4\Delta_{7/2}$ - $^4\Delta_{7/2}$) band of CoO....	73
3.V.	Assigned lines from the 6411 Å ($^4\Delta_{5/2}$ - $^4\Delta_{5/2}$) band of CoO....	74
3.VI.	Ground states and configurations of the first row diatomic transition metal oxides, with the fundamental frequency $\Delta G_{1/2}$, B and r for the $v''=0$ state, and the spin-orbit interval $\Delta\Lambda$ for the orbitally degenerate electronic states.....	83
4.I.	Molecular constants for the $^3\Phi$ - $^3\Delta$ system of NbN.....	105
4.II.	Rotational constants obtained for the $^3\Phi$ - $^3\Delta$ system of NbN with the A_D and γ parameters fixed to zero.....	110
5.I.	Vibrational fundamentals of gaseous $\text{NH}_2^{11}\text{BH}_2$	116
5.II.	Character table for the C_{2v} point group.....	128
5.III.	Character sets for an asymmetric top rotational wavefunction in the C_{2v} point group.....	132
5.IV.	Molecular constants of the ν_7 band of $\text{NH}_2^{11}\text{BH}_2$	143

LIST OF FIGURES

1.1.	Polar and Cartesian coordinates.....	5
1.2.	Vector diagram for Hund's coupling case (a).....	13
1.3.	Vector diagram for Hund's coupling case (b).....	15
1.4.	Vector diagram for Hund's coupling case (c).....	18
2.1.	Gaussian inhomogeneously Doppler-broadened velocity population profile.....	44
2.2.	Schematic diagram of the intermodulated fluorescence experiment.....	46
2.3.	a. The formation of crossover resonances. b. Stick diagram of a spectrum with four of the forbidden transitions that can accompany a $\Delta F = \Delta J = 0$ Q transition.....	48
2.4.	Schematic diagram of the laser-induced fluorescence experiment interfaced to the PDP-11/23 microcomputer.....	51
3.1.	Energy level diagram of a diatomic 3d transition metal oxide..	54
3.2.	Broadband laser excitation spectrum of the three bands of gaseous CoO analyzed in this work.....	59
3.3.	Bandhead of the $\Omega' = \Omega'' = 7/2$ transition at 6338 Å.....	62
3.4.	Upper state energy levels of the ${}^4\Delta_{7/2} - {}^4\Delta_{7/2}$ 6338 Å band....	68
3.5.	A section of the spectrum of the 6338 Å band containing Λ - doubling, two avoided crossings, and extra lines.....	69
3.6.	Upper state energy levels of the ${}^4\Delta_{7/2} - {}^4\Delta_{7/2}$ 6436 Å band....	71
3.7.	Bandhead of the $\Omega' = \Omega'' = 5/2$ transition at 6411 Å.....	75
3.8.	Upper state energy levels of the ${}^4\Delta_{5/2} - {}^4\Delta_{5/2}$ 6411 Å band....	76
4.1.	Broadband spectrum of the ${}^3\Phi - {}^3\Delta$ system of NbN.....	87

LIST OF FIGURES (cont.)

4.2.	The Q-head regions of the a) ${}^3\Phi_2$ - ${}^3\Delta_1$, b) ${}^3\Phi_3$ - ${}^3\Delta_2$, and c) ${}^3\Phi_4$ - ${}^3\Delta_3$ subbands of NbN.....	88
4.3.	The beginning of the Q head of the ${}^3\Phi_2$ - ${}^3\Delta_1$ subband.....	90
4.4.	The higher J portion of the ${}^3\Phi_2$ - ${}^3\Delta_1$ Q head, and the first resolved Q lines.....	91
4.5.	a) R(1), b) R(2), and c) R(3) of the ${}^3\Phi_2$ - ${}^3\Delta_1$ subband, illustrating the "forbidden" $\Delta F \neq \Delta J$ transitions and the crossover resonances between the rR and qR lines.....	92
4.6.	a) R2, b) R3 and c) R4 lines of the ${}^3\Phi_3$ - ${}^3\Delta_2$ subband of NbN, showing the rR, qR and pR transitions, and the crossover resonances associated with the rR and qR lines.....	93
4.6.	d) R5 and e) R6 lines of the ${}^3\Phi_3$ - ${}^3\Delta_2$ subband of NbN.....	94
4.7.	The reversal of hyperfine structure at high J in the ${}^3\Phi_4$ - ${}^3\Delta_3$ Q branch.....	95
4.8.	Partial energy level diagram for NbN.....	103
5.1.	A polychromatic signal in the frequency domain (above) Fourier transformed into the time domain (below).....	122
5.2.	A boxcar function D(x). The Fourier transform of a boxcar truncated interferogram is a spectrum with the line shape function $F\{D(x)\} = 2L\sin(2\pi\nu L)/2\pi\nu L$	124
5.3.	The triangular apodization function D(x) (above) produces a spectrum with the line shape function $F\{D(x)\} = 2L\sin(2\pi\nu L)/(2\pi\nu L)^2$ (below).....	125
5.4.	Schematic drawing of the C_{2v} NH_2BH_2 molecule in the x, y, z principal axis system and the a, b, c inertial axis system, showing the C_2 σ_v reflection planes.....	130

LIST OF FIGURES (cont.)

- 5.5. NH_2BH_2 spectrum of the ν_7 band, and the ν_5 and ν_{11} bands with which it undergoes Coriolis interactions.....140
- 5.5. Center of the ν_7 band of $\text{NH}_2^{11}\text{BH}_2$141

CHAPTER I
ELECTRONIC TRANSITIONS IN HETERONUCLEAR
DIATOMIC MOLECULES

I.A. Some Properties of Angular Momenta.

In a non-rotating molecule, the angular momentum operators \mathbf{J} , \mathbf{S} and \mathbf{L} have the following diagonal matrix elements:¹

$$\langle J\Omega | \hat{J}_z | J\Omega \rangle = \hbar\Omega \quad (1.1)$$

$$\langle S\Sigma | \hat{S}_z | S\Sigma \rangle = \hbar\Sigma \quad (1.2)$$

$$\langle L\Lambda | \hat{L}_z | L\Lambda \rangle = \hbar\Lambda \quad (1.3)$$

$$\langle J\Omega | \hat{J}^2 | J\Omega \rangle = \hbar^2 J(J+1) \quad (1.4)$$

$$\langle S\Sigma | \hat{S}^2 | S\Sigma \rangle = \hbar^2 S(S+1) \quad (1.5)$$

$$\langle L\Lambda | \hat{L}^2 | L\Lambda \rangle = \hbar^2 L(L+1) \quad (1.6)$$

J , S and L are the total, spin and orbital angular momenta, respectively; J , S and L are their respective quantum numbers, and Ω , Σ and Λ are the projection quantum numbers in diatomic molecules (i.e., along the molecular z axis).

The ladder operator \hat{L}_\pm of a general angular momentum $\hat{\mathbf{L}}$ has the Cartesian form²

$$\hat{L}_\pm = \hat{L}_x \pm i\hat{L}_y \quad (1.8)$$

It has the property of transforming state $|L,m\rangle$ into state $|L,m\pm 1\rangle$, where m is the quantum number of L . For $\hat{\mathbf{J}}$ and $\hat{\mathbf{S}}$ the laddering operations are written:¹

$$\langle J,\Omega\pm 1 | \hat{J}_\mp | J\Omega \rangle = \hbar[J(J+1) - \Omega(\Omega\pm 1)]^{1/2} \quad (1.9)$$

$$\langle S,\Sigma\pm 1 | \hat{S}_\pm | S\Sigma \rangle = \hbar[S(S+1) - \Sigma(\Sigma\pm 1)]^{1/2} \quad (1.10)$$

J_{\mp} in equation (1.9) is not expressed as J_{\pm} because the commutation relations are different in the space-fixed and molecule-fixed axis systems:³

$$J_x J_y - J_y J_x = i J_z \quad \text{SPACE} \quad (1.11)$$

$$J_x J_y - J_y J_x = -i J_z \quad \text{MOLECULE} \quad (1.12)$$

This leads to a sign reversal upon transformation from the space-fixed to molecule-fixed systems (the anomalous sign of i):

$$J_{\pm} |JM\rangle = \hbar [J(J+1) - M(M\pm 1)]^{1/2} |J, M\pm 1\rangle \quad \text{SPACE} \quad (1.13)$$

$$J_{\mp} |JK\rangle = \hbar [J(J+1) - K(K\pm 1)]^{1/2} |J, K\pm 1\rangle \quad \text{MOLECULE} \quad (1.14)$$

Although the motion of the electrons about the axis defines a good quantum number Λ , L itself is not a good quantum number because a diatomic molecule is not a spherical system. Thus \hat{L}_x and \hat{L}_y do not obey the usual operator equations, and \hat{L}_{\pm} is left in the form $\langle \hat{L}_+ \hat{L}_- + \hat{L}_- \hat{L}_+ \rangle / 2$, or $\langle \hat{L}_{\perp}^2 \rangle$, with the quantity $B \langle L_{\perp}^2 \rangle$ appearing on the diagonal of the rotational Hamiltonian matrix as a minor, constant electronic isotope shift incorporated into the effective vibrational energy.¹

The dot product of two general angular momentum operators $\hat{\mathbf{A}}$ and $\hat{\mathbf{B}}$ is:

$$\hat{\mathbf{A}} \cdot \hat{\mathbf{B}} = A_z B_z + (A_+ B_- + A_- B_+) / 2 \quad (1.15)$$

The addition of angular momenta j_1 and j_2 to form j results in the coupled eigenfunction $|jm\rangle$:

$$|jm\rangle = \sum_{m_1 m_2} (-1)^{j_1 - j_2 + m} \sqrt{2j+1} \begin{pmatrix} j_1 & j_2 & j \\ m_1 & m_2 & -m \end{pmatrix} |j_1 m_1\rangle |j_2 m_2\rangle \quad (1.16)$$

where $|j_1 m_1\rangle$ and $|j_2 m_2\rangle$ are the uncoupled eigenfunctions, the first term is a phase factor, and $\sqrt{2j+1}$ is a normalization factor. The term in brackets is a coefficient called a Wigner 3-j symbol. Its definition is given by equation (1.16) rearranged as:⁴

$$\begin{pmatrix} j_1 & j_2 & j \\ m_1 & m_2 & -m \end{pmatrix} = \frac{(-1)^{j_1-j_2+m}}{\sqrt{2j+1}} \langle j_1 j_2 m_1 m_2 | j m \rangle \quad (1.17)$$

According to the angular momentum commutation relations for j_1 , j_2 and j ,⁵ the algebraic form for the 3-j symbol is determined by the requirement that $m_1 + m_2 = m$ and $|j_1 - j_2| \leq j \leq (j_1 + j_2)$ (the triangle, or vector addition, rule)⁴. If these conditions are not satisfied, the vector coupling coefficient $\langle j_1 j_2 m_1 m_2 | j m \rangle$ is 0.

I.B. Spherical Harmonics and Spherical Tensor Operators.

Spherical harmonics, $Y_{lm}(\theta, \varphi)$, are orbital angular momentum eigenfunctions normalized to unity on a unit sphere. To be exact they are the eigenfunctions of the differential operators \hat{L}^2 and \hat{L}_z , corresponding to the eigenvalues $l(l+1)$ and m :^{6,7}

$$\hat{L}^2 Y_{lm}(\theta, \varphi) = l(l+1) Y_{lm}(\theta, \varphi) \quad (1.17)$$

$$\hat{L}_z Y_{lm}(\theta, \varphi) = m Y_{lm}(\theta, \varphi) \quad (1.18)$$

The angles θ and φ are the usual polar coordinates as illustrated in Figure 1.1. The differential operators \hat{L}^2 and \hat{L}_z , defined in units where $\hbar = 1$, are⁶

$$\hat{L}_z = \partial/\partial\varphi \quad (1.19)$$

$$\hat{L}^2 = -[(\sin \theta)^{-1}(\partial/\partial\theta)(\sin \theta \partial/\partial\theta) + (\sin^2\theta)^{-1}\partial^2/\partial\theta^2] \quad (1.20)$$

Expressed in terms of the orbital angular momentum functions of θ and φ on the unit sphere, a spherical harmonic is:⁸

$$Y_{lm}(\theta, \varphi) = c_l (-1)^{l+m} [(l-m)!/(l+m)!]^{1/2} (\sin\theta)^m [\partial/\partial(\cos\theta)]^{l+m} \times (\sin\theta)^{2l} e^{im\varphi} \quad (1.21)$$

where c_l is a normalization factor:

$$|c_l| = [(2l+1)!]^{1/2}/(4\pi)^{1/2} 2^{l!} \quad (1.22)$$

Associated Legendre polynomials, $P_l^m(\cos \theta)$, are commonly exploited in quantum mechanics because of their connection to spherical harmonics:⁶

$$Y_{lm}(\theta, \varphi) = (-)^m [(2l+1)(l-m)!/4\pi(l+m)!]^{1/2} P_l^m(\cos \theta) e^{im\varphi} \quad (1.23)$$

where⁶

$$P_l^m(x) = (1-x^2)^{m/2}/2^{l!} [d^{l+m}/dx^{l+m}](x^2-1)^l \quad (1.24)$$

When the component $m = 0$, the spherical harmonic and Legendre polynomial differ only by a constant⁹

$$Y_{l0}(\theta, \varphi) = [(2l+1)/4\pi]^{1/2} P_l(\cos \theta) \quad (1.25)$$

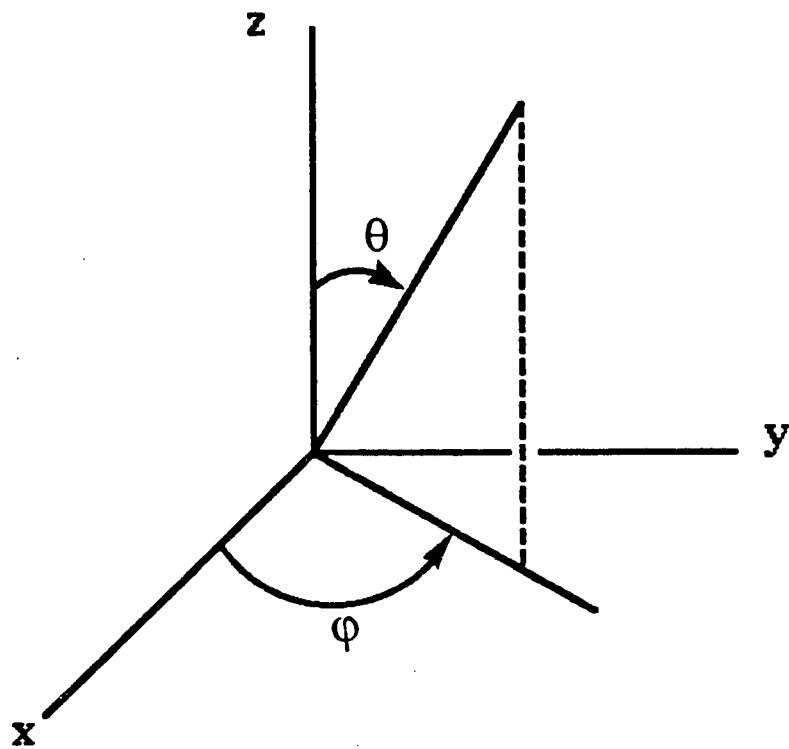


Fig. 1.1. Polar and Cartesian coordinates, in which $x = r\sin\theta\cos\phi$, $y = r\sin\theta\sin\phi$, $z = r\cos\theta$.⁸

The derivation of expressions describing the coupling of angular momenta, particularly those for the magnetic hyperfine and quadrupolar hyperfine interactions, is often best approached using irreducible spherical tensors. A brief explanation of spherical tensor operators, and the expressions required for their manipulation, follows. Spherical tensor methods are then applied where necessary in subsequent sections to derive the forms employed in the Hamiltonian representing the diatomic molecules in the present work.

The spherical components of a vector, or first rank tensor, operator acting on an angular momentum \mathbf{A} are related to their Cartesian counterparts by:^{2,4}

$$T^1_0(\mathbf{A}) = A_z \quad (1.26)$$

$$T^1_{\pm 1}(\mathbf{A}) = \mp(A_x \pm iA_y)/\sqrt{2} \quad (1.27)$$

A spherical tensor \mathbf{T} of rank k is defined as a set of $2k+1$ quantities ("components") which transform into one another upon rotation from one coordinate system to another (for example, between molecule- and space-fixed axis systems):^{10,11}

$$T^k_q = \sum_p T^k_p D_{pq}^{(k)}(\alpha\beta\gamma) \quad (1.28)$$

where q and p are the components of the tensor in the molecule- and space-fixed axis systems, respectively, and $D_{pq}^{(k)}(\alpha\beta\gamma)$ is the Wigner rotation matrix. The angles α , β and γ are the Euler angles corresponding to the three successive axis rotations required to transform between two coordinate systems. In spectroscopy, a beam of photons (in the space-fixed axis system) induces a change in the molecule in the molecule-fixed system. Wigner rotation

matrices function to project from one axis system to another in order to put the photon beam and the molecules being altered by the photons into the same frame of reference. In the reverse direction, from space- to molecule-fixed coordinates, the relation is:

$$T_p^k = \sum_q D_{pq}^{k*}(\alpha\beta\gamma) T_q^k \quad (1.29)$$

where the complex conjugation of a rotation matrix is given by

$$D_{MK}^{k*}(\alpha\beta\gamma) = (-1)^{M-K} D_{-M,-K}^k(\alpha\beta\gamma) \quad (1.30)$$

The complex conjugation is required to account for the anomalous sign of i .

A Wigner rotation matrix is a matrix describing how the eigenfunctions of \hat{J}^2 and \hat{J}_z , i.e., a spherical harmonic $|jm\rangle$, transform on coordinate rotation into other functions $|jm\rangle$:¹²

$$D(\alpha\beta\gamma)|jm\rangle = \sum |jm'\rangle D_{m'm}^{(j)}(\alpha\beta\gamma) \quad (1.31)$$

Premultiplying equation (1.31) by $|jm'\rangle^*$ (i.e., $\langle jm'|$) and integrating reduces the right hand side to $D_{m'm}^{(j)}$ due to the orthogonality of spherical harmonic functions:¹²

$$D_{m'm}^{(j)}(\alpha\beta\gamma) = \langle jm'|D(\alpha\beta\gamma)|jm\rangle \quad (1.32)$$

A D matrix element with one of its projections equal to zero collapses to a spherical harmonic, which depends on only two angles:¹²

$$D_{p0}^l(\alpha\beta\gamma) = (-1)^p [4\pi/(2l+1)]^{1/2} Y_{lp}(\beta,\alpha) \quad \text{SPACE} \quad (1.32)$$

$$D_{0q}^l(\alpha\beta\gamma) = [4\pi/(2l+1)]^{1/2} Y_{lq}(\beta,\gamma) \quad \text{MOLECULE} \quad (1.33)$$

If both projections are zero, the Wigner rotation matrix collapses to a Legendre polynomial:^{9,12}

$$D_{00}^l(\alpha\beta\gamma) = P_l(\cos \beta) = [4\pi/(2l+1)]^{1/2} Y_{l0}(\beta,0) \quad (1.34)$$

The Legendre polynomial $P_l(\cos\theta)$ is also related to the spherical harmonics by the spherical harmonic addition theorem:

$$P_l(\cos \theta) = (4\pi/2l+1) \sum_m Y_{lm}^*(\theta_1, \varphi_1) Y_{lm}(\theta_2, \varphi_2) \quad (1.35)$$

where $Y_{lm}^*(\theta, \varphi) = (-)^m Y_{l, -m}(\theta, \varphi)$.^{6,9,13,14} The angles $\theta_1, \theta_2, \varphi_1$ and φ_2 are as defined by Fig. 1.1 for vectors \mathbf{r}_1 and \mathbf{r}_2 , and θ is the angle between directions (θ_1, φ_1) and (θ_2, φ_2) . Using Racah's modified spherical harmonics to eliminate the factor of $[4\pi/(2l+1)]^{1/2}$:¹⁶

$$C_{lm}(\theta, \varphi) = [4\pi/(2l+1)]^{1/2} Y_{lm}(\theta, \varphi) \quad (1.36)$$

the spherical harmonic addition theorem becomes^{13,15}

$$P_l(\cos \theta) = \sum_m C_{lm}^*(\theta_1, \varphi_1) C_{lm}(\theta_2, \varphi_2) \quad (1.37)$$

or¹⁴

$$P_l(\cos \theta) = C_l(\theta_1, \varphi_1) \cdot C_l(\theta_2, \varphi_2) \quad (1.38)$$

The coupling of two tensor operators to form a compound tensor is similar to the addition of two angular momenta given in equation (1.16):¹⁰

$$[\mathbf{T}^{k_1(1)} \otimes \mathbf{T}^{k_2(2)}]_{q^k} = \sum (-1)^{k_1 - k_2 + q} \sqrt{2k+1} \begin{pmatrix} k_1 & k_2 & k \\ q_1 & q_2 & -q \end{pmatrix} \\ \times [\mathbf{T}^{k_1 q_1(1)}, \mathbf{T}^{k_2 q_2(2)}] \quad (1.39)$$

Here the tensor \mathbf{T}^{k_1} of rank k_1 , operating on system (1), is coupled to tensor \mathbf{T}^{k_2} [which operates on system (2)]. Shorter, alternative ways of denoting a compound tensor are $[\mathbf{T}^{k_1(1)}, \mathbf{T}^{k_2(2)}]$ or, for a tensor of rank k_1 coupled to itself, $[\mathbf{T}^k(1,1)]$, where $k = 2k_1$. If two tensors of the same rank k are coupled to give a scalar, i.e., a quantity invariant to a coordinate rotation, the compound tensor of equation (1.39) is also a scalar, or of rank zero. The resulting expression

becomes much simpler and lacks the orientation-dependent 3-j symbol:¹⁰

$$[T^k(1) \otimes T^k(2)]_{00} = (-1)^k(2k+1)^{-1/2} T^k(1) \cdot T^k(2) \quad (1.40)$$

where the conventional scalar product $T^k(1) \cdot T^k(2)$ is given as:^{10,11}

$$T^k(1) \cdot T^k(2) = \sum_q (-1)^q T^k_q(1) T^k_{-q}(2) \quad (1.41)$$

After a compound tensor equation is written which appropriately represents a particular physical interaction and breaks it into its constituent tensors, the Wigner-Eckart theorem is applied to evaluate the matrix elements T^k_q of the constituent tensors. According to the theorem the matrix elements of a tensor operator are factored into: 1) a 3-j symbol, which contains information on the geometry or orientation of the angular momentum; 2) a reduced matrix element (denoted by double vertical bars), related to the magnitude of the angular momentum but independent of its direction; and 3) a phase factor. Expressed in terms of the eigenfunctions $|j\gamma m\rangle$, where j is the quantum number acted upon by T^k , m is the projection of j , and γ contains any remaining quantum numbers not of interest in this particular basis, the Wigner-Eckart theorem is:¹⁶

$$\langle j'\gamma' m' | T^k_q | j\gamma m \rangle = (-1)^{j'-m'} \begin{pmatrix} j' & k & j \\ -m' & q & m \end{pmatrix} \langle j'\gamma' || T^k || j\gamma \rangle \quad (1.42)$$

Note that the reduced matrix element is independent of m .

A reduced matrix element is usually worked out by evaluating the simplest type of matrix element and then substituting into the Wigner-Eckart theorem. For example to obtain $\langle J || T^1(J) || J \rangle$, where J refers to a general angular momentum, we calculate the simplest type of matrix element of $T^1(J)$, namely its $q = 0$ (or z) component:¹⁷

$$\langle J'M' | T^1_0(J) | JM \rangle = \delta_{MM'} \delta_{JJ'} \quad (1.43)$$

This element is non-vanishing only if $J'M' = JM$. From the Wigner-Eckart theorem (equation 1.42),

$$M = (-1)^{J-M} \begin{pmatrix} J & 1 & J \\ -M & 0 & M \end{pmatrix} \langle J || T^1(J) || J \rangle \quad (1.44)$$

Substitution for the 3-j symbol¹¹ produces

$$M = (-1)^{J-M} (-1)^{J-M} M [J(J+1)(2J+1)]^{-1/2} \langle J || T^1(J) || J \rangle \quad (1.45)$$

Since J and M both have integral or half-integral values, $(-1)^{2(J-M)}$ is 1, which reduces equation (1.45) to:

$$\langle J || T^1(J) || J \rangle = [J(J+1)(2J+1)]^{1/2} \quad (1.46)$$

An important reduced matrix element is that of the rotation matrix element $D_{q^{(k)}}(\alpha\beta\gamma)$ (cf. equations 1.29 and 1.30):

$$\langle J'K' || D_{\cdot q^{k^*}}(\alpha\beta\gamma) || JK \rangle = (-1)^{J'-K'} [(2J+1)(2J'+1)]^{1/2} \begin{pmatrix} J' & k & J \\ -K' & q & K \end{pmatrix} \quad (1.47)$$

in which the dot replacing the p indicates that no reduction has been performed with respect to space-fixed axes, so there is no dependence on the M quantum number. Another useful formula gives the matrix elements of the scalar product of two commuting tensor operators (that is, ones which act on different parts of the system) in a coupled basis:¹⁸

$$\begin{aligned} & \langle \gamma' j_1' j_2' J'M' | T^k(1) \cdot U^k(2) | \gamma j_1 j_2 JM \rangle = \\ & (-1)^{j_1+j_2'+J} \delta_{J'J} \delta_{M'M} \left\{ \begin{matrix} J & j_2' & j_1' \\ k & j_1 & j_2 \end{matrix} \right\} \sum_{\gamma''} \langle \gamma' j_1' || T^k(1) || \gamma'' j_1 \rangle \langle \gamma'' j_2' || U^k(2) || \gamma j_2 \rangle \end{aligned} \quad (1.48)$$

in which T^k acts on j_1 and U^k on j_2 . The term in curly brackets is a Wigner 6-j symbol, a coefficient which arises in the coupling of three angular momenta, as compared to two in the 3-j symbol.¹⁹

I.C. Selection Rules and Hund's Coupling Cases.

An electronic transition can occur in a molecule only if there are non-zero matrix elements of the electric dipole moment operator \mathbf{M} which allow interaction with electromagnetic radiation.²⁰ The probability of such a transition occurring between electronic states n and m is proportional to the square of the transition moment, \mathbf{R}^{nm} :

$$\mathbf{R}^{nm} = \int \Psi_n^* \mathbf{M} \Psi_m d\tau, \quad (1.49)$$

where Ψ_n and Ψ_m are the eigenfunctions of states n and m .²⁰ The electric dipole moment \mathbf{M} for a total of N particles (electrons and nuclei) is²¹

$$\mathbf{M} = \sum_{i=1}^N e_i \mathbf{r}_i \quad (1.50)$$

where e_i is the charge on particle i which has coordinates \mathbf{r}_i . In the general case the transition moment integral vanishes unless the change in total angular momentum, J , is zero or unity, or²²

$$\Delta J = 0, \pm 1 \quad (1.51)$$

Changes in J of -1 , 0 and $+1$ are denoted by the letters P , Q and R , respectively.

The specific selection rules vary depending on the manner in which the spin, orbital and rotational angular momenta are coupled to one another and to the internuclear axis. The angular momentum coupling schemes in diatomic molecules are distinguished by sets of molecule-fixed basis functions called the Hund's coupling cases. The main property differentiating the four coupling cases described below is the number of angular momenta which have well-defined components (quantum numbers) along the internuclear axis. The

appropriate coupling case is the one which produces the smallest off-diagonal matrix elements for the rotational Hamiltonian, or diagonal elements which most closely reproduce the observed spectral pattern. The most common cases by far in molecules with no very heavy atoms are cases (a) and (b).

Hund's case (a) coupling has the maximum number of well-defined quantum numbers, such that the relations given in equations (1.1), (1.2) and (1.3) for a non-rotating molecule remain valid.^{1,23} The basis function for a case (a) coupling scheme is therefore $|(L)\Lambda\rangle|S\Sigma\rangle|J\Omega\rangle$, or $|\eta\Lambda;S\Sigma;J\Omega M\rangle$, where Λ , Σ and Ω are the eigenvalues of the z components of \hat{L} , \hat{S} and \hat{J} , with M being the space-fixed analog of Ω , and $\Omega = \Lambda + \Sigma$.¹ The semicolon separators indicate products of component wavefunctions. L is incorporated into the label η for the vibronic state, as it is not a good quantum number (cf. Section I.A). The case (a) representation is a good working approximation when there are no strong interactions in the Hamiltonian which uncouple these angular momenta from the axis. Case (a) occurs where there is a non-zero orbital angular momentum and fairly small spin-orbit coupling, where the coupling of L and S to each other is less important than the coupling of L to the axis.²⁴ The vector diagram for case (a) coupling is given in Fig. 1.2.

In case (b) coupling, S is coupled only weakly to the axis, but L remains strongly coupled. Given a large enough value of J , any case (a) state uncouples toward case (b) because as J increases the rotational and spin magnetic moments must ultimately be coupled more strongly to one another than L and S are. Formally it can be said that the rotation (R) has increased to the point where it couples

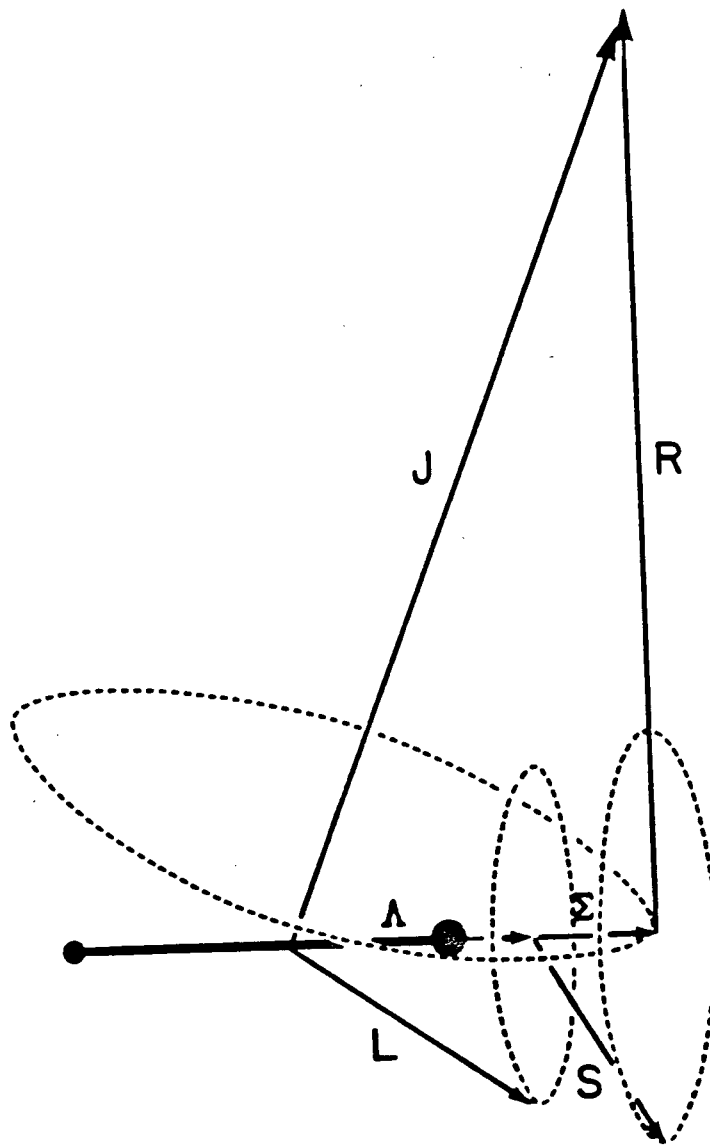


Fig. 1.2. Vector diagram of Hund's coupling case (a).²⁴

to the orbital angular momentum to form a resultant \mathbf{N} , causing \mathbf{S} to uncouple from \mathbf{L} , and therefore from the molecular axis. The effects of rotation become important when BJ becomes large compared to the separations between the spin-orbit components.¹ The transformation of a case (a) situation to case (b) occurs by way of the spin-uncoupling operator, $-B(\hat{J}_+\hat{S}_- + \hat{J}_-\hat{S}_+)$. With its selection rules ΔS and $\Delta \Lambda = 0$, and $\Delta \Omega = \Delta \Sigma = \pm 1$, this operator most commonly mixes spin-orbit components of a given $2S+1\Lambda$ state, which is consistent with the physical case (b) phenomenon of uncoupling \mathbf{L} from \mathbf{S} .²³ The case (b) representation also arises for Σ states in which there is no orbital angular momentum to couple the spin to the axis. The total angular momentum \mathbf{J} in case (b) is thus obtained as:²⁴

$$\mathbf{R} + \mathbf{L} = \mathbf{N}; \quad \mathbf{N} + \mathbf{S} = \mathbf{J} \quad (1.52)$$

instead of the case (a) situation

$$\mathbf{R} + \mathbf{L} + \mathbf{S} = \mathbf{J} \quad (1.53)$$

The case (b) basis function, $|\eta; N\Lambda S J\rangle$, is the more physically realistic representation in those cases where the rotational angular momentum \mathbf{N} is quantized about the axis, with electron spin providing only minor corrections to the total energy. Its vector diagram appears in Fig. 1.3.

When nuclear spin is included in the basis set describing angular momentum coupling in diatomic molecules, the Hund's coupling cases (a) and (b) must be further subdivided. In the majority of diatomic molecules, including those considered in the current work, \mathbf{I} is coupled so loosely to the internuclear axis or to \mathbf{S} that the dominant coupling is to the rotational angular momentum \mathbf{J} , or

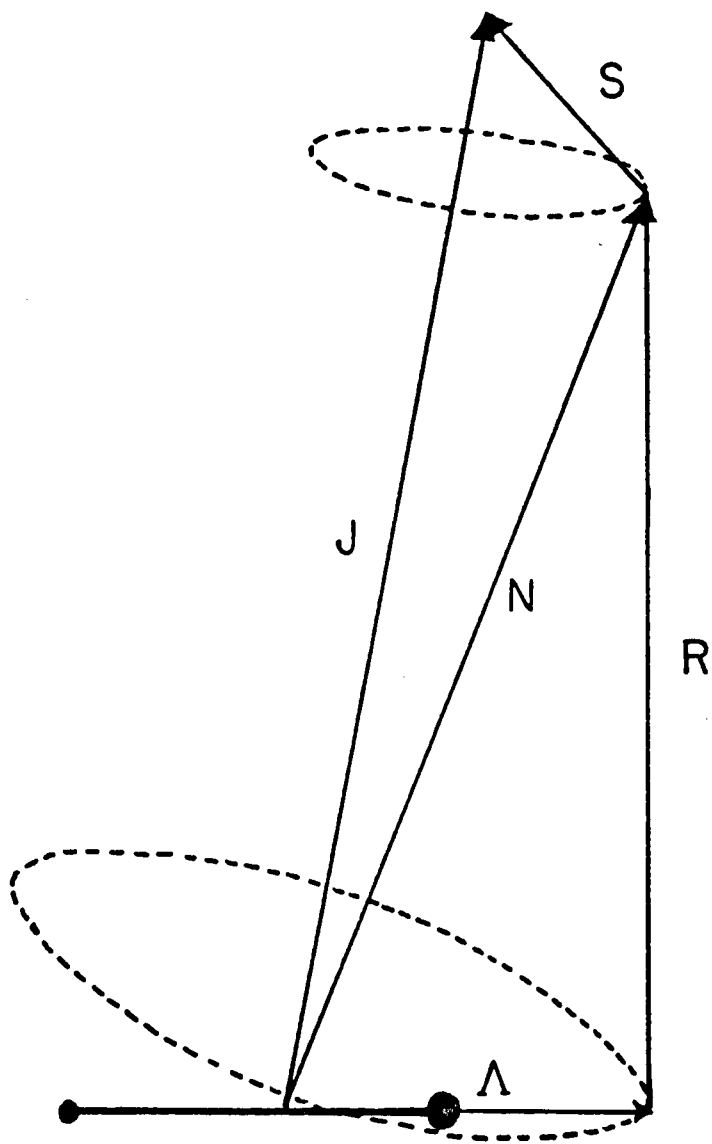


Fig. 1.3. Vector diagram of Hund's coupling case (b).²⁴

$$\mathbf{J} + \mathbf{I} = \mathbf{F} \quad (1.54)$$

By analogy with Hund's case (b), those coupling schemes following equation (1.54) are denoted by β subscripts. The extended Hund's coupling cases are called a_β and $b_{\beta J}$, corresponding to basis functions $|\Lambda S \Sigma J \Omega I F\rangle$ and $|N \Lambda S J I F\rangle$, respectively.^{25,26}

Coupling schemes in which \mathbf{I} is not coupled to \mathbf{J} are a_α , $b_{\beta N}$ and $b_{\beta S}$. In the a_α case, nuclear spin is coupled to the molecular axis with the projection quantum number I_z , though molecules exhibiting case (a_α) coupling have never been observed.²⁷ This is expected since nuclear magnetic moments are on the order of a thousand times smaller than that of the electron, making it unlikely that the dominant nuclear spin coupling will be to the internuclear axis by a magnetic interaction with the electronic and orbital angular momenta. In the $b_{\beta N}$ and $b_{\beta S}$ cases \mathbf{I} is coupled to \mathbf{N} and \mathbf{S} , respectively, rather than to \mathbf{J} as in case ($b_{\beta J}$). Case ($b_{\beta N}$) coupling is not expected to be observed, as the magnetic moment of \mathbf{N} (composed of $\mathbf{R} + \mathbf{L}$) is normally considerably less than that of either \mathbf{J} or \mathbf{S} , as \mathbf{S} has a large magnetic moment and \mathbf{J} is the sum of \mathbf{S} and \mathbf{L} .²⁷ In Hund's case ($b_{\beta S}$), \mathbf{I} couples to \mathbf{S} to form a vector \mathbf{G} , which couples to \mathbf{N} to form the total angular momentum \mathbf{F} :

$$\mathbf{I} + \mathbf{S} = \mathbf{G}$$

$$\mathbf{G} + \mathbf{N} = \mathbf{F}$$

In a nonrotating molecule, where any rotationally induced angular momenta are absent, case ($b_{\beta S}$) will be the dominant case (b) coupling scheme. In a rotating case (b) molecule, however, the coupling case that occurs depends on the relative sizes of the coupling of \mathbf{S} to \mathbf{I} and \mathbf{N} : if the $\mathbf{I}\text{-}\mathbf{S}$ coupling dominates, the ($b_{\beta S}$)

case occurs. The best condition for a case ($b\beta_S$) molecule is a Σ state which originates nearly completely from an atomic s orbital. Case ($b\beta_S$) coupling is therefore rather rare, though it has been extensively described in the ground $^2\Sigma$ state of scandium oxide, ScO .^{28,29,30} This molecule is ideal because the transition metal ion and closed shell oxygen have widely differing ionization potentials. This leaves the Sc^{2+} uncontaminated by contributions from O^{2-} , and the $^2\Sigma$ state far removed from the closed state of non-spherical symmetry with which it could mix.²⁷ Other molecules that have been observed to conform to case ($b\beta_S$) coupling are the $b^3\Sigma$ and $c^3\Sigma$ states of AlF^{31} , and the ground $^2\Sigma^+$ state of LaO ³². Note that both of these molecules also adhere to the conditions required for the $b\beta_S$ coupling case.

Case (c) coupling occurs in molecules containing an atom sufficiently heavy that the spin-orbit interaction which results is so large that electron motion can no longer be defined in either the \mathbf{L} or \mathbf{S} representations; one of the consequences is that spin multiplicity is no longer defined. This phenomenon is expressed as an axial \mathbf{J} (\mathbf{J}_a) equal to the sum of \mathbf{L} and \mathbf{S} , which is then coupled to \mathbf{R} to form the resultant \mathbf{J} , as illustrated in Fig. 1.4.²⁴ The basis function for case (c) is therefore $|\eta J_a; J\Omega M\rangle$, where the only well-defined axial component is Ω .¹ Case(c) molecules observed so far are ^{209}BiO ($X^2 \Pi_{1/2}$ state)^{33,34} and InH ($^3\Pi_1$ state)³⁵.

Case (d) coupling is normally only found in molecules where an electron has been promoted to a Rydberg orbital with higher principal quantum number n . The effect of the long distance between

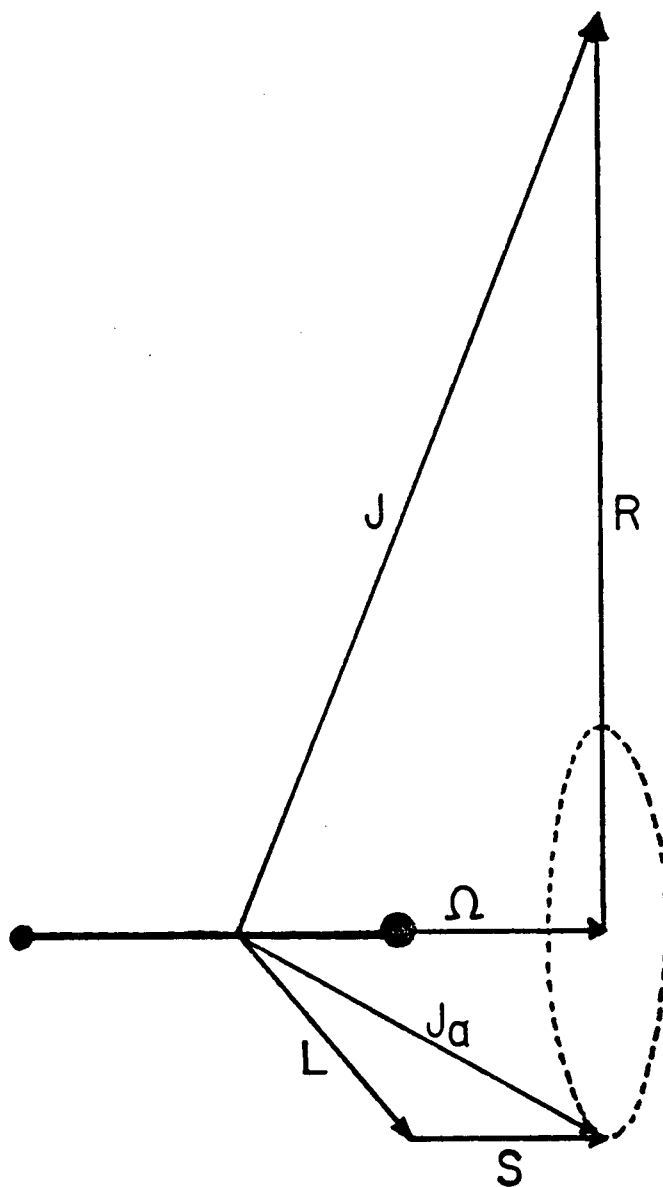


Fig. 1.4. Vector diagram for Hund's case (c).²⁴

the electron and the nuclei is that the electron orbital motion is coupled only weakly to the internuclear axis, but can instead couple more strongly to the rotational angular momentum, \mathbf{R} .^{21,24} Case (d) is equivalent to case (b) but with the difference that \mathbf{L} is uncoupled from the axis rather than \mathbf{S} ; the transition from case (a) is made by the L-uncoupling operator, $-B(\hat{J}_+\hat{L}_- + \hat{J}_-\hat{L}_+)$ rather than via the S-uncoupling operator.²³

While still in the case (a) or (b) limits, the L-uncoupling operator may induce Λ -doubling, which lifts the degeneracy of the $\pm\Lambda$ states. The selection rules for interactions by this operator are $\Delta\Omega = \Delta\Lambda = \pm 1$ and $\Delta S = 0$.²³ The phenomenon of Λ -doubling is discussed in more detail in the last section of this chapter. Case (d) becomes the appropriate representation when $-2B\hat{\mathbf{J}}\cdot\hat{\mathbf{L}}$ makes a contribution to the energy levels that is large with respect to the separation of states with differing Λ .

The Hund's coupling cases corresponding to the niobium nitride (NbN) and cobalt oxide (CoO) molecules in this work are most appropriately described by the case (a) and, with higher rotation, case (b) coupling schemes. As Λ and S are defined in both of these cases, the following selection rules can be stated for cases (a) and (b):²⁴

$$\Delta\Lambda = 0, \pm 1 \quad (1.55)$$

$$\Delta S = 0 \quad (1.56)$$

For case (a), with Σ and Ω as good quantum numbers, there are the more specific rules:

$$\Delta\Omega = 0, \pm 1 \quad (1.57)$$

$$\Delta\Sigma = 0 \quad (1.58)$$

where equation (1.57) follows from equations (1.55) and (1.56).²⁴ The $\Delta S = 0$ and $\Delta \Sigma = 0$ rules become less strict as the spin-orbit interaction increases, because the selection rules for the spin-orbit interaction are $\Delta \Omega = 0$ with either $\Delta \Lambda = \Delta \Sigma = 0$ or $\Delta \Lambda = -\Delta \Sigma = \pm 1$.^{24,36} In case (b) neither Σ nor Ω are well-defined, so the 'rotational' selection rule becomes

$$\Delta N = 0, \pm 1 \quad (1.59)$$

I.D. The Hamiltonian.

I.D.1. Nuclear rotational Hamiltonian.

From equation (1.53) it follows that the nuclear rotational Hamiltonian $B\hat{R}^2 - D\hat{R}^4$ should be written in the form appropriate for case (a) as:

$$\hat{H}_{\text{rot}} = B(\hat{J} - \hat{L} - \hat{S})^2 - D(\hat{J} - \hat{L} - \hat{S})^4 \quad (1.60)$$

where B is the rotational constant, and D is the centrifugal distortion constant representing the influence of centrifugal force due to rotation on bond length. Expansion of the B term of equation (1.60) gives

$$\hat{H} = B(\hat{J}^2 + \hat{L}^2 + \hat{S}^2 - 2\hat{J}\cdot\hat{L} - 2\hat{J}\cdot\hat{S} + 2\hat{L}\cdot\hat{S}) \quad (1.61)$$

Because the x and y components of \hat{L} are not defined in a non-spherical system, their effects are omitted in subsequent calculations¹. Equation (1.61) therefore simplifies to:

$$\hat{H} = B[\hat{J}^2 + \hat{L}^2 + \hat{S}^2 - 2\hat{J}_z\hat{L}_z - 2\hat{J}_z\hat{S}_z - (\hat{J}_+\hat{S}_- + \hat{J}_-\hat{S}_+) + 2\hat{L}_z\hat{S}_z] \quad (1.62)$$

The off-diagonal term, $-(\hat{J}_+\hat{S}_- + \hat{J}_-\hat{S}_+)$, is the spin-uncoupling operator discussed in Section 1.C.

The diagonal and off-diagonal rotational matrix elements are calculated by applying equations (1.1) through (1.10) and equation (1.15) to equation (1.61):

$$\langle J\Omega L\Sigma | \hat{H} | J\Omega L\Sigma \rangle = B[J(J+1) - \Omega^2 + S(S+1) - \Sigma(\Sigma+1)]^{1/2} \quad (1.63)$$

and

$$\begin{aligned} \langle JS, \Omega\pm 1, \Sigma\pm 1 | \hat{H} | JS\Omega\Sigma \rangle = & -B\{[(J(J+1) - \Omega(\Omega\pm 1))] \\ & \times [S(S+1) - \Sigma(\Sigma\pm 1)]\}^{1/2} \end{aligned} \quad (1.64)$$

The D terms are obtained by squaring the matrix of the coefficients of the B terms.

I.D.2. Spin Hamiltonian.

Spin-orbit coupling can be expressed as the scalar product of the many-electron electronic spin and orbital angular momentum operators, $\hat{\mathbf{S}}$ and $\hat{\mathbf{L}}$, which (using equations 1.8 and 1.15) is represented in Cartesian form as:

$$\begin{aligned}\hat{H}_{L\cdot S} &= A[(\hat{L}_x + i\hat{L}_y)(\hat{S}_x - i\hat{S}_y)/2 + \hat{L}_z\hat{S}_z + (\hat{L}_x - i\hat{L}_y)(\hat{S}_x + i\hat{S}_y)/2] \\ &= A\hat{L}_z\hat{S}_z + A(\hat{L}_+\hat{S}_- + \hat{L}_-\hat{S}_+)/2\end{aligned}\quad (1.65)$$

where A is the spin-orbit coupling constant. Neglecting the terms off-diagonal in L , equation (1.65) can be shortened to:³¹

$$\hat{H}_{L\cdot S} = A\hat{L}_z\hat{S}_z \quad (1.66)$$

which has the selection rule $\Delta S = 0$, and produces diagonal matrix elements of $A\Lambda\Sigma$.

The dipolar spin-spin interaction can be represented by the classical Hamiltonian for two bar magnets, or dipoles, μ :³⁷

$$\hat{H} = (\mu_1 \cdot \mu_2)/(r_{12})^3 - 3(\mu_1 \cdot \mathbf{r}_{12})(\mu_2 \cdot \mathbf{r}_{12})/(r_{12})^5 \quad (1.67)$$

in which \mathbf{r}_{12} is the vector between dipoles μ_1 and μ_2 , or $\mathbf{r}_1 - \mathbf{r}_2$. The magnetic dipole of spin \mathbf{S} is

$$\mu = -g\mu_B\mathbf{S} \quad (1.68)$$

where g is the dimensionless electronic g factor and μ_B is the Bohr magneton (the unit on an electronic magnetic moment, equal to $e\hbar/2m$ where e and m are the charge and mass of the electron, respectively).³⁸ The dipolar interaction in terms of two electron spin vectors separated by vector \mathbf{r} is therefore:

$$\hat{H}_{s-s} = (g^2\beta^2/r^3)\{\hat{\mathbf{S}}_1 \cdot \hat{\mathbf{S}}_2 - 3(\hat{\mathbf{S}}_1 \cdot \mathbf{r})(\hat{\mathbf{S}}_2 \cdot \mathbf{r})/r^2\} \quad (1.69)$$

Considering only the $q = 0$ terms (i.e., neglecting the components $q = \pm 1$ and ± 2), the interaction reduces to:³⁷

$$\hat{H}_{s-s} = (g^2\beta^2/r^3)\{\hat{S}_z^{(1)}\hat{S}_z^{(2)}(3\cos^2\theta_{12} - 1)\}$$

$$- (\hat{S}_-(1)\hat{S}_+(2) + \hat{S}_+(1)\hat{S}_-(2))(3\cos^2\theta_{12} - 1)/4 \quad (1.70)$$

Averaging over all orientations of r_1 and r_2 and expressed in terms of a total spin \mathbf{S} , equation (1.70) becomes:

$$\begin{aligned} \hat{H}_{s-s} &= (g^2\mu_B^2/r^3)[3\hat{S}_z^2 - \hat{S}^2 - (\hat{S}_+\hat{S}_+ + \hat{S}_+\hat{S}_-)/2] \\ &= (g^2\mu_B^2/r^3)[2\hat{S}_z - (\hat{S}_x + i\hat{S}_y)(\hat{S}_x - i\hat{S}_y)] \\ &= (g^2\mu_B^2/r^3)(3\hat{S}_z - \hat{S}^2) \end{aligned} \quad (1.71)$$

or in terms of the spin-spin coupling constant λ (or zero-field splitting parameter $2\lambda^{38}$),

$$\hat{H}_{s-s} = 2\lambda(3\hat{S}_z - \hat{S}^2)/3 \quad (1.72)$$

The spin-spin interaction originates from two mechanisms: the primary contribution to λ is from the dipolar interaction of two unpaired spins, but there is also an effect due to second order spin-orbit coupling, which may in fact be considerably larger:³⁹

$$\lambda = \lambda^{ss} + \lambda^{so} \quad (1.73)$$

Second order perturbation theory applied to the spin-orbit interaction produces a spin-spin interaction as follows. The second order contribution of the spin-orbit interaction in single particle terms is:

$$\begin{aligned} E_{so}^{(2)} &= \sum_{\eta'\Lambda'S'} [E_{\eta\Lambda S} - E_{\eta'\Lambda'S'}]^{-1} \sum_i \langle \eta\Lambda | a_i | \eta'\Lambda' \rangle \sum_j \langle \eta'\Lambda' | a_j | \eta\Lambda \rangle \\ &\quad \times \sum_{\Sigma'} \langle S\Sigma | \hat{s}_i | S'\Sigma' \rangle \langle S'\Sigma' | \hat{s}_j | S\Sigma \rangle \end{aligned} \quad (1.74)$$

The term summing over Σ' produces the dipolar spin-spin term $\langle S\Sigma | \hat{s}_i \hat{s}_j | S\Sigma \rangle$, as well as other matrix elements not of interest here because they are off-diagonal in Λ .

The dipolar spin-spin interaction matrix elements are obtained by applying equations (1.2) through (1.5) to equation (1.72):

$$\langle J\Omega L A S \Sigma | \hat{H}_{S-S} | J\Omega L A S \Sigma \rangle = 2\lambda[\Sigma^2 - S(S+1)/3] \quad (1.75)$$

The states they mix have $\Delta\Sigma$ ($=\Delta\Lambda$) and $\Delta S = 0, \pm 1, \pm 2$.⁴⁰

Centrifugal distortion corrections to the spin-orbit and spin-spin interactions-- A_D and λ_D , respectively--must also be considered. Terms containing the parameters A_D and λ_D are therefore added to the rotational Hamiltonian (equation 1.60) as follows:⁴¹

$$\hat{H}_{rot} = B\hat{R}^2 - D\hat{R}^4 + A_D\hat{R}^2\hat{L}_z\hat{S}_z + 2\lambda_D\hat{R}^2(3\hat{S}_z - \hat{S}^2)/3 \quad (1.76)$$

Since the products of the operators in the A_D and λ_D terms are not Hermitian, a Hermitian average must be taken by symmetrizing the products with the anticommutator. The diagonal matrix elements for the A_D and λ_D parameters therefore follow the rotational constant B , but are multiplied by the elements for the spin-orbit and spin-spin interactions, respectively. The off-diagonal elements do likewise, except that since there are no off-diagonal terms in A or λ , the factor for these interactions becomes the average of the two diagonal elements. As before, the operator \hat{R}^2 is simplified by omission of the x and y components of $-2\hat{J}\cdot\hat{L} + 2\hat{L}\cdot\hat{S} + \hat{L}^2$.

The spin-rotation operator, the dot product of the spin and rotational angular momenta, is written in Cartesian form as:³¹

$$\hat{H}_{S-R} = \gamma(\hat{J} - \hat{L} - \hat{S})\cdot\hat{S} \quad (1.77)$$

Neglecting L_{\pm} terms, equation (1.77) produces the expanded Hamiltonian:

$$\hat{H}_{S-R} = \gamma[\hat{J}_z\hat{S}_z - \hat{L}_z\hat{S}_z - \hat{S}_z^2 + (\hat{J}_+\hat{S}_- + \hat{J}_-\hat{S}_+)/2] \quad (1.78)$$

with diagonal elements:

$$\langle J\Omega L A S \Sigma | \hat{H}_{S-S} | J\Omega L A S \Sigma \rangle = \gamma[\Sigma^2 - S(S+1)] \quad (1.79)$$

and off-diagonal elements equal to those given in equation (1.64), but replacing B with $-\gamma/2$.

I.D.3. Magnetic hyperfine interactions.

The magnetic hyperfine interactions include all interactions of the nuclear spin, I , with the other angular momenta in the basis set, which for the case(a) basis are J , L and S . Nuclear magnetic moments interact weakly with the rotational magnetic moment giving rise to a scalar interaction term written:²⁵

$$\hat{H}_{I,J} = c_I \hat{I} \cdot \hat{J} \quad (1.80)$$

where c_I denotes the interaction constant. From equation (1.54),

$$\mathbf{F}^2 = \mathbf{J}^2 + 2\mathbf{I} \cdot \mathbf{J} + \mathbf{I}^2 \quad (1.81)$$

so that the $I \cdot J$ interaction can be expressed in terms of F as:

$$\hat{H}_{I,J} = c_I (\hat{F}^2 - \hat{J}^2 - \hat{I}^2)/2 \quad (1.82)$$

The matrix elements can be obtained directly from equation (1.4) as:

$$\langle \Lambda S \Sigma J \Omega I F | \hat{H}_{I,J} | \Lambda S \Sigma J \Omega I F \rangle = c_I [F(F+1) - J(J+1) - I(I+1)]/2 \quad (1.83)$$

The interactions of electronic and nuclear spins are represented by the Hamiltonian:²⁶

$$\hat{H}_{I,S} = b \hat{I} \cdot \hat{S} + c \hat{I}_z \hat{S}_z \quad (1.84)$$

with

$$b = a_F - c/3 \quad (1.85)$$

where a_F and c are the isotropic (Fermi-contact) and dipolar hyperfine constants, respectively. The former interaction is directly proportional to the quantity of electron density at the spinning nucleus, while the dipolar, or bar magnet, interaction between I_z and S_z is the same as given in equation (1.67). The interaction of nuclear spin with the electronic orbital magnetic moment is a scalar product of I and L which is treated in the same manner as the $L \cdot S$ interaction described by equations (1.65) and (1.66). The resulting Hamiltonian is therefore:^{26,31}

$$\hat{H}_{I,L} = a\hat{l}_z\hat{L}_z \quad (1.86)$$

in which a is the interaction constant.

The b term of equation (1.84) is expressed in spherical tensor form as:

$$\hat{H}_{I,S} = bT^1(I) \cdot T^1(S) \quad (1.87)$$

To derive the matrix elements of the interaction, I is first uncoupled from J by application of equation (1.48):

$$\begin{aligned} <\eta\Lambda S \Sigma J \Omega | F | T^1(I) \cdot T^1(S) | \eta'\Lambda S' \Sigma' J' \Omega' | F > = \\ & (-1)^{I+J'+F} \begin{Bmatrix} F & J & I \\ 1 & I & J' \end{Bmatrix} [(I+1)(2I+1)]^{1/2} <\eta\Lambda S \Sigma J \Omega || T^1(S) || \eta'\Lambda S' \Sigma' J' \Omega' > \end{aligned} \quad (1.88)$$

where the $[(I+1)(2I+1)]^{1/2}$ term is the reduced matrix element of $T^1(I)$ according to equation (1.46). By projecting the reduced matrix element in equation (1.87) from the space-fixed axis system to the molecule-fixed system, using Wigner rotation matrices as in equation (1.47), the general matrix element can be expressed as:³¹

$$\begin{aligned} <\eta\Lambda S \Sigma J \Omega | F | \hat{H}_{I,S} | \eta'\Lambda S' \Sigma' J' \Omega' | F > = \\ & (-1)^{I+J'+F} \begin{Bmatrix} F & J & I \\ 1 & I & J' \end{Bmatrix} [(I+1)(2I+1)(2J+1)(2J'+1)]^{1/2} \sum_q (-1)^{J-\Omega} \begin{pmatrix} J & 1 & J' \\ -\Omega & q & \Omega' \end{pmatrix} \\ & \times (-1)^{S-\Sigma} \begin{pmatrix} S & 1 & S' \\ -\Sigma & q & \Sigma' \end{pmatrix}^i <S || T^1(S) || S' > <\eta\Lambda S | b_i | \eta'\Lambda S' > \end{aligned} \quad (1.89)$$

The $c\hat{l}_z\hat{S}_z$ and $a\hat{l}_z\hat{L}_z$ Hamiltonians are treated by the same method.

Evaluation of the 3-j and 6-j symbols with the appropriate formulae^{5,42}, yields the matrix elements for $b\hat{I} \cdot \hat{S}$, $c\hat{l}_z\hat{S}_z$ and $a\hat{l}_z\hat{L}_z$, except that the only matrix elements written for the a and c constants are those diagonal in Λ and Σ , respectively. The resulting matrix elements employed in the hyperfine analysis of NbN are as follows:

$$\langle JIF\Omega\Sigma M | \hat{H}_{hf} | JIF\Omega\Sigma M \rangle = \Omega h R(J) / [2J(J+1)] \quad (1.90)$$

$$\begin{aligned} \langle JIF\Omega\Sigma M | \hat{H}_{hf} | J-1, IF\Omega\Sigma M \rangle = \\ -h(J^2 - \Omega^2)^{1/2} P(J) Q(J) / [2J(4J^2 - 1)^{1/2}] \end{aligned} \quad (1.91)$$

$$\begin{aligned} \langle JIF\Omega\Sigma M | \hat{H}_{hf} | JIF\Omega\pm 1, \Sigma\pm 1, M \rangle = \\ b[(J+\Omega)(J\pm\Omega+1)]^{1/2} R(J) V(S) / [4J(J+1)] \end{aligned} \quad (1.92)$$

$$\begin{aligned} \langle JIF\Omega\Sigma M | \hat{H}_{hf} | J-1, IF\Omega\pm 1, \Sigma\pm 1, M \rangle = \\ \mp b[(J\mp\Omega)(J\mp\Omega+1)]^{1/2} P(J) Q(J) V(S) / [4J(4J^2 - 1)^{1/2}] \end{aligned} \quad (1.93)$$

where the following abbreviations have been used:

$$R(J) = F(F+1) - J(J+1) - I(I+1) \quad (1.94)$$

$$P(J) = [(F-I+J)(F+J+I+1)]^{1/2} \quad (1.95)$$

$$Q(J) = [(J+I-F)(F-J+I+1)]^{1/2} \quad (1.96)$$

$$V(S) = [S(S+1) - \Sigma(\Sigma\pm 1)]^{1/2} \quad (1.97)$$

The constant b is that given in equation (1.84), while h is used in the diagonal elements in order to incorporate the a , b and c constants into one:

$$h = a\Lambda + (b+c)\Sigma \quad (1.98)$$

I.D.3.a. The sign of nuclear hyperfine coupling constants in transition metal complexes.

I.D.3.a.i. The sign of the Fermi contact interaction.

For an isotropic (Fermi contact) interaction involving only pure s electrons, the isotropic hyperfine constant a_F is positive because the magnetic field generated at the nucleus by the interaction is in the same direction as the electronic spin. However, negative contributions to the isotropic hyperfine interaction occur when there are open shell d or p electrons which polarize s electrons in inner (filled) orbitals via an exchange interaction which promotes an

electron from an inner s orbital to an outer empty one.⁴³ For example, a ground electronic configuration with a single unpaired 3d electron,

$$\Psi_0 = (3s^+)(3s^-)(3d^+)$$

can mix with excited states resulting from the promotion of an electron from a 3s to 4s orbital to produce the three functions:⁴³

$$\Psi_1 = (4s^+)(3s^-)(3d^+)$$

$$\Psi_2 = (3s^+)(4s^-)(3d^+)$$

$$\Psi_3 = (3s^+)(4s^+)(3d^+)$$

This is known as a configuration interaction, in which the ground and excited states possess different spin distributions yet form the basis for the same irreducible representation, in keeping with the requirement that the energy of the system remains constant.⁴⁴ First order perturbation theory is applied to describe the mixing, yielding an expression for the hyperfine contribution due to configuration interaction that is a function of the product of the ns and ms orbitals evaluated at the nucleus $[ns(0)ms(0)]$, times an exchange integral $J(ms,3d,3d,ns)$, divided by the energy separation between the ms and ns orbitals:

$$\chi = 8\pi \sum_{n=1}^3 \sum_{m=4}^{\infty} [ns(0)ms(0) \times J(ms,3d,3d,ns)] / (E_m - E_n) \quad (1.99)$$

The quantity χ is independent of charge⁴³ and is related to the isotropic Fermi contact coupling constant, a_F , by:⁴⁴

$$a_F = (2/3)g_e\mu_B g_n\mu_n\chi \quad (1.100)$$

where g_e and g_n are the electronic and nuclear g factors and μ_B and μ_n are the Bohr and nuclear magnetons. The quantity $[ns(0)4s(0)] / (E_4 -$

E_n) for the $n = 1, 2, 3$ s orbitals of the neutral atoms of the first row transition metals from V to Cu was found to increase by about 20% across the series. The exchange integrals varied in the opposite sense, though more gradually, decreasing by an overall 14% from V to Cu.⁴³

An alternative approach to the configuration interaction (CI) is core (or spin) polarization, a treatment which may be easier to conceptualize but is not as theoretically sound.⁴⁴ This theory differs from CI in that the orbitals involved belong to a single configuration which originates from spin-dependent one-electron orbitals. The resulting hyperfine interaction is therefore a function of the amount of spin density of each sign. CI requires two spin-independent configurations to represent the wavefunction. The wavefunction for the core polarization model is a spin-polarized unrestricted Hartree-Fock function (UHF) where UHF differs from the conventional, or restricted, Hartree-Fock function in that the trial one-electron wavefunctions are not required to be independent of the orientation of the spin.⁴⁴ The radial functions whose spins are being polarized, corresponding to spin up and spin down, differ from one another because they couple differently with the unpaired d or p electrons. The resulting hyperfine interaction is negative because the polarized spin has the opposite sense to the unpaired electron which induces the polarization.⁴⁴

I.D.3.a.ii. The sign of the dipolar nuclear hyperfine interaction.

The sign and magnitude of the dipolar hyperfine interaction depends on the number and type of open shell d and p electrons. The interaction constant for such an electron in orbital η is⁴⁵

$$c_i = 3g_e\mu_B g_n \mu_n \langle \eta | r^{-3} (3\cos^2\theta - 1) / 2 | \eta \rangle \quad (1.101)$$

where θ is the angle between the nucleus and the i th unpaired electron at a distance r ; closed shell electrons do not contribute to $\langle 3\cos^2\theta - 1 \rangle$. Using for sake of illustration the ground electronic $4\Sigma^-$ state of VO, with the configuration $(\sigma^2\pi^4\sigma_n^1\delta^2)$, there are three non-bonding $\sigma_n^1\delta^2$ open shell electrons contributing to the I-S interaction. If the assumption is made that the interacting electrons are metal centered, the hyperfine constants are:⁴⁶

$$(A_{iso})_{VO} \approx (1/3)(A_{iso})_{4s\sigma} \quad (1.102)$$

$$(A_{dip})_{VO} \approx (2/3)(A_{dip})_{3d\delta} \quad (1.103)$$

where these A parameters are related to a_F , b and c by:

$$A_{iso} = A_{\perp} + A_{dip} = a_F \quad (1.104)$$

$$A_{\perp} = b = a_F - c/3 \quad (1.105)$$

$$A_{dip} = c/3 \quad (1.106)$$

$$A_{\parallel} = b + c \quad (1.107)$$

Combining equations (1.101), (1.103) and (1.106), the expression for c becomes:

$$c = 3g_e\mu_B g_n \mu_n (2/3) \langle 3d\delta | r^{-3} (3\cos^2\theta - 1) / 2 | 3d\delta \rangle \quad (1.108)$$

Using the algebraic expression for the spherical harmonic Y_{20} (see Section I.B)⁴⁷, the matrix element portion of equation (1.108) can be written in terms of the n, l and m quantum numbers as:

$$\langle nlm | r^{-3} (3\cos^2\theta - 1) / 2 | nlm \rangle = (1/2) \langle lm | 3\cos^2\theta - 1 | lm \rangle \langle n | r^{-3} | n \rangle$$

$$c = \frac{3m^2 - l(l+1)}{(2l-1)(2l+3)} \langle r^{-3} \rangle_{nl} \quad (1.109)$$

For a δ orbital, equation (1.109) reduces to $(2/7)\langle r^{-3} \rangle_{nl}$, producing a value for c (in cm^{-1}) of⁴⁶

$$c = -(4/7)g_e\mu_B g_n\mu_n \langle r^{-3} \rangle_{3d} / hc \quad (1.110)$$

When an electron is promoted from the $4s\sigma$ to $4p\sigma$ orbital to produce the $C^4\Sigma^-$ excited state, all three electrons contribute to the dipolar term and c becomes (in cm^{-1}):

$$c = 3g_e\mu_B g_n\mu_n \left[\frac{2}{3} \langle r^{-3} (3\cos^2\theta - 1)/2 \rangle_{3d\delta} + \frac{1}{3} \langle r^{-3} (3\cos^2\theta - 1)/2 \rangle_{4p\sigma} \right] / hc$$

$$c = g_e\mu_B g_n\mu_n \left[-(4/7) \langle r^{-3} \rangle_{3d\delta} + (2/5) \langle r^{-3} \rangle_{4p\sigma} \right] / hc \quad (1.111)$$

Using this method the different values for c corresponding to the various possible electron configurations of an electronic state can be estimated, which assists in the assignment of an electronic state.

I.D.4. The nuclear electric quadrupole interaction.

The nuclear electric quadrupole interaction involves two second rank tensors, representing the electric field gradient and the nuclear quadrupole moment. A simple method by which to derive the quadrupolar Hamiltonian is with the use of spherical harmonics and Legendre polynomials.

To obtain the Hamiltonian for the electrostatic interaction of the nuclear quadrupole moment with the electric field gradient at the nucleus, a multipole expansion is made for the scalar coupling of the charges of the nucleons with those of the electrons. A multipole

expansion is a spherical harmonic expansion (or Legendre polynomial expansion) where the values of l in the spherical harmonic Y_{lm} are referred to as monopole, dipole, quadrupole and octopole for $l = 0, 1, 2$ and 3 .⁴⁸ By Coulomb's law⁴⁹, the electrostatic Hamiltonian is

$$\hat{H} = \sum_n eq_n/R_n \quad (1.112)$$

which describes the interaction between n nucleons with charge q_n and an electron with charge e , with an electron-nucleon separation of R_n . The electrostatic potential at the electron is

$$V = \sum q_n/R_n \quad (1.113)$$

The distance R_n is the resultant of the two vectors originating from the nuclear center to the n th nucleon (r_n) and to the electron (R), with the angle between vectors r_n and R denoted by θ_n . The law of cosines⁵⁰ gives the relation between R_n , r_n , R and θ_n :

$$\begin{aligned} R_n &= (R^2 + r_n^2 - 2Rr_n\cos\theta_n)^{1/2} \\ &= R[1 + (r_n/R)^2 - 2(r_n/R)\cos\theta_n]^{1/2} \end{aligned} \quad (1.114)$$

By the generating function for Legendre polynomials⁵¹,

$$[1 - 2(r_n/R)\cos\theta_n + (r_n/R)^2]^{1/2} = \sum P_l(\cos\theta_n)(r_n/R)^l \quad (1.115)$$

equation (1.113) can be written in terms of a Legendre polynomial as:⁵²

$$V = \sum_{l=0} \sum_n P_l(\cos\theta_n)q_n r_n^l / R^{l+1} \quad (1.116)$$

Each Legendre polynomial represents the scalar product of electronic and nuclear tensor operators (from the spherical harmonic addition theorem), producing from equations (1.112) and (1.116) the multipole expansion:^{48,52}

$$\begin{aligned} \hat{H}_{\text{multipole}} &= eV \\ &= \sum_{l=0} \sum_m (-1)^m \left[\sum_e (e/R^{l+1}) C_{lm}(\theta_e, \varphi_e) \times \sum_n q_n r_n^l C_{l,-m}(\theta_n, \varphi_n) \right] \quad (1.117) \end{aligned}$$

where the summations over e electrons and n nucleons represent terms in electronic (θ_e, φ_e) and nuclear (θ_n, φ_n) angular coordinates, respectively.

The first term in this expansion which is non-vanishing describes the quadrupolar interaction. The $l = 0$ term can be represented by $Z_e V_0$, or the Coulombic interaction between the nuclear charge and the electrons, and is included in the electronic Hamiltonian.⁵³ The dipole term, $l = 1$, is the product of the electric dipole moment of the nucleus, which is zero, and the electrostatic field of the electrons, which is invariant over the nuclear volume and therefore produces no interaction.⁵³ The $l = 2$ quadrupole term, however, is the interaction of the nuclear electric quadrupole moment, \hat{Q} , with the electric field gradient ($\hat{\nabla}E$) experienced by the nucleus due to the charge distribution of the electrons. For those nuclei possessing a quadrupole moment, then, the quadrupolar Hamiltonian is the scalar product of these two tensor quantities:⁵⁴

$$\hat{H}_Q = -T^2(\hat{\nabla}E) \cdot T^2(\hat{Q}) \quad (1.118)$$

where the minus sign is present due to the negative charge of the electron.

The quadrupole moment is a measure of how spherical the nucleus is, as indicated by the value of the nuclear spin, I . The deviation of nuclear charge distribution from spherical symmetry is given by: $3z^2_{\text{ave}} - (x^2 + y^2 + z^2)_{\text{ave}}$ or $3\cos^2\theta_n - 1$ (where θ_n is the nuclear angular coordinate).⁵⁵ This value is non-zero if I is greater than

1/2, which is dictated by the number of odd nucleons (i.e., differences in the number of neutrons with respect to protons). The mechanism giving rise to specific values of I is imperfectly understood, though it seems to approximate the same shell model that applies to electrons. Thus, zero spin results from spin-pairing if the number of protons (Z) equals the number of neutrons (N), and predictions for I can usually be made for nuclei possessing odd N or Z based on the number of particles occupying open shells.⁵⁵

By convention, the nuclear electric quadrupole moment is defined classically as¹¹

$$\hat{Q} = e \int (3z^2 - r^2) \rho(r) d\tau \quad (1.119)$$

where $\rho(r)$ is the nuclear charge density, and $d\tau$ denotes integration over the nuclear volume. Quantum mechanically the definition becomes:⁵²

$$\hat{Q} = e^{-1} \sum_n q_n r_n^2 (3 \cos^2 \theta_n - 1) \quad (1.120)$$

The quantum mechanical observable corresponding to equation (1.120) is the nuclear quadrupole moment, Q , defined by convention as⁵⁴

$$Q = \langle l, m_l = l | \hat{Q} | l, m_l = l \rangle \quad (1.121)$$

The definition of \hat{Q} was made prior to the invention of spherical tensors and therefore lacks the factor of 1/2 needed for the expressions $P_2(\cos\theta) = T^2_0(X) = (3\cos^2\theta - 1)/2$; \hat{Q} was also defined without the electron charge e . The spherical tensor definition is therefore

$$T^2_0(\hat{Q}) = e\hat{Q}/2 \quad (1.122)$$

with the corresponding scalar quantity

$$eQ/2 = \langle l, m_l = l | T^2_o(\hat{Q}) | l, m_l = l \rangle \quad (1.123)$$

The quadrupole tensor, from equation (1.117), is of the form

$$T^2(\hat{Q}) = \sum_n q_n r_n^2 C^2(\theta_n, \varphi_n) \quad (1.124)$$

The electric field gradient (EFG) evaluated at the nucleus, $(\partial^2 V / \partial z^2)_o$, has the spherical tensor form (from equation 1.117) of:

$$-T^2(\hat{V}E) = \sum_e e R^{-3} C^2(\theta_e, \varphi_e) \quad (1.125)$$

with the corresponding field gradient coupling constant defined as

$$q = \langle J, m_J = J | (\partial^2 V / \partial z^2)_o | J, m_J = J \rangle \quad (1.126)$$

where $(\partial^2 V / \partial z^2)_o = e R^{-3} (3 \cos \theta_e - 1)$. Thus, with the factor of 1/2 required by the spherical harmonic definition of the quadrupole moment, the EFG tensor can be expressed as:

$$-T^2_o(\hat{V}E) = q/2 \quad (1.127)$$

To derive the matrix elements for the quadrupolar interaction (equation 1.116), equation (1.48) is applied to evaluate the scalar coupling of two commuting tensor operators in a coupled basis (l must be unravelled from J):

$$\begin{aligned} & \langle \eta' \Lambda'; S' \Sigma'; J' \Omega' | F | \hat{H}_Q | \eta \Lambda; S \Sigma; J \Omega | F \rangle \\ &= (-1)^{J+l+F} \delta_{FF} \begin{Bmatrix} F & 1 & J' \\ 2 & J & 1 \end{Bmatrix} \langle \eta' \Lambda'; J' \Omega' | -T^2(\hat{V}E) | \eta \Lambda; J \Omega \rangle \langle l | T^2(\hat{Q}) | l \rangle \end{aligned} \quad (1.128)$$

Then project $T^2(\hat{V}E)$ from space- to molecule-fixed axes with equation (1.29):

$$\begin{aligned} \langle \eta' \Lambda'; J' \Omega' | -T^2(\hat{V}E) | \eta \Lambda; J \Omega \rangle &= \sum_q \langle J' \Omega' | D^2_{q^*}(\alpha \beta \gamma) | J \Omega \rangle \langle \eta' \Lambda' | -T^2_q(\hat{V}E) | \eta \Lambda \rangle \\ &= \sum_q (-1)^{J'-\Omega'} [(2J+1)(2J'+1)]^{1/2} \begin{Bmatrix} J' & 2 & J \\ -\Omega' & q & \Omega \end{Bmatrix} \langle \eta' \Lambda' | -T^2_q(\hat{V}E) | \eta \Lambda \rangle \end{aligned} \quad (1.129)$$

The last term of equation (1.128) is evaluated with the Wigner-Eckart theorem, in conjunction with equation (1.123):

$$\langle l, m_l = l | T^2_o(\hat{Q}) | l, m_l = l \rangle = eQ/2 = (-1)^{l-1} \begin{pmatrix} 1 & 2 & 1 \\ -1 & 0 & 1 \end{pmatrix} \langle l || T^2(\hat{Q}) || l \rangle \quad (1.130)$$

Substituting for the 3-j symbol⁵⁷ and solving for the reduced matrix element gives

$$\begin{aligned} \langle l || T^2(\hat{Q}) || l \rangle &= eQ/2 \begin{pmatrix} 1 & 2 & 1 \\ -1 & 0 & 1 \end{pmatrix}^{-1} \\ &= eQ/2 [(2l+1)(2l+2)(2l+3)/2l(2l-1)]^{1/2} \quad (1.131) \end{aligned}$$

In terms of the molecule-fixed $T^2(\hat{V}E)$ tensor in equation (1.129), the coupling constant q is defined by the diagonal reduced element of $T^2(\hat{V}E)$:

$$\langle \Lambda || -T^2_o(\hat{V}E) || \Lambda \rangle = q/2 \quad (1.132)$$

A first order approximation was made in the current study to neglect the ± 1 and ± 2 components of $T^2(\hat{V}E)$, that is, to exclude quadrupole matrix elements off-diagonal in Ω . Appropriate combination of equations (1.128), (1.129), (1.131) and (1.132) therefore yields the matrix elements

$$\begin{aligned} &\langle \eta' \Lambda'; S' \Sigma'; J' \Omega' | F | -T^2(\hat{V}E) \cdot T^2(\hat{Q}) | \eta \Lambda; S \Sigma; J \Omega | F \rangle \\ &= (1/4)eqQ(-1)^{J+1+F} \begin{pmatrix} F & 1 & J' \\ 2 & J & 1 \end{pmatrix} [(2l+1)(2l+2)(2l+3)/2l(2l-1)]^{1/2} \\ &\quad \times \sum_q (-1)^{J'-\Omega'} [(2J+1)(2J'+1)]^{1/2} \begin{pmatrix} J' & 2 & J \\ -\Omega' & q & \Omega \end{pmatrix} \quad (1.133) \end{aligned}$$

From the triangle condition for a 3-j symbol, which states that the third J value must not lie outside the sum and difference of the first two J values¹⁸, the 3-j symbol in equation (1.133) requires ΔJ to be 0, ± 1 or ± 2 . From equation (1.133) and these selection rules, the specific matrix elements employed in this work are as follows:

$$\langle JIF\Omega\Sigma M | \hat{H}_Q | JIF\Omega\Sigma M \rangle = \frac{eQq[3\Omega^2 - J(J+1)]\{3R(J)[R(J)+1] - 4J(J+1)l(l+1)\}}{8l(2l-1)J(J+1)(2J-1)(2J+3)} \quad (1.134)$$

$$\langle JIF\Omega\Sigma M | \hat{H}_Q | J-1, IF\Omega\Sigma M \rangle = \frac{-eQq3\Omega[R(J)+J+1](J^2-\Omega^2)^{1/2}P(J)Q(J)}{2J(2J-2)(2J+2)(2l-1)(4J^2-1)^{1/2}} \quad (1.135)$$

$$\langle JIF\Omega\Sigma M | \hat{H}_Q | J-2, IF\Omega\Sigma M \rangle = \frac{eQq3[(J-1)^2-\Omega^2]^{1/2}(J^2-\Omega^2)^{1/2}P(J)Q(J)P(J-1)Q(J-1)}{4l(2l-1)4J(J-1)(2J-1)[(2J-3)(2J+1)]^{1/2}} \quad (1.136)$$

The terms $R(J)$, $P(J)$, $Q(J)$, $P(J-1)$ and $Q(J-1)$ are as in equations (1.93), (1.94) and (1.95).

I.D.5. Λ -Doubling.

The phenomenon of Λ -doubling results from the breakdown of the Born-Oppenheimer approximation, which allows the separation of electronic and nuclear motion.²⁶ It is the lifting of $\pm\Lambda$ degeneracy which occurs when molecular rotation interferes with the well-defined quantization of the z component of electronic orbital angular momentum about the molecular axis. The operators in the spin and rotational Hamiltonian responsible for Λ -doubling are the x and y components of the electronic orbital angular momentum operators which produce matrix elements off-diagonal in Λ . In the rotational Hamiltonian, this is the L-uncoupling operator, $-2B\hat{J}\cdot\hat{L}$. Among the spin-interaction terms of the Hamiltonian, the spin-orbit operator is used, yielding the complete Λ -doubling Hamiltonian:⁵⁷

$$V = -2B\hat{J}\cdot\hat{L} + \sum_i a_i \hat{l}_i \cdot \hat{s}_i \quad (1.137)$$

The Λ -doubling interaction is treated by degenerate perturbation theory⁵⁸, which for Δ states must be taken to fourth order in order

to connect $|\Lambda = 2\rangle$ to $|\Lambda = -2\rangle$ via states with $\Lambda = 1$ and 0 (i.e., Π and Σ states). For this reason the interaction is smaller than that in Π states, since the mixing of $|\Lambda = 1\rangle$ and $|\Lambda = -1\rangle$ states requires only second order perturbation theory.⁵⁷ The unperturbed Hamiltonian contains those terms adhering to the Born-Oppenheimer approximation which are diagonal in Λ and independent of the orbital degeneracy. The perturbation can be treated through the use of a fourth-order effective Hamiltonian, which is obtained by subtracting out the unperturbed energy from the complete Hamiltonian expression to leave an effective Hamiltonian which operates only on the vibronic state of interest, $|l_0 k\rangle$ ^{57,59}

$$\begin{aligned} \hat{H}_{\text{eff}}^{(4)} = & P_0 V(Q_0/a) V(Q_0/a) V(Q_0/a) V P_0 - P_0 V(Q_0/a^2) V P_0 V(Q_0/a) V P_0 \\ & - P_0 V(Q_0/a^2) V(Q_0/a) V P_0 V P_0 - P_0 V(Q_0/a) V(Q_0/a^2) V P_0 V P_0 \\ & + P_0 V(Q_0/a^3) V P_0 V P_0 V P_0 \end{aligned} \quad (1.138)$$

The operator P_0 , extending over the k -fold degeneracy of l_0 , is defined as

$$P_0 = \sum_k |l_0 k\rangle \langle l_0 k| \quad (1.139)$$

while

$$(Q_0/a^n) = \sum_{l=l_0} \sum_k |lk\rangle \langle lk| / (E_0 - E_l)^n \quad (1.140)$$

where l denotes any vibronic state with energy E_l , E_0 is the energy of state $\langle l_0 k|$, and k labels all rotational, spin and electronic quantum numbers in a vibronic state l_0 or l .

The Hamiltonian in equation (1.137) has $2\Lambda+1$ terms of the form $(\hat{H}_{\text{rot}})^{2\Lambda-n} (\hat{H}_{\text{s.o.}})^n$, where n ranges from zero to 2Λ . In the case (a) form it is written:⁵⁷

$$\begin{aligned}
\hat{H}_{L.D.,\Delta} = & \tilde{m}_{\Delta}(\hat{S}_+^4 + \hat{S}_-^4)/2 - \tilde{n}_{\Delta}(\hat{S}_+^3\hat{J}_+ + \hat{S}_-^3\hat{J}_-)/2 \\
& + \tilde{o}_{\Delta}(\hat{S}_+^2\hat{J}_+^2 + \hat{S}_-^2\hat{J}_-^2)/2 - \tilde{p}_{\Delta}(\hat{S}_+\hat{J}_+^3 + \hat{S}_-\hat{J}_-^3)/2 \\
& + \tilde{q}_{\Delta}(\hat{J}_+^4 + \hat{J}_-^4)
\end{aligned} \tag{1.141}$$

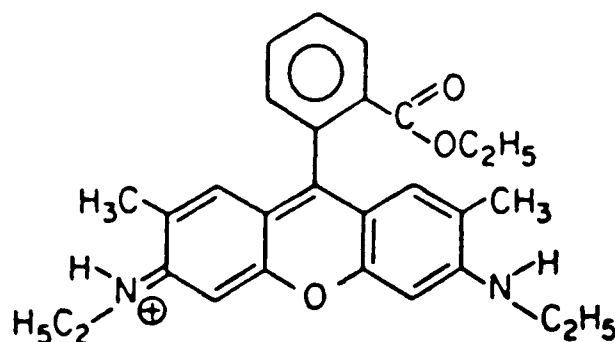
where the factors of 1/2 are included to be consistent with the notation of Mulliken and Christy⁶⁰ for Π states. Thus the \tilde{q}_{Δ} parameter accompanies $(\hat{H}_{rot})^{2\Lambda}$, \tilde{p}_{Δ} is with $(\hat{H}_{rot})^{2\Lambda-1}(\hat{H}_{s.o.})$ and so on to \tilde{m}_{Δ} with $(\hat{H}_{s.o.})^{2\Lambda}$. The number of those parameters that can be determined equals the spin multiplicity up to a maximum of 5. In a $^4\Delta$ state, for example, only four of the five parameters are included in the Λ -doubling matrix elements, with \tilde{m}_{Δ} excluded because the spin-orbit interaction need not be extended to fourth order. In a $^4\Delta$ state where there are four Ω substates, the terms appear in the 4 x 4 matrix as \pm terms which split a given level into two levels of different parity, labelled *e* and *f*. By convention, the *e* levels have parity $+(-1)^{j-k}$ and *f* levels have parity $-(-1)^{j-k}$, where *k* is 1/2 and 0 for half-integer and integer values of spin, respectively.^{61,62} The magnitude of the Λ -doubling observed in this work in the $^4\Delta_{7/2}$ - $^4\Delta_{7/2}$ transition of CoO ranged from 0.2 to 1.2 cm^{-1} , while that in the $^3\Pi_0$ state of NbN is on the order of six wavenumbers.

CHAPTER II

THE COMPUTERIZED LASER-INDUCED FLUORESCENCE EXPERIMENTS

II.A. Experimental Details.

The laser excitation experiments were performed using a Coherent Radiation model CR-599-21 scanning single frequency (standing wave) dye laser, pumped by a Coherent Radiation model Innova-18 argon ion laser operated at a wavelength of 514 nm and a power of 2.0 to 3.5 W. Output power from the dye laser was normally 100 to 150 mW. The tunability of the laser comes from selecting portions of the broad fluorescence band of an organic dye.⁶³ Two dyes were employed for both the cobalt oxide (CoO) and niobium nitride (NbN) studies. For maximum output at 590 nm (ranging from 570 to 620 nm or 17540 to 16130 cm^{-1}), the dye used was rhodamine 6G (Exciton Chemical Co.), with the structure⁶³



made to a concentration of 2×10^{-3} M in ethylene glycol. To reach the lower energy regions, the dye DCM (4-dicyanomethylene-2-methyl-6-p-dimethylaminostyryl-4H-pyran, from Exciton Chemical Co.) was dissolved in 3:7 benzyl alcohol to ethylene glycol to form nearly saturated 2.5×10^{-3} M solutions. At a pump wavelength of 514 nm, DCM's maximum output power occurs at 640 nm, and

broadband laser operation occurs over the range 600 to 695 nm (16670 to 14390 cm^{-1}). The benzyl alcohol required to dissolve the DCM leads to bubble formation, so the solution was cooled to minimize bubbling by running the dye tubing through a $-30\text{ }^{\circ}\text{C}$ slush of dry ice mixed with a 1:3 solution of water to CaCl_2 . All chemicals were used as obtained.

A small fraction of the output beam was diverted to an iodine absorption or emission cell for absolute frequency calibration. Another fraction was sent to a Tropel fixed-length semiconfocal Fabry-Perot interferometer with a 299 MHz free-spectral range, providing a common ladder of frequency markers against which the sample and iodine spectra could be referenced. The beam containing the majority of the output power was passed down the longitudinal axis of the stream of sample molecules, with the laser-induced fluorescence (LIF) detected at right angles to the beam with a photomultiplier tube equipped with a high transmittance low pass optical filter to reduce scattered light, and powered by 300 to 500 V from a high voltage power supply. Phase-sensitive detection was achieved with a Princeton Applied Research (PAR) model 128A lock-in amplifier receiving chopped sample and reference signals, with the reference beam supplied by a Spectra-Physics model 132 Lablite He-Ne gas laser.

The resolved fluorescence experiments were performed with a 0.7 m Spex Industries model 1702 spectrometer which dispersed the spectrum onto the detector elements of a microchannel-plate intensified array detector (PAR model 1461), mounted at the output

end of the spectrometer. The spectral window of the array detector was calibrated with a Burleigh model WA-20VIS wavemeter.

II.B. Intermodulated Fluorescence.

A laser-induced fluorescence transition has a Gaussian velocity population profile forming an inhomogeneously broadened line, because of the Doppler effect, the frequency absorbed by molecules moving away from the light source appears to be lower than that absorbed by molecules moving toward it. At the center of the profile (zero velocity) the transition frequency Ω is not Doppler-shifted; that is, the molecules have zero velocity with respect to the light wave with which the molecules interact.^{65,66} In Doppler-free (or "sub-Doppler") spectroscopy, two travelling waves (laser beams) with frequency ω propagate in opposite directions through the sample gas molecules. Molecules moving with velocity v along the axis of the laser beams absorb radiation from one beam at a frequency $\Omega = \omega(1 + v/c)$, and from the other beam at $\Omega = \omega(1 - v/c)$. These opposite Doppler shifts cause each beam to depopulate a portion of the lower state velocity profile symmetrically about the profile center at $v = c(\Omega \pm \omega)/\Omega$ (see Fig. 2.1). This depletion is termed "burning a Bennett hole", creating a homogeneous profile in the lower state.⁶⁶ As the laser is scanned, and the laser frequency approaches the non-Doppler-shifted resonance frequency, the two Bennett holes converge until they meet at the center, or zero velocity (see Fig. 2.1). The resulting lower state population depletion causes a corresponding depletion in the intensity profile of the fluorescence, called a "Lamb dip".

Intermodulated fluorescence (IMF) is a technique which enables relatively small Lamb dips to be detected against the large Doppler-broadened profile so that they are directly measured as spectral

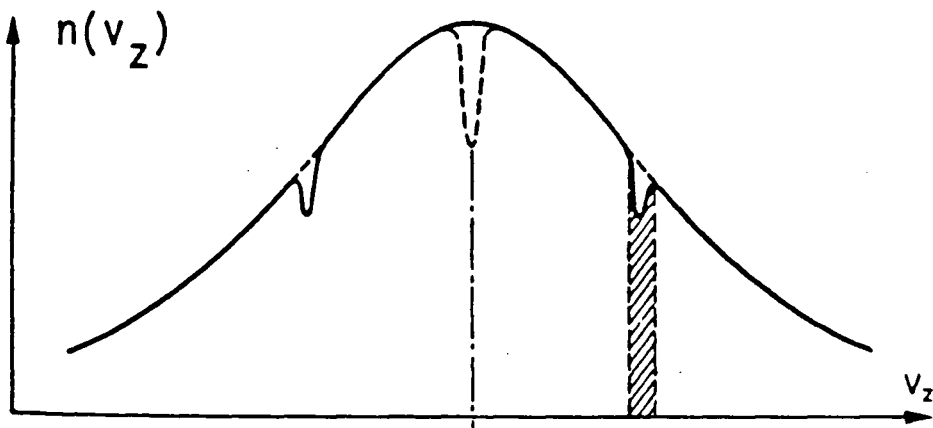


Fig. 2.1. Gaussian inhomogeneously Doppler-broadened velocity (v_z) population (n) profile, showing two Bennett holes (solid lines) which converge at zero velocity (dotted line) to form a Lamb dip in the profile of intensity versus laser tuning frequency.⁶⁶

peaks. The two laser beams are modulated (i.e., chopped to produce certain phase trains) with frequencies f_1 and f_2 . The lock-in amplifier, with the phase sensitive detector referenced to a frequency of $f_1 + f_2$, passes only $(f_1 + f_2)$ -modulated input signals, such as those occurring when two Bennet holes meet⁶⁶. A schematic diagram of the IMF experiment used to obtain the niobium nitride sub-Doppler spectra is illustrated in Fig. 2.2. In practice, the two counterpropagating laser beams must be slightly misaligned from one another to avoid feedback into the laser.

A LIF signal normally arises from Bennet holes caused by allowed $\Delta F = \Delta J$ transitions meeting at the velocity profile center. However, Lamb dips also originate from holes burned by "forbidden" $\Delta F \neq \Delta J$ transitions meeting at the center. Since the selection rules²⁴ on F and J are $\Delta F = 0, \pm 1$ and $\Delta J = 0, \pm 1$, transitions with $\Delta F = \Delta J \pm 1$ and ± 2 are also possible. For a Q transition, with $\Delta J = 0$, the F selection rule requiring that $\Delta F = 0, \pm 1$ allows the transitions rQ ($\Delta F = \Delta J + 1$), qQ ($\Delta F = \Delta J$) and pQ ($\Delta F = \Delta J - 1$). If $\Delta J = +1$, $\Delta F = +1, 0$ and -1 corresponds to the transitions rR, qR and pR (or $\Delta F = \Delta J, \Delta J - 1$ and $\Delta J - 2$). The same occurs for P branches where $\Delta F = \Delta J, \Delta J + 1$ and $\Delta J + 2$ lines (pP, qP and rP) occur. These satellite branches are observed only at low values of J because the intensity of the transitions is proportional to the angle between the vectors \mathbf{J} and \mathbf{F} .⁶⁷ When \mathbf{J} and \mathbf{F} are large with respect to \mathbf{I} this angle approaches zero, and only $\Delta F = \Delta J$ transitions are observed. The large value of $9/2$ for the nuclear spin of Nb allows $\Delta F \neq \Delta J$ transitions to be seen at higher values of J than is normally possible.

Accompanying a pair of $\Delta F = \Delta J$ and $\Delta F = \Delta J \pm 1$ transitions, or a

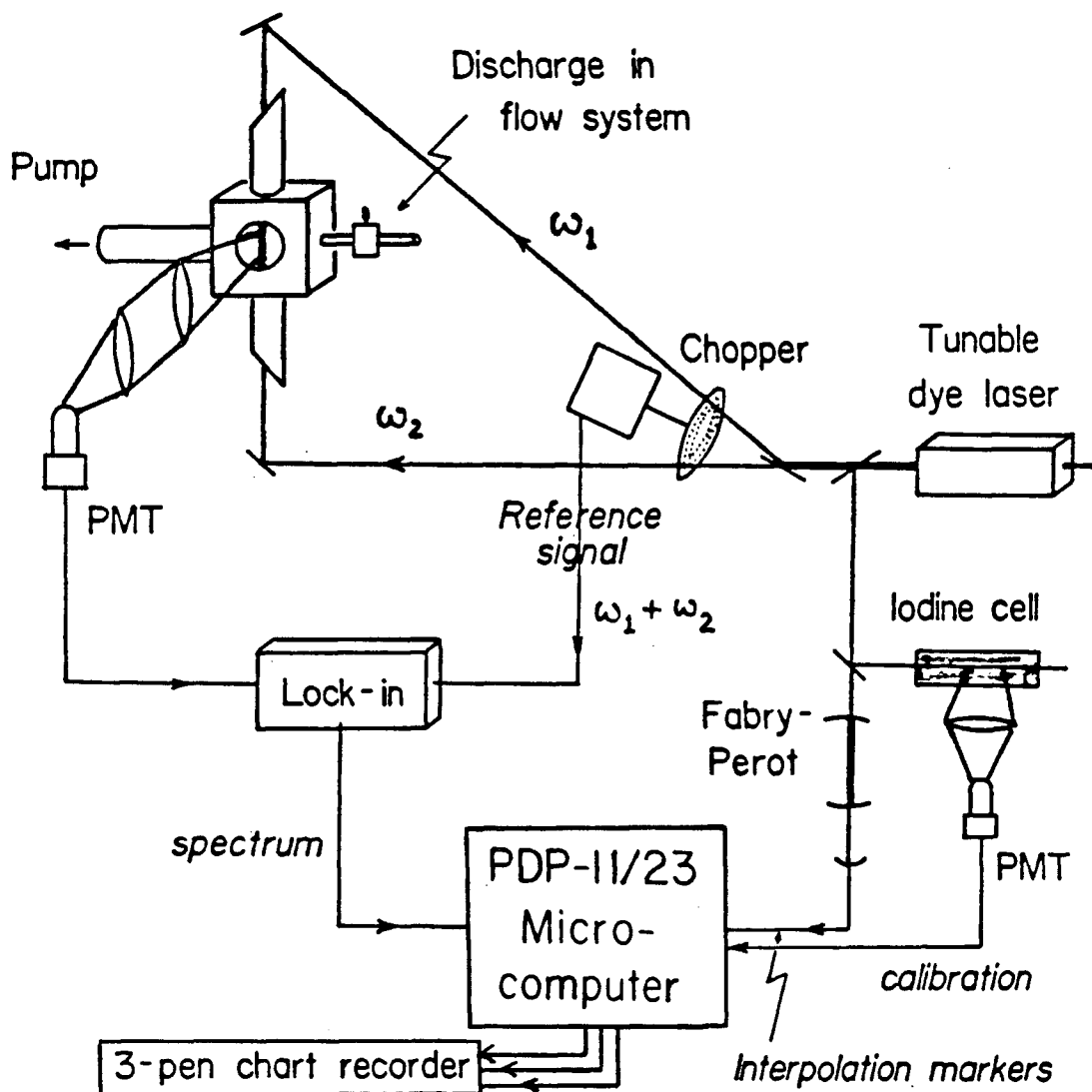


Fig. 2.2. Schematic drawing of the intermodulated fluorescence experiment used in this laboratory. The discharge cube where the sample and laser light are combined is shown in the top left corner.

$\Delta F = \Delta J \pm 1$ and $\Delta F = \Delta J \pm 2$ pair, may be a "crossover resonance" occurring exactly mid-way between the two. Such a phenomenon requires that the two transitions sharing a common level lie within the same Doppler profile. Crossover resonances occur in the IMF spectra of the nearly coincident transitions of closely spaced hyperfine components. The means by which crossover resonances are generated is depicted in Fig. 2.3, with a schematic stick drawing of the resulting spectrum.

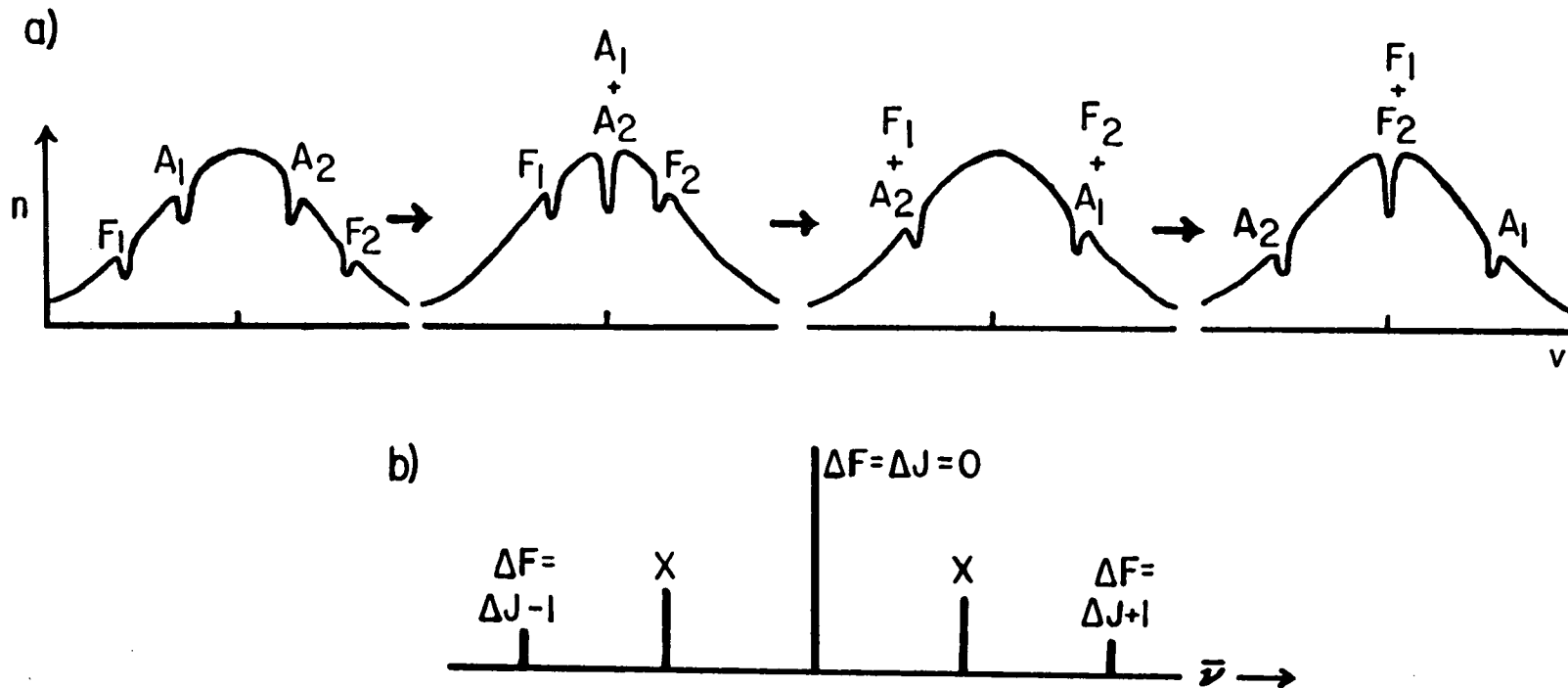


Fig. 2.3. a) The formation of crossover resonances ($F_1 + A_2$ and $F_2 + A_1$) as the result of allowed $\Delta J = \Delta F$ transitions (A_1 and A_2) occurring within the same Doppler-broadened velocity profile as forbidden $\Delta J \neq \Delta F$ transitions (F_1 and F_2). The diagram shows the laser scanning toward the non-Doppler-shifted $\Delta F = \Delta J$ transition (occurring at $A_1 + A_2$) and beyond toward higher frequency to the $\Delta F = \Delta J + 1$ transition ($F_1 + F_2$). If the F's and A's are exchanged, the first central Lamb dip is the $\Delta F = \Delta J - 1$ transition. b) Stick diagram of the spectrum of the four forbidden transitions that can accompany a $\Delta F = \Delta J = 0$ Q transition (X denotes a crossover). With an R line, the $\Delta F = 0$ and $\Delta F = -1$ transitions and the associated crossovers occur to the red of the $\Delta F = \Delta J + 1$ transition, while with a P line the forbidden transitions lie to the blue to the $\Delta F = \Delta J - 1$ transition.

II.C. Computerization.

Part of the work for this thesis involved computerizing all stages of the Doppler-limited and intermodulated fluorescence (sub-Doppler) LIF experiments on a PDP-11/23 microcomputer with an RSX-11M operating system. These stages included: 1) laser scanning, and data acquisition and storage; 2) peak finding; and 3) frequency calibration. Each stage comprises a separate program. All of the software was written with FORTRAN-77 except for the laser scanning and data acquisition, programmed in MACRO. The PDP-11 computer is structured such that space for executable code is quite limited. This constraint required that the three programs be overlaid. Overlaying is a method of memory management which allows the sum of the individual subroutines to far exceed the memory limitations of the computer. When an overlaid program is executed, only a portion of the subroutines are sent into memory, while the remainder resides in the relatively limitless disk space. A set of overlay directives is written which describes the program in terms of a calling "root" segment and any number of subprogram "branch" segments; the branches may themselves call "subbranches". The computer uses these directives to build the task file such that during program execution the memory space at any given time is occupied only by the root segment and the branch being called at that time. Since the main responsibility of the root is to call subroutines in the branches, the root is made as short as possible to allow most of the software to remain disk-resident throughout program execution.

The heart of the first program is the MACRO routine which orchestrates laser scanning and data acquisition via its control of the following hardware peripheral devices:

- The 16-bit digital-to-analog converter (D/A), which sends a voltage ramp to the laser so that it scans a range of up to 1.4 cm^{-1} .

- The 4-channel, 12-bit analog-to-digital converter (A/D), containing two registers to process incoming data. The control status register (CSR) receives the voltages (data points) from the sample, iodine and interferometer detectors. The buffer preset register receives the point from the CSR, stores it temporarily, then delivers it both to the 12-bit output D/A and to the appropriate storage buffer for transfer to disk. The sample spectrum is signal averaged over four points prior to transfer to the buffer.

- Three 12-bit D/A's, which send the three data points to the chart recorder for a hardcopy of the spectra.

- The real-time (crystal-oscillator) clock, by which the above peripheral devices are interrupt-driven to operate at a user-chosen rate producing a resolution compatible with the lock-in time constant and the frequency range scanned by the laser. The use of interrupts ensures that the task will be serviced by the computer's central processing unit exactly as dictated by the clock.

The interfacing of computer and experiment is illustrated schematically in Fig. 2.4. Upon return from the MACRO routine after scanning is complete, the three spectral vectors are stored in unformatted files with the first record of the sample file serving as a housekeeping record containing spectral identification and experimental parameters.

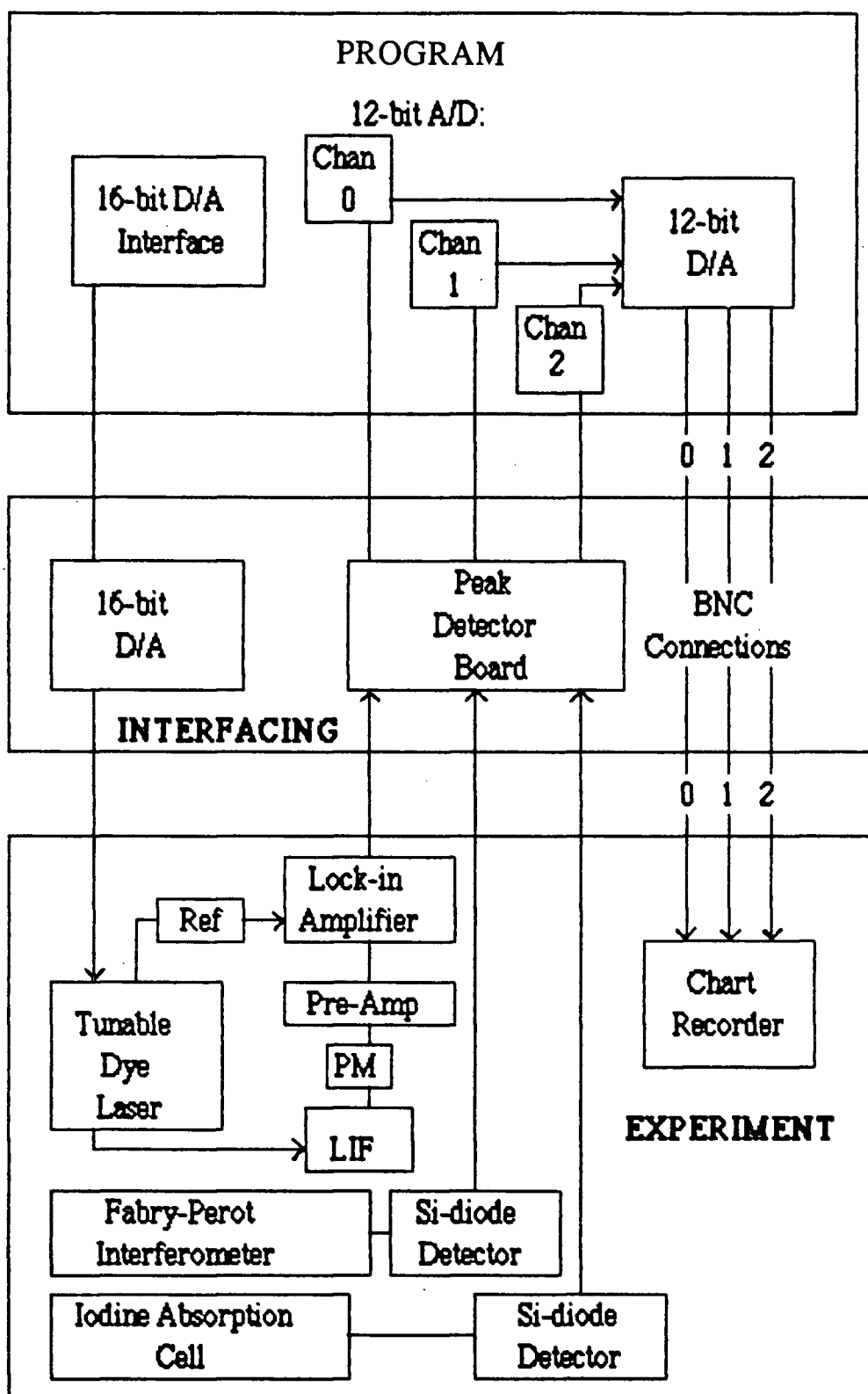


Fig. 2.4. Schematic diagram of the laser-induced fluorescence experiment and how it is interfaced to the PDP-11/23 micro-computer.

CHAPTER III

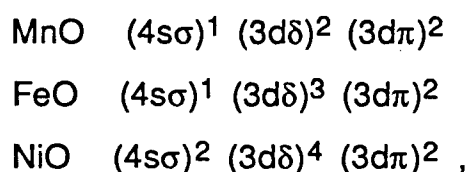
ROTATIONAL ANALYSIS OF THE RED SYSTEM OF COBALT OXIDE

III.A. Introduction.

In German-occupied Belgium during World War II, Malet and Rosen observed a number of electronic bands of gaseous cobalt oxide (CoO) between 5000 and 10000 Å using the exploding wire technique.⁶⁹ The lower state vibrational frequency (i.e., the separation of the $v''=0$ and $v''=1$ vibrational states) was found to be 840 cm^{-1} , and this state was assumed to be the ground electronic state. The next spectroscopic experiments on CoO came years later, in 1979. The first was a low resolution infrared spectrum of CoO (with $\pm 0.2\text{ cm}^{-1}$ line precision) obtained with a microwave discharge source, giving a vibrational frequency of 842.2 cm^{-1} , an equilibrium rotational constant (B_e) of 0.522, and an equilibrium bond length (r_e) of 1.60 Å.⁷⁰ The absence of a Q branch in the spectrum led to the tentative assignment of a Σ ground state²⁴, though the possibility was not ruled out that the spectrum was that of a low-lying excited state.⁷⁰ A matrix isolation infrared study followed shortly afterwards⁷¹, in which cobalt from a cobalt cathode sputtering source and oxygen were codeposited at low temperature (14 K) into a solid matrix of argon. The ground state vibrational frequency was measured in this work to be 846.4 cm^{-1} . In the next year, matrix isolation electron spin resonance (ESR) studies of a large group of transition metal-containing molecules with high spin multiplicities were reported, including CoO.⁷² In spite of high concentrations of CoO within the matrices and the expertise of the laboratory in conducting

experiments of this type, no CoO ESR signal was observed. CoO was therefore concluded to possess an orbitally degenerate ground state, because orbital degeneracy in linear molecules (in matrices of low enough temperature that only the ground state is populated) causes a g tensor anisotropy so large that the spectrum is spread out over such a large magnetic field that it cannot be observed. The ESR spectrum of a paramagnetic Σ state, on the other hand, will possess little or no g anisotropy and will exhibit only a small deviation from the free electron value, $g_e = 2.0023$, due to the spherical symmetry of the overall orbital angular momentum.^{72,73} The value of g is deduced from the relation $h\nu = g\mu_B H$, where ν is the resonance frequency, μ_B the Bohr magneton, H the applied magnetic field, and h Planck's constant; the g anisotropy is taken as $g_{\perp} - g_{\parallel}$. No further work has been published on CoO since this ESR study, leaving the ground state of the molecule to be the only one of the first row transition metal oxides yet to be established.

Field-free atomic orbitals of a diatomic transition metal molecule are split by the axial field of the other atom, as shown in Fig. 3.1. From the electron configurations of manganese, iron and nickel monoxides,



it can be seen that there are two possible candidates for the ground electronic state of CoO. If the seventh valence electron occupies the $4s\sigma$ orbital, the spin multiplicity and direct products given by the resulting $\sigma^2\delta^3\pi^2$ configuration produce a ${}^4\Delta_i$ electronic state⁷⁴; if

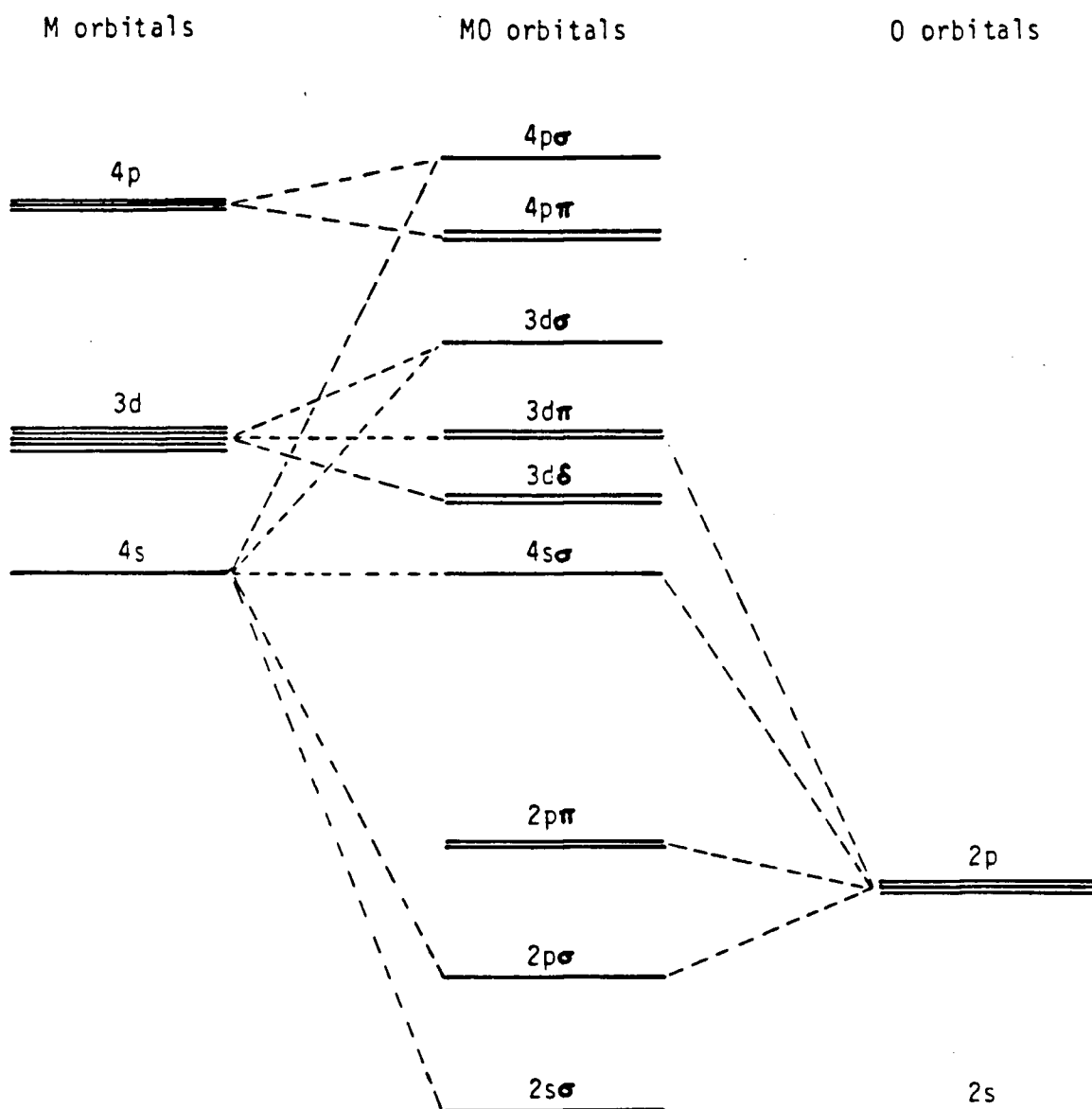


Fig. 3.1. Relative orbital energies of a diatomic 3d transition metal oxide.⁹² The ordering of the 3d δ and 4s σ molecular orbitals is variable.

instead it fills up the δ orbital, a $4\Sigma^-$ state results. However, the uncertain ordering of the $4s\sigma$ orbital with respect to the $3d\delta$ orbital⁷⁵ left the problem in the hands of the theoreticians. Multi-configuration self-consistent-field complete active space (CAS MCSCF) calculations on FeO were extrapolated to CoO to predict a $4\Sigma^-$ ground state.⁷⁶ Weltner, however, first predicted a state of Δ symmetry based on trends in the other TM oxides⁷⁷, then later predicted a 4Φ ground state based on ESR experiments⁷². It was from this stage of development that the current study proceeded.

III.B. Experimental

III.B.1. Synthesis of gaseous cobalt oxide.

Cobalt oxide was made in a Broida-type oven assembly⁷⁴ as follows: an alumina crucible containing cobalt metal powder (Fisher Scientific Co.; 0.14% Ni, 0.11% Fe) was heated resistively in a tungsten basket. The basket was enclosed in a radiation shield comprising an inner ceramic sleeve enveloped by an outer copper sleeve and fitted lid, with zirconia felt packed very tightly around the basket. To produce cobalt oxide (CoO) in quantities sufficient for measurable fluorescence, temperatures approaching the melting point of the alumina crucible (1920 °C) were required, well in excess of cobalt's melting point of 1495 °C. CoO was formed in the gaseous stream of vaporized cobalt atoms, argon carrier gas and molecular oxygen at a pressure of roughly 1 Torr, with a ratio of approximately 150(±15):1 argon to oxygen. Fluorescence, however, occurs only in the presence of laser excitation, which is as with NiO in which only the ground state is populated by the reaction of metal and O₂.⁷⁸ Unlike the production of CuO⁷⁹, which is more efficient with N₂O than O₂, no CoO fluorescence was observed using N₂O as the oxidant. The requirement of high temperature drastically hampered the efficiency of CoO synthesis in two ways. First, there was extensive formation of Thénard's Blue⁸⁰ (cobalt aluminate) deposits on the crucible and on the surface of the liquid cobalt; this phenomenon was also reported in 1966 by Grimely and coworkers who heated solid CoO in an alumina cell to high temperatures⁸¹. Second, the reaction of cobalt vapor with the tungsten basket produces an alloy that renders the basket very susceptible to

cracking, with breakage occurring after at most three heatings of a basket assembly.

III.B.2. The spectrum.

The laser excitation spectrum of gaseous CoO was investigated over the range of 7000 to 5800 Å at Doppler-limited resolution, as described in Section II.A. It is evident that the system extends further to both higher and lower energies. The bands observed by Malet and Rosen with the exploding wire technique⁶⁹ correspond in frequency to those we have measured, though the intensities sometimes varied dramatically between the two techniques. With the superior sensitivity provided by the LIF method, a number of additional bands were observed. The most prominent ones, as measured from a broadband laser spectrum (i.e., one obtained without the intracavity assembly), are listed in Table 3.1. The portion of the spectrum rotationally analyzed thus far covers the range from 15450 to 15790 cm⁻¹ (6470 to 6335 Å), which includes three red-degraded bands whose heads lie at 15778 cm⁻¹ (6338 Å), 15598 cm⁻¹ (6411 Å) and 15538 cm⁻¹ (6436 Å). The broadband spectrum of this region is shown in Fig. 3.2.

Table 3.1. The most prominent bandheads in the 7000 to 5800 Å broadband emission spectrum of gaseous CoO. Values are accurate to roughly ± 3 cm⁻¹, with band strength denoted by: s = strong, m = medium, w = weak.

Wavelength group	5920 Å	6120 Å	6320 Å	6650 Å	6900 Å
Wavenumber	16916 m	16366 w	15832 w	15296 vw	14704 w
and intensity	16846 s	16322 s	15778 s	15228 w	14477 m
		16256 m	15597 w	15036 m	14469 s
		16088 w	15538 m	15004 s	

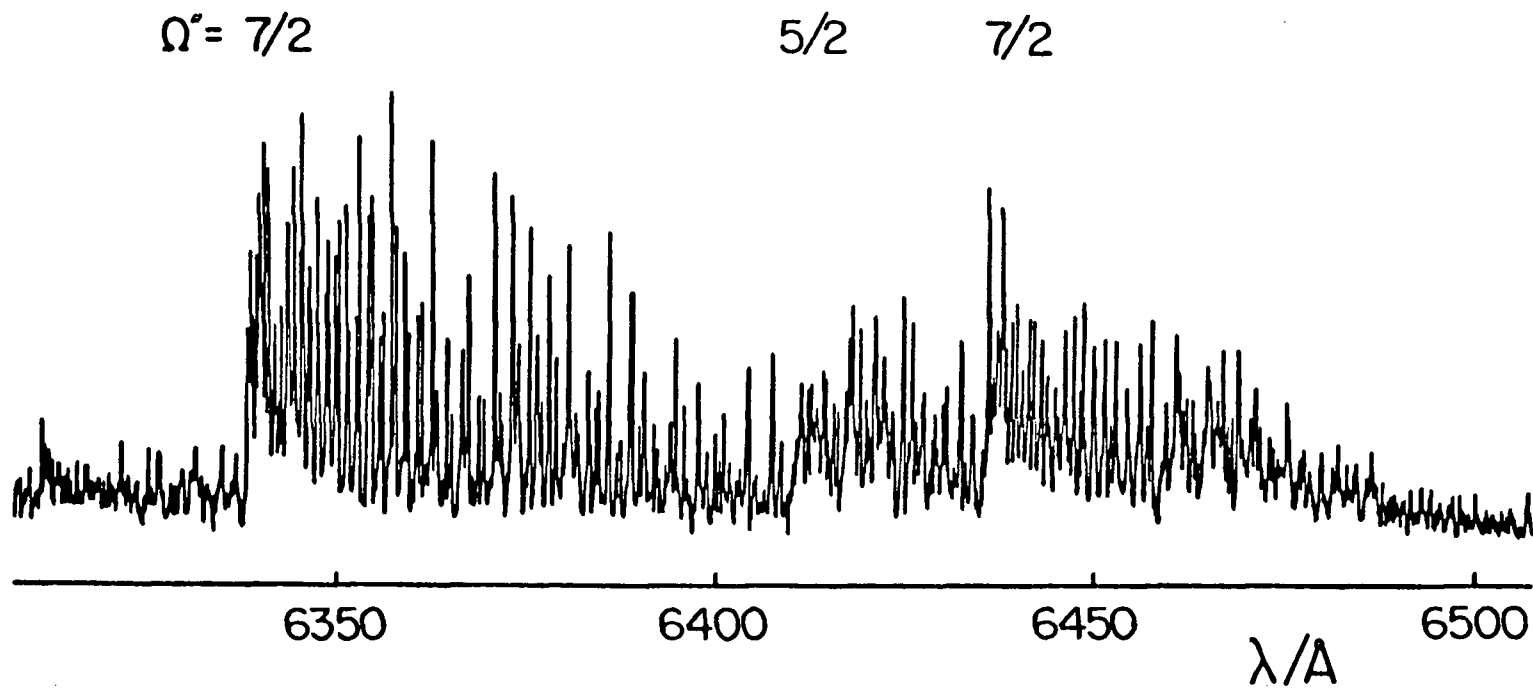


Fig. 3.2. Broadband laser excitation spectrum of the three bands of gaseous CoO analyzed in this work (linewidths are on the order of 1 cm^{-1}).

III.C. Analysis.

III.C.1. Rotational analysis of the 6338 Å subband.

III.C.1.a. Rotational constants and hyperfine structure.

The strongest band, at 6338 Å, was the only band of the three for which a complete analysis was possible, given the available data. The line assignments, listed in Table 3.II, were made using lower state combination differences. For added assurance, some wavelength-resolved fluorescence experiments were performed to verify that certain lines possessed common upper levels. For example, if a pair of lines with a common upper level, such as Q(J") and R(J"-1), are excited, the fluorescence pattern produced as a result of the R line excitation will be identical to that obtained from the Q line, barring changes in the scattered laser light at the excitation wavelength.

Lower state combination differences measure differences between lines with a common upper state that differ in their J" value, thereby providing information on the lower state energy structure:¹

$$\Delta_1 F''(J) = R(J) - Q(J + 1) = Q(J) - P(J + 1) \quad (3.1)$$

$$\Delta_2 F''(J) = R(J - 1) - P(J + 1) \quad (3.2)$$

From the definitions of R, Q and P, and from the energy level expressions, it can be shown that⁸³

$$\Delta_1 F''(J) = 2B''(J + 1) - 4D''(J + 1)^3 \quad (3.6)$$

$$\Delta_2 F''(J) = (4B'' - 6D'')(J + 1/2) - 8D''(J + 1/2)^3 \quad (3.7)$$

The lowest Q line of this band was assigned as J' = J" = 7/2, using the average of the $\Delta_1 F''$ combination differences from the first R and P lines, and a rough estimate of 0.5 cm⁻¹ for the value of B. The

possible electronic states corresponding to a value of Ω of $7/2$ are 4Δ and 2Φ , but only the 4Δ state has an electronic configuration that can reasonably be expected to belong to the ground state. The three subbands analyzed in the current work demonstrate that the most intense CoO transitions are those with $\Omega'' = 7/2$. Presumably these must come from the lowest spin-orbit component of the ground state. Since the spin-orbit manifold must be inverted for its lowest energy component to be $7/2$, the electronic state is assigned as $4\Delta_i$. The relatively low intensity of the Q lines¹ (see Fig. 3.3), identifies the transition as parallel, or $\Omega' = \Omega'' = 7/2$. The lower state vibrational level can definitely be assigned as $v'' = 0$, based on resolved fluorescence experiments where the Q(3.5) line was excited: strong fluorescence was observed 851.7 cm^{-1} to the red of the Q(3.5) transition, but nothing to the blue. In the absence of isotopic labelling studies, such as with Co^{18}O , no information is available on the upper state quantum number.⁸³ Extensive structure to the red of the 6338 \AA band indicates that there are lower lying vibrational levels; on this basis, the upper state vibrational quantum number is suggested to be at least two.

The lower state rotational constants B and D were calculated by least squares from the Δ_2F'' combination difference formula in equation (3.7). The $\Delta_2F''(J)$ combination differences are given in Table 3.II along with the assigned lines of the 6338 \AA band. Using these B'' and D'' values to calculate the lower state energy levels, the upper state energy levels were calculated; then a least squares fit to the expression

$$E(J) = T_0 + BJ(J + 1) - DJ^2(J + 1)^2 \quad (3.8)$$

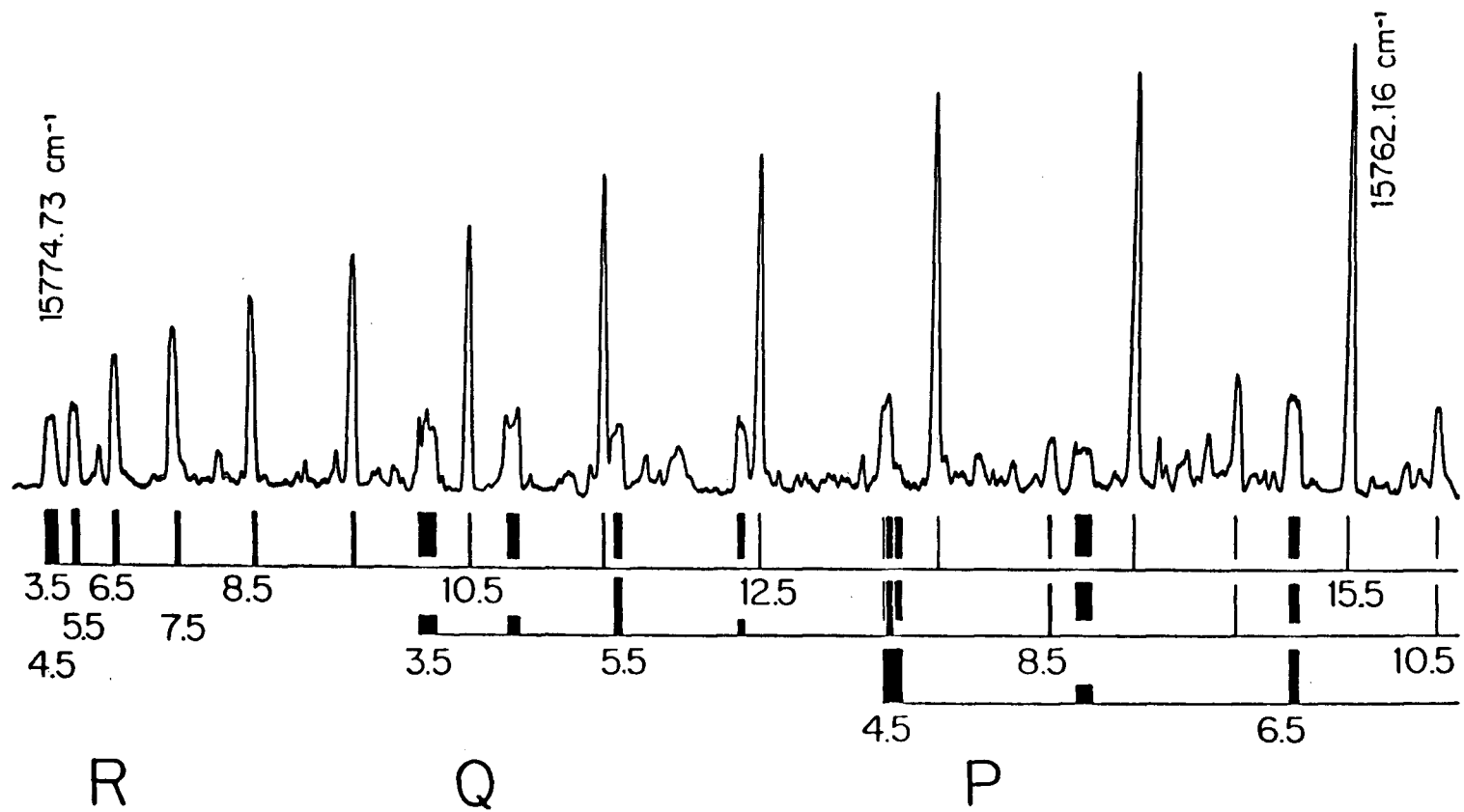


Fig. 3.3. Bandhead of the $\Omega' = \Omega'' = 7/2$ transition at 6338 Å, exhibiting the broadening due to hyperfine interactions and the weak Q branch signifying a parallel transition. The weak background is reproducible.

Table 3.II. Assigned lines from the 6338 Å band (${}^4\Delta_{7/2} - {}^4\Delta_{7/2}$) of CoO with the lower state combination differences, Δ_2F'' , in cm^{-1} . An asterisk denotes a blended line.

J''	R	Q	P	Δ_2F''	10^3 O-C	
3.5	15774.7*	15771.060				
4.5	15774.7*	15770.2*	15766.64*			
5.5	15774.509	15769.2*	15764.737			
6.5	15774.110	15768.002	15762.704	14.015	1	
7.5	15773.526	15766.64*	15760.494	16.014	-2	
8.5	15772.760	15765.024	15758.096	18.011	-6	
9.5	15771.810	15763.259	15775.515	20.013	-5	
10.5	15770.668	15761.291	15752.747	22.015	-3	
11.5	15769.343	15759.158	15749.791	24.021	2	
12.5	15767.828	15756.829	15746.647	26.024	6	
13.5	15766.126	15754.316	15743.319	28.017	-1	
14.5	15764.236	15751.615	15739.811	30.019	2	
15.5	15762.159	15748.715	15736.107	32.018	2	
16.5	15759.892		15732.219	34.011	-3	
17.5	15757.445		15728.147	36.012	1	
18.5	15754.806		15723.880	38.006	-2	
19.5	15751.994		15719.439	40.005	1	
20.5	15749.350	15747.947	15714.801	42.000	0	
	15748.821	15749.039				
21.5	15745.600	15745.906	15709.994	43.995	0	
		15745.720				
22.5	15742.273	15742.345	15705.347	15703.946	45.987	-3
			15704.829	15705.045		
23.5	15738.696	15738.769	15699.615	15699.914	47.984	1
			15699.735			
24.5	15734.923	15735.005	15694.290	15694.360	49.980	4
25.5	15730.951	15731.051	15688.720	15688.786	51.975	6
26.5	15726.783	15726.911	15682.948	15683.030	53.968	8
27.5	15722.428	15722.592	15767.986	15677.080	55.956	6
28.5	15717.883	15718.106	15670.826	15670.954	57.938	-2

Table 3.II. continued.

J"	R		P		$\Delta_2 F''$	10^3 O-C
29.5	15713.130	15713.500	15664.491	15664.654	59.929	0
30.5	15709.131	15708.185	15657.951	15658.178	61.908	-9
	15707.960					
31.5	15703.047	15703.110	15651.226	15651.589	63.903	0
32.5	15697.705	15697.888	15645.226	15644.282	65.890	1
			15644.057			
33.5	15692.171	15692.441	15637.158	15637.220	67.870	-4
34.5	15686.424	15686.786	15629.837	15630.015	69.861	3
35.5	15680.487	15680.945	15622.311	15622.580	71.836	-5
36.5	15674.251	15674.893	15614.591	15614.950	73.820	-2
37.5	15667.933	15668.678	15606.670	15607.122	75.787	-15 ^a
38.5	15661.347	15662.251	15598.464	15599.106	77.783	1
39.5	15654.547	15665.638	15590.150	15590.896	79.752	-8
40.5	15647.498	15648.844	15581.594	15582.500	81.738	2
41.5	15640.453*	15641.831	15572.810	15573.900	83.713	1
42.5		15634.643	15563.785	15565.131	85.684	-2
43.5		15627.272	15554.769	15556.159	87.641	-18 ^a
44.5		15619.712		15547.002	89.615	-15 ^a
45.5		15611.954		15537.657	91.591	-9 ^a
46.5		15604.010		15528.121		
47.5				15518.405*		

^aNot included in the least squares fit.

was used to obtain B' and D' from the unperturbed levels with $J' = 5.5$ to 19.5. The results appear in Table 3.III. Note that since the upper state B value is only 81% of the lower state, by the relation $r''/r' = (B'/B'')^{1/2}$ the CoO bond length increases by a full 10% upon electronic excitation.

The hyperfine structure in CoO arising from the ^{59}Co nuclear spin of $7/2$ follows the case ($a\beta$) pattern where the hyperfine widths decrease with increasing rotation, described to a first approximation by equation (1.90):⁸⁵

$$E_{\text{Hfs}} \approx \Omega[a\Lambda + (b + c)\Sigma](1/J)\{[F(F+1) - J(J+1) - I(I+1)]/2(J+1)\} \quad (3.9)$$

(In case ($b\beta_J$) coupling the hyperfine widths are independent of N for each of the spin components.) The hyperfine splitting in the P lines is found to be wider than that in R lines of the same J'' , while P and R lines possessing the same upper state J are of comparable widths. Since a comparison of P and R lines of the same J'' demonstrate upper state properties, while those with equal J' represent the lower state, it can be seen that the hyperfine interactions produce larger splittings in the upper state than in the lower state. From equation (3.9) it can also be seen that the eight hyperfine components of a rotational line will be more widely spaced at higher values of F . Partially resolved hyperfine splittings in some low J lines, for instance P(5.5), show that the highest F value component is on the high frequency side. This ordering of the hyperfine components shows that the change in the Fermi contact parameter, $b' - b''$, is positive.⁸⁴

Table 3.III. Rotational constants for the analyzed bands of the red system of CoO.^a

	T_0	B	10^7D	σ
Upper Levels:				
6338 Å, $\Omega = 7/2$	15772.513 ± 3	0.40531 ± 9	6.4 ± 19	0.0038
6411 Å, $\Omega = 5/2$	$a+15594.974 \pm 2$	$0.4250_3 \pm 24$	27 ± 7	0.0049
6436 Å, $\Omega = 7/2$	15535.77	0.422_4^b
Lower Levels ($X^4\Delta_i$):				
$\Omega = 5/2$	a	$0.5026_6 \pm 9$	3.6 ± 14	0.0024
$\Omega = 7/2$	0	0.50058 ± 4	6.50 ± 15	0.0031

^aValues in cm^{-1} , with error limits of three standard deviations in units of the last significant figure. $a = A\Lambda \approx 244 \text{ cm}^{-1}$.

^bNo least squares fit; see text.

III.C.1.b. Perturbations.

A plot of the upper state energy levels as a function of $J(J + 1)$ illustrates the perturbations in the upper states. The lower state appears to be free of Λ -doubling (cf. Section 1.B.6) and other perturbations, since the lower state combination differences are entirely regular: the two $\Delta_2F''(J)$ values, given by the two Λ -doubling components, are equal to within experimental error. Figure 3.4 shows that upper state Λ -doublings begin at $J' = 21.5$, and that in some places extra transitions occur; the section of spectrum in Fig. 3.5 illustrates these perturbations. The extra lines could be securely identified because they give exactly the same $\Delta_2F''(J)$ combination differences as the main lines and their relative intensities are in the same ratio.

Two avoided crossings can be seen in Fig. 3.4: a strong one, where both of the Λ components are perturbed, at $J' = 30.5 - 31.5$, and a weaker one where the lower Λ component is mildly perturbed at $J' = 37.5$. Since the avoided crossings affect the Λ -components differently, the perturbing state is orbitally non-degenerate, or alternatively has a very large Λ -doubling of its own. The state perturbing the $J' = 22.5$ level appears to have a relatively small Λ - or Ω -doubling. (Λ -doubling exhibited by a Σ state is referred to here as Ω -doubling⁸⁵.)

The state responsible for all of the above perturbations could conceivably be a single case (a) 4Σ state. The small Ω -doubling occurring near $J' = 22.5$ could arise from the $4\Sigma_{3/2}$ component, while the considerably larger Ω -type splitting associated with the $4\Sigma_{1/2}$ component⁸⁵ is capable of affecting upper state levels that are

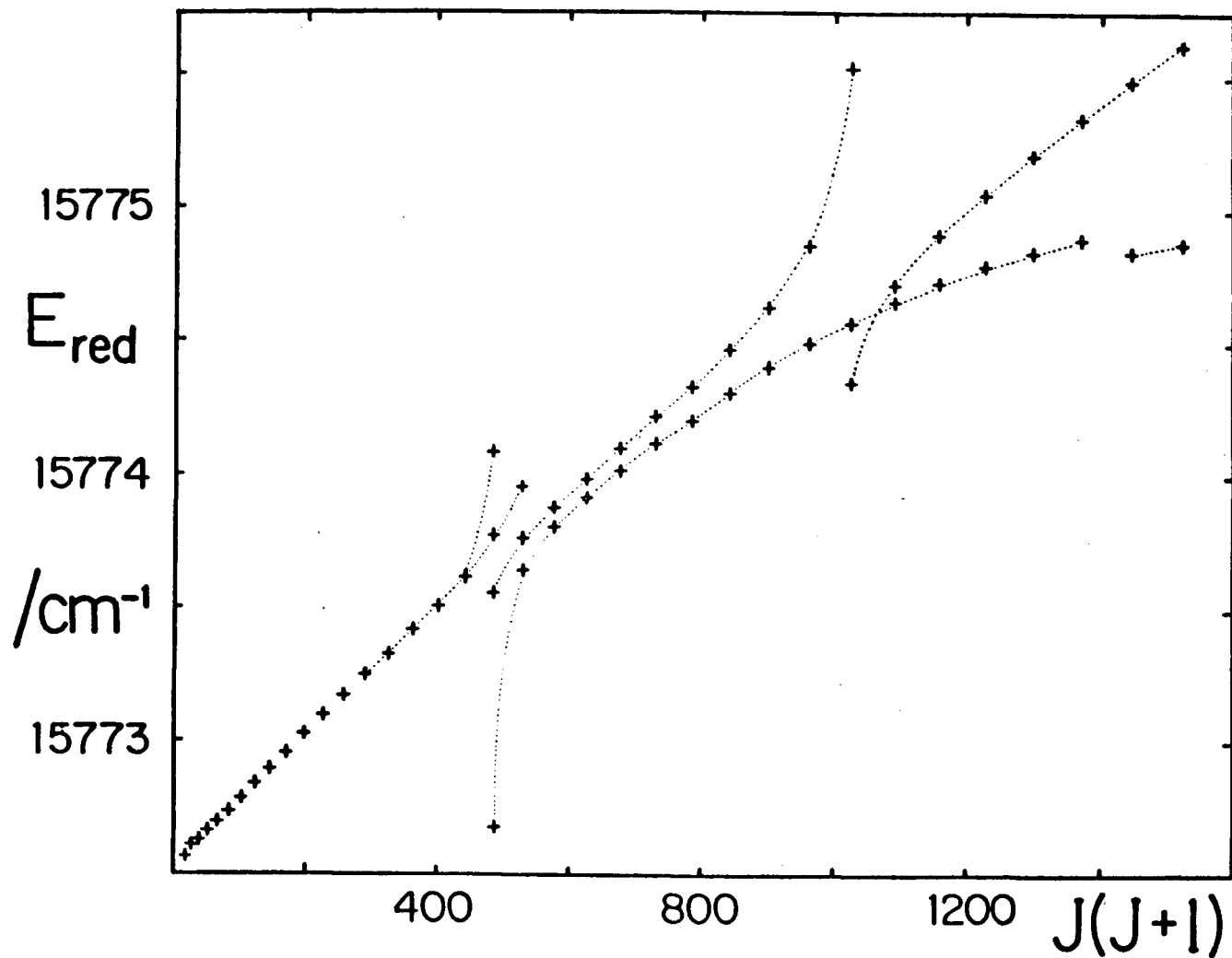


Fig. 3.4. Upper state energy levels of the ${}^4\Delta_{7/2} - {}^4\Delta_{7/2}$ 6338 Å band, scaled by subtracting the quantity $0.405J(J + 1) - 6.4 \times 10^{-7}J^2(J + 1)^2$, plotted against $J(J + 1)$.

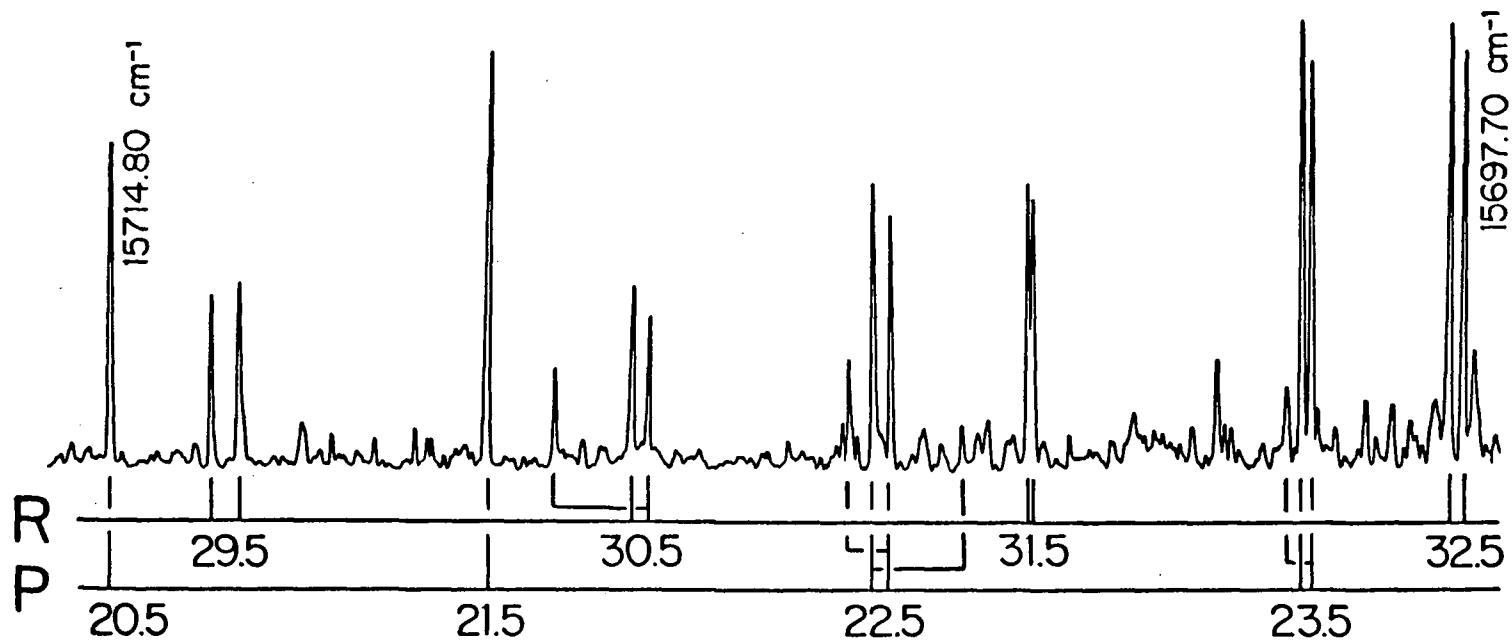


Fig. 3.5. A section of the spectrum of the 6338 Å band containing Λ -doubling, two avoided crossings, and extra lines. The extra R(30.5) line to the blue of the Λ -doubled R(30.5) lines corresponds to the anomalous point in Fig. 3.4 near $J(J + 1) = 1000$. All lines, down to the weakest, are reproducible, though relative intensities between lines at either end of the spectrum may not be accurate since the spectrum is compiled from several laser scans.

widely spaced in J , analogous to the situation observed in Fig. 3.4.

III.C.2. Rotational analysis of the 6436 Å subband.

The fairly intense 6436 Å band is another $\Omega' = \Omega'' = 7/2$ parallel transition whose lower state is the same as that of the 6338 Å band, as the lower state combination differences of the two bands are equal to within experimental error. Because the upper level lies only 237 cm^{-1} below that of the 6338 Å upper state, and the frequency separating the strong groups of subbands (cf. Table 3.1) is on the order of 600 cm^{-1} , it cannot belong to the same upper electronic state as the 6338 Å band. Also, the hyperfine structure is considerably wider than in the 6338 Å subband, which also points to a different upper electronic state. There is not enough information available to say what this other electronic state is. Although its high intensity suggests that it is another ${}^4\Delta_{7/2} - {}^4\Delta_{7/2}$ transition, there are other channels through which intensity can be derived. In the very dense, perturbed "orange" system of FeO, for example, transitions to the high vibrational levels of various lower electronic states acquire considerable intensity by interacting with the upper state of the system.⁸⁶

The upper state energy levels are plotted as a function of $J(J + 1)$ in Fig. 3.6, up to the limit of our analysis thus far at $J' = 26.5$. Λ -doubling is first observed at $J' = 20.5$, very much like the 6338 Å band upper levels which are first seen to split at $J' = 21.5$. Perturbations in the upper state have scattered the levels to such a degree that a good least squares fit to the upper state constants was not possible, though a value of B' could be estimated (see Table

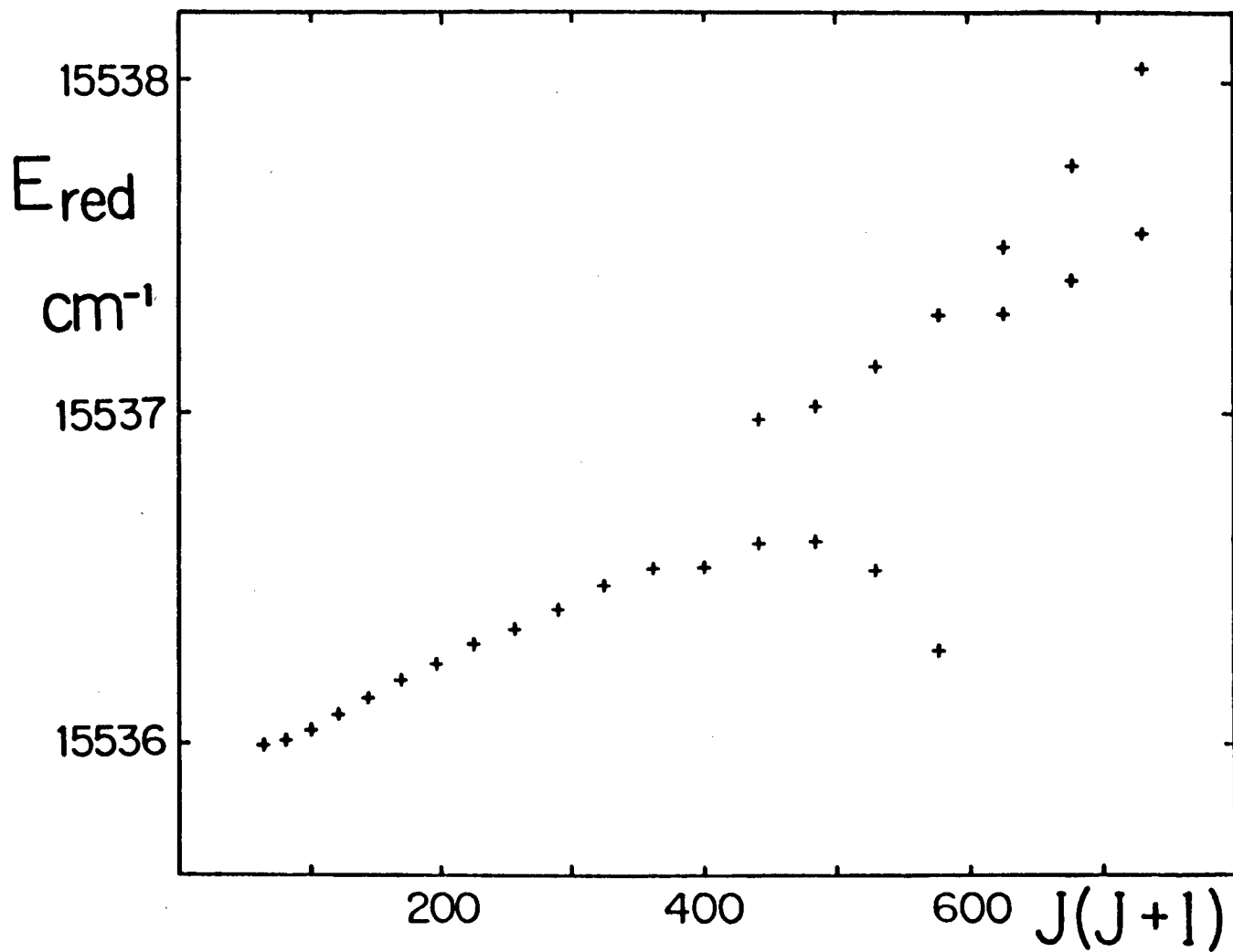


Fig. 3.6. Upper state energy levels of the $4\Delta_{7/2} - 4\Delta_{7/2}$ 6436 Å band, scaled by subtracting the quantity $0.42J(J + 1)$, plotted against $J(J + 1)$.

3.III). The lines assigned in the 6436 Å band are compiled in Table 3.IV.

III.C.3. Rotational analysis of the 6411 Å subband.

The $\Omega' = \Omega'' = 5/2$ subband whose head lies at 6411 Å is much weaker than the other two subbands, and is also badly perturbed, which has precluded analysis beyond $J' = 20.5$. All the lines assigned so far are listed in Table 3.V. The transition was assigned as $\Omega' = \Omega'' = 5/2$ by the methods used previously for the 6338 Å subband, and it appears that the lower state is the $\Omega = 5/2$ spin-orbit component of the ground electronic state. The crowded head region of the band is shown in Fig. 3.7.

The perturbations in the $\Omega' = 5/2$ upper state are illustrated by the plot of the scaled upper state energy levels as a function of $J(J + 1)$ in Fig. 3.8. The Λ -doubling is much larger than in the upper levels of the $\Omega = 7/2$ bands, with the splitting first discernible at Doppler-limited resolution at $J' = 10.5$. At $J' = 16.5$ one of the Λ -components is drastically pushed to lower energy, and no further J' levels could be assigned. The other component also disappears abruptly at $J' = 20.5$. The suddenness with which the branches break off is surprising, because there is no appreciable loss of intensity before the rotational structure ceases. This fragmentary behavior has been observed before, for example in the 5866 Å band of FeO where the structure disappears suddenly at $J' = 15$, and then reappears 12 cm^{-1} to the blue.⁸⁶ The 6411 Å upper level in CoO has obviously suffered a massive perturbation near $J' = 20.5$. To find where the branches resume will require extensive wavelength resolved

Table 3.IV. Assigned lines from the 6436 Å ($4\Delta_{7/2}-4\Delta_{7/2}$) band of CoO, in cm^{-1} .

J"	R		P	
7.5	15537.998		15524.45	
8.5	15537.505		15522.347	
9.5	15536.866		15519.996	
10.5	15536.061		15517.490	
11.5	15535.096		15514.839	
12.5	15533.976		15512.039	
13.5	15532.692		15509.082	
14.5	15531.241		15505.950	
15.5	15529.644		15502.682	
16.5	15527.897		15499.226	
17.5	15525.955		15495.625	
18.5	15523.820		15491.877	
19.5	15521.589	15521.967	15487.959	
20.5	15519.589	15519.536	15483.815	
21.5	15516.412	15517.029	15479.586	15479.959
22.5	15513.383	15514.393	15475.130	15475.539
23.5	15511.448	15511.650	15470.420	15471.035
24.5	15508.438	15508.784	15465.395	15466.408
25.5			15461.468	15461.670
26.5			15456.463	15456.809
27.5			15451.345	15451.840

Table 3.V. Assigned lines from the 6411 Å band (${}^4\Delta_{5/2}$ - ${}^4\Delta_{5/2}$) of CoO, in cm^{-1} . An asterisk denotes a blended line.

J''	R	Q	P	
2.5	15597.270*	15594.293		
3.5	15597.577*	15593.751		
4.5	15597.730*	15593.067	15589.2*	
5.5	15597.730*	15592.23*	15587.557	
6.5	15597.577*	15591.183	15585.670	
7.5	15597.270*	15590.039*	15583.654	
8.5	15596.194	15588.739	15581.492	
9.5	15596.194	15596.240	15579.076	
10.5	15595.432	15595.512	15576.718	
11.5	15594.523	15594.647	15574.076*	15574.125
12.5	15593.461	15593.618	15571.307	15571.389
13.5	15592.254	15592.708	15568.389	15568.512
14.5	15590.896	15591.441	15565.323	15565.493
15.5	15589.390	15588.739	15562.106	15562.559
16.5	15587.729		15582.734	15559.270
17.5	15585.958		15555.222	15554.561
18.5	15583.958		15551.558	
19.5	15581.845		15547.736	
20.5			15543.770	
21.5			15539.646	

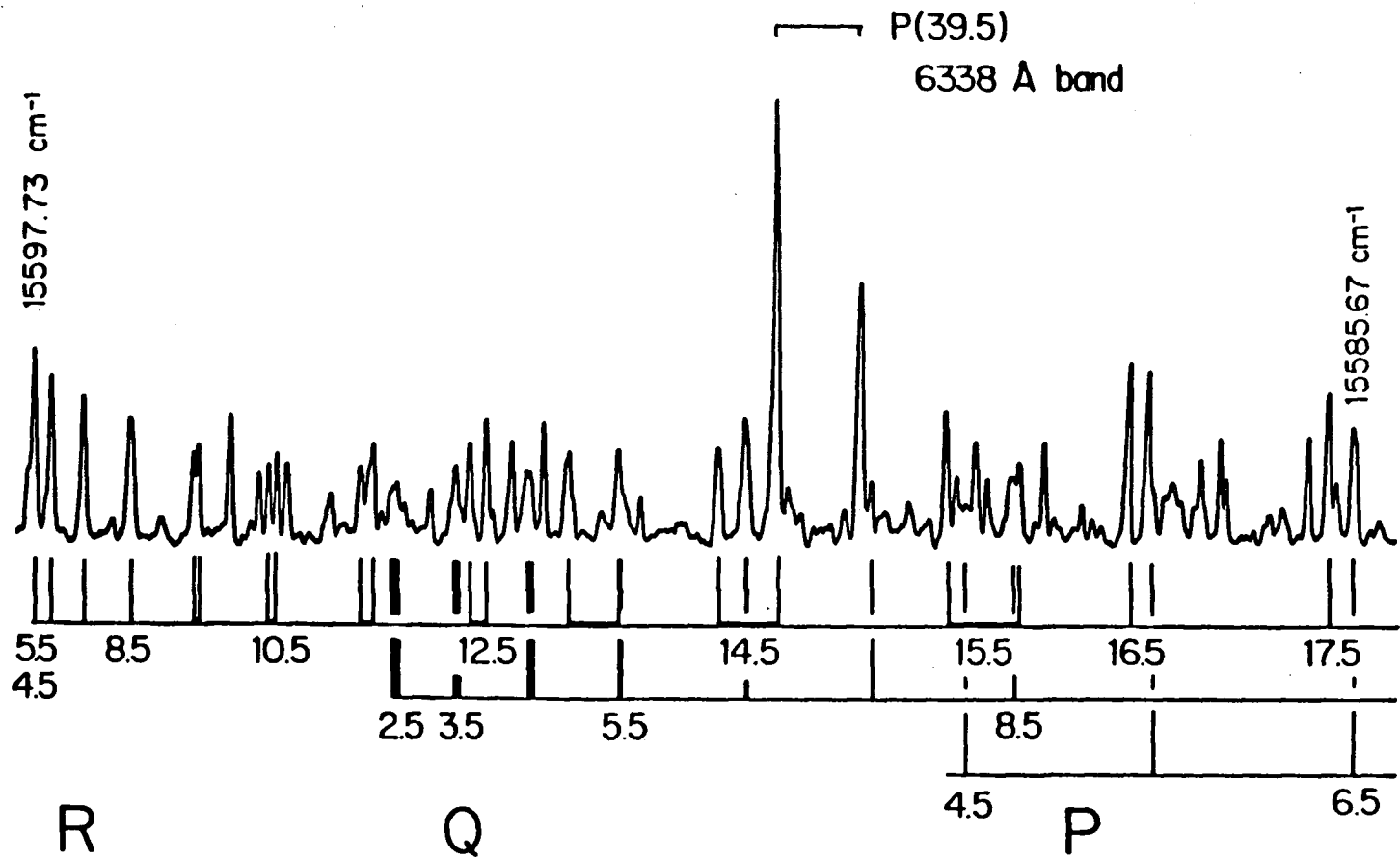


Fig. 3.7. Bandhead of the $\Omega' = \Omega'' = 5/2$ transition at 6411 Å. The band is extensively overlapped by other bands, as evidenced by the dense collection of unassigned lines.

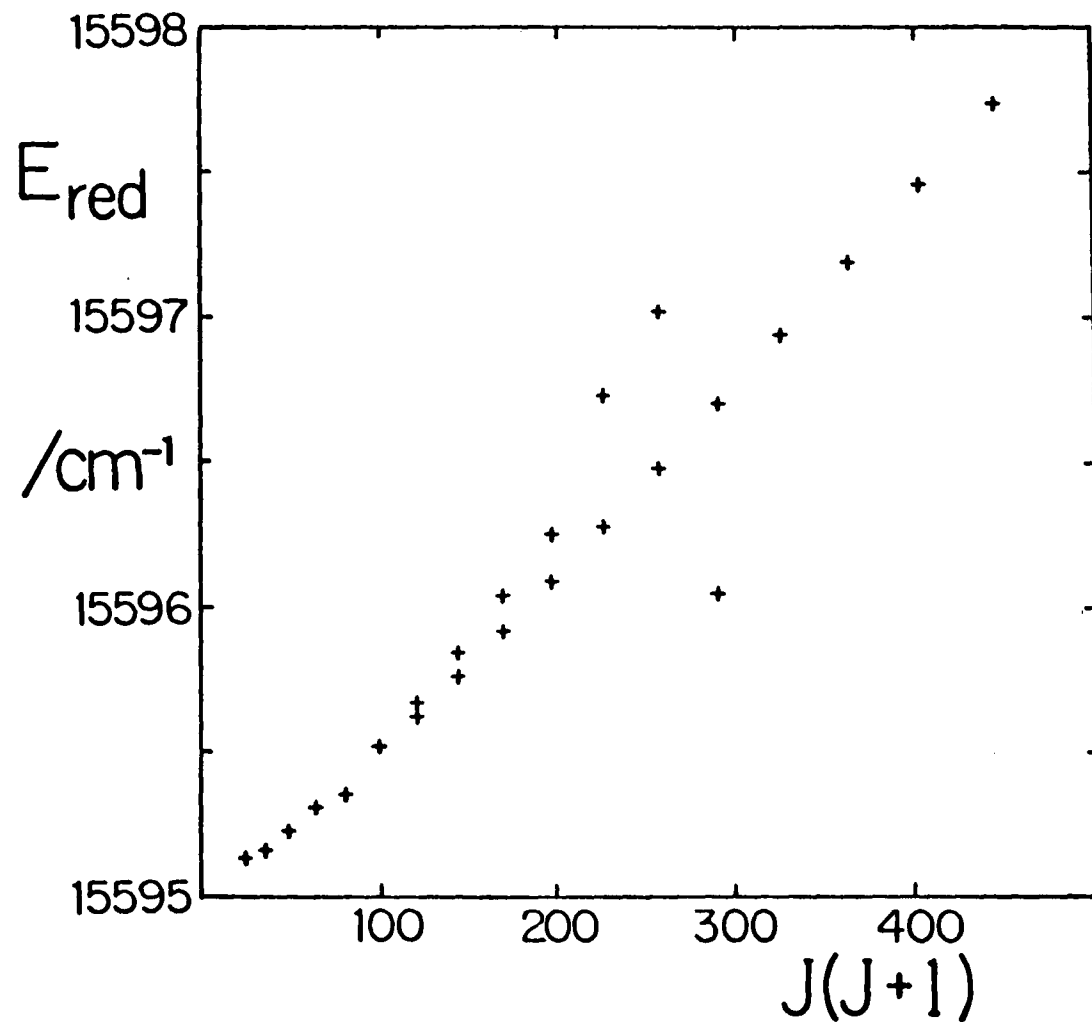


Fig. 3.8. Upper state energy levels of the $4\Delta_{5/2} - 4\Delta_{5/2}$ 6411 Å band, scaled by subtracting the quantity $0.42J(J + 1)$, plotted against $J(J + 1)$.

fluorescence measurements in the surrounding region. Such studies must be postponed until we develop a less cumbersome method by which to synthesize gaseous CoO.

The upper and lower state B and D rotational constants, calculated in the same manner as for the 6338 Å band, are given in Table 3.III. Kratzer's relationship⁸³,

$$D_e = 4B_e^3/\omega_e^2 \quad (3.10)$$

for the equilibrium values of the rotational constants and the vibrational frequency (ω_e) can be approximated for the $v = 0$ level by

$$D_0 = 4B_0^3/\Delta G_{1/2}^2 \quad (3.11)$$

Using equation (3.11) to calculate an approximate value for D'' , it is found to be about 60% larger than the observed value.

III.D. Discussion.

Of the two possible ground electronic state configurations for CoO, $4\Sigma^- (\sigma\pi^2\delta^4)$ or $4\Delta(\sigma^2\pi^2\delta^3)$, evidence has been presented in the rotational analysis of the excitation spectrum of gaseous CoO which strongly supports that the ground state is $4\Delta_i$. The fundamental vibrational frequency of 846.4 cm^{-1} measured by infrared spectroscopy in low-temperature (14 K) matrix isolation⁷¹ closely matches the value of 851.7 cm^{-1} obtained from this laser induced fluorescence work. Since the ground electronic state should be the only one populated at 14 K, and a 5.3 cm^{-1} shift from the solid to gas phase is not unreasonable, this suggests that the lower electronic state of the three bands studied here is the ground state. The matrix isolation electron spin resonance study⁷² which could not produce a signal from CoO eliminates the possibility for $4\Sigma^-$ as the ground state, taking this absence of a result as valid. The only condition under which an orbitally non-degenerate electronic state with case (a) coupling can produce no ESR signal when isolated in a low-temperature matrix is if it possesses an odd spin multiplicity with the $\Omega = 0$ level the only one populated. The band intensities support an inverted order for the spin-orbit manifold since the $\Omega' = \Omega'' = 7/2$ bands are strongest, followed by $\Omega' = \Omega'' = 5/2$.

The rotational analysis of two Ω spin-orbit components of the same electronic state provides the information required to determine the true B value and an estimate for the spin-orbit interval, $A\Lambda$. For molecules in which spin uncoupling is small because the spin-orbit interaction is very large, the effective B value for a given spin-orbit component differs from the true B value

by an amount that depends on the spin-uncoupling operator, $-2B\hat{J}\cdot\hat{S}$. A second order perturbation treatment of two Ω substates separated by $A\Lambda$ and connected by this operator produces the relation:²⁴

$$B_{\text{eff},\Omega} = B(1 + 2B\Sigma/A\Lambda) \quad (3.12)$$

Solving equation (3.12) simultaneously for both $A\Lambda$ and the true B value for the $v'' = 0$ level, using the effective $B_{\Omega=7/2}$ and $B_{\Omega=5/2}$ values in Table 3.III, gives

$$B = 0.5037 ; \quad A\Lambda \approx -244 \text{ cm}^{-1} \quad (3.13)$$

The spin-orbit coupling interval $A\Lambda$ is not expected to be accurate to better than 10%, as equation (3.12) does not take into account the centrifugal distortion corrections to A and λ , called A_D and λ_D (cf. Section I.B.3). For example, the initial estimate of $|A\Lambda|$ made for FeO^{75} was 180 cm^{-1} , based on the approximation in equation (3.12), yet the value was later found⁸⁷ to be 190 cm^{-1} . The definition of B , as a function of the mean value of the bond length r during the vibration, is⁸³

$$B = (h/8\pi^2c\mu)\langle r^{-2} \rangle \quad (3.14)$$

where μ is the reduced mass of the molecule. With the B value in equation (3.13), the bond length in the zero point vibrational level is calculated from equation (3.14) to be:

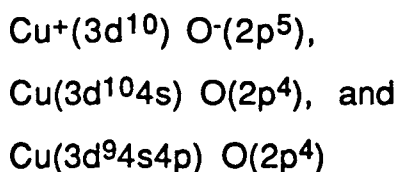
$$r_0(X^4\Delta_i) = 1.631 (\pm 0.001) \text{ \AA} \quad (3.15)$$

The 10% increase in bond length to 1.80 \AA upon electronic excitation to the upper $^4\Delta_i$ state is quite large compared to transitions in the other first row diatomic transition metal oxides. The $A^4\Pi \leftarrow X^4\Sigma^-$ transition of VO produces a 7% increase⁴⁵; $A^5\Sigma \leftarrow X^5\Pi_r$ and $B^5\Pi_r \leftarrow X^5\Pi_r$ in CrO give 2-1/2 and 5-1/2% increases⁹⁰; the $^6\Sigma^+ \leftarrow ^6\Sigma^+$ parallel transition of MnO at 6500 \AA shows a 4% increase⁹¹; but

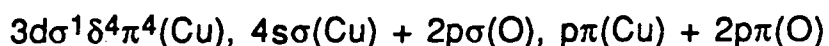
various subbands of the orange system of FeO do show bond length increases of up to as much as 11%⁸⁷, and a state perturbing the MnO $A^6\Sigma^+$ state has a bond 10% longer than that of the ground state⁹¹.

The magnetic hyperfine structure and spin-orbit coupling constant can be used to give information about the excited states as well as the ground state. The insignificant hyperfine structure in the ground state is consistent with the lack of unpaired s electron density in the $4\Delta \sigma^2\pi^2\delta^3$ configuration. The upper state configuration can be assigned as $\sigma\pi^2\delta^3\sigma^*$ for three reasons:

1) the large, positive hyperfine splittings in the upper state indicate a strong Fermi contact interaction due to open shell s electrons (cf. Section I.B.3). When an unpaired s electron is present in a diatomic transition metal oxide it usually shows up clearly in the Fermi contact parameter. Most states with unpaired s electrons have positive values for a_F : a_F for $\text{ScO}^{73} \sigma^2\Sigma^+ = +0.0667 \text{ cm}^{-1}$; a_F for $\text{VO}^{45} \sigma\delta^2 4\Sigma^- = +0.02593 \text{ cm}^{-1}$; a_F for $\text{MnO}^{90} \sigma\delta^2\pi^2 6\Sigma^+ = +0.0151 \text{ cm}^{-1}$. An exception is the ground state of CuO, which has a large, negative Fermi contact parameter in spite of the presence of open shell s σ electrons.⁷⁹ Three configurations are believed to make significant contributions to the $^2\Pi_i$ ground state:



Only the last one has open shell metal-centered orbitals which will participate significantly in the hyperfine interactions. In terms of molecular orbitals, this configuration is proposed to be:⁷⁹



The wavefunction can therefore be expressed as a linear combination of Slater determinants (showing only the unpaired electrons for clarity):

$$\begin{aligned} \psi(^2\Pi_i) = (1/\sqrt{6})\{ & 2|d\sigma(\alpha) p\sigma(\alpha) p\pi(\beta)| - |d\sigma(\alpha) p\sigma(\beta) p\pi(\alpha)| \\ & - |d\sigma(\beta) p\sigma(\alpha) p\pi(\alpha)|\} \end{aligned} \quad (3.16)$$

The authors propose that the negative terms in the wavefunction are responsible for the negative value for a_F of -0.0139 cm^{-1} . The $C^4\Sigma^-$ state of VO, with a $3d\delta^2\sigma^*$ configuration, is an example where the promotion of an electron from $s\sigma$ to a non-s type σ orbital produces a negative value for the I-S interaction constant of -0.00881 cm^{-1} , as a result of spin polarization.⁴⁵ The σ^* orbital is believed to be a linear combination of $3d\sigma$, $4s\sigma$ and $O(2p\sigma)$.

2) the fact that the $\Omega = 7/2$ and $\Omega = 5/2$ subbands lie very close in the spectrum shows that the spin-orbit intervals $A\Lambda''$ and $A\Lambda'$ are nearly equal. The $^4\Delta$ states of the configurations $\sigma^2\pi^2\delta^3$ and $\sigma\pi^2\delta^3\sigma^*$ will have orbital angular momentum coming only from the 'δ' hole, so that they should have roughly the same spin-orbit couplings.

3) Following from 2), the negative sign of A also suggests a δ hole, or δ^3 configuration.

The $\sigma\pi^2\delta^3\sigma^*$ configuration can give rise to 19 electronic states from the different arrangements of the electrons within the orbitals.⁷⁴ The result will be a dense collection of states ranging up to $S = 5/2$ and $\Lambda = 4$, among which are, for example, a $^4\Gamma$ state with the configuration $\sigma(\uparrow)\pi(\uparrow\downarrow)\delta(\uparrow\downarrow\uparrow)\sigma^*(\uparrow)$, and a $\sigma(\uparrow)\pi(\uparrow\uparrow)\delta(\uparrow\downarrow\uparrow)\sigma^*(\uparrow)$ $^6\Delta$ state. As the states comprising such a melange are expected to interact strongly with one another, this

could explain the extensive perturbations experienced by the upper states of CoO investigated here. As discussed in Section III.C.1.c, the only perturbing state for which we have clear evidence appears to be a 4Σ state, arising possibly from a $\sigma\pi^2\delta^3\sigma^*$ configuration, or $2\Sigma \times 1\Delta \times 2\Delta \times 2\Sigma = 4\Sigma$.

Now that the ground state configuration of CoO has been determined in this work, the entire series of first row diatomic transition metal oxide ground states is now established. The ground states and some major molecular constants of the 3d transition metal monoxides appear in Table 3.V. Although many more excited states of cobalt oxide remain to be discovered, the most interesting results for the immediate future would be the direct measurements of the spin-orbit coupling intervals, and sub-Doppler measurements of the hyperfine structure. However, the experiments would require a more efficient means of generating CoO than has been used so far.

Table 3.VI. Ground states and configurations of the first row diatomic transition metal oxides, with the fundamental vibrational frequency $\Delta G_{1/2}$, B and r for the $v'' = 0$ state, and the spin-orbit interval $A\Lambda$ for the orbitally degenerate electronic states. The $A\Lambda$ value for CoO has not been established with certainty.

Ground state	Electron configuration	$\Delta G_{1/2}$ (cm^{-1})	B_0 (cm^{-1})	r_0 (\AA)	$A\Lambda$	Ref
ScO $^2\Sigma^+$	σ	964.65	0.51343	1.668	-	29,30
TiO $^3\Delta_r$	$\sigma\delta$	1000.02	0.53384	1.623	101.30	89
VO $^4\Sigma^-$	$\sigma\delta^2$	1001.81	0.54638	1.592	-	45,88
CrO $^5\Pi_r$	$\sigma\delta^2\pi$	884.98	0.52443	1.621	63.22	90
MnO $^6\Sigma^+$	$\sigma\delta^2\pi^2$	832.41	0.50122	1.648	-	91
FeO $^5\Delta_i$	$\sigma\delta^3\pi^2$	871.15	0.51681	1.619	-189.89	87
CoO $^4\Delta_i$	$\sigma^2\delta^3\pi^2$	851.7	0.5037 ₀	1.631	(-240)	this work
NiO $^3\Sigma^-$	$\sigma^2\delta^4\pi^2$	825.4	0.505 ₈	1.631	-	78
CuO $^2\Pi_i$	$\sigma^2\delta^4\pi^3$	629.39	0.44208	1.729	-277.04	92,93

CHAPTER IV

HYPERFINE ANALYSIS OF NIOBIUM NITRIDE

IV.A. Introduction.

Niobium nitride (NbN) is an exemplary molecule in which to study hyperfine interactions in diatomic molecules, because the nuclear magnetic moment (μ_N) of ^{93}Nb exceeds that of any other non-radioactive atom. The magnetic hyperfine structure which results is proportionately large and well-resolved, allowing precise, informative analysis. Following the initial observation of NbN in 1969 by Dunn and Rao⁹⁴, the first low resolution hyperfine analysis of the $^3\Phi$ - $^3\Delta$ system was performed in 1975 by Féménias *et al*⁹⁵ with a grating spectrograph. The study produced values for the magnetic hyperfine constants a , b and c which suggested that the excited $^3\Phi$ state makes a non-negligible contribution to the hyperfine structure. The spectra also exhibited line broadening at very high J values, indicating either Λ -doubling in the $^3\Delta$ state or a transition from case (a_β) to ($b_{\beta J}$) coupling with increasing rotation. In the meantime, the fundamental frequencies of the ground states of Nb^{14}N and Nb^{15}N were measured to be 1002.5 cm^{-1} and 974 cm^{-1} by IR spectroscopy in a 14 K argon matrix.⁹⁶ A Russian group published a number of papers on the $^3\Phi$ - $^3\Delta$ system^{97,98,99}, culminating in the 1986 publication by Pazyuk *et al*¹⁰⁰, in which they proposed a set of rotational, centrifugal distortion and spin-orbit coupling constants (B , D and A), and an energy level scheme for the system. However, the spin-orbit splittings for both states were drastically miscalculated, and the ordering of the spin-orbit

manifolds was inverted, due to their interpretation of bands they observed near 5600 Å as ${}^3\Phi_3 - {}^3\Delta_3$ and ${}^3\Phi_2 - {}^3\Delta_2$ spin-orbit satellites, rather than as parts of the $\Pi - \Delta$ system to which they actually belong. In 1979, an optical emission study measured eight subbands belonging to five systems, including ${}^3\Phi - {}^3\Delta$, and determined the upper and lower state B values for each.¹⁰¹ Most recent was a grating spectrograph analysis of the ${}^3\Phi - {}^3\Delta$ system performed by the same investigators involved in the preliminary 1975 study, but at a higher resolution ($\pm 0.01 \text{ cm}^{-1}$ line position), and up to $J'' = 88$.¹⁰² Their work produced the following set of molecular constants for the (0,0) band, in units of cm^{-1} with the uncertainty in the last digit given in parentheses:

	T_0	A	δ	B	$10^7 D$	$10^5 A_D$
$X^3\Delta$	fixed to 0	183.0(2)	-33.1(2)	0.50144(4)	4.56(6)	≈ -4
$A^3\Phi$	16504.938(3)	241.6(1)	7.39(2)	0.49578(4)	4.88(6)	≈ -4

The central shift parameter δ accounts for the shift in the ${}^3\Phi_3 - {}^3\Delta_3$ subband because of second order spin-orbit effects. The investigations described in the current work mark the first high resolution laser spectroscopy performed on NbN.

IV.B. Experimental.

IV.B.1. Synthesis of gaseous niobium nitride.

Niobium nitride was formed in a flow system by reacting the vapor from a sample of warmed niobium (V) chloride ($\approx 80^\circ\text{C}$) with nitrogen. The nitrogen was entrained with argon in a ratio of approximately 1:18 (v/v) at 1 Torr pressure. A few centimeters upstream from the fluorescence cell, the vapor was passed through a 2450 MHz microwave discharge (powered by a Microtron model 200 microwave generator). To obtain intermodulated fluorescence spectra, two nearly coincident laser beams were passed in opposite directions across the lavender-colored flame of the discharge, with the fluorescence detected at right angles to the beams through a deep red low pass filter to the photomultiplier tube, as described in Section II.A.

IV.B.2. Description of the $^3\Phi\text{-}^3\Delta$ spectrum.

Broadband spectra of the three subbands of the $^3\Phi\text{-}^3\Delta$ system of NbN are illustrated in Fig. 4.1. The middle spin-orbit component, $^3\Phi_3\text{-}^3\Delta_2$, is shifted to higher energy rather than being equidistant between the outer subbands, and is also considerably weaker, presumably due to intensity stealing by an unseen state. The vibrational sequences are plainly visible, up to $(v',v'') = (5,5)$ in the $^3\Phi_4\text{-}^3\Delta_3$ subband.

At sub-Doppler resolution, the variation in hyperfine structure between the three subbands is apparent from the Q head regions shown in Fig. 4.2. The hyperfine interaction in the $^3\Phi_3\text{-}^3\Delta_2$ subband is much less pronounced than that in the other two because

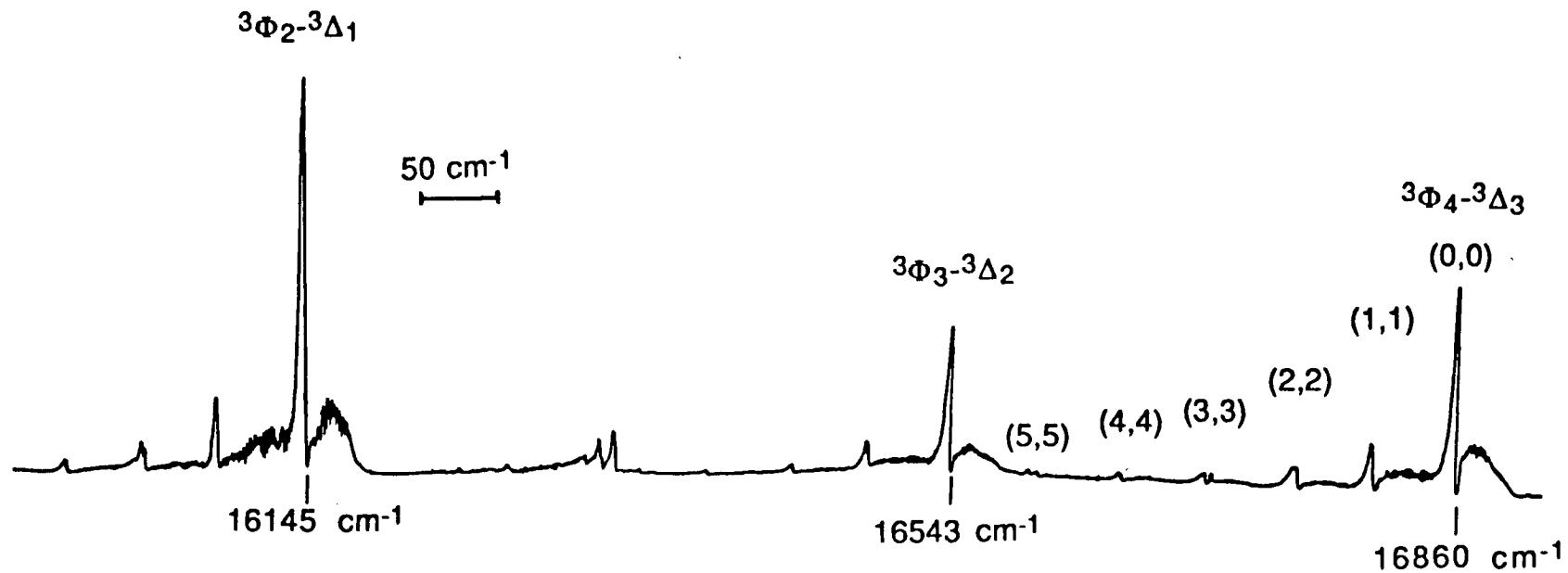


Fig. 4.1. Broadband spectrum of the ${}^3\Phi-{}^3\Delta$ system of NbN, obtained with the intracavity assembly removed, using the dye rhodamine 6G. Note that the vibrational sequence of the ${}^3\Phi_4-{}^3\Delta_3$ subband is visible up to $(v',v'') = (5,5)$.

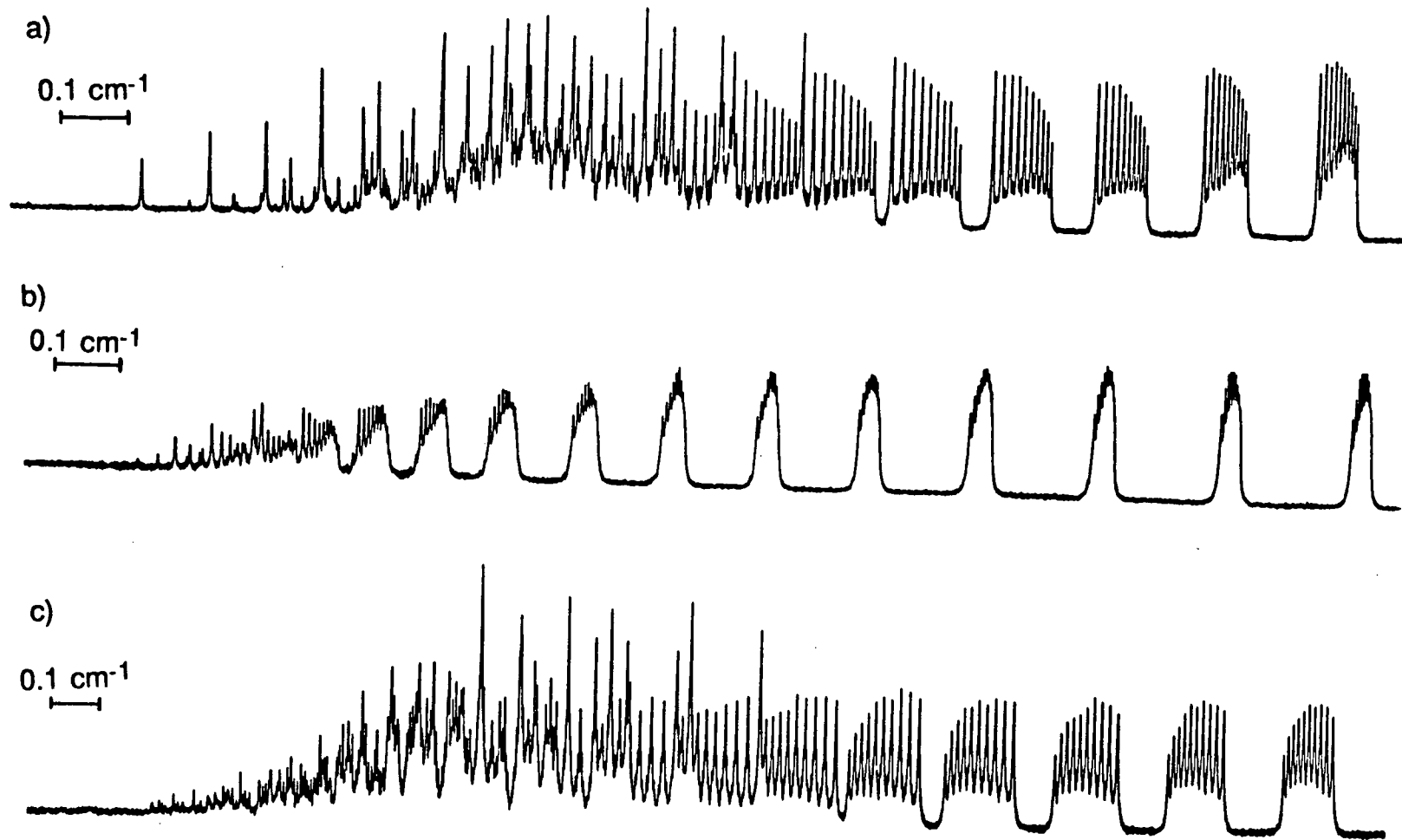


Fig. 4.2. The Q heads of the a) ${}^3\Phi_2$ - ${}^3\Delta_1$, b) ${}^3\Phi_3$ - ${}^3\Delta_2$, and c) ${}^3\Phi_4$ - ${}^3\Delta_3$ subbands of NbN.

the value of Σ in both states is zero. In the ${}^3\Phi_4$ - ${}^3\Delta_3$ subband the hyperfine splitting is considerably larger than that in ${}^3\Phi_2$ - ${}^3\Delta_1$, since Ω is three times as large in the former subband (cf. equations 1.90 and 1.98). The assignment of the densely overlapped ${}^3\Phi_2$ - ${}^3\Delta_1$ Q head is shown in Figs. 4.3 and Fig. 4.4. The low-J R branches of the ${}^3\Phi_2$ - ${}^3\Delta_1$ subband, illustrated in Fig. 4.5, are exemplary for their completely resolved $\Delta F \neq \Delta J$ transitions and crossover resonances (cf. Section II.B for a discussion of these transitions). The hyperfine pattern is quite different in the central subband: at $J'' = 2$ the high F component is on the low frequency side, but at $J'' = 3$ the hyperfine structure reverses order and continues on at higher J values with the highest F component at high frequency. The development of this ${}^3\Phi_3$ - ${}^3\Delta_2$ R branch hyperfine structure is shown in Fig. 4.6.

As the rotation of the molecule increases, spin-uncoupling is observed in the Q branches of the outer two subbands as a reversal in the hyperfine structure: the hyperfine splitting narrows with increasing J until the components collapse into a spike; then they reverse their order and widen with increasing rotation (see Fig. 4.7). Therefore hyperfine structure which begins with its components increasing in F toward increasing frequency reverse to an order in which the F values decrease with frequency. The reversal in the Q branches occurs at $J = 27$ and $J = 38$ in the ${}^3\Phi_2$ - ${}^3\Delta_1$ and ${}^3\Phi_4$ - ${}^3\Delta_3$ subbands, respectively. The hyperfine structure in the ${}^3\Phi_3$ - ${}^3\Delta_2$ transition is less sensitive to the effects of rotation, since its diagonal matrix elements are independent of b and c. The Q branch of

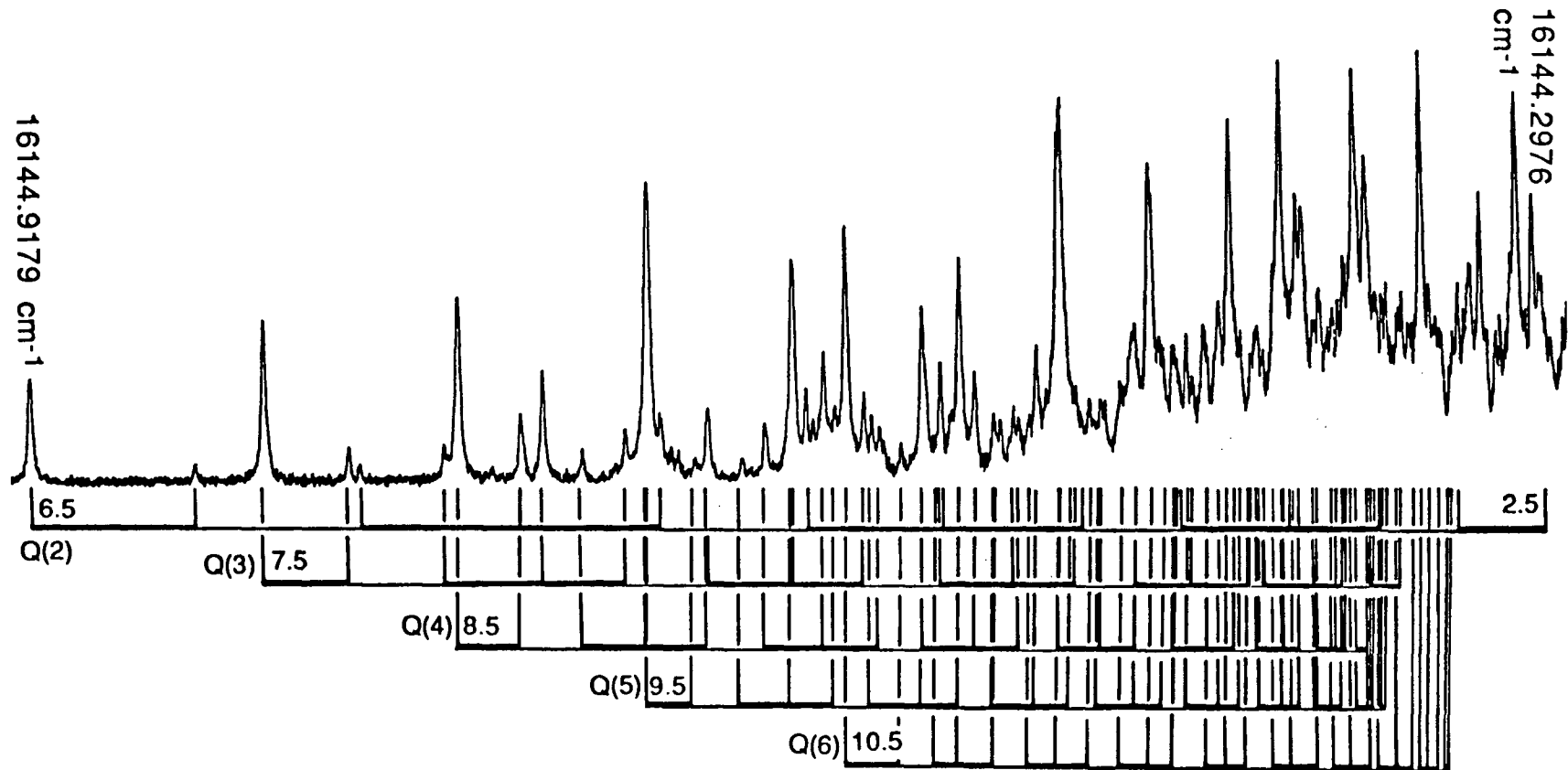


Fig. 4.3. The beginning of the Q head of the ${}^3\Phi_2$ - ${}^3\Delta_1$ subband. Each $\Delta F = 0$ line is connected to the $\Delta F = \pm 1$ lines with the same F'' value by a thick horizontal line. Components of the Q(7) and Q(8) lines are also present in this region, but are not labelled.

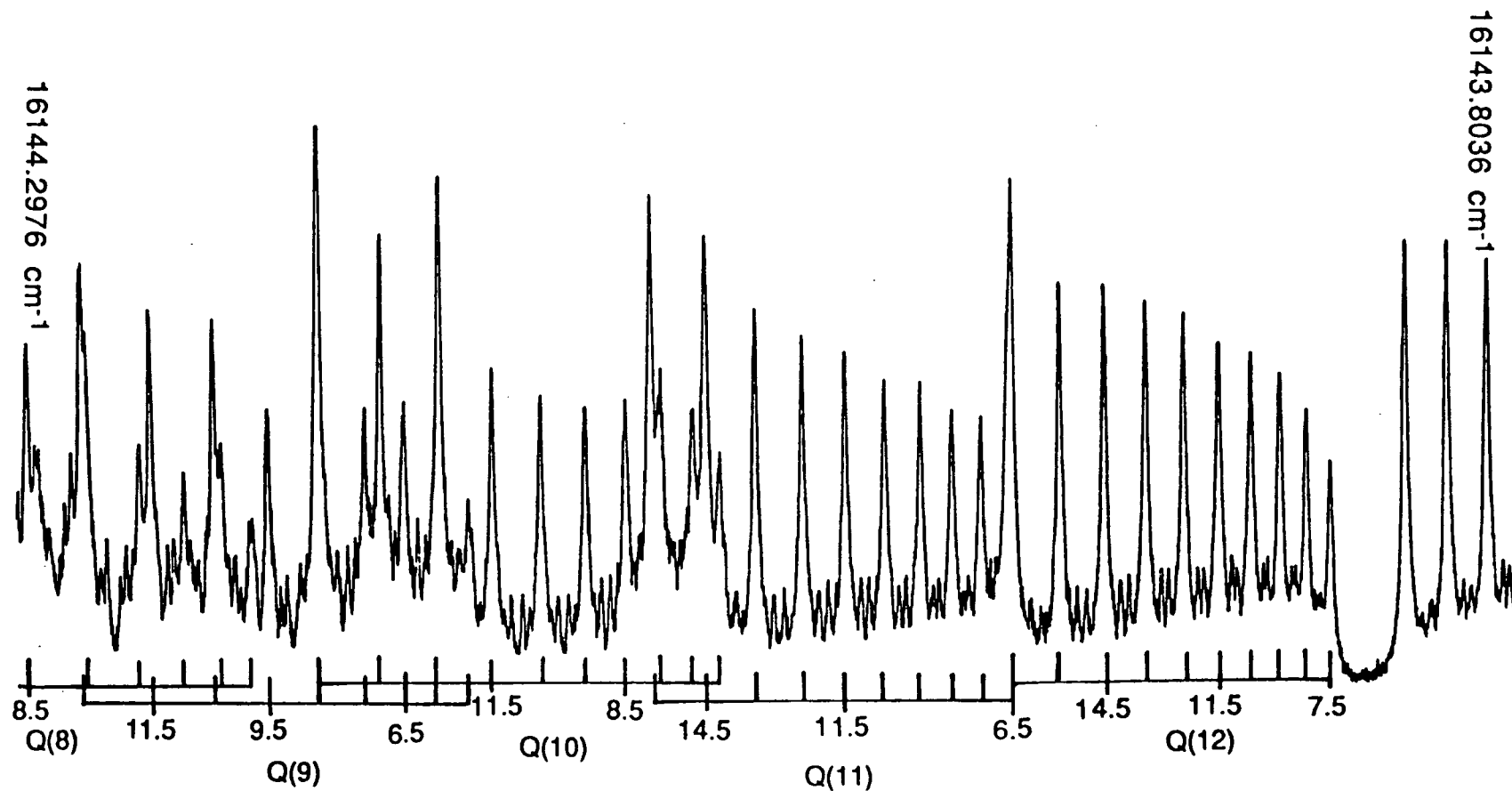


Fig. 4.4. The higher J portion of the ${}^3\Phi_2$ - ${}^3\Delta_1$ Q head, and the first resolved Q lines. The crossover resonances are not labelled.

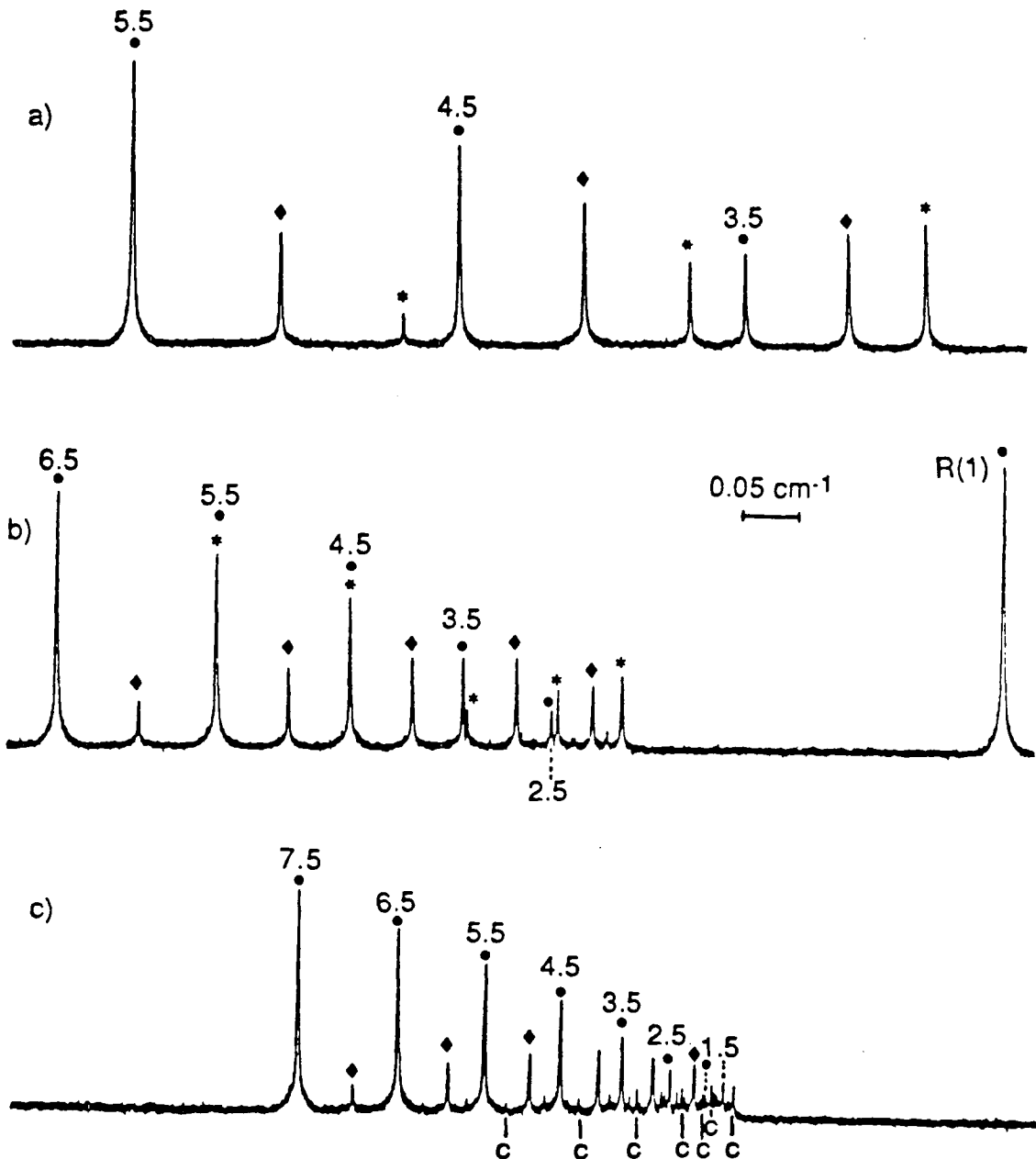


Fig. 4.5. a) R1, b) R2, and c) R3 lines of the ${}^3\Phi_2$ - ${}^3\Delta_1$ subband, illustrating the "forbidden" $\Delta F \neq \Delta J$ transitions (◆ for qR, * for pR) and the crossover resonances (c) between the rR and qR lines. Each $\Delta F = \Delta J$ transition (●) is labelled with the lower state F value, with the corresponding satellite transitions following it to the red (right) in the order: c (if seen), ◆, * (if seen). The scale shown in (b) is the same for all spectra.

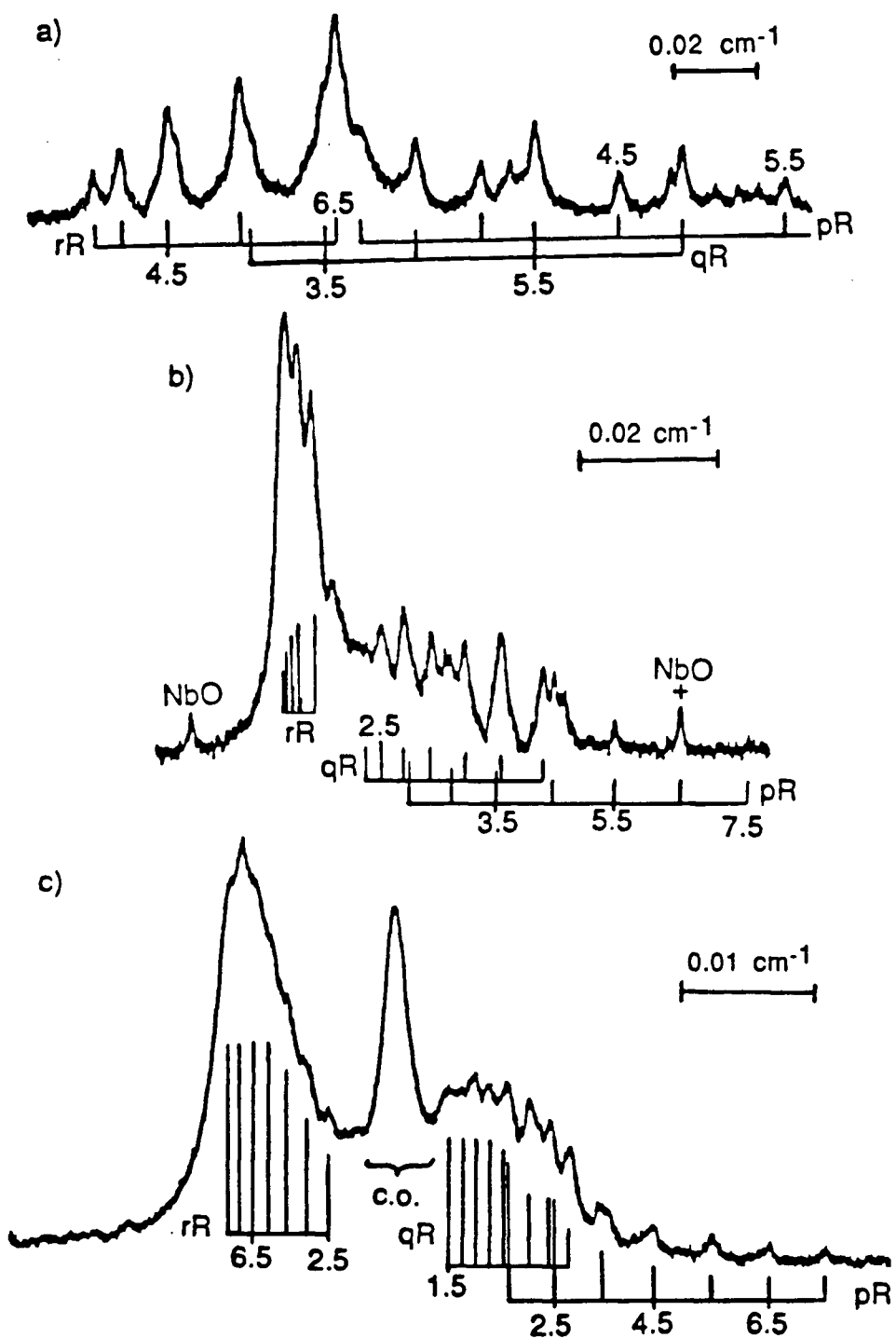


Fig. 4.6. a) R2, b) R3 and c) R4 lines of the ${}^3\Phi_3-{}^3\Delta_2$ subband of NbN, showing the rR, qR and pR transitions and the crossover resonances associated with the rR and qR lines (denoted by c.o.).

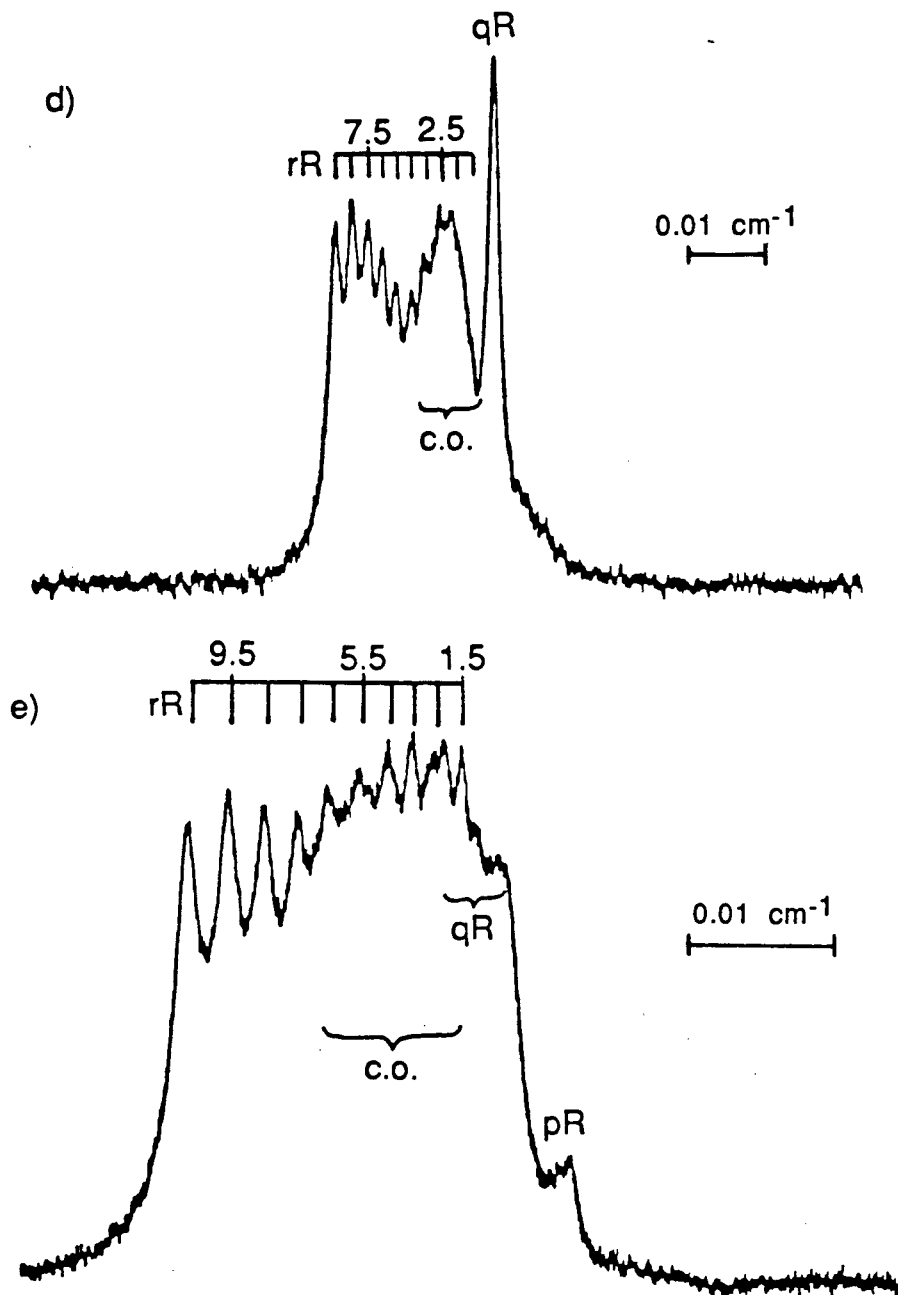


Fig. 4.6. d) R5 and e) R6 lines of the ${}^3\Phi_3$ - ${}^3\Delta_2$ subband of NbN; the labelling follows that of Fig. 4.6 a, b and c.

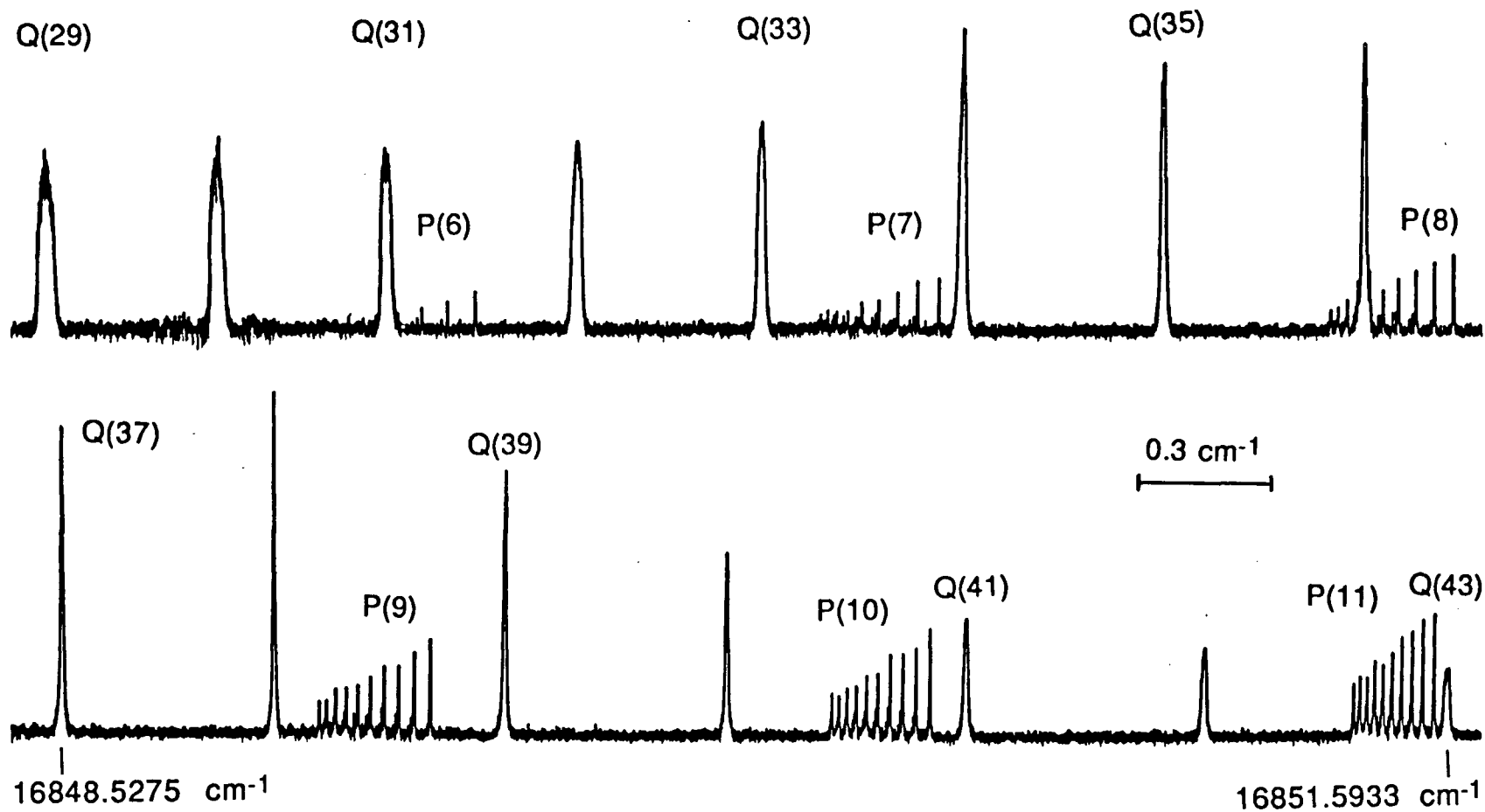


Fig. 4.7. The reversal of hyperfine structure at high J in the ${}^3\Phi_4-{}^3\Delta_3$ Q branch, caused by the effects of spin-uncoupling. Actual reversal occurs in the line of maximum intensity, Q(38).

this subband therefore narrows up to about $J = 12$, and then remains nearly constant in width up to the limit of our data at $J = 27$.

IV. C. Non-Linear Least Squares Fitting of Spectroscopic Data.

In order to acquire the best set of molecular constants in a Hamiltonian, one must iteratively improve an estimated set of constants until a satisfactory fit of the observed data is obtained. In approaching the non-linear type of Hamiltonian typically describing a spectroscopic problem, the Hamiltonian is divided into its two constituents: the coefficients containing the quantum number dependence, and the molecular constants, or¹⁰³

$$\hat{H} = \sum_{m=1}^p X_m H_m \quad (4.1)$$

X_m is the m th parameter (or molecular constant) out of a total of p parameters, and H_m is the "skeleton matrix" containing the quantum number dependence of the m th parameter. For example, a simple ${}^2\Pi$ Hamiltonian may be expressed as:¹⁰³

$$\hat{H} = T_0 \cdot \begin{bmatrix} 1 & 0 \\ 0 & 1 \end{bmatrix} + A \cdot \begin{bmatrix} 1/2 & 0 \\ 0 & -1/2 \end{bmatrix} + B \cdot \begin{bmatrix} (J + 1/2)^2 - 2 & -[(J + 1/2)^2 - 1]^{1/2} \\ -[(J + 1/2)^2 - 1]^{1/2} & (J + 1/2)^2 \end{bmatrix}$$

The matrix of eigenvalues (or energy levels) \mathbf{E} of the Hamiltonian is obtained by diagonalization with the eigenvectors \mathbf{U} :

$$\mathbf{U}^\dagger \hat{H} \mathbf{U} = \mathbf{E} \quad (4.2)$$

\mathbf{U} is a unitary matrix such that the adjoint of \mathbf{U} (\mathbf{U}^\dagger , or the conjugate of the transpose \mathbf{U}^T) equals the inverse of \mathbf{U} (\mathbf{U}^{-1}).

The combination of equations (4.1) and (4.2) allows the Hellmann-Feynman theorem to be employed, which states:¹⁰⁴

$$\partial E_m / \partial X = \int \Psi_m^* (\partial H / \partial X) \Psi_m d\tau \quad (4.3)$$

For a single matrix element ii of parameter m , the Hellmann-Feynman theorem becomes:¹⁰³

$$[\mathbf{U}^T(\partial\hat{H}/\partial X_m)\mathbf{U}]_{ii} = \partial E_i/\partial X_m = B_i \quad (4.4)$$

Using equation (4.1), equation (4.4) can also be written as:

$$B_{im} = [\mathbf{U}^T\hat{H}_m\mathbf{U}]_{ii} \quad (4.5)$$

The Hellmann-Feynman derivatives B_{im} form the derivatives matrix, \mathbf{B} , which give the dependence of the energy on variations in the parameters.

To apply this relation to an iterative solution of unknown molecular parameters, equation (4.2) is expressed in terms of a single energy level, E_i^{calc} :

$$E_i^{\text{calc}} = (\mathbf{U}^T\hat{H}\mathbf{U})_{ii} \quad (4.6)$$

Substituting equation (4.1) into equation (4.6) gives

$$E_i^{\text{calc}} = \sum_{m=1}^p X_m (\mathbf{U}^T\hat{H}_m\mathbf{U})_{ii} \quad (4.7)$$

With the relations in equations (4.4) and (4.5), the energy can be written:

$$E_i^{\text{calc}} = \sum_{m=1}^p X_m B_{im} \quad (4.8)$$

To express equation (4.8) in terms of transitions rather than energy levels, the upper and lower state eigenvalue vectors (\mathbf{E}' and \mathbf{E}'') are subtracted to give \mathbf{y} , and \mathbf{B}' and $-\mathbf{B}''$ are combined into one derivatives matrix \mathbf{B} . Equation (4.8) therefore transforms to:¹⁰⁵

$$\mathbf{y} = \mathbf{B}\mathbf{X} \quad (4.9)$$

where \mathbf{y} is the vector of calculated transitions, \mathbf{B} is the matrix of known derivatives, and \mathbf{X} is the vector of estimated parameters. If

there are N transitions and p parameters to be determined, \mathbf{y} has length N , \mathbf{B} is a matrix of size N by p , and \mathbf{X} has length p . To obtain \mathbf{X} , both sides of equation (4.9) are multiplied by $(\mathbf{B}^T\mathbf{B})^{-1}\mathbf{B}^T$:

$$\begin{aligned}(\mathbf{B}^T\mathbf{B})^{-1}(\mathbf{B}^T\mathbf{B})\mathbf{X} &= (\mathbf{B}^T\mathbf{B})^{-1}\mathbf{B}^T\mathbf{y} \\ \mathbf{X} &= (\mathbf{B}^T\mathbf{B})^{-1}\mathbf{B}^T\mathbf{y}\end{aligned}\quad (4.10)$$

In a problem where the estimated parameters \mathbf{X} are iteratively improved, we calculate parameter changes $\Delta\mathbf{X}$, rather than \mathbf{X} itself. Equation (4.10) is therefore expressed as:¹⁰⁶

$$\Delta\mathbf{X} = (\mathbf{B}^T\mathbf{B})^{-1}\mathbf{B}^T\Delta\mathbf{y}\quad (4.11)$$

where $\Delta\mathbf{y}$ is the vector of residuals (i.e., the observed transitions minus the calculated). The fitting process begins with a set of estimates for the molecular constants, which are used to generate calculated transitions (y^{calc}) and their residuals ($\Delta\mathbf{y}$). The set of corrections to the constants, given by equation (4.11), is added to the initial estimates to provide improved constants for the next iteration. The process is repeated, iteratively producing improved sets of calculated transitions, residuals and constants until the magnitude of the residuals is reduced to a satisfactory level, for example, to the vicinity of the experimental precision.

The least squares program for the ${}^3\Phi - {}^3\Delta$ system of NbN was written in FORTRAN 77 by the author, except for UBC Amdahl library routines for diagonalizing and inverting matrices, and calculating parameter changes from the Hellman-Feynman derivatives. The Hamiltonian matrices for the ${}^3\Phi$ and ${}^3\Delta$ states have a maximum dimension of $(2I + 1)(2S + 1)$, or 30. The 30×30 matrices (one for each F) were diagonalized in two steps. In the first step, only the rotational part of the Hamiltonian was diagonalized, in ten separate

J submatrices. In the second step, the entire matrix (rotational and hyperfine) was diagonalized. Two steps were employed because the ordering of eigenvalues from step one was used in the second diagonalization to preserve the matching of eigenvalues with the original basis functions. This is possible because the separation of the spin-orbit components is large compared to the perturbation made by the hyperfine interactions.

Analogous to the common formula for the standard deviation,

$$s = [\sum(x^{\text{obs}} - x^{\text{calc}})^2/n]^{1/2} \quad (4.12)$$

the weighted least squares standard deviation is obtained from:¹⁰⁵

$$\sigma = \left[\sum_{i=1}^n (y_i^{\text{obs}} - y_i^{\text{calc}})^2 W_{ii} / (n-m) \right]^{1/2} \quad (4.13)$$

where n is the number of independent measurements, m the number of unknowns to be estimated, $n-m$ the degrees of freedom, and W_{ii} the diagonal element of the weight matrix for point i .¹⁰⁵ To determine estimates of the precision of the estimated constants, a variance-covariance matrix Θ is calculated by:¹⁰⁵

$$\Theta = \sigma^2(\mathbf{B}^T\mathbf{B})^{-1} \quad (4.14)$$

A diagonal element Θ_{ii} is called the variance (not to be confused with the variance that is the square of the standard deviation, σ^2). The square root of Θ_{ii} gives the standard error, or precision, of estimated molecular constant i . The off-diagonal elements Θ_{ij} are covariances. Both the variances and covariances are only estimated values, because they depend on the precision of the measurements, σ^2 . The goodness of the structure of the model lies in $(\mathbf{B}^T\mathbf{B})^{-1}$.

Normalization of the variance-covariance matrix gives the correlation matrix, \mathbf{C} , with elements

$$c_{ij} = \Theta_{ij}/(\Theta_{ii}\Theta_{jj})^{1/2} \quad (4.15)$$

where $c_{ij} = 1$ for $i = j$, and $(-1 < c_{ij} < +1)$ for $i \neq j$. \mathbf{C} is independent of the precision of the measurements since σ^2 has been cancelled out. Therefore the off-diagonal elements represent the interdependence of the molecular constants on one another, for a given data set. A value for c_{ij} that closely approaches unity indicates that constants i and j cannot be determined independently.

IV.D. Results and Discussion.

Initial line assignments were facilitated by the unpublished grating spectrograph work of Dunn *et al*¹⁰², who listed the positions of the P, Q and R rotational lines. Initial attempts to obtain a least squares fit to the hyperfine constants in a case (a) basis (i.e., as they were presented in Sections I.D.3 and I.D.4) did not succeed, because the hyperfine constants required to fit the three subbands are not consistent with one another. In the light of this observation, and the unequal first order spin-orbit spacings, it was concluded that the various substates are perturbed differently by second order spin-orbit interactions. According to the $\Delta\Omega = 0$ selection rule for this interaction¹⁰⁹, the electronic states perturbing the $^3\Phi$ substate include $^3\Gamma_{3,4}$, $^1\Gamma_4$, $^1\Phi_3$, $^3\Delta_{2,3}$ and $^1\Delta_2$. The $^3\Delta$ substates can interact with $^3\Phi_{2,3}$, $^1\Phi_3$, $^1\Delta_2$, $^3\Pi_{1,2}$ and $^1\Pi_1$. The $^1\Phi$ and $^1\Delta$ states isoconfigurational with $^3\Phi$ and $^3\Delta$ are expected to be the closest of these states to $^3\Phi$ and $^3\Delta$, and therefore the ones most responsible for the perturbations (see Fig. 4.8). The effect would be to shift the central spin-orbit components, $^3\Phi_3$ and $^3\Delta_2$, to lower energy. However, the hyperfine constants suggest that there could also be second order spin-orbit interactions occurring with the other members of the manifolds, though we can say nothing about their relative sizes. The $^3\Phi$ - $^3\Delta$ system of NbN is the first observed instance of a molecule represented by Hund's case (a) which requires modifications to the Hamiltonian because of extensive second order spin-orbit interactions. This phenomenon can be considered a slight tendency toward the case (c) coupling scheme.¹⁰⁹

The molecular constants obtained for the $^3\Phi$ - $^3\Delta$ system of NbN

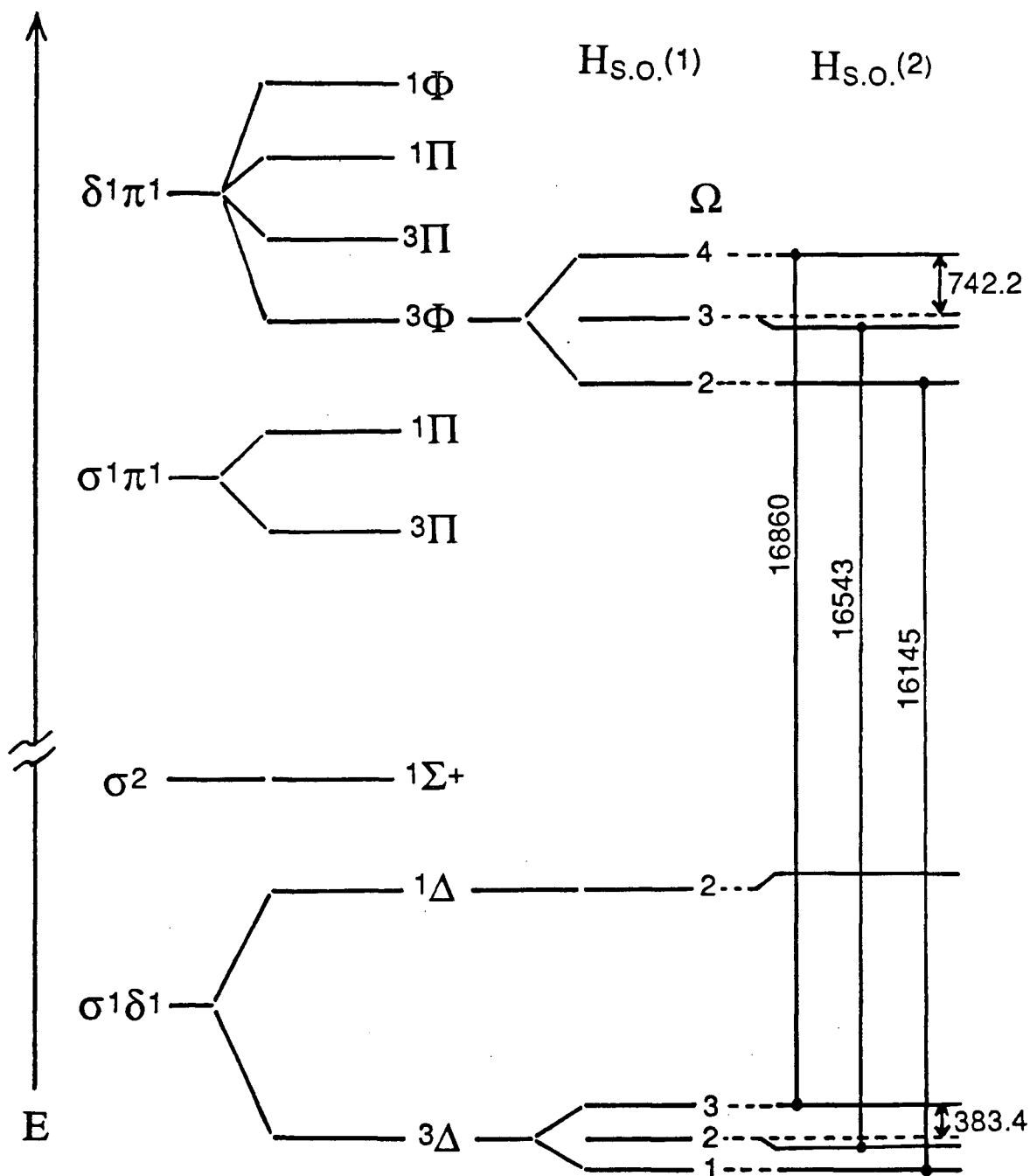


Fig. 4.8. Partial energy level diagram for NbN. The figure is not to scale, but illustrates the relative ordering of states, except in the case of the low-lying configurations σ^2 and $\sigma\delta$ where the ordering is uncertain.

are given in Table 4.1. The unequal perturbations in the ${}^3\Phi$ and ${}^3\Delta$ spin-orbit manifolds means that, in the magnetic hyperfine structure, only the h constants in the matrix elements diagonal in Ω and Σ can be determined, rather than individual a , b and c constants (cf. equations 1.90 and 1.98). The h constants, subscripted by their Σ values, are as follows:

$$h_{-1} = a\Lambda - b - c = a\Lambda - (b + c)_{-1} \quad (4.16)$$

$$h_0 = a\Lambda \quad (4.17)$$

$$h_{+1} = a\Lambda + b + c = a\Lambda + (b + c)_{+1} \quad (4.18)$$

In an unperturbed system, the average of h_{-1} and h_{+1} equals h_0 ; that is, $(b + c)_{-1}$ and $(b + c)_{+1}$ in equations (4.16) and (4.18) are equal. This is far from the case in the ${}^3\Phi$ - ${}^3\Delta$ system of NbN, where $(b + c)_{+1}$ is 39% smaller than $(b + c)_{-1}$ in the ${}^3\Delta$ state, and 10% larger in ${}^3\Phi$. It was also found, in the ${}^3\Delta$ state, that two distinct b constants are required in the $\langle \Sigma = -1 | \Sigma = 0 \rangle$ and $\langle \Sigma = 0 | \Sigma = +1 \rangle$ matrix elements (referred to here as $b_{-1/0}$ and $b_{0/+1}$, respectively). Therefore, a total of five magnetic hyperfine constants are required to fit the data, rather than the usual three: h_{-1} , h_0 , h_{+1} , $b_{-1/0}$ and $b_{0/+1}$ replace a , b and c .

It is clear that the perturbations in the ${}^3\Delta$ state are much more pronounced than those in ${}^3\Phi$. The ${}^3\Delta$ $b_{+1/0}$ value is 34% smaller than $b_{0/-1}$, comparable to the 39% difference between the ${}^3\Delta$ $(b + c)_{-1}$ and $(b + c)_{+1}$ constants. In the upper state, however, two distinct b values off-diagonal in Σ are not necessary: attempts to distinguish two ${}^3\Phi$ b constants produced values that were very highly correlated (-0.998) and with standard errors so high that the constants were indeterminable. It is evident, then, that the ${}^1\Delta$ state lies closer to

Table 4.1. Molecular constants for the ${}^3\Phi\text{-}{}^3\Delta$ system of NbN.^a

	Φ	Δ
T_0	16518.509(1)	0
A	247.4116(5)	191.7038(8)
B	0.495814(4)	0.501465(4)
D	$0.4943(4) \times 10^{-6}$	$0.4622(2) \times 10^{-6}$
λ	-16.817(2)	3.430(2)
γ	0.011(2)	-0.0217(6)
A_D	$-0.58(2) \times 10^{-4}$	$-0.105(3) \times 10^{-3}$
λ_D	$-0.150(6) \times 10^{-4}$	$-0.1314(6) \times 10^{-3}$
h_{-1}	0.0633(2)	-0.0616(3)
h_0	0.0411(4)	0.0458(5)
h_{+1}	0.0168(2)	0.1112(3)
b	-0.02(1)	-
$b_{-1/0}$	-	0.085(5)
$b_{0/+1}$	-	0.056(5)
e^2Qq_0	$-0.39(8) \times 10^{-2}$	fixed to zero
Derived constants:		
$(b+c)_{-1}$	-0.0222(4)	0.1074(6)
$(b+c)_{+1}$	-0.0246(5)	0.0654(6)
σ	0.000547	

^a Values are in cm^{-1} . The numbers in parentheses are three times the standard errors of the constants, in units of the last significant figure. The standard deviation of the transition measurements is given by σ . The magnetic hyperfine constants, h , $(b + c)$ and b , are explained in the text.

the ${}^3\Delta$ state than ${}^1\Phi$ does to ${}^3\Phi$. Note from Fig. 4.8 that the ordering of states in the $\delta\pi$ manifold is contrary to that dictated by Hund's rule¹¹⁰, which would place the higher multiplicity ${}^1\Phi$ state below ${}^1\Pi$ (and therefore closer to the ${}^3\Phi$ state). The dipolar hyperfine constant c cannot be extracted since separate b constants are required for the three substates.

The $(b + c)$ and b constants clearly support the $5s\sigma^1 4d\delta^1$ and $4d\pi^1 \delta^1$ configurations for the ${}^3\Delta$ and ${}^3\Phi$ states, respectively. The ${}^3\Delta$ $(b + c)$ and b values are large and positive, indicating that the dominant mechanism for the coupling of electronic and nuclear spins is the Fermi contact interaction. This is consistent with the presence of an unpaired $s\sigma$ electron, as in the $s\sigma^1 d\delta^1$ configuration of ${}^3\Delta$. The ${}^3\Phi$ $(b + c)$ and b constants are negative, and small compared to those in ${}^3\Delta$. This is characteristic of a hyperfine interaction which occurs because of spin polarization by electrons in orbitals having nodes at the nucleus, such as $\pi^1 \delta^1$. The difference between the Fermi contact and spin polarization hyperfine constants in NbN is similar to that found in the VO states⁴⁵ $4s\sigma^1 3d\delta^2 X^4\Sigma^-$ and $4p\sigma^1 3d\delta^2 C^4\Sigma^-$. The ratio of ${}^3\Delta(b + c)_{ave}/{}^3\Phi(b + c)_{ave} = -3.7$, while $b(X^4\Sigma^-)/b(C^4\Sigma^-) = -3.1$.

The quadrupole coupling constant for the lower state is $-3.9 (\pm 0.8) \times 10^{-3} \text{ cm}^{-1}$, while that of the upper state was fixed to zero after it was found to be too small to be determined. The sign of the ${}^3\Phi$ state e^2Qq_0 is consistent with the quadrupole moment for ${}^{93}\text{Nb}$ of $-2 \times 10^{-24} \text{ e}\cdot\text{cm}^2$. The upper and lower state constants for the interaction of nuclear spin and rotation (c_i) were fixed to zero, as they were found to be on the order of -10^{-5} to -10^{-6} cm^{-1} , almost completely

correlated (.999), and with standard errors as large as the values themselves. It is the usual case for diatomics containing a transition metal for c_l to be too small to be determined (see for example references 31, 45, 79 and 91).

In the rotational part of the Hamiltonian, the A, B and D constants are very well determined in spite of the high correlations between A' and A" (.9985) and B' and B" (.995). The high rotational lines carrying information about the spin-uncoupling operator, $-2BJ \cdot S$, allow B and D to be determined individually, rather than simply determining their differences, B' - B" and D' - D". Since all three subbands were fitted simultaneously, and B was extracted with good precision, A could also be determined. This is possible since A, B and the effective B values for each subband are related by:²⁴

$$B_{\text{eff},\Omega} = B(1 + 2B\Sigma/A\Lambda) \quad (4.19)$$

From the B values, the bond lengths are calculated to be:

$$r_0(^3\Delta) = 1.6618 \text{ \AA}$$

$$r_0(^3\Phi) = 1.6712 \text{ \AA}$$

There have been very few rotational studies of transition metal mononitrides. Aside from the current work, the known bond lengths (r_0 , in \AA) are:

TiN ¹¹¹	X ² Σ	1.583
	A ² Π _r	1.597
	B ² Σ	1.646
ZrN ¹¹²	X ² Σ	1.696
	B ² Σ	1.740
	A ² Π	1.702
MoN ¹¹³	X ⁴ Σ ⁻	1.634

A⁴Π 1.654

The 3d transition metal monoxide series isovalent with ZrN (and TiN), NbN, MoN is ScO, TiO, VO, whose ground state bond lengths go as 1.668 Å³⁰, 1.623 Å⁸⁹ and 1.592 Å⁴⁵. Here the bond length decreases with each addition of a bonding δ electron. The ³Δ and ³Φ NbN bond lengths show that the nitrides are consistent with this trend, with values intermediate between those of ZrN and MoN.

The very large spin-spin interaction constants λ (equations 1.72 and 1.73) are caused by contributions from the second order spin-orbit interactions which induce the substantial shift of the ³Φ₃-³Δ₂ subband. The centrifugal distortion correction to λ , however, is considerably larger than its expected value of $\lambda_D \approx \lambda(A_D/A)$. The reason for this probably lies in the fact that we have not yet made direct measurements of the spin-orbit intervals. In this context, then, the centrifugal distortion correction constants A_D and λ_D are essentially fudge factors which enable the least squares fit to converge to a minimum lying within a broad minimum which contains the true molecular constants. So although this set of constants is an internally consistent one which fits the data, once the derived A values are replaced by direct measurements the constants may change slightly to enable the fit to converge to the true, nearby minimum. With the data we now possess, however, the A_D and λ_D values given in Table 4.1 are necessary to obtain a fit.

To demonstrate this fact, a fit of the rotational constants was made in which λ_D and γ were fixed to zero, and all hyperfine constants were fixed at the values determined in this work. The initial values for the floated constants were taken from the grating

spectrograph work of Dunn *et al*¹⁰² (see p. 85), with the exception of A_D which was given an initial value of zero; the parameter δ in their work is equal to -2λ . The fit converged to a standard deviation of 0.00138 cm^{-1} , which is about 2.5 times higher than the fit which incorporates λ_D and γ . As expected, the final set of constants (Table 4.II) is very similar to those determined by the grating spectrograph analysis, with the exception of T_0 , which was found from LIF data to be 13.5 cm^{-1} higher than that from the grating work. The residuals contain systematic errors in the positions of the rotational lines, as compared to the random residuals generated by the full set of constants. The systematic errors and higher standard deviation reflect the inability of the model to fit the data without λ_D , A_D and γ . However, as stated above, the resulting rotational constants, other than B and D, are only effective ones. Another important feature of this fit is that the first order spin-orbit coupling constants A' and A'' are 100% correlated, as are the second order spin-orbit parameters λ' and λ'' (see the correlation matrix in Table 4.II). This is a direct reflection of the fact that the spin-orbit coupling constants are derived rather than measured. As a result, only the difference $\Delta\lambda$ can be determined, rather than separate λ' and λ'' values. For these reasons, a fit excluding λ_D and γ may produce a set of rotational constants that more accurately represents the real situation, though the addition of λ_D and γ creates a model which is able to fit the data. It is worth noting that in a purely case (a) basis, γ , A_D and λ_D are correlated such that only two of the three can be determined.⁴¹ In the ${}^3\Phi$ - ${}^3\Delta$ system of NbN this correlation is broken

Table 4.II. Rotational constants obtained for the $3\Phi-3\Delta$ system of NbN with the λ_D and γ parameters fixed to zero, and the hyperfine constants fixed to the values in Table 4.I.^a The correlation matrix follows the constants.

	Φ	Δ
T_0	16518.4653(2)	0
A	242.59(8)	184.5(1)
B	0.495796(8)	0.501447(8)
D	$0.5005(7) \times 10^{-6}$	$0.4685(4) \times 10^{-6}$
λ	-3.70(8)	16.53(8)
A_D	$-0.484(5) \times 10^{-4}$	$-0.793(8) \times 10^{-4}$
σ	0.00138	

^aThe format of the table follows that of Table 4.I.

Correlation Matrix

	T_0	A'	B'	D'	λ	A_D
T_0	1.0000	0.0996	0.0820	-0.4333	0.3401	0.1538
A'		1.0000	-0.0473	0.1235	0.5124	-0.0645
B'			1.0000	-0.0973	0.0934	-0.3204
D'				1.0000	0.0366	-0.4503
λ'					1.0000	-0.0664
A_D'						1.0000

	A''	B''	D''	λ''	A_D''
T_0	0.0995	0.1580	-0.2227	0.3408	0.1715
A'	1.0000	-0.0335	0.3977	0.5115	0.3233
B'	-0.0474	0.9936	-0.0789	0.0928	-0.3322
D'	0.1233	-0.1874	0.4224	0.0360	-0.2099
λ'	0.5124	0.1025	-0.2270	1.0000	0.0874
A_D'	-0.0643	-0.2737	-0.0883	-0.0659	0.8660
A''	1.0000	-0.0336	0.3976	0.5116	0.3233
B''		1.0000	-0.0839	0.1020	-0.2929
D''			1.0000	-0.2275	0.0982
λ''				1.0000	0.0875
A_D''					1.0000

to some extent by the high J data where there is a distinct tendency towards case (b) (see the correlation matrices in Appendix I and Table 4.II).

For the future, a direct measurement of the spin-orbit intervals must be made. The most likely method for doing this is to locate forbidden "spin-orbit satellite" transitions which disobey the case (a) selection rule $\Delta\Sigma = 0$ (equation 1.57). Since these transitions are very weak, resolved fluorescence experiments can be performed to enhance the signal. To record the spectrum of a ${}^3\Phi_2$ - ${}^3\Delta_2$ line, for example, an allowed ${}^3\Phi_2$ - ${}^3\Delta_1$ transition is excited. The resulting emission spectrum of the satellite transition is recorded over a long exposure time using the microchannel-plate intensified array detector. The lines which hold the most promise for producing spin-orbit satellites are high J lines affected by spin-uncoupling, since the $\Delta\Sigma = 0$ selection rule weakens with increasing rotation. However, it is also important that the excited line be strong, so a compromise must be made between high J and line strength when choosing lines for excitation.

Other important tasks are to locate the singlet states which interact with the ${}^3\Delta_2$ and ${}^3\Phi_3$ spin-orbit components, and to search for the expected $\sigma^2 {}^1\Sigma^+$ state to determine if the ground state is ${}^3\Delta$ or ${}^1\Sigma^+$. The ordering of the $\sigma\delta$ states (${}^3\Delta$ and ${}^1\Delta$) and the σ^2 state (${}^1\Sigma^+$) depends on the relative ordering of the $4s\sigma$ and $3d\delta$ metal-centered molecular orbitals (see Fig. 3.1). Diatomic transition metal oxides and fluorides isoelectronic with NbN demonstrate that these orbitals lie very close to one another. Therefore one cannot readily predict in NbN whether the ${}^3\Delta_r$ or ${}^1\Sigma^+$ state will be lower in energy.

For example, the d²-transition metal monoxide series, consisting of titanium oxide (TiO), zirconium oxide (ZrO) and hafnium oxide (HfO), is variable in this respect. TiO has a $^3\Delta_r$ ground state¹¹⁴, with the $^1\Delta$ state lying 3500 cm⁻¹ above that¹¹⁵. However, ZrO has a $^1\Sigma^+$ ground state¹¹³ which lies 1650 cm⁻¹ below the $^3\Delta_r$ state¹¹⁶. HfO is believed to have a $^1\Sigma^+$ ground state also, but with the $\sigma\delta$ states further removed from the ground state than those in ZrO due to the greater ligand field splitting between the σ and δ orbitals in HfO.¹¹⁴ In the d¹-transition metal monofluoride series, comprising scandium fluoride (ScF), yttrium fluoride (YF) and lanthanum fluoride (LaF), ScF¹¹⁵ and YF have $^1\Sigma^+$ ground states, while the ordering of $^1\Sigma^+$ and $^3\Delta_r$ in LaF is not known¹¹⁸. Tantalum nitride (TaN), the 5d counterpart of NbN, is predicted from matrix isolation studies to have a $^1\Sigma$ ground state, though the possibility of $^3\Delta$ has not been entirely ruled out.¹¹⁹ To identify the ground state of NbN securely, then, the relative position of the $^1\Sigma^+$ and $^3\Delta_r$ states must be determined experimentally.

CHAPTER V
ROTATIONAL ANALYSIS OF THE ν_7 -FUNDAMENTAL
OF AMINOBORANE, NH_2BH_2

V.A. Background.

This work examines the BH_2 out-of-plane wagging fundamental of aminoborane (NH_2BH_2), the simplest alkene in the B=N homologues of the hydrocarbons. Long before NH_2BH_2 was studied experimentally, its small size and the interest in B-N compounds led to extensive theoretical studies of it. In particular, the donor-acceptor nature of the B-N bond attracted attention, as Hückel theory calculations¹²⁰ done in 1964 predicted that the bond moment was in the direction B to N rather than the reverse, as required by formal valence theory. These preliminary calculations, covering charge distributions, electronic structures and geometries for a number of B-N compounds, were followed by CNDO (complete neglect of differential overlap)¹²¹ and ab initio^{122,123,124} calculations predicting these and other properties such as the dipole moment, force constants, barriers to rotation and stabilities. Aminoborane's extreme instability at room temperature, however, imposed practical difficulties for experimentalists to verify or refute the theoreticians' predictions. Its first synthesis was in 1966 from the symmetrical cleavage of vacuum sublimed cycloborazine pyrolyzed at 135°C, where NH_2BH_2 and other decomposition products could be trapped in a liquid nitrogen cold trap, and then identified by mass spectroscopy¹²⁵. The aminoborane was found to have decomposed spontaneously after warming to room temperature. In

1968, gaseous aminoborane and diborane (B_2H_6) were observed by molecular beam mass spectroscopy as products of the spontaneous decomposition of solid ammonia borane (NH_3BH_3) at room temperature.¹²⁶ When Kwon and McGee performed both pyrolysis and radiofrequency discharge experiments on borazine (the BN analog of benzene), NH_2BH_2 and B_2H_6 were again the products.¹²⁷ They were recovered in a $-168\text{ }^\circ\text{C}$ trap, then separated by vacuum distillation of diborane from aminoborane at $-155\text{ }^\circ\text{C}$. At this temperature, small amounts of both evaporation and polymerization of NH_2BH_2 were observed. Polymerization becomes the dominant process at temperatures above this, and is fairly significant at $-130\text{ }^\circ\text{C}$.¹²⁷ The pronounced instability of monomeric aminoborane led Pusatcioglu *et al*¹²⁸ in 1977 to investigate the possibility of using NH_2BH_2 to build thermally stable inorganic polymers. They pyrolyzed gaseous ammonia borane, condensed the monomeric NH_2BH_2 product at 77 K, then allowed it to polymerize as it warmed. In 1979 a microwave spectrum of NH_2BH_2 was obtained, using a sample formed from the reaction of 5-10 mTorr each of ammonia and diborane at $500\text{ }^\circ\text{C}$.¹²⁹ Molecular constants calculated by a least-squares fit were consistent with a planar configuration, thereby establishing the symmetrical structure $NH_2=BH_2$ for aminoborane, rather than the asymmetrical NH_3BH . Perhaps the most important outcome of this work was the determination of the dipole moment to be 1.844 D in the direction from N to B, as opposed to the theoretical predictions of B to N.^{120,121} The assumption of an $N \rightarrow B$ direction for the dipole moment was based on the observation that the dipole moment of NH_2BH_2 is 0.751 D smaller than that in BH_2BF_2 .

The same group recently reported microwave spectra of five isotopic species of NH_2BH_2 , improving the constants and geometric parameters obtained in the previous study.¹³⁰

Recently, at the University of British Columbia, the first gas phase Fourier transform infrared spectrum of aminoborane was measured.¹³¹ The synthesis combined the solid-state and vapor-phase ammonia borane pyrolysis techniques. Solid NH_3BH_3 was heated to about 70 °C in a flow system maintained at approximately 200 microns, and the vapors produced were passed through a furnace at about 400 °C, to pyrolyze unreacted sublimed sample. Nine of aminoborane's eleven infrared (IR) active fundamental vibrations were recorded at medium resolution (0.05 cm^{-1}), with the ν_4 A-type band at 1337 cm^{-1} being also recorded at very high resolution (0.004 cm^{-1}). Since that time the bands of all of the IR active fundamentals have been recorded at UBC at 0.004 cm^{-1} resolution (see Table 5.1), though ν_5 is vanishingly weak because its dipole derivative appears to be very small. Some analysis has been completed^{132,133,134}, with the remainder currently underway. The present work is a contribution to the high resolution Fourier transform IR study of aminoborane, being the rotational analysis of the C-type ν_7 fundamental whose origin is at 1004.7 cm^{-1} .

Table 5.I. Vibrational fundamentals of gaseous $\text{NH}_2^{11}\text{BH}_2$.

Symmetry		cm^{-1}	Type of motion
A ₁	v ₁	3451	NH symmetric stretch
	v ₂	2495	BH symmetric stretch
	v ₃	1617	NH ₂ symmetric bend
	v ₄	1337.474 ¹	BN stretch
	v ₅	1145	BH ₂ symmetric bend
A ₂	v ₆	837	Torsion (twist)
B ₁	v ₇	1004.6842	BH ₂ wag
	v ₈	612.1987 ²	NH ₂ wag
B ₂	v ₉	3533.8	NH asymmetric stretch
	v ₁₀	2564 ³	BH asymmetric stretch
	v ₁₁	1122.2	NH ₂ rock
	v ₁₂	742	BH ₂ rock

¹Reference (131)

²Reference (133): v₈ (1,0) band; reference (132): v₈ (2,0) band

³Reference (134)

V.B. The Michelson Interferometer and Fourier Transform Spectroscopy.

The infrared interferogram was recorded and Fourier transformed with a BOMEM DA3.002 Michelson interferometer and associated software (version 3.1). Three sources of infrared light are available depending on the wavelength region desired: a quartz-halogen lamp for the near IR and visible regions, a globar for the mid-IR, and a mercury-xenon lamp for the far IR. After first being filtered and focused at an aperture, the infrared light passes to a collimating mirror and is reflected as a parallel beam to a beamsplitter, where it is divided in two. One beam continues through to a fixed mirror, while the other is reflected onto a mirror moving at constant velocity. As one of the beams has a fixed path length and the other a constantly varying one, the recombination of the beams at the beamsplitter produces a resultant of sinusoidal waves that are out of phase.¹³⁵ The portion of the resultant not absorbed by the sample is measured at the detector as the interferogram. The point along the moving mirror's travel at which the fixed and moving mirrors are exactly equidistant--called the zero path difference (ZPD)--should in principle bring all the sinusoidal waves into phase, with constructive interference producing a maximum in the amplitude.¹³⁵

Because the interference patterns producing the infrared interferogram result from the optical path difference between the two light beams, it is essential that signal sampling occur at constant intervals of mirror displacement. This is achieved in the BOMEM DA3 spectrophotometer by a He-Ne laser. Operating at 632.8

nm, or 15796 cm^{-1} , the laser provides an extremely precise time base of 31,592 cycles per cm of mirror travel.¹³⁶ The cycles, called fringes, trigger spectral sampling at a frequency normally equal to one sample/laser fringe, though the rate can be increased to up to eight times the laser fringe frequency. The phase coherence provided by this laser is excellent: its single-mode operation prevents destructive interference by two other closely lying transition frequencies, and its thermal stabilization removes temperature dependent fluctuations in the laser optics. The resulting uncertainty in the mirror's position is 0.0025 fringes per cm of mirror travel, which even at the maximum translation of 125 cm amounts to a variation of only 0.3 fringes over the length of the mirror's scan.¹³⁶

The interferogram not only requires that its points be sampled at precise intervals, but also that one of these points occurs at an origin that is exactly reproducible from scan to scan. The BOMEM DA3 spectrophotometer achieves this by triggering the commencement of each scan at the ZPD of an interferogram of white light. The beams from the white light source follow the same optical path as that of the radiation of interest, with the incoherent nature of the white light producing an interferogram characterized by an intense pulse at ZPD (the WLZPD), and low intensity amplitudes at non-zero mirror translations. The occurrence of the pulse is precise to well within one laser fringe, so the actual WLZPD trigger is marked as the laser fringe immediately following the pulse. The result is a synchronization signal which references the points in the

IR interferogram to a constant position along the scanning mirror's path.^{136,137}

A Fourier transform infrared experiment is therefore the process of obtaining the infrared interferogram in conjunction with the white light reference interferogram and the time base generated by the He-Ne laser. These data are processed by Fourier transformation from the IR interferogram time domain to an IR spectrum in the frequency domain. The integrals of the Fourier transformation can be understood in terms of the phase differences between the IR beams split by the beamsplitter. When a wave with angular frequency ω reflects off a mirror moving with velocity v , the frequency is Doppler shifted by an amount¹³⁸

$$\Delta\omega = 4\pi v/\lambda \quad (5.1)$$

Expressed as a function of the speed of light and the incident frequency, using the relation $\lambda = 2\pi c/\omega$, the phase shift becomes¹³⁸

$$\Delta\omega = (v/c)2\omega \quad (5.2)$$

The magnitude of $\Delta\omega$ is on the order of 1 kHz to 100 kHz, a frequency that can be processed easily as compared to the 10^{13} to 10^{15} Hz frequencies of IR radiation itself.

The time-averaged beat intensity, I , produced by the combination of two waves out of phase by $\Delta\omega$ is¹³⁸

$$I = I_0(1 + \cos\Delta\omega t)\cos^2[(\omega + \omega')t/2] = (I_0/2)(1 + \cos\Delta\omega t) \quad (5.3)$$

where I_0 is the signal intensity when $\Delta\omega = 0$. Represented in terms of amplitude or electric field strength $[E_0(\omega)]$, phase difference $[\delta(\omega) = \Delta\omega t]$, and the reflectivity (R) and transmittance (T) of the beamsplitter, equation (5.3) becomes¹³⁸:

$$I(\omega, \delta) = c\epsilon_0 RT |E_0(\omega)|^2 [1 + \cos\delta(\omega)] \quad (5.4)$$

where c is the speed of light and ϵ_0 is the vacuum permittivity¹³⁹, equal to $8.85 \times 10^{-12} \text{ C}^2\text{J}^{-1}\text{m}^{-1}$. Integrating over all frequencies of the spectral components,

$$I(\delta) = \int I(\omega, \delta) d\omega = c\epsilon_0 RT \left[\int |E_0(\omega)|^2 d\omega + \int |E_0(\omega)|^2 \cos \delta d\omega \right] \quad (5.5)$$

At zero path difference, or $\delta = 0$, the two terms in brackets in equation (5.5) are equal, so the ZPD intensity is given by:

$$I_0 = 2c\epsilon_0 RT \int |E_0(\omega)|^2 d\omega \quad (5.6)$$

The time-averaged signal intensity as a function of phase difference, $I(\delta)$, is the quantity measured at the detector. The interferogram points themselves are taken to be the oscillations of these intensities about $I_0/2$:¹³⁸

$$|I(\delta) - I_0/2| = c\epsilon_0 RT \int |E_0(\omega)|^2 \cos \delta d\omega \quad (5.7)$$

The cosine Fourier transform of an interferogram of the form of equation (5.7) yields a spectral intensity distribution function $I(\omega)$ in which intensity is a function of discrete frequencies:

$$I(\omega) = (1/\pi RT) \int [I(\delta) - I_0/2] \cos \delta d\delta \quad (5.8)$$

However, since imperfections in manufacture do not produce equivalent reflectivities in the fixed and moving mirrors, sine components as well as cosine are introduced into the interferogram. The actual Fourier transform therefore employs the complex form of the expression^{138,140,141}

$$I(v) = C \int [I(\delta) - I_0/2] e^{-i2\pi v \delta} d\delta \quad (5.9)$$

In general form, the Fourier transform of function $f(x)$ is¹⁴²

$$\mathfrak{F}\{f(x)\} = F(\alpha) = \int f(x) e^{-i\alpha x} dx \quad (5.10)$$

The inverse Fourier transform of $F(\alpha)$ is therefore

$$\mathfrak{F}^{-1}\{F(\alpha)\} = f(x) = (1/2\pi) \int F(\alpha) e^{i\alpha x} d\alpha \quad (5.11)$$

Likewise, the spectrum expressed in equation (5.9) is one member of a Fourier pair, which consists of two non-periodic functions related by the Fourier integral transforms¹⁴¹:

$$g(\nu) = \int f(\delta) e^{i2\pi\nu\delta} d\delta \quad (5.12)$$

$$f(\delta) = \int g(\nu) e^{-i2\pi\nu\delta} d\nu \quad (5.13)$$

A Fourier pair is illustrated graphically in Fig. 5.1.

Fourier transform spectroscopy is able to exploit the Fourier pair relationship between the time domain (phase, δ) and the frequency domain (ω or ν), because frequency can be obtained with greater accuracy, resolution and speed by measuring and transforming phase differences rather than by directly measuring relative frequency. With the Michelson interferometer the integration cannot be performed over all space ($-\infty$ to $+\infty$) but is limited to the range $0 - L$ where L is the total mirror displacement. As the distance travelled by the mirror increases, the number of terms included in the integration increases, extending the amount of information available for extraction into the spectrum $I(\nu)$.¹⁴¹ The theoretical maximum spectral resolution of an interferometer is therefore inversely proportional to the maximum optical path difference between the fixed and moving mirrors.¹⁴² Defining resolution as the full width at half height, the maximum unapodized resolution is:¹⁴⁴

$$\Delta\nu_{1/2} = 1/(2L) \quad (5.14)$$

Imposing the 0 to L limits on an interferogram is known as a "boxcar" truncation (see Fig. 5.2).¹⁴⁴ When a boxcar-truncated interferogram is Fourier transformed, the spectral line shape contains the sinc function [$\text{sinc } z = (\sin z)/z$]:^{146,147}

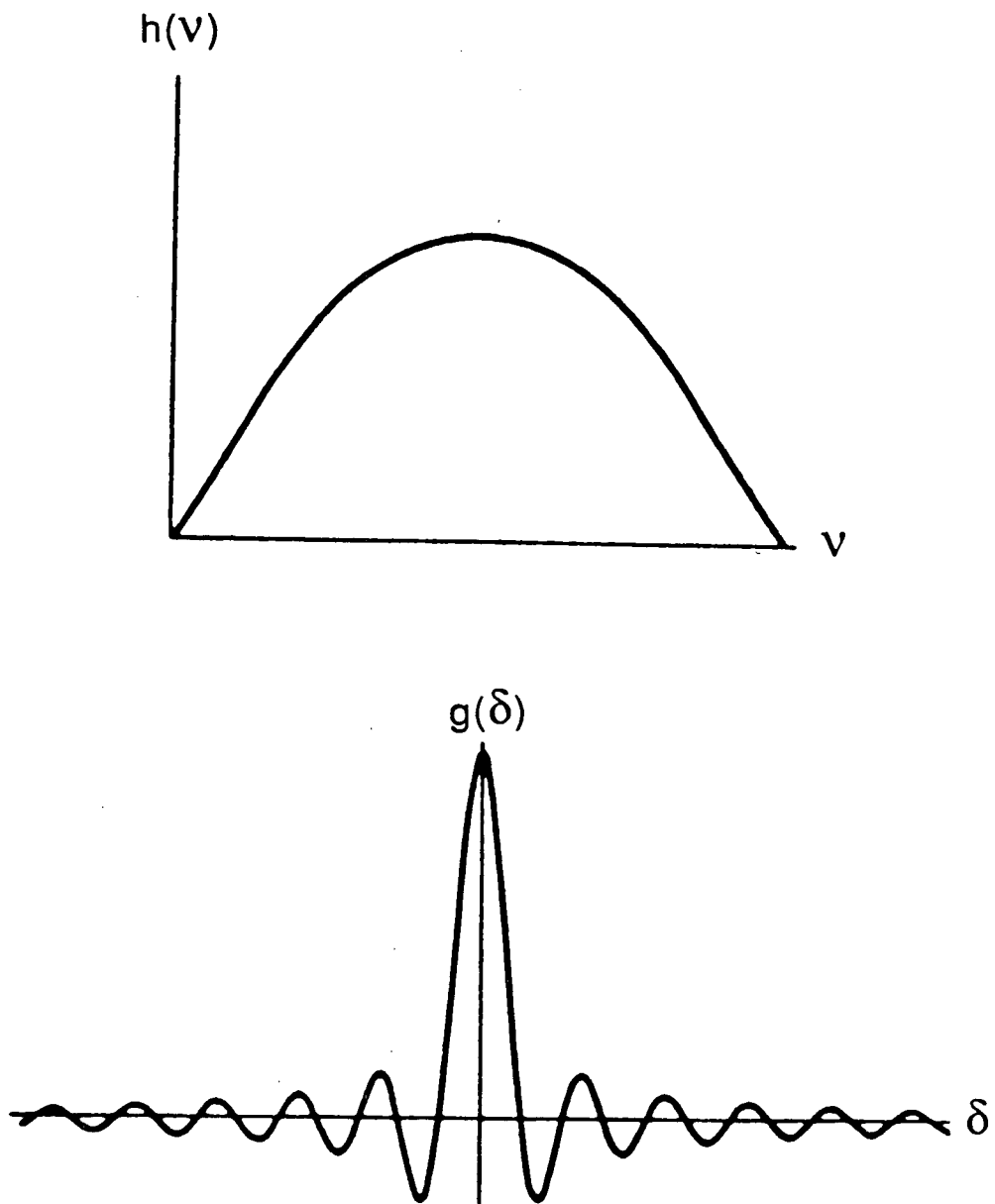


Fig. 5.1. A polychromatic signal in the frequency domain (above) Fourier transformed into the time domain (below).¹⁴¹

$$F\{D(x)\} = 2L(\text{sinc } z) \quad (5.15)$$

where $z = 2\pi(\sigma - \sigma_0)L$. The half-width of the center spike of this form is very narrow: $\Delta\sigma = 1.207/2L$, or about 20% wider than the theoretical resolution of $1/2L$. However, the sidelobes next to the central peak have about 21% of its intensity, and the amplitudes of subsequent lobes are slow to die away.¹⁴⁵ In order to approximate more closely the true frequency domain spectrum, an apodization function is often included in the data processing. This process dampens the effects caused by truncating the interferogram at a definite mirror displacement of L . Though there are many forms of apodization functions, the effect is to give decreasing weight to the data points recorded at large mirror displacements.^{145,146} One of the simplest is the triangular function in Fig. 5.3, in which all sidelobes are positive and the largest is only about 4.5% that of the center spike; the linewidth is increased by almost 50% over the boxcar case.^{146,147} The apodization applied to the aminoborane experiment in this work was a cosine function referred to as "Hamming" or "Happ-Genzel". It produces spectral lines with negative sidelobes of only 0.0071 the height of the maximum peak, and lines about 2% broader than those from the triangular apodization.¹⁴⁵

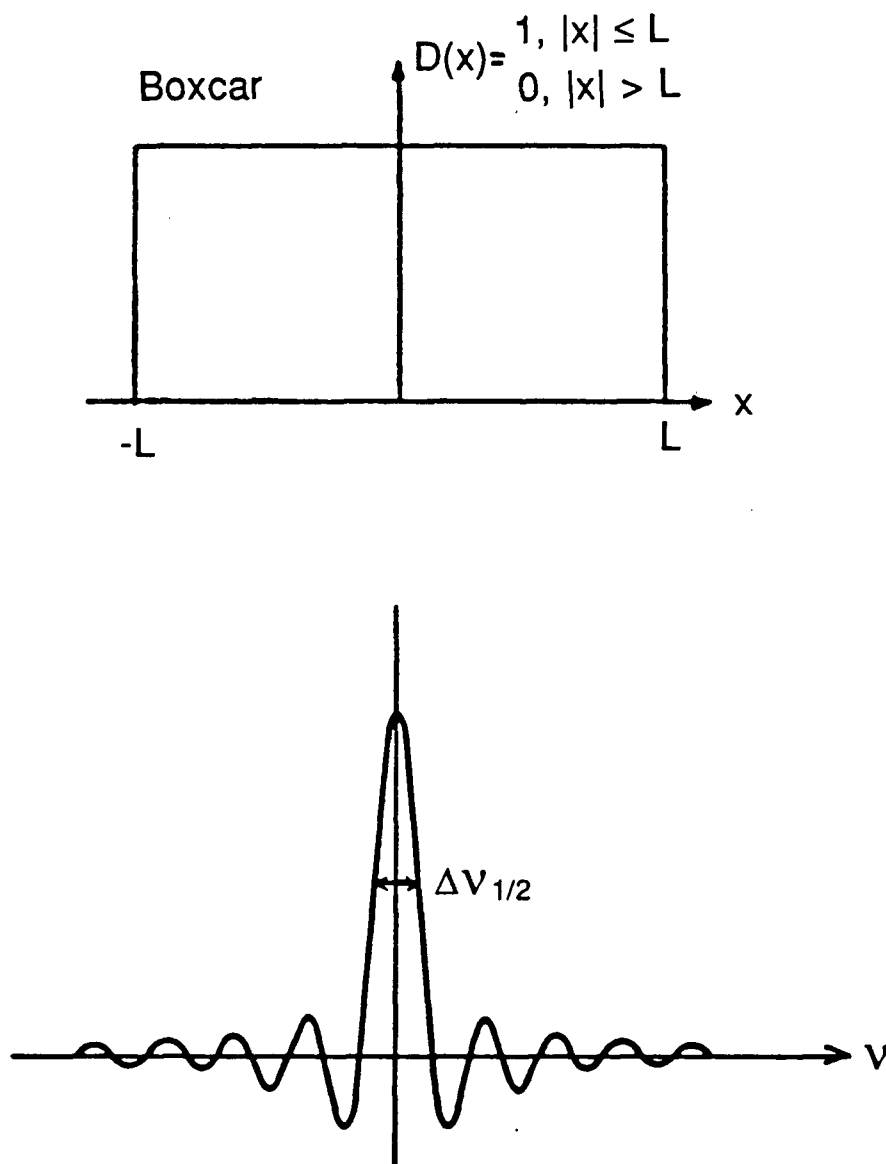


Fig. 5.2. A boxcar function $D(x)$ (above). The Fourier transform of a boxcar truncated interferogram is a spectrum with the line shape function $F\{D(x)\} = 2L\sin(2\pi\nu L)/2\pi\nu L$ (where L denotes the maximum mirror displacement.) The full width at half-height ($\Delta\nu_{1/2}$) is $1.207/2L$, and the strongest sidelobe has 21% the intensity of the maximum.¹⁴⁵

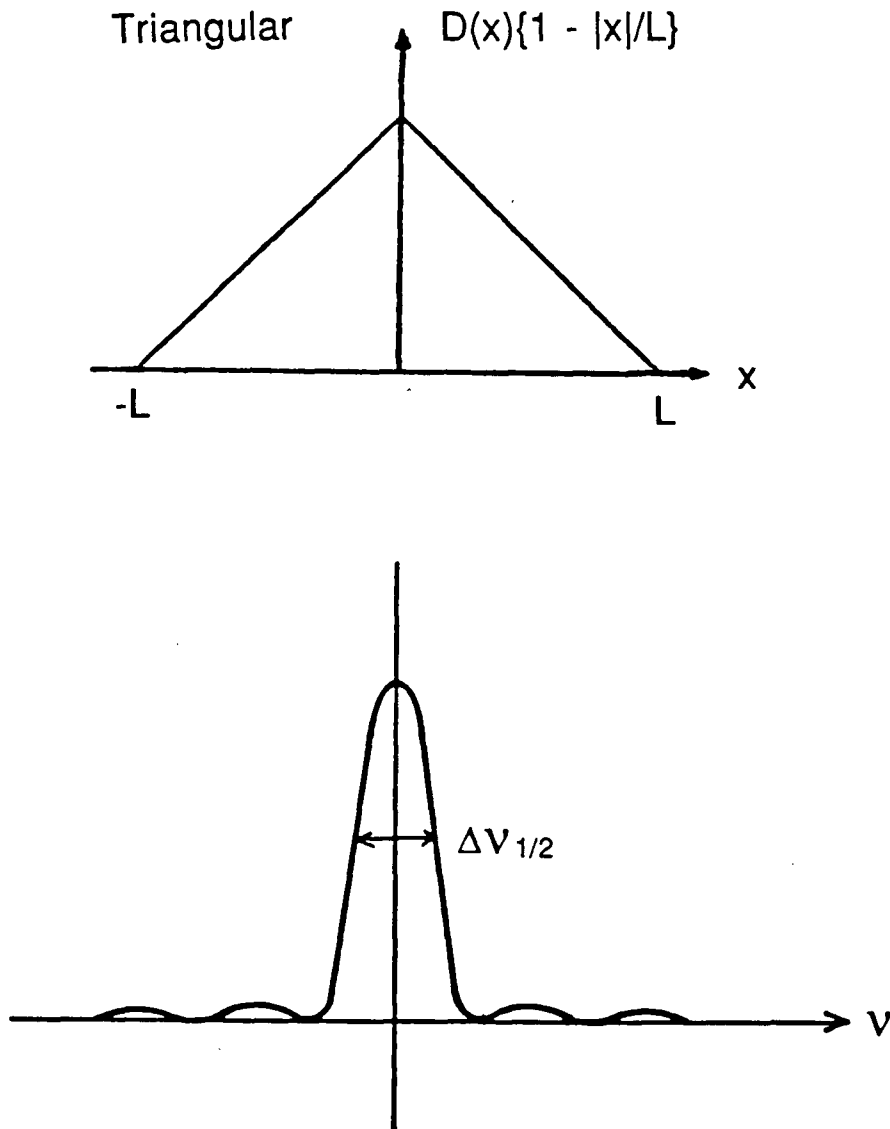


Fig. 5.3. The triangular apodization function $D(x)$ (above) produces a spectrum with the line shape function $F\{D(x)\} = 2L\sin(2\pi\nu L)/(2\pi\nu L)^2$ (below). The full width at half-height ($\Delta\nu_{1/2}$) is $1.772/2L$, with the strongest sidelobe only 4.5% of the maximum intensity.¹⁴⁵

V.C. Experimental.

The aminoborane was prepared by pyrolysis of borane ammonia (BH_3NH_3 , Alfa Products) according to the procedure of Gerry and coworkers¹³¹, except that in the present work the temperature of the solid NH_3BH_3 was raised to only 67 °C - 68 °C for the first several hours, then lowered to 63 °C - 65 °C for the remainder of the experiment. The 70 °C pyrolysis temperature employed in reference 131 was found to be unnecessarily close to the temperature of uncontrolled thermal decomposition, which initiates violently at approximately 71 °C. At the time the interferogram was measured, the temperature of the solid ammonia borane was 63.5 (± 0.5) °C. The sample absorption cell, set to an optical path of 9.75 m, was maintained at a pressure of 100 μ during data acquisition. The BOMEM DA3.002 interferometer was fitted with a potassium chloride beam splitter and a liquid nitrogen-cooled HgCdTe detector.

V.D. The Asymmetric Rotor.

A vibrational fundamental is infrared active if the dipole moment μ changes as a result of motion along the normal coordinate Q_k , or in other words if the derivative $(\partial\mu/\partial Q_k)_0$ in the Taylor series expansion of the dipole moment

$$\mu = \mu^0 + \sum (\partial\mu/\partial Q_k)_0 Q_k \quad (5.16)$$

is non-zero.¹⁴⁸ The linear character of the dipole operator means that its components transform as translations along the principal axes, and therefore so do the various $(\partial\mu/\partial Q_k)_0 Q_k$'s.

Aminoborane is a prolate asymmetric top molecule belonging to the point group C_{2v} , whose character table is given in Table 5.II. The irreducible representations of the normal vibrations are: $5A_1 + A_2 + 2B_1 + 2B_2$, for a total of twelve fundamental vibrations. The BH_2 out-of-plane wagging vibration is antisymmetric with respect to reflection in the yz plane, and therefore transforms as the B_1 representation (see Fig. 5.4). Thus the ν_7 vibration represents translation along the c inertial axis and generates a C-type infrared band.

Accompanying any molecular vibration are the rotational transitions involving changes in the total angular momentum, J . In order to understand the rotational selection rules for an asymmetric top molecule, one must write down asymmetric top rotational wave functions which are eigenfunctions of the symmetry operations of the molecular point group, in this case C_{2v} . We begin by examining the effects of the C_{2v} symmetry operations on the symmetric top wave functions, $Y_{JK}(\theta, \phi)$. From equation (1.23) we know that:

$$Y_{JK}(\theta, \phi) = NP_J^K(\cos \theta) e^{iK\phi} \quad (5.17)$$

Table 5.II. Character table for the C_{2v} point group, and the correlation of the axes of translation to infrared band type. The molecule-fixed axes x , y , z given here are related to the inertial axes a , b , c by the I' representation.

C_{2v}	E	C_2	$\sigma_v(xz)$	$\sigma_v'(yz)$	Rotation (R) and Translation (T) axes
A_1	1	1	1	1	T_a
A_2	1	1	-1	-1	$R_a (R_z)$
B_1	1	-1	1	-1	$T_c, R_b (R_y)$
B_2	1	-1	-1	1	$T_b, R_c (R_x)$

where N is a normalization factor, $P_J^K(\cos \theta)$ is an associated Legendre polynomial, and the spherical polar angles θ and ϕ are shown in Fig. 5.4.

A C_2 rotation about the a inertial axis ($C_2^{(a)}$) adds an amount π to ϕ , but does not change the θ coordinate:

$$C_2^{(a)}Y_{JK}(\theta, \phi) = NP_J^K(\cos \theta)e^{iK(\phi+\pi)} \quad (5.18a)$$

$$= NP_J^K(\cos \theta)e^{iK\phi}e^{iK\pi} \quad (5.18b)$$

$$= e^{iK\pi}Y_{JK}(\theta, \phi) \quad (5.18c)$$

where

$$e^{iK\pi} \begin{cases} = 1 & \text{for even } K \\ = -1 & \text{for odd } K \end{cases} \quad (5.19)$$

Note that the operation of C_2 on $Y_{JK}(\theta, \phi)$ gives a multiple of the original spherical harmonic, $Y_{JK}(\theta, \phi)$. C_2 rotations about the b and c inertial axes are not symmetry operations of the C_{2v} point group.

Unlike $C_2^{(a)}$, the σ_v^{ac} and σ_v^{ab} operators reverse the directions of the angles θ and ϕ . Both reflections change θ into $-\theta$, causing the associated Legendre polynomial to become $P_J^K(-\cos \theta)$. By the Rodrigues formula¹⁴⁹

$$P_J^K(-\cos \theta) = (-1)^{J+K}P_J^K(\cos \theta) \quad (5.20)$$

The operation of σ_v^{ac} changes ϕ to $-\phi$. σ_v^{ab} projects the c axis in the opposite direction and changes ϕ to $\pi - \phi$. The overall effects of the reflections are therefore:

$$\sigma_v^{ac}Y_{JK}(\theta, \phi) = (-1)^{J+K}NP_J^K(\cos \theta)e^{-iK\phi} \quad (5.21)$$

and

$$\sigma_v^{ab}Y_{JK}(\theta, \phi) = (-1)^{J+K}NP_J^K(\cos \theta)e^{iK\pi}e^{-iK\phi} \quad (5.22)$$

Clearly the spherical harmonics themselves are not eigenfunctions of the reflection operators, though the linear combinations obtained

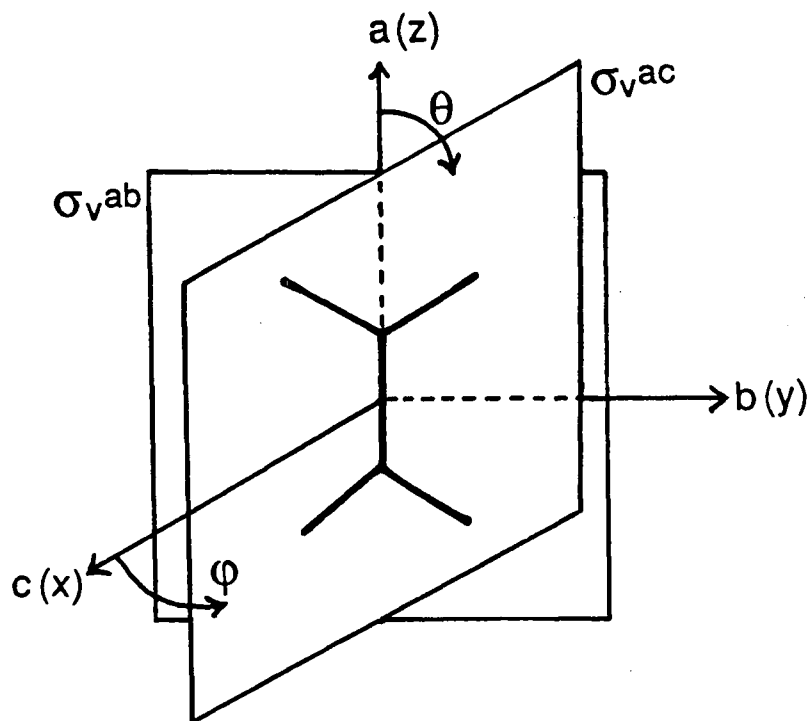


Fig. 5.4. Schematic drawing of the C_{2v} NH_2BH_2 molecule in the x , y , z principal axis system and the a , b , c inertial axis system, showing the $C_2 \sigma_v$ reflection planes.

by taking Wang sum and difference functions¹⁵⁰ are eigenfunctions of these operators:

$$\Psi_{JK\pm} = (1/\sqrt{2})(Y_{JK} \pm Y_{J,-K}) \quad (5.23)$$

In equation (5.23) the sums and differences (JK_+ and JK_- , respectively) correspond to the upper and lower asymmetry components of a JK level.

The effects of the C_{2v} symmetry operations, performed on asymmetric top rotational wavefunctions, follow from equations (5.18c), (5.19), (5.21), (5.22) and (5.23):

$$C_{2(a)} \Psi_{JK\pm} = (-1)^K \Psi_{JK\pm} \quad (5.24)$$

$$\begin{aligned} \sigma_{v^{ac}} \Psi_{JK\pm} &= (1/\sqrt{2})(-1)^{J-K} Y_{J,-K} \pm (1/\sqrt{2})(-1)^{J+K} Y_{JK} \\ &= \pm(-1)^{J+K}(1/\sqrt{2}) (Y_{JK} \pm Y_{J,-K}) \\ &= \pm(-1)^{J+K} \Psi_{JK\pm} \end{aligned} \quad (5.25)$$

$$\begin{aligned} \sigma_{v^{ab}} \Psi_{JK\pm} &= (-1)^K(-1)^{J+K} \Psi_{JK\pm} \\ &= \pm(-1)^J \Psi_{JK\pm} \end{aligned} \quad (5.26)$$

For even and odd values of K , and the + and - asymmetry components, the result of each operation can be tabulated using (5.24) through (5.26), as given in the first two sections of Table 5.III. The irreducible representations in the third section of Table 5.III are obtained by substituting even and odd values for J into section 2. The quantum numbers K_a and K_c in section 3 denote the projections of the angular momentum components J_a and J_c along the axes of lowest and highest inertia. The values of K_a and K_c corresponding to each irreducible representation are derived from the rule that $K_c = J - K_a$ and $K_c = J - K_a + 1$, for the + and - asymmetry components, respectively. For example, for even J , even K_a and the - asymmetry component, K_c must be odd, giving $K_a K_c = eo$. The eo notation

Table 5.III. Character sets for an asymmetric top rotational wavefunction in the C_{2v} point group.

Wang sum & difference						Irred. representations ($K_a K_c$)		E^\pm/O^\pm notation
J	K_a functions	E	C_2	$\sigma_{v^{ac}}$	$\sigma_{v^{ab}}$	J_{even}	J_{odd}	
J	K_{even} +	1	1	$(-1)^J$	$(-1)^J$	$A_1(ee)$	$A_2(eo)$	E^+
J	K_{even} -	1	1	$-(-1)^J$	$-(-1)^J$	$A_2(eo)$	$A_1(ee)$	E^-
J	K_{odd} +	1	-1	$-(-1)^J$	$(-1)^J$	$B_2(oe)$	$B_1(oo)$	O^+
J	K_{odd} -	1	-1	$(-1)^J$	$-(-1)^J$	$B_1(oo)$	$B_2(oe)$	O^-

indicates that the rotational wavefunction is symmetric with respect to rotation about the a inertial axis and antisymmetric with respect to rotation about the c inertial axis.¹⁵¹ The E^\pm/O^\pm notation given in the last column of Table 5.III is explained in Section V.E. From Table 5.III, the selection rules for a C-type band are:

$$A_1 \Leftrightarrow B_2 \text{ and } A_2 \Leftrightarrow B_1 \quad (5.27)$$

or in $K_a K_c$ notation:

$$ee \Leftrightarrow oe \text{ and } eo \Leftrightarrow oo \quad (5.28)$$

The restrictions on changes in K_a and K_c are therefore:

$$\Delta K_a = \pm 1, \pm 3, \pm 5, \dots \text{ and } \Delta K_c = 0, \pm 2, \pm 4, \dots \quad (5.29)$$

so that C-type bands consist of the following branches, in $\Delta K_a \Delta J$ notation:

<u>Branch</u>	<u>ΔJ</u>	<u>ΔK_a</u>	<u>ΔK_c</u>	<u>Intensity</u>
rR	+1	+1	0,0	strong
pP	-1	-1	0,0	strong
rQ	0	+1	0,-2	intermediate
pQ	0	-1	0,+2	intermediate
rP	-1	+1	-2,-2	weak
pR	+1	-1	+2,+2	weak

V.E. The Rotational Hamiltonian.

V.E.1. The Hamiltonian without vibration interaction.

The rotational Hamiltonian representing the purely kinetic energy, T , of a freely rotating rigid asymmetric top molecule is:

$$\hat{H}^{\text{rigid}} = (B_x + B_y) \hat{J}^2/2 + [B_z - (B_x + B_y)/2] \hat{J}_z^2/2 + (B_x - B_y)(\hat{J}_+^2 + \hat{J}_-^2)/4 \quad (5.20)$$

where $\hat{J}_+^2 + \hat{J}_-^2 = (\hat{J}_x + i\hat{J}_y)^2 + (\hat{J}_x - i\hat{J}_y)^2$, and the quantities $B_\alpha = h/8\pi^2cl_\alpha$ (in cm^{-1}) are the rotational constants.¹⁵² B_x , B_y and B_z are to be identified with the rigid-rotor rotational constants B , C and A , respectively, for the I^r representation which is appropriate for a near-prolate asymmetric top molecule.

The third term of equation (5.20) (which vanishes in a symmetric top) produces a matrix representation for \hat{H}^{rigid} that contains off-diagonal matrix elements with $\Delta K \pm 2$:

$$\langle J, K \pm 2 | \hat{J}_\pm^2 | JK \rangle = (\hbar^2/4)[J(J+1) - K(K \pm 1)]^{1/2} \times [J(J+1) - (K \pm 1)(K \pm 2)]^{1/2} \quad (5.21)$$

The matrix of \hat{H}^{rigid} can be factorized at once into blocks containing only odd or even values of K in the basis set (because no matrix elements of the type $\Delta K = \pm 1$ arise from (5.20)). These submatrices can be further factorized by taking sums and differences of the original symmetric top basis functions by means of a Wang similarity transformation¹⁵⁰:

$$\begin{aligned} |J, 0^+\rangle &= |J, 0\rangle \\ |J, K^\pm\rangle &= (1/\sqrt{2})\{|J, K\rangle \pm |J, -K\rangle\}, \quad (K > 0) \end{aligned} \quad (5.22)$$

The four submatrices constructed from the basis functions $|J, K^\pm\rangle$ are designated E^\pm and O^\pm for even and odd K , respectively.

To obtain a more accurate description of the rotational structure of an asymmetric top, centrifugal distortion must be considered. Centrifugal forces cause expansion (or stretching) and distortion in a rotating molecule, which lead to deviations from the rigid rotor Hamiltonian that increase with increasing angular momentum. The distortion Hamiltonian, H'_d , is therefore treated as a power series which adds higher degree angular momentum terms to the rigid rotor Hamiltonian:

$$\hat{H}'_d = (\hbar^4/4) \sum_{\alpha\beta\gamma\delta} \tau_{\alpha\beta\gamma\delta} J_\alpha J_\beta J_\gamma J_\delta \quad (5.23)$$

where $\tau_{\alpha\beta\gamma\delta}$ is the centrifugal distortion constant and α, β, γ and $\delta = x, y$ or z .¹⁵³ The number of terms in the general power series of equation (5.23) is 81. However, symmetry constraints reduce the number to 6 for an orthorhombic molecule (i.e., one which possesses at least two perpendicular planes of symmetry), since all terms vanish which are antisymmetric with respect to one or more of the symmetry operations. All of the remaining terms have only even powers of J , since those with odd powers change sign under the operation of Hermitian conjugation and time reversal.^{152,154} Further reduction of the orthorhombic Hamiltonian follows one of two routes: the "asymmetric top reduction" for the general asymmetric top, or the "symmetric top reduction" for asymmetric tops that are nearly symmetric. In the A-reduction the $J_+^4 + J_-^4$ term is eliminated, leaving only terms of the type $\Delta K = 0, \pm 2$, whereas the "S" reduced Hamiltonian retains $\Delta K = \pm 4, \pm 6, \dots$ terms. Aminoborane was treated using Watson's "A" reduced

Hamiltonian.¹⁵² Written out completely up to terms in J^8 , this is:¹⁵⁴

$$\begin{aligned}
 \hat{H}_{\text{rot}}^{(A)} = & B_x(A)\hat{J}_x^2 + B_y(A)\hat{J}_y^2 + B_z(A)\hat{J}_z^2 - \Delta_J\hat{J}^4 - \Delta_{JK}\hat{J}^2\hat{J}_z^2 - \Delta_K\hat{J}_z^4 \\
 & - 2\delta_J\hat{J}^2(\hat{J}_x^2 - \hat{J}_y^2) - \delta_K[\hat{J}_z^2(\hat{J}_x^2 - \hat{J}_y^2) + (\hat{J}_x^2 - \hat{J}_y^2)\hat{J}_z^2] + \Phi_J\hat{J}^6 \\
 & + \Phi_{JK}\hat{J}^4\hat{J}_z^2 + \Phi_{KJ}\hat{J}^2\hat{J}_z^4 + \Phi_K\hat{J}_z^6 + 2\phi_J\hat{J}^4(\hat{J}_x^2 - \hat{J}_y^2) \\
 & + \phi_{JK}\hat{J}^2[\hat{J}_z^2(\hat{J}_x^2 - \hat{J}_y^2) + (\hat{J}_x^2 - \hat{J}_y^2)\hat{J}_z^2] + \phi_K[\hat{J}_z^4(\hat{J}_x^2 - \hat{J}_y^2) \\
 & + (\hat{J}_x^2 - \hat{J}_y^2)\hat{J}_z^4] + L_J\hat{J}^8 + L_{JK}\hat{J}^6\hat{J}_z^2 + L_{JK}\hat{J}^4\hat{J}_z^4 + L_{KKJ}\hat{J}^2\hat{J}_z^6 \\
 & + L_K\hat{J}_z^8 + 2l_J\hat{J}^6(\hat{J}_x^2 - \hat{J}_y^2) + l_{JK}\hat{J}^4[\hat{J}_z^2(\hat{J}_x^2 - \hat{J}_y^2) + (\hat{J}_x^2 - \hat{J}_y^2)\hat{J}_z^2] \\
 & + l_{KJ}\hat{J}^2[\hat{J}_z^4(\hat{J}_x^2 - \hat{J}_y^2) + (\hat{J}_x^2 - \hat{J}_y^2)\hat{J}_z^4] + l_K[\hat{J}_z^6(\hat{J}_x^2 - \hat{J}_y^2) \\
 & + (\hat{J}_x^2 - \hat{J}_y^2)\hat{J}_z^6] \tag{5.24}
 \end{aligned}$$

The fitting program employed in this work to analyze the aminoborane ν_7 band included all matrix elements through to the off-diagonal sextic terms (J^6), plus the diagonal elements from the octic terms:

$$\begin{aligned}
 E_{K,K} = & \langle J,K | \hat{H}_{\text{rot}}^{(A)} | J,K \rangle \\
 = & [B_x(A) + B_y(A)]J(J+1)/2 + \{B_z(A) + [B_x(A) + B_y(A)]/2\}K^2 \\
 & - \Delta_JJ^2(J+1)^2 - \Delta_{JK}J(J+1)K^2 - \Delta_KK^4 + \Phi_JJ^3(J+1)^3 \\
 & + \Phi_{JK}J^2(J+1)^2K^2 + \Phi_{KJ}J(J+1)K^4 + \Phi_KK^6 + L_JJ^4(J+1)^4 \\
 & + L_{JK}J^3(J+1)^3K^2 + L_{JK}J^2(J+1)^2K^4 + L_{KKJ}J(J+1)K^6 + L_KK^8 \tag{5.25}
 \end{aligned}$$

$$\begin{aligned}
 E_{K\pm 2,K} = & \langle J,K\pm 2 | \hat{H}_{\text{rot}}^{(A)} | J,K \rangle \\
 = & \{[B_x(A) - B_y(A)]/4 - \delta_JJ(J+1) - \delta_K[(K\pm 2)^2 + K^2]/2 + \\
 & + \phi_JJ^2(J+1)^2 + \phi_{JK}J(J+1)[(K\pm 2)^2 + K^2]/2 + \phi_K[(K\pm 2)^4 + K^4]/2\} \\
 & \{[J(J+1 - K(K\pm 1))][J(J+1) - (K\pm 1)(K\pm 2)]\}^{1/2} \tag{5.26}
 \end{aligned}$$

V.E.2. Coriolis interaction.

The only perturbation present in the ν_7 fundamental, up to the limit of this analysis at $K_a' = 11$, is a Coriolis interaction globally affecting all levels to an extent which increases quadratically with the rotational quantum number K . A Coriolis interaction is the coupling of two vibrations by the rotation of the molecule. Put simply, certain combinations of vibrations generate an internal angular momentum which is part of the total angular momentum of the molecule.¹⁵⁵ In other words, rotational and vibrational motion are not separable. This internal, or vibrational, angular momentum is a vector, written Π , whose components are Π_x , Π_y and Π_z . To obtain the rotational Hamiltonian, the vibrational angular momentum must be subtracted from the total angular momentum, P , to give the rotational angular momentum. Instead of the simple form

$$\hat{H} = \hbar^2(\hat{J}_x^2/I_x + \hat{J}_y^2/I_y + \hat{J}_z^2/I_z)/2 + \hat{H}_{\text{vib}} \quad (5.27)$$

the rotation-vibration Hamiltonian (in joules) becomes^{155,156,157}:

$$\hat{H} = \hbar^2\{ [(\hat{P}_x - \hat{\Pi}_x)]^2/I_x + [(\hat{P}_y - \hat{\Pi}_y)]^2/I_y + [(\hat{P}_z - \hat{\Pi}_z)]^2/I_z \}/2 + \hat{H}_{\text{vib}} \quad (5.28)$$

$$\hat{H} = \hbar^2(\hat{P}_x^2/I_x + \hat{P}_y^2/I_y + \hat{P}_z^2/I_z)/2 - \hbar^2(\hat{\Pi}_x\hat{P}_x/I_x + \hat{\Pi}_y\hat{P}_y/I_y + \hat{\Pi}_z\hat{P}_z/I_z) + \hbar^2(\hat{\Pi}_x^2/I_y + \hat{\Pi}_y^2/I_y + \hat{\Pi}_z^2/I_z) + \hat{H}_{\text{vib}} \quad (5.29)$$

The first term in equation (5.29), independent of the vibrational angular momentum, is the rigid rotor Hamiltonian, while the third term, independent of rotational angular momentum, affects only the vibrational energy. The second term, a function of both the vibrational and the total angular momenta, represents Coriolis coupling. The Coriolis interaction can therefore be considered as the scalar product of the rotational and vibrational angular momenta,

the magnitude of which increases the faster the molecule rotates and the nearer the vibrations approach degeneracy. According to Jahn's rule two normal coordinates Q_k and Q_l are coupled via an α -axis Coriolis interaction only if the product of their irreducible representations is of the same symmetry as P_α .¹⁵⁷ Thus the ν_7 (B_1) fundamental at 1005 cm^{-1} undergoes an a-axis Coriolis interaction with the nearby ν_{11} (B_2) fundamental at 1122 cm^{-1} , since $B_1 \times B_2$ gives the A_2 symmetry species (corresponding to rotation around the a-axis). The ν_{11} vibration in turn interacts with ν_5 (A_1) at 1145 cm^{-1} (the BH_2 symmetric bending vibration) by a c-axis Coriolis interaction, while the direct product of the ν_7 and ν_5 symmetries produces B_1 symmetry for a b-axis Coriolis interaction. Each of these three vibrations is therefore affected by the other two.

The vibrational angular momentum, in units of \hbar , is defined as¹⁵⁵:

$$\Pi_\alpha = \sum_{k,l} \zeta_{kl}^{(\alpha)} q_k p_l (\omega_l/\omega_k)^{1/2} \quad (5.30)$$

where the normal coordinate Q and its momentum conjugate, $P = -i\hbar\partial/\partial Q$, are expressed in the dimensionless forms, q and p :

$$q_k = \gamma_k^{1/2} Q_k \quad (5.31)$$

$$p_k = P_k/\gamma_k^{1/2}\hbar \quad (5.32)$$

$$\gamma_k = 2\pi c\omega_k/h \quad (5.33)$$

The Coriolis coupling constant, $\zeta_{kl}^{(\alpha)}$, is a measure of the angular momentum about the α -axis induced by the interaction of two normal vibrational modes, Q_k and Q_l , having frequencies (in cm^{-1}) of ω_k and ω_l .

V.F. Band Analysis and Discussion.

Aminoborane's BH_2 -wag forms a C-type band whose appearance is characterized by a central spike, due to the asymmetry of the molecule causing low-K Q branches to pile up about the band origin (see Fig. 5.5).¹⁵⁸ At high resolution (Fig. 5.6), it can be seen that the spike is composed largely of the two lowest Q branches, PQ_1 and RQ_0 (using the notation $\Delta K_a \Delta J_{K_a}$). The lines of the ^{11}B form of NH_2BH_2 were assigned by a process of successive refinement of the upper state constants. The ground state constants were held fixed at the best values available so far,¹³³ and the structure of the band was calculated using a prediction program. As the upper state constants were improved the prediction became more accurate so that more lines could be assigned. The assignments were limited to a maximum upper state value of K_a equal to 11, as a result of the Boltzmann distribution at room temperature. Lines of ammonia, present as an impurity in the spectrum, were used as an internal standard for absolute frequency calibration. The NH_3 frequencies were taken from the diode laser study by Job *et al.*¹⁵⁹

A complete set of molecular constants cannot be given at this time because the ν_5 fundamental has not yet been observed directly since its dipole derivative is very small. Without lines from ν_5 , it is extremely difficult to analyze the ν_5 - ν_7 - ν_{11} Coriolis interactions. However, it is hoped that a sufficient portion of the ν_5 band can be assigned in the near future to allow a fit to be made. The data were fitted to the matrix elements in equation (5.25) and (5.26) by means of a least-squares program written by Dr. Wyn Lewis-Bevan. In this program the Hellmann-Feynman theorem is used to calculate the

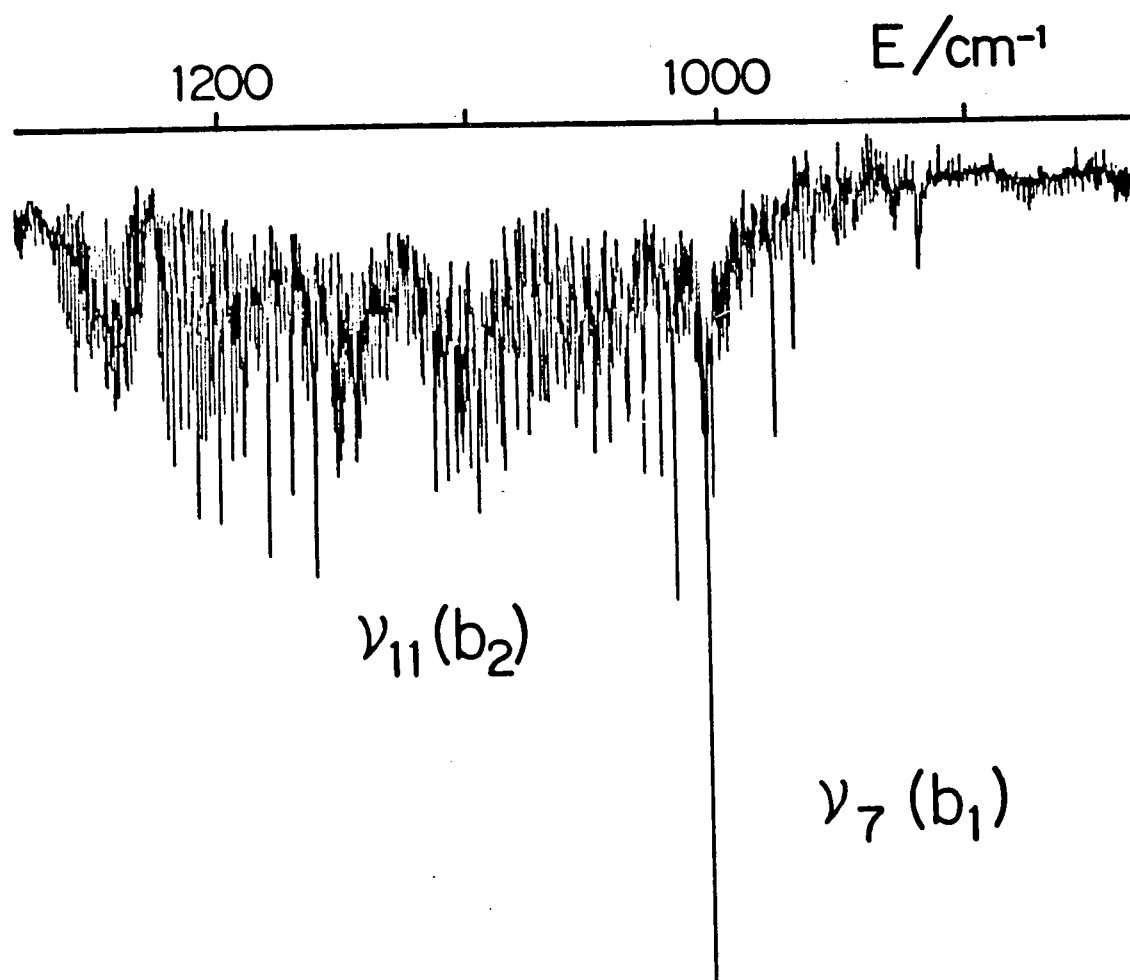


Fig. 5.5. NH_2BH_2 spectrum of the ν_7 band and the ν_5 and ν_{11} bands with which it undergoes Coriolis interactions.

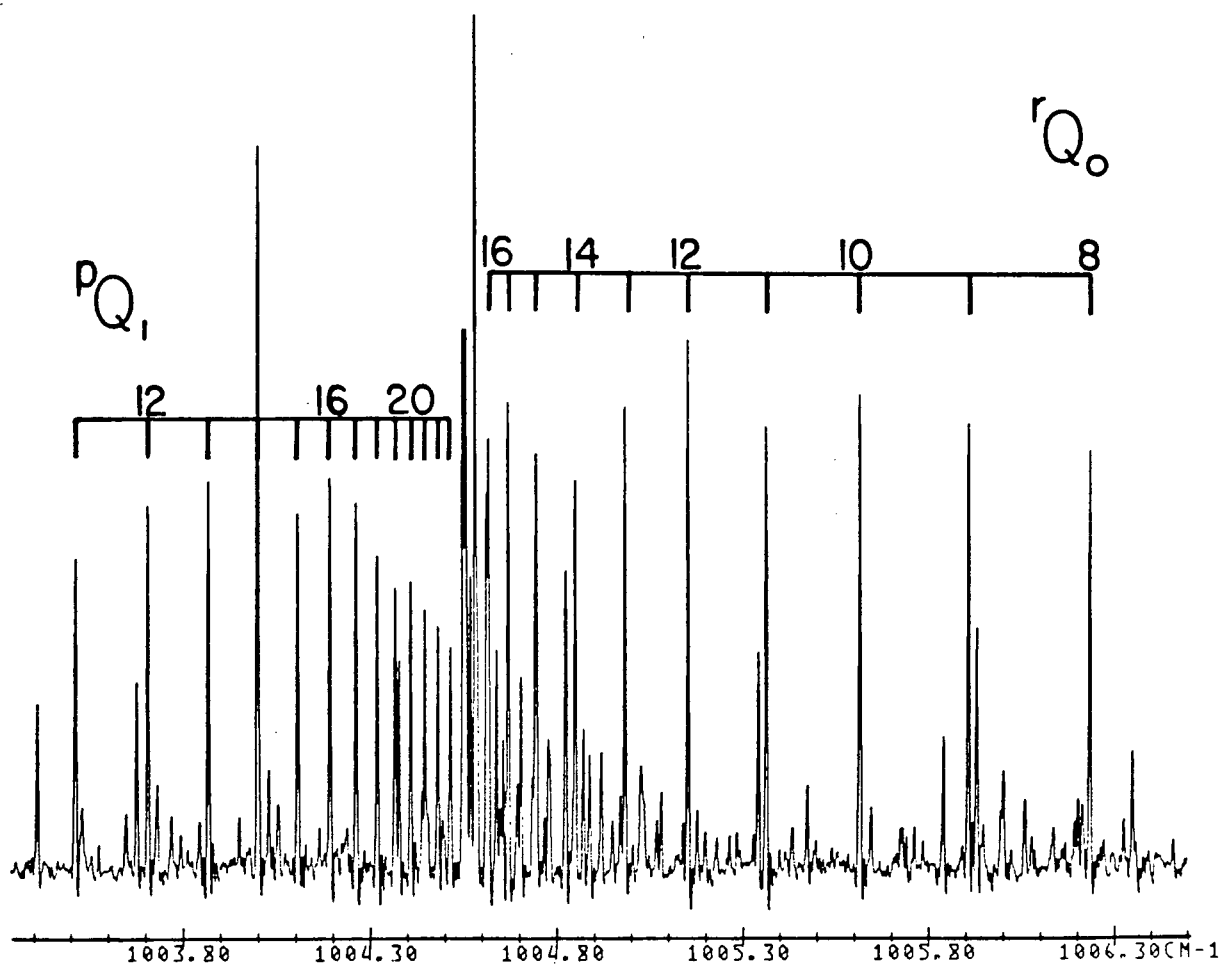


Fig. 5.6. Center of the ν_7 band of $\text{NH}_2^{11}\text{BH}_2$.

derivatives of the energy levels with respect to the parameters (see Section IV.C). The computations were performed on the University of British Columbia Computing Centre Amdahl 470 V/8 mainframe computer.

Two sets of molecular constants appear in Table 5.IV. Both were obtained by ignoring the Coriolis perturbation, but one was produced from a reduced data set of 606 transitions with a maximum K_a' of 6. In the excited state, all constants were floated except the off-diagonal sextics, namely ϕ_J , ϕ_{JK} , and ϕ_K . Eliminating all K_a' values above six reduces the standard deviation in the line positions from 0.001 cm^{-1} to 0.0003 cm^{-1} . This is expected from the K dependence of the Coriolis coupling. The standard errors of most constants improved when the data set was reduced, except for very small ones ($\approx 10^{-8} \text{ cm}^{-1}$) and with matrix elements dependent on K . Note in particular that Φ_{KJ} , L_{KKJ} and L_K , which accompany the variables K^6 , $J(J+1)K^6$ and K^8 , are very poorly determined in the reduced data set. This reflects the importance of a wide range of K values in determining terms containing high powers of K .

Without including Coriolis terms in the Hamiltonian, the constants in Table 5.IV are not true values. Rather, they comprise internally consistent sets which have incorporated the effects of the Coriolis interactions in order to fit the data. This is particularly evident in that the Δ_K and δ_K constants are negative, rather than positive as they should be. Since Δ_K and δ_K accompany the variables $-K^4$ and $-[(K\pm 2)^2 + K^2]$, these terms are the most sensitive to Coriolis interactions. An estimate of -0.406 was made for the ν_7 - ν_{11} a-axis Coriolis coupling constant ($\zeta_{7,11}$) from the ν_7

Table 5.IV. Molecular constants of the ν_7 band of $\text{NH}_2^{11}\text{BH}_2$ (in cm^{-1}), for both the full and reduced ($K_a' \leq 6$) data sets. The numbers in parentheses denote one standard deviation in units of the last significant figures. Where a ground state constant is blank, it was fixed to zero.

	EXCITED STATE		GROUND STATE
	Reduced	Full	
T_0	1004.68420(5)	1004.6831(2)	
A	4.51446(2)	4.51512(3)	4.610569(8)
B	0.9060531(8)	0.90605(2)	0.916897(2)
C	0.7646658(7)	0.76467(2)	0.763137(2)
Δ_J	$1.173(1) \times 10^{-6}$	$1.161(3) \times 10^{-6}$	$1.542(2) \times 10^{-6}$
Δ_{JK}	$1.04(1) \times 10^{-5}$	$1.15(2) \times 10^{-5}$	$9.87(3) \times 10^{-6}$
Δ_K	$-1.17(3) \times 10^{-4}$	$-0.68(1) \times 10^{-4}$	$8.692(8) \times 10^{-5}$
δ_J	$1.116(6) \times 10^{-7}$	$1.06(2) \times 10^{-7}$	$2.86(3) \times 10^{-7}$
δ_K	$-1.197(6) \times 10^{-5}$	$-1.89(2) \times 10^{-5}$	$1.016(2) \times 10^{-5}$
Φ_{JK}	$6.7(2.2) \times 10^{-10}$	$-3.3(2) \times 10^{-10}$	
Φ_{KJ}	$-4.3(7) \times 10^{-8}$	$5.7(4) \times 10^{-8}$	$7.0(32) \times 10^{-11}$
Φ_K	$-6.7(1.6) \times 10^{-7}$	$3.7(2) \times 10^{-7}$	$5.94(30) \times 10^{-9}$
L_{JK}	$-2.5(7) \times 10^{-11}$	$6.4(3) \times 10^{-11}$	
L_{KKJ}	$4.6(1.3) \times 10^{-10}$		
L_K	$3.8(2.3) \times 10^{-9}$		
σ	0.0003	0.001	

and v_{11} data.¹⁶⁰ This is in good agreement with a force field estimate of -0.40 .¹⁶¹

Appendix I. NbN 3Φ - 3Δ Correlation Matrix

	B'	A _D '	λ _D '	A'	λ'	γ'	D'	h ₋₁ '	h ₀ '	h ₊₁ '	b'	e ² qQ'
B'	1	-0.462	0.105	0.028	-0.107	0.034	0.055	-0.002	0.039	0.022	0.025	0.013
A _D '		1	-0.159	-0.258	-0.158	0.333	0.157	-0.032	0.022	0.047	-0.319	-0.004
λ _D '			1	0.248	-0.273	0.004	0.049	-0.072	0.242	-0.143	0.133	-0.005
A'				1	0.241	-0.515	-0.235	0.012	-0.073	-0.004	0.671	0.049
λ'					1	-0.573	-0.187	0.124	-0.391	0.151	0.392	0.011
γ'						1	0.517	-0.117	0.121	-0.011	-0.706	-0.013
D'							1	0.002	0.066	0.151	-0.119	-0.016
h ₋₁ '								1	-0.027	-0.004	-0.002	-0.068
h ₀ '									1	-0.027	-0.075	-0.002
h ₊₁ '										1	0.101	-0.018
b'											1	0.041
e ² qQ'												1

	T_0	B''	A_D''	λ_D''	A''	λ''	γ''	D''	h_{-1}''	h_0''	h_{+1}''	$b_{-1/0}''$	$b_{0/+1}''$
B'	-0.038	0.995	-0.462	-0.017	0.026	-0.113	0.011	-0.131	-0.025	0.032	0.021	0.027	0.023
A_D'	-0.278	-0.464	0.974	-0.181	-0.275	-0.100	0.272	0.232	0.013	0.030	0.027	-0.318	-0.318
λ_D'	-0.108	0.091	-0.206	0.884	0.250	-0.255	-0.168	-0.257	-0.068	0.195	-0.106	0.127	0.146
A'	0.152	0.026	-0.355	0.396	0.999	0.235	-0.882	-0.455	-0.026	-0.078	0.041	0.670	0.672
λ'	0.592	-0.091	-0.060	-0.114	0.242	0.965	-0.268	-0.067	0.084	-0.345	0.150	0.398	0.377
γ'	-0.902	-0.004	0.227	-0.267	-0.520	-0.382	0.680	0.284	-0.063	0.123	-0.050	-0.701	-0.701
D'	-0.512	-0.022	0.089	-0.145	-0.247	-0.053	0.246	0.518	0.017	0.077	0.134	-0.116	-0.012
h_{-1}'	0.111	0.008	-0.017	-0.031	0.021	0.106	-0.060	0.152	0.848	-0.016	0.003	0.010	0.002
h_0'	-0.116	0.036	0.005	0.221	-0.073	-0.415	0.072	0.105	-0.011	0.910	-0.012	-0.082	-0.062
h_{+1}'	0.034	0.034	0.073	-0.110	-0.020	0.151	0.056	0.356	0.000	-0.006	0.933	0.096	0.081
b'	0.408	0.025	-0.350	0.312	0.670	0.330	-0.877	-0.191	-0.050	-0.078	0.153	0.996	0.994
e^2qQ'	-0.016	0.015	-0.017	-0.003	0.047	0.018	-0.058	-0.008	-0.047	0.001	-0.012	0.043	0.036
T_0	1	0.007	-0.097	0.147	0.159	0.368	-0.301	-0.110	0.074	-0.112	0.050	0.401	0.400
B''		1	-0.453	-0.024	0.025	-0.108	0.012	-0.130	-0.017	0.028	0.031	0.027	0.022
A_D''			1	-0.197	-0.364	-0.045	0.346	0.269	0.028	0.014	0.045	-0.350	-0.352
λ_D''				1	0.397	-0.176	-0.351	-0.308	-0.042	0.187	-0.069	0.307	0.324
A''					1	0.234	-0.883	-0.460	-0.021	-0.078	0.028	0.669	0.671
λ''						1	-0.221	-0.048	0.069	-0.365	0.148	0.339	0.316
γ''							1	0.442	-0.005	0.078	-0.008	-0.877	-0.880
D''								1	0.149	0.121	0.318	-0.186	-0.200
h_{-1}''									1	-0.010	-0.004	-0.051	-0.051
h_0''										1	-0.011	-0.079	-0.078
h_{+1}''											1	0.153	0.150
$b_{-1/0}''$												1	0.993
$b_{0/+1}''$													1

APPENDIX II. Transitions of the ${}^3\Phi\text{-}{}^3\Delta$ System of NbN.^aAppendix II.A. ${}^3\Phi_2\text{-}{}^3\Delta_1$.

R			Q			P					
J"	F"		J"	F"		J"	F"				
1	4.5	pR	16146.4540	2	5.5	qQ	16144.7074	3	6.5	pP	16141.7114
1	4.5	qR	16146.5474	2	6.5	qQ	16144.9179	3	7.5	pP	16141.8930
1	4.5	rR	16146.6629	3	5.5	qQ	16144.5975	4	3.5	pP	16140.4155
1	5.5	pR	16146.7154	3	6.5	qQ	16144.6982	4	4.5	pP	16140.4653
1	5.5	qR	16146.8310	3	7.5	qQ	16144.8162	4	5.5	pP	16140.5293
1	5.5	rR	16146.9692	4	5.5	qQ	16144.5255	5	4.5	pP	16139.4474
2	2.5	pR	16147.3250	4	6.5	qQ	16144.5854	5	5.5	pP	16139.4858
2	2.5	qR	16147.3517	4	8.5	qQ	16144.7337	5	6.5	pP	16139.5321
2	2.5	co	16147.3705	5	4.5	qQ	16144.4281	5	7.5	pP	16139.5875
2	2.5	rR	16147.3890	5	5.5	qQ	16144.4622*	5	8.5	pP	16139.6506
2	3.5	pR	16147.3833	5	6.5	qQ	16144.5010	5	9.5	pP	16139.7216
2	3.5	qR	16147.4205	5	7.5	qQ	16144.5462	6	3.5	pP	16138.3884*
2	3.5	co	16147.4442	5	8.5	qQ	16144.5975	6	4.5	pP	16138.4083*
2	3.5	rR	16147.4682	5	9.5	qQ	16144.6555	6	5.5	pP	16138.4339
2	4.5	pR	16147.4643	6	5.5	qQ	16144.3961*	6	6.5	pP	16138.4648
2	4.5	qR	16147.5121	6	6.5	qQ	16144.4232*	6	7.5	pP	16138.5015
2	4.5	rR	16147.5698	6	7.5	qQ	16144.4556*	6	8.5	pP	16138.5435
2	5.5	qR	16147.6272	6	9.5	qQ	16144.5314	6	9.5	pP	16138.5909
2	5.5	rR	16147.6948	6	10.5	qQ	16144.5764	6	10.5	pP	16138.6441
2	6.5	qR	16147.7669	7	2.5	qQ	16144.2829	7	2.5	pP	16137.3347
2	6.5	rR	16147.8436	7	3.5	qQ	16144.2937	7	3.5	pP	16137.3449
3	1.5	pR	16148.3506	7	4.5	qQ	16144.3069*	7	4.5	pP	16137.3592
3	1.5	qR	16148.3604*	7	5.5	qQ	16144.3241	7	5.5	pP	16137.3773
3	1.5	co	16148.3684*	7	6.5	qQ	16144.3445*	7	6.5	pP	16137.3992
3	1.5	rR	16148.3763	7	7.5	qQ	16144.3674	7	7.5	pP	16137.4251
3	2.5	pR	16148.3712*	7	8.5	qQ	16144.3938	7	8.5	pP	16137.4548
3	2.5	qR	16148.3873	7	9.5	qQ	16144.4232	7	9.5	pP	16137.4886
3	2.5	co	16148.3985	7	10.5	qQ	16144.4556	7	10.5	pP	16137.5263
3	2.5	rR	16148.4098	7	11.5	qQ	16144.4915	7	11.5	pP	16137.5678
3	3.5	pR	16148.4032	8	3.5	qQ	16144.2216	8	3.5	pP	16136.2870
3	3.5	qR	16148.4257	8	4.5	qQ	16144.2325	8	4.5	pP	16136.2976
3	3.5	co	16148.4399	8	5.5	qQ	16144.2450	8	5.5	pP	16136.3108
3	3.5	rR	16148.4541	8	6.5	qQ	16144.2600	8	6.5	pP	16136.3270
3	4.5	pR	16148.4469	8	7.5	qQ	16144.2781*	8	7.5	pP	16136.3461
3	4.5	qR	16148.4755	8	8.5	qQ	16144.2976	8	8.5	pP	16136.3682
3	4.5	co	16148.4930	8	9.5	qQ	16144.3198	8	9.5	pP	16136.3931
3	4.5	rR	16148.5103	8	10.5	qQ	16144.3445	8	10.5	pP	16136.4211
3	5.5	qR	16148.5375	8	11.5	qQ	16144.3719	8	11.5	pP	16136.4520
3	5.5	co	16148.5582	8	12.5	qQ	16144.4024	8	12.5	pP	16136.4858
3	5.5	rR	16148.5782	9	4.5	qQ	16144.1476*	9	4.5	pP	16135.2249
3	6.5	qR	16148.6118	9	5.5	qQ	16144.1575*	9	5.5	pP	16135.2350
3	6.5	rR	16148.6583	9	6.5	co	16144.1647*	9	6.5	pP	16135.2472
3	7.5	qR	16148.6996	9	6.5	qQ	16144.1695*	9	7.5	pP	16135.2616
3	7.5	rR	16148.7512	9	6.5	co	16144.1750*	9	8.5	pP	16135.2784
4	0.5	rR	16149.3518	9	7.5	qQ	16144.1830	9	9.5	pP	16135.2974
4	1.5	qR	16149.3553	9	7.5	co	16144.1888*	9	10.5	pP	16135.3187
4	1.5	co	16149.3607	9	8.5	qQ	16144.1989	9	11.5	pP	16135.3422
4	1.5	rR	16149.3661	9	8.5	co	16144.2049*	9	12.5	pP	16135.3681
4	2.5	qR	16149.3725	9	9.5	co	16144.2092*	9	13.5	pP	16135.3961
4	2.5	co	16149.3801	9	9.5	qQ	16144.2157				
4	2.5	rR	16149.3875	9	9.5	co	16144.2226*				
4	3.5	qR	16149.3969	9	10.5	co	16144.2279*				
4	3.5	co	16149.4064	9	10.5	qQ	16144.2350				
4	3.5	rR	16149.4159	9	10.5	co	16144.2431*				
4	4.5	qR	16149.4282	9	11.5	co	16144.2485*				
4	4.5	co	16149.4397	9	11.5	qQ	16144.2562				
4	4.5	rR	16149.4514	9	11.5	co	16144.2645*				
4	5.5	qR	16149.4670	9	12.5	co	16144.2710*				
4	5.5	co	16149.4807	9	12.5	qQ	16144.2794				

Appendix II.A, continued. $3\Phi_2-3\Delta_1$.

<u>R</u>				<u>Q</u>				<u>P</u>
J"	F"			J"	F"			
4	5.5	rR	16149.4943	9	13.5	co	16144.2947*	
4	6.5	qR	16149.5134	9	13.5	qQ	16144.3047*	
4	6.5	co	16149.5292	10	5.5	qQ	16144.0616*	
4	6.5	rR	16149.5446	10	6.5	qQ	16144.0707*	
4	7.5	qR	16149.5678	10	6.5	co	16144.0749*	
4	7.5	rR	16149.6026	10	7.5	qQ	16144.0815*	
4	8.5	qR	16149.6298	10	8.5	co	16144.0888*	
4	8.5	rR	16149.6681	10	8.5	qQ	16144.0937	
5	1.5	co	16150.3267	10	8.5	co	16144.0989*	
5	1.5	rR	16150.3306	10	9.5	co	16144.1018*	
5	2.5	qR	16150.3348	10	9.5	qQ	16144.1075	
5	2.5	co	16150.3401	10	9.5	co	16144.1132*	
5	2.5	rR	16150.3454	10	10.5	co	16144.1167*	
5	3.5	qR	16150.3513	10	10.5	qQ	16144.1226	
5	3.5	co	16150.3581	10	10.5	co	16144.1289*	
5	3.5	rR	16150.3649	10	11.5	co	16144.1328*	
5	4.5	qR	16150.3726	10	11.5	qQ	16144.1393	
5	4.5	co	16150.3808	10	12.5	co	16144.1507*	
5	4.5	rR	16150.3891	10	12.5	qQ	16144.1575	
5	5.5	qR	16150.3989	10	13.5	qQ	16144.1775	
5	5.5	co	16150.4086	10	14.5	qQ	16144.1989	
5	5.5	rR	16150.4184	11	7.5	co	16143.9767	
5	6.5	qR	16150.4302	11	8.5	co	16143.9783	
5	6.5	co	16150.4414	11	8.5	qQ	16143.9824	
5	6.5	rR	16150.4528	11	8.5	co	16143.9869	
5	7.5	qR	16150.4669	11	9.5	co	16143.9889	
5	7.5	co	16150.4795	11	9.5	qQ	16143.9933	
5	7.5	rR	16150.4921	11	9.5	co	16143.9982	
5	8.5	qR	16150.5088	11	10.5	co	16144.0004	
5	8.5	co	16150.5228	11	10.5	qQ	16144.0053	
5	8.5	rR	16150.5364	11	10.5	co	16144.0106	
5	9.5	rR	16150.5862	11	11.5	co	16144.0134	
6	1.5	rR	16151.2772	11	11.5	qQ	16144.0188	
6	2.5	co	16151.2838	11	11.5	co	16144.0246	
6	2.5	rR	16151.2878	11	12.5	co	16144.0278	
6	3.5	qR	16151.2917	11	12.5	qQ	16144.0334	
6	3.5	co	16151.2968	11	12.5	co	16144.0396	
6	3.5	rR	16151.3019	11	13.5	co	16144.0431	
6	4.5	qR	16151.3071	11	13.5	qQ	16144.0494*	
6	4.5	co	16151.3133	11	14.5	qQ	16144.0666*	
6	4.5	rR	16151.3195	11	15.5	qQ	16144.0852	
6	5.5	qR	16151.3260	12	7.5	co	16143.8591	
6	5.5	co	16151.3332	12	8.5	co	16143.8609	
6	5.5	rR	16151.3407	12	8.5	co	16143.8671	
6	6.5	qR	16151.3485	12	9.5	co	16143.8684	
6	6.5	co	16151.3569	12	9.5	qQ	16143.8722	
6	6.5	rR	16151.3652	12	9.5	co	16143.8763	
6	7.5	qR	16151.3748	12	10.5	co	16143.8778	
6	7.5	co	16151.3843	12	10.5	qQ	16143.8819	
6	7.5	rR	16151.3937	12	10.5	co	16143.8864	
6	8.5	qR	16151.4046	12	11.5	co	16143.8882	
6	8.5	co	16151.4153	12	11.5	qQ	16143.8928	
6	8.5	rR	16151.4256	12	11.5	co	16143.8977	
6	9.5	qR	16151.4385	12	12.5	co	16143.8997	
6	9.5	co	16151.4501	12	12.5	qQ	16143.9046	
6	9.5	rR	16151.4613	12	12.5	co	16143.9097	
6	10.5	rR	16151.5009	12	13.5	co	16143.9121	
7	2.5	rR	16152.2180	12	13.5	qQ	16143.9175	
7	3.5	co	16152.2246	12	13.5	co	16143.9230	
7	3.5	rR	16152.2287	12	14.5	co	16143.9257	
7	4.5	co	16152.2370	12	14.5	qQ	16143.9315	
7	4.5	rR	16152.2419	12	14.5	co	16143.9374	
7	5.5	qR	16152.2461	12	15.5	co	16143.9405	
7	5.5	co	16152.2521	12	15.5	qQ	16143.9464	
7	5.5	rR	16152.2578	12	15.5	co	16143.9525	

Appendix II.A, continued. ${}^3\Phi_2-{}^3\Delta_1$.

R				Q				P
J"	F"			J"	F"			
7	6.5	qR	16152.2632	12	16.5	co	16143.9559	
7	6.5	co	16152.2697	12	16.5	qQ	16143.9626*	
7	6.5	rR	16152.2762	13	9.5	qQ	16143.7435	
7	7.5	qR	16152.2827	13	10.5	qQ	16143.7524	
7	7.5	co	16152.2900	13	10.5	co	16143.7553	
7	7.5	rR	16152.2972	13	11.5	co	16143.7562	
7	8.5	qR	16152.3047	13	11.5	qQ	16143.7602	
7	8.5	co	16152.3130	13	12.5	qQ	16143.7698	
7	8.5	rR	16152.3210	13	12.5	co	16143.7744	
7	9.5	qR	16152.3298	13	13.5	co	16143.7756	
7	9.5	co	16152.3388	13	13.5	qQ	16143.7801	
7	9.5	rR	16152.3477	13	13.5	co	16143.7851	
7	10.5	qR	16152.3578	13	14.5	co	16143.7870	
7	10.5	co	16152.3676	13	14.5	qQ	16143.7916	
7	10.5	rR	16152.3772	13	14.5	co	16143.7966	
7	11.5	co	16152.3995	13	15.5	co	16143.7986	
7	11.5	rR	16152.4096	13	15.5	qQ	16143.8036	
8	3.5	rR	16153.1443	13	15.5	co	16143.8099	
8	4.5	co	16153.1507	13	16.5	co	16143.8113	
8	4.5	rR	16153.1546	13	16.5	qQ	16143.8168	
8	5.5	co	16153.1621	13	17.5	qQ	16143.8307	
8	5.5	rR	16153.1668	14	10.5	qQ	16143.6131	
8	6.5	co	16153.1758	14	11.5	qQ	16143.6199	
8	6.5	rR	16153.1810	14	12.5	qQ	16143.6279	
8	7.5	co	16153.1914	14	13.5	qQ	16143.6365	
8	7.5	rR	16153.1973	14	14.5	qQ	16143.6459	
8	8.5	co	16153.2091	14	15.5	qQ	16143.6557	
8	8.5	rR	16153.2157	14	16.5	qQ	16143.6662	
8	9.5	co	16153.2290	14	17.5	qQ	16143.6778	
8	9.5	rR	16153.2362	14	18.5	qQ	16143.6901	
8	10.5	qR	16153.2432	15	10.5	qQ	16143.4662*	
8	10.5	co	16153.2511	15	11.5	qQ	16143.4721*	
8	10.5	rR	16153.2589	15	12.5	qQ	16143.4787	
8	11.5	co	16153.2754	15	13.5	qQ	16143.4854	
				15	14.5	qQ	16143.4931	
				15	15.5	qQ	16143.5011	
				15	16.5	qQ	16143.5100	
				15	17.5	qQ	16143.5193	
				15	18.5	qQ	16143.5293	
				15	19.5	qQ	16143.5401	
				16	12.5	qQ	16143.3211*	
				16	13.5	qQ	16143.3267	
				16	14.5	qQ	16143.3331	
				16	15.5	qQ	16143.3393	
				16	16.5	qQ	16143.3465	
				16	17.5	qQ	16143.3544	
				16	18.5	qQ	16143.3625	
				16	19.5	qQ	16143.3713	
				16	20.5	qQ	16143.3805	
				17	12.5	qQ	16143.1555	
				17	13.5	qQ	16143.1602	
				17	14.5	qQ	16143.1650	
				17	15.5	qQ	16143.1706	
				17	16.5	qQ	16143.1763	
				17	17.5	qQ	16143.1824	
				17	18.5	qQ	16143.1890	
				17	19.5	qQ	16143.1963	
				17	20.5	qQ	16143.2037	
				17	21.5	qQ	16143.2118	
				18	13.5	qQ	16142.9849	
				18	14.5	qQ	16142.9887	
				18	15.5	qQ	16142.9932	
				18	16.5	qQ	16142.9978	
				18	17.5	qQ	16143.0028	
				18	18.5	qQ	16143.0081	

Appendix II.A, continued. ${}^3\Phi_2\text{-}{}^3\Delta_1$.

<u>R</u>		<u>Q</u>	<u>P</u>
	J*	F*	
18	19.5	qQ	16143.0140
18	20.5	qQ	16143.0200
18	21.5	qQ	16143.0266
18	22.5	qQ	16143.0336
19	15.5	qQ	16142.8074
19	22.5	qQ	16142.8404
19	23.5	qQ	16142.8462
20	15.5	qQ	16142.6139
20	16.5	qQ	16142.6166
20	17.5	qQ	16142.6194
20	18.5	qQ	16142.6230
20	19.5	qQ	16142.6262
20	20.5	qQ	16142.6301
20	21.5	qQ	16142.6341
20	22.5	qQ	16142.6387
20	23.5	qQ	16142.6433
20	24.5	qQ	16142.6486
21	16.5	qQ	16142.4132
21	17.5	qQ	16142.4152
21	18.5	qQ	16142.4182
21	19.5	qQ	16142.4207
21	20.5	qQ	16142.4233
21	21.5	qQ	16142.4261
21	22.5	qQ	16142.4299
21	23.5	qQ	16142.4337
21	24.5	qQ	16142.4378
21	25.5	qQ	16142.4417
31	27.5	qQ	16139.8508*
31	28.5	qQ	16139.8488*
31	29.5	qQ	16139.8467*
31	30.5	qQ	16139.8423*
31	31.5	qQ	16139.8408*
31	32.5	qQ	16139.8382*
31	33.5	qQ	16139.8366*
32	28.5	qQ	16139.5394*
32	29.5	qQ	16139.5368*
32	31.5	qQ	16139.5321*
32	32.5	qQ	16139.5293*
32	33.5	qQ	16139.5268*
32	34.5	qQ	16139.5242*
32	35.5	qQ	16139.5217*
33	28.5	qQ	16139.2199
33	29.5	qQ	16139.2171
33	30.5	qQ	16139.2143
33	31.5	qQ	16139.2113
33	32.5	qQ	16139.2083
33	33.5	qQ	16139.2053
33	34.5	qQ	16139.2023
33	35.5	qQ	16139.1994
33	36.5	qQ	16139.1966
33	37.5	qQ	16139.1938
34	29.5	qQ	16138.8863
34	30.5	qQ	16138.8832
34	31.5	qQ	16138.8798
34	32.5	qQ	16138.8764
34	33.5	qQ	16138.8730
34	34.5	qQ	16138.8696
34	35.5	qQ	16138.8662
34	36.5	qQ	16138.8628
34	37.5	qQ	16138.8596
34	38.5	qQ	16138.8562
35	32.5	qQ	16138.5376*
35	34.5	qQ	16138.5299
35	35.5	qQ	16138.5261
35	36.5	qQ	16138.5222

Appendix II.A, continued. ${}^3\Phi_2-{}^3\Delta_1$.

<u>R</u>		<u>Q</u>	<u>P</u>
J"	F"		
35	37.5	qQ	16138.5184
35	38.5	qQ	16138.5147
35	39.5	qQ	16138.5110
36	31.5	qQ	16138.1934
36	32.5	qQ	16138.1893
36	33.5	qQ	16138.1853
36	34.5	qQ	16138.1812
36	35.5	qQ	16138.1773
36	36.5	qQ	16138.1729
36	37.5	qQ	16138.1686
36	38.5	qQ	16138.1642
36	39.5	qQ	16138.1601
36	40.5	qQ	16138.1559
37	32.5	qQ	16137.8315
37	33.5	qQ	16137.8270
37	34.5	qQ	16137.8226
37	35.5	qQ	16137.8181
37	36.5	qQ	16137.8136
37	37.5	qQ	16137.8087
37	38.5	qQ	16137.8044
37	39.5	qQ	16137.7995
37	40.5	qQ	16137.7950
37	41.5	qQ	16137.7904
38	33.5	qQ	16137.4595
38	34.5	qQ	16137.4548*
38	35.5	qQ	16137.4505
38	36.5	qQ	16137.4449
38	37.5	qQ	16137.4403
38	38.5	qQ	16137.4352
38	39.5	qQ	16137.4305
38	40.5	qQ	16137.4251*
38	41.5	qQ	16137.4199
38	42.5	qQ	16137.4150
39	34.5	qQ	16137.0771
39	35.5	qQ	16137.0720
39	36.5	qQ	16137.0669
39	37.5	qQ	16137.0617
39	38.5	qQ	16137.0563
39	39.5	qQ	16137.0510
39	40.5	qQ	16137.0455
39	41.5	qQ	16137.0403
39	42.5	qQ	16137.0346
39	43.5	qQ	16137.0293
40	35.5	qQ	16136.6841
40	36.5	qQ	16136.6787
40	37.5	qQ	16136.6732
40	38.5	qQ	16136.6677
40	39.5	qQ	16136.6619
40	40.5	qQ	16136.6562
40	41.5	qQ	16136.6505
40	42.5	qQ	16136.6444
40	43.5	qQ	16136.6387
40	44.5	qQ	16136.6329
41	36.5	qQ	16136.2810
41	37.5	qQ	16136.2749
41	38.5	qQ	16136.2689
41	39.5	qQ	16136.2631
41	40.5	qQ	16136.2569
41	41.5	qQ	16136.2510
41	42.5	qQ	16136.2448
41	43.5	qQ	16136.2387
41	44.5	qQ	16136.2324
41	45.5	qQ	16136.2261
42	37.5	qQ	16135.8672

Appendix II.A, continued. $3\Phi_2-3\Delta_1$.

R		Q		P
J"	F"	J"	F"	
42	38.5	qQ	16135.8612	
42	39.5	qQ	16135.8549	
42	40.5	qQ	16135.8485	
42	41.5	qQ	16135.8421	
42	42.5	qQ	16135.8356	
42	43.5	qQ	16135.8293	
42	44.5	qQ	16135.8227	
42	45.5	qQ	16135.8158	
42	46.5	qQ	16135.8091	
43	38.5	qQ	16135.4427	
43	39.5	qQ	16135.4362	
43	40.5	qQ	16135.4298	
43	41.5	qQ	16135.4230	
43	42.5	qQ	16135.4164	
43	43.5	qQ	16135.4093	
43	44.5	qQ	16135.4024	
43	45.5	qQ	16135.3961	
43	46.5	qQ	16135.3889	
43	47.5	qQ	16135.3816	
44	39.5	qQ	16135.0081	
44	40.5	qQ	16135.0014	
44	41.5	qQ	16134.9947	
44	42.5	qQ	16134.9875	
44	43.5	qQ	16134.9804	
44	44.5	qQ	16134.9733	
44	45.5	qQ	16134.9664	
44	46.5	qQ	16134.9588	
44	47.5	qQ	16134.9515	
44	48.5	qQ	16134.9442	

Appendix II.B. $3\Phi_3-3\Delta_2$.

J"	F"		J"	F"			
2	2.5	rR	16545.9680*	3	5.5	qQ	16542.8992*
2	3.5	pR	16545.8810	3	5.5	rQ	16542.9654*
2	3.5	rR	16545.9621	3	6.5	qQ	16542.9180*
2	4.5	pR	16545.8495	3	6.5	rQ	16542.9944*
2	4.5	qR	16545.8954	3	7.5	qQ	16542.9403*
2	4.5	rR	16545.9511*	4	1.5	qQ	16542.8182*
2	5.5	qR	16545.8684	4	3.5	qQ	16542.8289*
2	5.5	rR	16545.9350*	4	4.5	qQ	16542.8379*
2	6.5	rR	16545.9133*	4	5.5	qQ	16542.8465*
3	2.5	qR	16546.8608	4	6.5	qQ	16542.8574*
3	3.5	qR	16546.8555	4	6.5	rQ	16542.9034
3	4.5	pR	16546.8233*	4	7.5	qQ	16542.8707*
3	4.5	qR	16546.8492*	4	7.5	rQ	16542.9224
3	5.5	pR	16546.8087*	4	8.5	qQ	16542.8858*
3	5.5	qR	16546.8422*	5	1.5	co	16542.7690*
3	6.5	qR	16546.8339	5	2.5	co	16542.7723*
3	6.5	rR	16546.8792*	6	2.5	qQ	16542.6976*
3	7.5	qR	16546.8246*	6	2.5	co	16542.7028*
3	7.5	rR	16546.8763*	6	3.5	qQ	16542.7009*
4	2.5	qR	16547.7981*	6	4.5	qQ	16542.7054*
4	2.5	rR	16547.8109*	6	5.5	qQ	16542.7107*
4	3.5	qR	16547.7965*	6	6.5	qQ	16542.7165*
4	3.5	rR	16547.8139*	6	7.5	qQ	16542.7227*
4	4.5	qR	16547.7948*	6	8.5	qQ	16542.7298*
4	4.5	rR	16547.8158*	6	9.5	qQ	16542.7382*
4	5.5	qR	16547.7931*	6	10.5	qQ	16542.7473*
4	5.5	rR	16547.8178*	7	4.5	qQ	16542.6228*
4	6.5	qR	16547.7910*	7	5.5	qQ	16542.6265*
4	6.5	rR	16547.8197*	7	6.5	qQ	16542.6312*
4	7.5	qR	16547.7888*	7	7.5	qQ	16542.6354*
4	7.5	rR	16547.8209*	7	8.5	qQ	16542.6408*

Appendix II.B, continued. ${}^3\Phi_3-{}^3\Delta_2$.

R				Q				P			
J"	F"			J"	F"			J"	F"		
4	8.5	qR	16547.7864*	7	9.5	qQ	16542.6473*				
4	8.5	rR	16547.8221*	7	10.5	qQ	16542.6544*				
15	10.5	rR	16557.3963	7	11.5	qQ	16542.6623*				
15	11.5	rR	16557.3980	8	4.5	qQ	16542.5271				
15	12.5	rR	16557.4003	8	5.5	qQ	16542.5310*				
15	13.5	rR	16557.4027	8	6.5	qQ	16542.5344*				
15	14.5	rR	16557.4053	8	7.5	qQ	16542.5377*				
15	15.5	rR	16557.4076	8	8.5	qQ	16542.5420				
15	16.5	rR	16557.4110	8	9.5	qQ	16542.5469				
15	17.5	rR	16557.4146	8	10.5	qQ	16542.5526				
15	18.5	rR	16557.4176	8	11.5	qQ	16542.5589				
15	19.5	rR	16557.4219	8	12.5	qQ	16542.5657				
16	11.5	rR	16558.1965*	9	7.5	qQ	16542.4283*				
16	12.5	rR	16558.1986	9	8.5	qQ	16542.4318*				
16	13.5	rR	16558.2008	9	10.5	qQ	16542.4407*				
16	14.5	rR	16558.2029*	9	11.5	qQ	16542.4458*				
16	15.5	rR	16558.2056	9	12.5	qQ	16542.4515*				
16	16.5	rR	16558.2086	9	13.5	qQ	16542.4580*				
16	17.5	rR	16558.2116	10	8.5	qQ	16542.3107*				
16	18.5	rR	16558.2150	10	9.5	qQ	16542.3142*				
16	19.5	rR	16558.2186	10	10.5	qQ	16542.3181*				
16	20.5	rR	16558.2222	10	11.5	qQ	16542.3227*				
17	12.5	rR	16558.9853*	10	12.5	qQ	16542.3273*				
17	13.5	rR	16558.9869	10	13.5	qQ	16542.3325*				
17	14.5	rR	16558.9892	10	14.5	qQ	16542.3382*				
17	15.5	rR	16558.9917	11	8.5	qQ	16542.1788*				
17	16.5	rR	16558.9943	11	9.5	qQ	16542.1816*				
17	17.5	rR	16558.9972	11	10.5	qQ	16542.1849*				
17	18.5	rR	16559.0004	11	11.5	qQ	16542.1888*				
17	19.5	rR	16559.0036	11	12.5	qQ	16542.1927*				
17	20.5	rR	16559.0071	11	13.5	qQ	16542.1970*				
17	21.5	rR	16559.0109	11	14.5	qQ	16542.2020*				
18	13.5	rR	16559.7605*	11	15.5	qQ	16542.2074*				
18	14.5	rR	16559.7635*	12	9.5	qQ	16542.0373*				
18	15.5	rR	16559.7652*	12	10.5	qQ	16542.0400*				
18	16.5	rR	16559.7679	12	11.5	qQ	16542.0434*				
18	17.5	rR	16559.7702	12	12.5	qQ	16542.0468*				
18	18.5	rR	16559.7732	12	13.5	qQ	16542.0508*				
18	19.5	rR	16559.7765	12	14.5	qQ	16542.0548*				
18	20.5	rR	16559.7798	12	15.5	qQ	16542.0595*				
18	21.5	rR	16559.7832	12	16.5	qQ	16542.0648*				
18	22.5	rR	16559.7872	13	10.5	qQ	16541.8833*				
19	14.5	rR	16560.5248	13	11.5	qQ	16541.8864*				
19	15.5	rR	16560.5268	13	12.5	qQ	16541.8894*				
19	16.5	rR	16560.5291	13	13.5	qQ	16541.8929*				
19	17.5	rR	16560.5314	13	14.5	qQ	16541.8964*				
19	18.5	rR	16560.5344	13	15.5	qQ	16541.9005*				
19	19.5	rR	16560.5371	13	16.5	qQ	16541.9050*				
19	20.5	rR	16560.5404	13	17.5	qQ	16541.9100*				
19	21.5	rR	16560.5437	14	10.5	qQ	16541.7165*				
19	22.5	rR	16560.5474	14	11.5	qQ	16541.7191*				
19	23.5	rR	16560.5514	14	12.5	qQ	16541.7215*				
20	16.5	rR	16561.2782	14	13.5	qQ	16541.7245*				
20	17.5	rR	16561.2808	14	14.5	qQ	16541.7278*				
20	18.5	rR	16561.2834	14	15.5	qQ	16541.7313*				
20	19.5	rR	16561.2863	14	16.5	qQ	16541.7355*				
20	20.5	rR	16561.2891	14	17.5	qQ	16541.7397*				
20	21.5	rR	16561.2922	14	18.5	qQ	16541.7445*				
20	22.5	rR	16561.2957	15	12.5	qQ	16541.5414*				
20	23.5	rR	16561.2991	15	13.5	qQ	16541.5438*				
20	24.5	rR	16561.3032	15	14.5	qQ	16541.5469*				
21	16.5	rR	16562.0156	15	15.5	qQ	16541.5501*				
21	17.5	rR	16562.0181	15	16.5	qQ	16541.5536*				
21	18.5	rR	16562.0203	15	17.5	qQ	16541.5575*				

Appendix II.B, continued. $3\Phi_3-3\Delta_2$.

		R			Q			P
J"	F"		J"	F"		J"	F"	
21	19.5	rR	16562.0228	15	18.5	qQ	16541.5616*	
21	20.5	rR	16562.0256	15	19.5	qQ	16541.5662*	
21	21.5	rR	16562.0287	16	13.5	qQ	16541.3521*	
21	22.5	rR	16562.0321	16	14.5	qQ	16541.3547*	
21	23.5	rR	16562.0355	16	15.5	qQ	16541.3577*	
21	24.5	rR	16562.0389	16	16.5	qQ	16541.3608*	
21	25.5	rR	16562.0425	16	17.5	qQ	16541.3644*	
22	17.5	rR	16562.7433	16	18.5	qQ	16541.3683*	
22	18.5	rR	16562.7456	16	19.5	qQ	16541.3725*	
22	19.5	rR	16562.7483	16	20.5	qQ	16541.3767*	
22	20.5	rR	16562.7506	17	14.5	qQ	16541.1503*	
22	21.5	rR	16562.7536	17	15.5	qQ	16541.1529*	
22	22.5	rR	16562.7569	17	16.5	qQ	16541.1558*	
22	23.5	rR	16562.7599	17	17.5	qQ	16541.1591*	
22	24.5	rR	16562.7633	17	18.5	qQ	16541.1628*	
22	25.5	rR	16562.7669	17	19.5	qQ	16541.1664*	
22	26.5	rR	16562.7706	17	20.5	qQ	16541.1707*	
23	18.5	rR	16563.4585	17	21.5	qQ	16541.1748*	
23	19.5	rR	16563.4608	18	14.5	qQ	16540.9346*	
23	20.5	rR	16563.4635	18	15.5	qQ	16540.9370*	
23	21.5	rR	16563.4660	18	16.5	qQ	16540.9397*	
23	22.5	rR	16563.4689	18	17.5	qQ	16540.9428*	
23	23.5	rR	16563.4722	18	18.5	qQ	16540.9460*	
23	24.5	rR	16563.4748	18	19.5	qQ	16540.9494*	
23	25.5	rR	16563.4785	18	20.5	qQ	16540.9530*	
23	26.5	rR	16563.4821	18	21.5	qQ	16540.9571*	
23	27.5	rR	16563.4864	18	22.5	qQ	16540.9611*	
24	19.5	rR	16564.1609	19	15.5	qQ	16540.7098	
24	20.5	rR	16564.1637	19	16.5	qQ	16540.7123	
24	21.5	rR	16564.1668	19	17.5	qQ	16540.7150	
24	22.5	rR	16564.1690	19	18.5	qQ	16540.7180	
24	23.5	rR	16564.1724	19	19.5	qQ	16540.7214	
24	24.5	rR	16564.1752	19	20.5	qQ	16540.7247	
24	25.5	rR	16564.1785	19	21.5	qQ	16540.7283	
24	26.5	rR	16564.1818	19	22.5	qQ	16540.7322	
24	27.5	rR	16564.1857	19	23.5	qQ	16540.7365	
24	28.5	rR	16564.1897	20	16.5	qQ	16540.4728	
25	20.5	rR	16564.8514	20	17.5	qQ	16540.4755	
25	21.5	rR	16564.8543	20	18.5	qQ	16540.4781	
25	22.5	rR	16564.8568	20	19.5	qQ	16540.4810	
25	23.5	rR	16564.8597	20	20.5	qQ	16540.4843	
25	24.5	rR	16564.8627	20	21.5	qQ	16540.4877	
25	25.5	rR	16564.8660	20	22.5	qQ	16540.4912	
25	26.5	rR	16564.8687	20	23.5	qQ	16540.4953	
25	27.5	rR	16564.8729	20	24.5	qQ	16540.4993	
25	28.5	rR	16564.8765	21	17.5	qQ	16540.2245	
25	29.5	rR	16564.8803	21	18.5	qQ	16540.2269	
26	21.5	rR	16565.5304	21	19.5	qQ	16540.2297	
26	22.5	rR	16565.5326	21	20.5	qQ	16540.2327	
26	23.5	rR	16565.5349	21	21.5	qQ	16540.2357	
26	24.5	rR	16565.5381	21	22.5	qQ	16540.2391	
26	25.5	rR	16565.5411	21	23.5	qQ	16540.2427	
26	26.5	rR	16565.5441	21	24.5	qQ	16540.2466	
26	27.5	rR	16565.5474	21	25.5	qQ	16540.2507	
26	28.5	rR	16565.5510	22	18.5	qQ	16539.9633	
26	29.5	rR	16565.5547	22	19.5	qQ	16539.9660	
26	30.5	rR	16565.5590	22	20.5	qQ	16539.9688	
27	22.5	rR	16566.1951	22	21.5	qQ	16539.9717	
27	23.5	rR	16566.1975	22	22.5	qQ	16539.9751	
27	24.5	rR	16566.2006	22	23.5	qQ	16539.9784	
27	25.5	rR	16566.2034	22	24.5	qQ	16539.9822	
27	26.5	rR	16566.2068	22	25.5	qQ	16539.9858	
27	27.5	rR	16566.2103	22	26.5	qQ	16539.9901	
27	28.5	rR	16566.2138	23	19.5	qQ	16539.6903	
27	29.5	rR	16566.2171	23	20.5	qQ	16539.6928*	

Appendix II.B, continued. ${}^3\Phi_3\text{-}{}^3\Delta_2$.

R		Q		P
J"	F"	J"	F"	
27	30.5	rR	16566.2211	
27	31.5	rR	16566.2254	
23	21.5	qQ	16539.6956	
23	22.5	qQ	16539.6988	
23	23.5	qQ	16539.7021	
23	24.5	qQ	16539.7054	
23	25.5	qQ	16539.7092	
23	26.5	qQ	16539.7130	
23	27.5	qQ	16539.7172	
24	21.5	qQ	16539.4074	
24	22.5	qQ	16539.4100	
24	23.5	qQ	16539.4131	
24	24.5	qQ	16539.4165	
24	25.5	qQ	16539.4200	
24	26.5	qQ	16539.4236	
24	27.5	qQ	16539.4275	
24	28.5	qQ	16539.4317	
25	21.5	qQ	16539.1073	
25	22.5	qQ	16539.1099	
25	23.5	qQ	16539.1129	
25	24.5	qQ	16539.1158	
25	25.5	qQ	16539.1191	
25	26.5	qQ	16539.1227	
25	27.5	qQ	16539.1264	
25	28.5	qQ	16539.1307	
25	29.5	qQ	16539.1344	
26	22.5	qQ	16538.7988	
26	23.5	qQ	16538.8014	
26	24.5	qQ	16538.8043	
26	25.5	qQ	16538.8077	
26	26.5	qQ	16538.8107	
26	27.5	qQ	16538.8146	
26	28.5	qQ	16538.8183	
26	29.5	qQ	16538.8225	
26	30.5	qQ	16538.8264	
27	23.5	qQ	16538.4771	
27	24.5	qQ	16538.4802	
27	25.5	qQ	16538.4829	
27	26.5	qQ	16538.4859	
27	27.5	qQ	16538.4895	
27	28.5	qQ	16538.4931	
27	29.5	qQ	16538.4969	
27	30.5	qQ	16538.5010	
27	31.5	qQ	16538.5050	

Appendix II.C. ${}^3\Phi_4\text{-}{}^3\Delta_3$.

J"	F"		J"	F"		J"	F"				
3	3.5	pR	16864.5123	7	2.5	qQ	16860.1995*	6	7.5	pP	16854.1702
3	3.5	qR	16864.5240	7	3.5	qQ	16860.1811*	6	8.5	pP	16854.1221
3	3.5	co	16864.5312	7	4.5	qQ	16860.1613*	6	9.5	pP	16854.0689
3	3.5	rR	16864.5385	7	5.5	qQ	16860.1358*	6	10.5	pP	16854.0117
3	4.5	pR	16864.4016	7	6.5	qQ	16860.1061*	7	3.5	pP	16853.2286
3	4.5	qR	16864.4167	7	8.5	qQ	16860.0329*	7	4.5	pP	16853.2077
3	4.5	co	16864.4255	7	10.5	qQ	16859.9436*	7	5.5	pP	16853.1823
3	4.5	rR	16864.4348	8	5.5	qQ	16860.0412*	7	6.5	pP	16853.1531
3	5.5	pR	16864.2657	9	4.5	qQ	16859.9476*	7	7.5	pP	16853.1202
3	5.5	qR	16864.2841	9	6.5	qQ	16859.9134*	7	8.5	pP	16853.0836
3	5.5	co	16864.2950	9	8.5	qQ	16859.8685*	7	9.5	pP	16853.0431
3	5.5	rR	16864.3058	9	9.5	qQ	16859.8420*	7	10.5	pP	16852.9993
3	6.5	pR	16864.1039	9	11.5	qQ	16859.7819*	7	11.5	pP	16852.9518*
3	6.5	qR	16864.1256	9	12.5	qQ	16859.7482*	8	3.5	pP	16852.1317
3	6.5	co	16864.1383	10	6.5	qQ	16859.7938*	8	4.5	pP	16852.1151
3	6.5	rR	16864.1509	10	7.5	qQ	16859.7770*	8	5.5	pP	16852.0958
3	7.5	qR	16863.9396	10	8.5	qQ	16859.7572	8	6.5	pP	16852.0726*

Appendix II.C, continued. ${}^3\Phi_4-{}^3\Delta_3$.

R		Q		P							
J"	F"	J"	F"	J"	F"						
3	7.5	co	16863.9543	10	9.5	qQ	16859.7360	8	8.5	pP	16852.0184
3	7.5	rR	16863.9686	10	10.5	qQ	16859.7124*	8	9.5	pP	16851.9865
4	0.5	rR	16865.5243*	10	11.5	qQ	16859.6872	8	10.5	pP	16851.9520
4	2.5	qR	16865.4658*	10	12.5	qQ	16859.6598	8	11.5	pP	16851.9147
4	2.5	co	16865.4690*	10	13.5	qQ	16859.6301	8	12.5	pP	16851.8748
4	2.5	rR	16865.4729*	10	14.5	qQ	16859.5991	9	4.5	pP	16851.0102
4	3.5	pR	16865.4072	11	7.5	qQ	16859.6461	9	5.5	pP	16850.9946
4	3.5	qR	16865.4154	11	8.5	qQ	16859.6301*	9	6.5	pP	16850.9764
4	3.5	co	16865.4201	11	9.5	qQ	16859.6124	9	7.5	pP	16850.9558
4	3.5	rR	16865.4250*	11	10.5	qQ	16859.5931	9	8.5	pP	16850.9325
4	4.5	pR	16865.3407	11	11.5	qQ	16859.5719	9	9.5	pP	16850.9072
4	4.5	qR	16865.3509	11	12.5	qQ	16859.5494	9	10.5	pP	16850.8793
4	4.5	co	16865.3568	11	13.5	qQ	16859.5251	9	11.5	pP	16850.8494
4	4.5	rR	16865.3630	11	14.5	qQ	16859.4999	9	12.5	pP	16850.8171
4	5.5	pR	16865.2600	11	15.5	qQ	16859.4725*	9	13.5	pP	16850.7827
4	5.5	qR	16865.2726	12	8.5	qQ	16859.4874	10	5.5	pP	16849.8802
4	5.5	co	16865.2796	12	9.5	qQ	16859.4725*	10	6.5	pP	16849.8656
4	5.5	rR	16865.2870	12	10.5	qQ	16859.4567	10	7.5	pP	16849.8488
4	6.5	pR	16865.1656	12	11.5	qQ	16859.4389	10	8.5	pP	16849.8298
4	6.5	qR	16865.1802	12	12.5	qQ	16859.4202	10	9.5	pP	16849.8089
4	6.5	co	16865.1886	12	13.5	qQ	16859.3998	10	10.5	pP	16849.7861
4	6.5	rR	16865.1970	12	14.5	qQ	16859.3781	10	11.5	pP	16849.7615
4	7.5	pR	16865.0577	12	15.5	qQ	16859.3552	10	12.5	pP	16849.7352
4	7.5	qR	16865.0743	12	16.5	qQ	16859.3310	10	13.5	pP	16849.7070
4	7.5	co	16865.0841	13	8.5	qQ	16859.3310*	10	14.5	pP	16849.6771
4	7.5	rR	16865.0936	13	9.5	qQ	16859.3183	11	6.5	pP	16848.7402
4	8.5	qR	16864.9557	13	10.5	qQ	16859.3046	11	7.5	pP	16848.7261
4	8.5	co	16864.9664	13	11.5	qQ	16859.2896	11	8.5	pP	16848.7106
4	8.5	rR	16864.9773	13	12.5	qQ	16859.2736	11	9.5	pP	16848.6934
5	3.5	qR	16866.3218	13	13.5	qQ	16859.2564	11	10.5	pP	16848.6745
5	3.5	co	16866.3247	13	14.5	qQ	16859.2383	11	11.5	pP	16848.6534
5	3.5	rR	16866.3283	13	15.5	qQ	16859.2187	11	12.5	pP	16848.6316
5	4.5	pR	16866.2717	13	16.5	qQ	16859.1983	11	13.5	pP	16848.6086
5	4.5	qR	16866.2792	13	17.5	qQ	16859.1771	11	14.5	pP	16848.5835
5	4.5	co	16866.2833	14	9.5	qQ	16859.1494	11	15.5	pP	16848.5575
5	4.5	rR	16866.2876	14	10.5	qQ	16859.1377				
5	5.5	pR	16866.2183	14	11.5	qQ	16859.1248				
5	5.5	qR	16866.2274	14	12.5	qQ	16859.1112				
5	5.5	co	16866.2326	14	13.5	qQ	16859.0964				
5	5.5	rR	16866.2378	14	14.5	qQ	16859.0808				
5	6.5	pR	16866.1563	14	15.5	qQ	16859.0642				
5	6.5	qR	16866.1667	14	16.5	qQ	16859.0468				
5	6.5	co	16866.1726	14	17.5	qQ	16859.0283				
5	6.5	rR	16866.1785	14	18.5	qQ	16859.0092				
5	7.5	pR	16866.0852	15	10.5	qQ	16858.9562				
5	7.5	qR	16866.0975	15	11.5	qQ	16858.9451				
5	7.5	co	16866.1043	15	12.5	qQ	16858.9332				
5	7.5	rR	16866.1109	15	13.5	qQ	16858.9205				
5	8.5	qR	16866.0198	15	14.5	qQ	16858.9070				
5	8.5	co	16866.0273	15	15.5	qQ	16858.8928				
5	8.5	rR	16866.0350	15	16.5	qQ	16858.8777				
5	9.5	qR	16865.9338	15	17.5	qQ	16858.8617				
5	9.5	rR	16865.9508	15	18.5	qQ	16858.8453				
6	1.5	rR	16867.2702	15	19.5	qQ	16858.8279				
6	2.5	rR	16867.2546	16	11.5	qQ	16858.7512				
6	4.5	qR	16867.1976	16	12.5	qQ	16858.7407				
6	4.5	co	16867.2007	16	13.5	qQ	16858.7298				
6	4.5	rR	16867.2037	16	14.5	qQ	16858.7182				
6	5.5	qR	16867.1611	16	15.5	qQ	16858.7057				
6	5.5	co	16867.1647	16	16.5	qQ	16858.6926				
6	5.5	rR	16867.1687	16	17.5	qQ	16858.6787				
6	6.5	qR	16867.1182	16	18.5	qQ	16858.6644				
6	6.5	co	16867.1225	16	19.5	qQ	16858.6499				
6	6.5	rR	16867.1270	16	20.5	qQ	16858.6338				
6	7.5	qR	16867.0689	17	12.5	qQ	16858.5344				

Appendix II.C, continued. $3\Phi_4-3\Delta_3$.

R			Q			P	
J"	F"		J"	F"			
6	7.5	co	16867.0742	17	13.5	qQ	16858.5253
6	7.5	rR	16867.0792	17	14.5	qQ	16858.5158
6	8.5	qR	16867.0141	17	15.5	qQ	16858.5037
6	8.5	co	16867.0197	17	16.5	qQ	16858.4922
6	8.5	rR	16867.0254	17	17.5	qQ	16858.4801
6	9.5	qR	16866.9532	17	18.5	qQ	16858.4676
6	9.5	co	16866.9597	17	19.5	qQ	16858.4546
6	9.5	rR	16866.9659	17	20.5	qQ	16858.4412
6	10.5	qR	16866.8967	17	21.5	qQ	16858.4269
6	10.5	co	16866.8940	18	13.5	qQ	16858.3054
6	10.5	rR	16866.9008	18	14.5	qQ	16858.2967
7	2.5	rR	16868.1433	18	15.5	qQ	16858.2868
7	3.5	rR	16868.1266	18	16.5	qQ	16858.2771
7	5.5	qR	16868.0739	18	17.5	qQ	16858.2665
7	5.5	co	16868.0768	18	18.5	qQ	16858.2556
7	5.5	rR	16868.0795	18	19.5	qQ	16858.2439
7	6.5	qR	16868.0420	18	20.5	qQ	16858.2325
7	6.5	co	16868.0456	18	21.5	qQ	16858.2197
7	6.5	rR	16868.0488	18	22.5	qQ	16858.2072
7	7.5	qR	16868.0057	19	15.5	qQ	16858.0564
7	7.5	co	16868.0097	19	16.5	qQ	16858.0475
7	7.5	rR	16868.0136	19	17.5	qQ	16858.0383
7	8.5	qR	16867.9650	19	18.5	qQ	16858.0284
7	8.5	co	16867.9695	19	19.5	qQ	16858.0186
7	8.5	rR	16867.9738	19	20.5	qQ	16858.0081
7	9.5	qR	16867.9200	19	21.5	qQ	16857.9973
7	9.5	co	16867.9247	19	22.5	qQ	16857.9862
7	9.5	rR	16867.9297				
7	10.5	qR	16867.8706				
7	10.5	co	16867.8760				
7	10.5	rR	16867.8815				
7	11.5	qR	16867.8172				
7	11.5	co	16867.8234				
7	11.5	rR	16867.8292				
8	3.5	rR	16869.0122				
8	4.5	rR	16868.9957				
8	6.5	qR	16868.9467*				
8	6.5	co	16868.9496*				
8	6.5	rR	16868.9521				
8	7.5	qR	16868.9187*				
8	7.5	co	16868.9219*				
8	7.5	rR	16868.9250				
8	8.5	qR	16868.8873				
8	8.5	co	16868.8909				
8	8.5	rR	16868.8943				
8	9.5	qR	16868.8526				
8	9.5	co	16868.8566				
8	9.5	rR	16868.8604				
8	10.5	qR	16868.8144				
8	10.5	co	16868.8188				
8	10.5	rR	16868.8231				
8	11.5	qR	16868.7731				
8	11.5	co	16868.7779				
8	11.5	rR	16868.7826				
8	12.5	qR	16868.7289				
8	12.5	co	16868.7341				
8	12.5	rR	16868.7390				
9	4.5	rR	16869.8738				
9	5.5	rR	16869.8579				
9	6.5	qR	16869.8346				
9	6.5	co	16869.8369				
9	6.5	rR	16869.8391				
9	7.5	qR	16869.8123				
9	7.5	co	16869.8152				
9	7.5	rR	16869.8177				

Appendix II.C, continued. $3\Phi_4-3\Delta_3$.

R			Q			P
J"	F"		J"	F"		
9	8.5	qR 16869.7877	19	23.5	qQ 16857.9745	
9	8.5	co 16869.7907	20	15.5	qQ 16857.8116	
9	8.5	rR 16869.7936	20	16.5	qQ 16857.8037	
9	9.5	qR 16869.7600	20	17.5	qQ 16857.7960	
9	9.5	co 16869.7635	20	18.5	qQ 16857.7872	
9	9.5	rR 16869.7668	20	19.5	qQ 16857.7782	
9	10.5	qR 16869.7299	20	20.5	qQ 16857.7689	
9	10.5	co 16869.7335	20	21.5	qQ 16857.7593	
9	10.5	rR 16869.7369	20	22.5	qQ 16857.7492	
9	11.5	qR 16869.6975	20	23.5	qQ 16857.7390	
9	11.5	co 16869.7013	20	24.5	qQ 16857.7286	
9	11.5	rR 16869.7051	21	16.5	qQ 16857.5463	
9	12.5	qR 16869.6621	21	17.5	qQ 16857.5393	
9	12.5	co 16869.6663	21	18.5	qQ 16857.5318	
9	12.5	rR 16869.6704	21	19.5	qQ 16857.5236	
9	13.5	qR 16869.6246*	21	20.5	qQ 16857.5155	
9	13.5	co 16869.6292	21	21.5	qQ 16857.5070	
9	13.5	rR 16869.6334	21	22.5	qQ 16857.4983	
22	17.5	rR 16880.0768	21	23.5	qQ 16857.4894	
22	18.5	rR 16880.0699	21	24.5	qQ 16857.4800	
22	19.5	rR 16880.0628	21	25.5	qQ 16857.4706	
22	20.5	rR 16880.0557	22	17.5	qQ 16857.2691	
22	21.5	rR 16880.0476	22	18.5	qQ 16857.2621	
22	22.5	rR 16880.0398	22	19.5	qQ 16857.2550	
22	23.5	rR 16880.0313	22	20.5	qQ 16857.2480	
22	24.5	rR 16880.0228	22	21.5	qQ 16857.2410	
22	25.5	rR 16880.0151	22	22.5	qQ 16857.2330	
22	26.5	rR 16880.0063	22	23.5	qQ 16857.2250	
24	19.5	rR 16881.4627	22	24.5	qQ 16857.2167	
24	20.5	rR 16881.4569	22	25.5	qQ 16857.2084	
24	21.5	rR 16881.4512	22	26.5	qQ 16857.1997	
24	22.5	rR 16881.4450	23	18.5	qQ 16856.9789	
24	23.5	rR 16881.4387	23	19.5	qQ 16856.9727	
24	24.5	rR 16881.4320	23	20.5	qQ 16856.9664	
24	25.5	rR 16881.4251	23	21.5	qQ 16856.9598	
24	26.5	rR 16881.4181	23	22.5	qQ 16856.9528	
24	27.5	rR 16881.4113	23	23.5	qQ 16856.9457	
24	28.5	rR 16881.4043	23	24.5	qQ 16856.9386	
25	20.5	rR 16882.1360	23	25.5	qQ 16856.9309	
25	21.5	rR 16882.1305	23	26.5	qQ 16856.9233	
25	22.5	rR 16882.1254	23	27.5	qQ 16856.9157	
25	23.5	rR 16882.1193	24	19.5	qQ 16856.6761	
25	24.5	rR 16882.1138	24	20.5	qQ 16856.6706	
25	25.5	rR 16882.1085	24	21.5	qQ 16856.6645	
25	26.5	rR 16882.1020	24	22.5	qQ 16856.6585	
25	27.5	rR 16882.0958	24	23.5	qQ 16856.6522	
25	28.5	rR 16882.0897	24	24.5	qQ 16856.6461	
25	29.5	rR 16882.0832	24	25.5	qQ 16856.6391	
26	21.5	rR 16882.7961	24	26.5	qQ 16856.6324	
26	22.5	rR 16882.7919	24	27.5	qQ 16856.6256	
26	23.5	rR 16882.7862	24	28.5	qQ 16856.6185	
26	24.5	rR 16882.7815	25	20.5	qQ 16856.3611	
26	25.5	rR 16882.7766	25	21.5	qQ 16856.3560	
26	26.5	rR 16882.7712	25	22.5	qQ 16856.3509	
26	27.5	rR 16882.7660	25	23.5	qQ 16856.3454	
26	28.5	rR 16882.7603	25	24.5	qQ 16856.3396	
26	29.5	rR 16882.7548	25	25.5	qQ 16856.3342	
26	30.5	rR 16882.7491	25	26.5	qQ 16856.3277	
			25	27.5	qQ 16856.3217	
			25	28.5	qQ 16856.3154	
			25	29.5	qQ 16856.3093	
			26	21.5	qQ 16856.0330	
			26	22.5	qQ 16856.0284	
			26	23.5	qQ 16856.0234	
			26	24.5	qQ 16856.0188	

Appendix II.C, continued. ${}^3\Phi_4\text{-}{}^3\Delta_3$.

<u>R</u>		<u>Q</u>	<u>P</u>
	J"	F"	
26	25.5	qQ	16856.0135
26	26.5	qQ	16856.0079
26	27.5	qQ	16856.0028
26	28.5	qQ	16855.9973
26	29.5	qQ	16855.9916
26	30.5	qQ	16855.9862
27	22.5	qQ	16855.6942
27	24.5	qQ	16855.6846
27	25.5	qQ	16855.6800
27	26.5	qQ	16855.6754
27	27.5	qQ	16855.6705
27	28.5	qQ	16855.6663
27	29.5	qQ	16855.6610
27	30.5	qQ	16855.6560
27	31.5	qQ	16855.6509
28	23.5	qQ	16855.3426*
28	24.5	qQ	16855.3366
28	25.5	qQ	16855.3329
28	26.5	qQ	16855.3288
28	27.5	qQ	16855.3251
28	28.5	qQ	16855.3199
28	30.5	qQ	16855.3117
28	31.5	qQ	16855.3064
28	32.5	qQ	16855.3030
29	24.5	qQ	16854.9763
29	25.5	qQ	16854.9724
29	26.5	qQ	16854.9690
29	27.5	qQ	16854.9656
29	28.5	qQ	16854.9620
29	29.5	qQ	16854.9575
29	30.5	qQ	16854.9542
29	31.5	qQ	16854.9505
29	32.5	qQ	16854.9466
29	33.5	qQ	16854.9423

^aTransitions in units of cm^{-1} . Blended lines are denoted by an asterisk.

APPENDIX III. Transitions of the v_7 Fundamental of $\text{NH}_2^{11}\text{BH}_2^a$

		R			Q			P
Branch	J"		Branch	J"		Branch	J"	
rRO	0	1010.1049	rQO	1	1008.2841*	rPO	2	1005.0696
	1	1011.9077		2	1008.1281		3	1003.5316*
	2	1013.7738		3	1007.9039		4	1002.0797*
	3	1015.7095		4	1007.6227		5	1000.7299*
	4	1017.7244*		5	1007.2983*		6	999.4985
	5	1019.8287*		6	1006.9468		7	998.4016*
	6	1022.0408*		7	1006.5875*		8	997.4567*
	7	1024.3696		8	1006.2366		9	996.6731
	8	1026.8280		9	1005.9094		10	996.0551
	9	1029.4214*		10	1005.6170		11	995.6010
	10	1032.1525*		11	1005.3645		12	995.3008
	11	1035.0115		12	1005.1540		13	995.1399*
	12	1037.9854		13	1004.9840*		14	995.0959
	13	1041.0538		14	1004.8502		15	995.1471*
	14	1044.1942		15	1004.7468*		16	995.2669
	15	1047.3830		16	1004.6711*		17	995.4321
	16	1050.5983*		17	1004.6182*		18	995.6203
	17	1053.8206*	rQ1	3	1016.0602		19	995.8127
	18	1057.0349		2	1015.3731		20	995.9953
	19	1060.2328*		2	1015.8385		21	996.1585*
	20	1063.4078		3	1015.1179*	rP1	4	1008.1281*
	21	1066.5582		4	1016.3770*		5	1008.3194*
	22	1069.6846*		4	1014.7801*		5	1006.0794*
	23	1072.7885		5	1016.8055		6	1007.0793*
rR1	1	1019.0407*		5	1014.3608		7	1005.9205*
	1	1018.8912		6	1017.3657		7	1001.9174*
	2	1020.8460*		6	1013.8658		8	999.8510*
	2	1020.4058*		7	1018.0803		9	1003.8456
	3	1021.8576*		7	1013.2978		9	997.8300
	3	1022.7189		8	1018.9708*		10	1002.9319
	4	1024.6586*		8	1012.6643*		10	995.8851
	4	1023.2645		9	1020.0551		11	1002.1016*
	5	1026.6682		9	1011.9726		11	994.0435*
	5	1024.6459*		10	1021.3496*		12	992.3300*
	6	1028.7450*		10	1011.2327		13	1000.6831
	6	1026.0253		11	1022.8611		13	990.7678
	7	1030.8941		11	1010.4563		14	1001.0897*
	7	1027.4255		12	1024.5963		14	989.3753
	8	1033.1127		12	1009.6590		15	999.5678*
	8	1028.8737*		13	1008.8556		15	988.1679
	9	1035.4025		13	1026.5538		16	987.1582*
	9	1030.3893		14	1008.0649		17	986.3492
	10	1037.7617		15	1007.2983*		18	985.7379*
	10	1031.9923		16	1006.5875*		19	985.3241*
	11	1040.1900*		17	1005.9323		20	985.0787*
	11	1033.7003		18	1005.3433		21	984.9990
	12	1042.6999*		19	1004.8253*	rP2	4	1015.9509*
	12	1035.5309*		20	1004.3791*		5	1014.2566*
	13	1045.2437		21	1004.0011*		6	1012.5641*
	13	1037.4928		22	1003.6786		7	1010.8849*
	14	1048.8616*		23	1003.4115		8	1009.2266
	14	1039.6025		24	1003.1891		9	1007.5971*
	15	1050.5364*		25	1003.0034		9	1006.2047*
	15	1041.8683		26	1002.8478*		10	1006.0037*
	16	1053.2621		27	1002.7176		10	1004.0011*
	16	1044.2964*		28	1002.6062*		11	1001.7142
	17	1058.0367*		29	1002.5345*		12	1002.9580
	17	1046.8873*	rQ2	3	1022.6457*		12	999.3473*
	18	1058.8497*		3	1022.6724*		13	1001.5208
	18	1049.6386*		4	1022.5746		13	996.9305
	19	1061.7981*		4	1022.6457*		14	1000.1527*
	19	1052.5335*		5	1022.4583		14	994.4831*
	20	1064.7856*		5	1022.6225*		15	998.8561*
	20	1055.5552*		6	1022.2841		15	992.0420

R			Q			P		
Branch	J"		Branch	J"		Branch	J"	
rR1	21	1058.6813*	rQ2	6	1022.6132*	rP2	16	997.6372
	22	1061.8709*		7	1022.0408*		16	989.6367
	23	1065.1156*		7	1022.6225*		17	996.5003
rR2	2	1027.7066*	8	1021.6947	17	987.3044		
	2	1027.7066*	8	1022.6619*	18	995.4475*		
	3	1029.3599	9	1021.2534	18	985.0787*		
	3	1029.3377*	9	1022.7473*	19	982.9912		
	4	1031.0100	10	1020.7012*	20	993.5984*		
	4	1030.9418	10	1022.8919	20	981.0716		
	5	1032.6636	11	1020.0366	21	992.8029*		
	5	1032.5071	11	1023.1151	21	979.3436*		
	6	1034.3278*	12	1019.2616	23	976.5387*		
	6	1034.0212*	12	1023.4372*	24	975.4816*		
	7	1036.0076	13	1018.3825	pP1	2	997.3140	
	7	1035.4699	13	1023.8812		3	995.3837	
	8	1037.7110	14	1017.4096*		4	993.3620	
	8	1036.8455	14	1024.4698	5	991.2423		
	9	1039.4445	15	1016.3552	6	989.0151		
	9	1038.1416	15	1025.2282	7	986.6704		
	10	1041.2140	16	1015.2320	8	984.1997		
	10	1039.3617	16	1026.1794	9	981.5953		
	11	1043.0269	17	1014.0559	10	978.8544		
	11	1040.5153	17	1027.3419	11	975.9802		
	12	1044.8897*	18	1012.8439*	12	972.9832		
	12	1041.6205	18	1028.7324*	13	969.8798		
	13	1046.8063	19	1011.6111	14	966.6919		
	13	1042.6999*	19	1030.3594*	15	963.4440		
	14	1048.7838*	20	1010.3800*	16	960.1606		
	14	1043.7824	20	1032.2262*	17	956.8643		
	15	1050.8236	21	1009.1683*	18	953.5738		
15	1044.8975*	22	1007.9954	pP2	2	989.9796		
16	1052.9239*	23	1006.8817*		3	989.8431*		
16	1046.0744	24	1005.8420*		3	988.4041		
17	1055.1066	25	1004.8886*	3	988.0031			
17	1047.3408	26	1004.0550*	4	986.8626			
18	1057.3523	27	1003.2674*	4	986.0845			
18	1048.7218*	28	1002.5995*	5	985.3387			
19	1059.6674	29	1002.0207*	5	984.0876			
19	1050.2396*	rQ3	4	1029.5455*	6	983.8095		
20	1062.0510		4	1029.5455*	6	982.0125		
20	1051.9110		5	1029.4912*	7	982.2515		
21	1064.5001		5	1029.4912*	7	979.8592		
21	1053.7518		7	1029.3290*	8	980.6406*		
22	1067.0120*		7	1029.3475	8	977.6288		
23	1069.5835		8	1029.2137	9	978.9530		
23	1057.9821		8	1029.2551	9	975.3221*		
24	1072.2165*		9	1029.0685	10	977.1707*		
24	1060.3822		9	1029.1510*	10	972.9398		
25	1074.8836		10	1028.8846	11	975.2746		
25	1062.9708		10	1029.0362*	11	970.4851		
26	1077.7030*		11	1028.6512	12	973.2551*		
26	1065.7372		11	1028.9174	12	967.9602		
27	1080.3614*		12	1028.3568	13	971.1009		
rR3	3		1036.2744*	12	1028.7961	13	965.3686	
	3		1036.2744*	13	1027.9869	14	968.7443*	
	4		1037.9060*	13	1028.6796	14	962.7151	
	4	1037.9060*	14	1027.5265	15	960.0028		
	5	1039.5262*	14	1028.5772	16	963.7555		
	5	1039.5262*	15	1026.9597*	16	957.2391		
	6	1041.1383*	15	1026.9597*	17	960.9989		
	6	1041.1304*	16	1026.2778*	17	954.4276		
	7	1042.7363*	16	1028.4608	18	951.5756		
	7	1042.7184*	17	1025.4670	19	955.0372		
8	1044.3233	17	1028.4753	19	948.6880			
8	1044.2834	18	1024.5247*	20	951.8544			

Appendix III, continued.

R		Q		P				
Branch	J"	Branch	J"	Branch	J"			
rR3	9	1045.8996	18	1028.5612*	pP2	20	945.7720	
	9	1045.8216	19	1023.4506*	21	948.5616		
	10	1047.4676*	20	1022.2521	21	942.8300*		
	10	1047.3248	20	1029.0362*	22	945.1839*		
	11	1049.0294	21	1020.9383	22	939.8683		
	11	1048.7838*	21	1029.4670	23	941.7475		
	12	1050.5882*	22	1030.0639	23	936.8755*		
	12	1050.1895	22	1019.5236	24	938.2798*		
	13	1052.1491	23	1018.0056*	25	934.8032		
	13	1051.5302	rQ4	5	1036.2669*	pP3	4	978.7082
	14	1053.7169		5	1036.2669*		4	978.6884
	14	1052.7941		6	1036.2034*		5	977.0116
	15	1055.2980		6	1036.2034*		5	976.9555*
	15	1053.9720*		7	1036.1289*		6	975.3303*
	16	1056.8992		7	1036.1289*		6	975.1961
	16	1055.0612		8	1036.0395*		7	973.6720
	17	1058.5274		8	1036.0395*		7	973.4099
	17	1056.0591		9	1035.9358*		8	972.0465*
	18	1060.1880*		9	1035.9358*		8	971.5892*
	18	1056.9737		10	1035.8159*		9	970.4631
	19	1061.8923*		10	1035.8159*		9	969.7282
	19	1057.8196		11	1035.6753*		10	968.9224
	20	1063.6434	11	1035.6843*	10	967.8217		
	20	1058.6198*	12	1035.5144	11	967.4219*		
	21	1065.4484	12	1035.5309*	11	965.8621		
	21	1059.4005	13	1035.3291	12	965.9497		
22	1067.3136*	13	1035.3631	12	963.8465			
22	1060.1829*	14	1035.1149*	13	964.4893			
24	1061.9630*	14	1035.1769	13	961.7748*			
25	1062.9990*	15	1034.8680	14	963.0167			
26	1064.1769*	15	1034.9734	14	959.6248*			
rR4	4	1044.6741	16	1034.5800	15	961.5062		
	4	1044.6741	16	1034.7537	15	957.4145*		
	5	1046.2965	17	1034.5206	16	959.9296		
	5	1046.2965	18	1033.8482*	16	955.1299		
	6	1047.9076	18	1034.2783	17	958.2623		
	6	1047.9076	19	1033.3823	17	952.7749		
	7	1049.5070*	19	1034.0309*	18	956.4808		
	7	1049.5070*	20	1032.8330	18	950.3476		
	8	1051.0941*	20	1033.7838*	19	954.5650*		
	8	1051.0941*	21	1032.1853*	19	947.8489		
	9	1052.6676*	22	1031.4235	20	952.5032		
	9	1052.6676*	23	1030.5349	20	945.2803		
	10	1054.2260*	23	1033.1511	21	950.2831		
	10	1054.2260*	24	1029.5080	21	942.6462*		
	11	1055.7739*	24	1033.0169	22	947.8973		
	11	1055.7658*	25	1028.3354*	22	939.9468		
	12	1057.3044*	25	1032.9486	23	945.3408		
	12	1057.2868*	26	1027.0079	23	937.1897*		
	13	1058.8177*	26	1032.9670	24	942.6114		
	13	1058.7858	27	1025.5505	24	934.3056*		
	14	1060.3155	27	1033.0915*	25	939.7111*		
	14	1060.2586*	rQ5	6	1042.8357*	pP4	4	970.7243*
	15	1061.7981*		6	1042.8357*		4	970.7243*
	15	1061.7008*		7	1042.7645		5	969.0060*
	16	1063.2645		7	1042.7645		5	969.0060*
	16	1063.1060		9	1042.5844		6	967.2789*
17	1064.7190*	9		1042.5844	6		967.2789*	
17	1064.4676	10		1042.4754	7		965.5417*	
18	1066.1620	10		1042.4754	7		965.5467*	
18	1065.7771	11		1042.3520*	8		963.8095	
19	1067.5976	11		1042.3520*	8		963.7943*	
19	1067.0244*	12		1042.2139	9		962.0712	
20	1069.0303*	12		1042.2139	9		962.0391	
20	1068.1959*	13		1042.0604	10		960.3347	

Appendix III, continued.

R		Q		P			
Branch	J"	Branch	J"	Branch	J"		
rR4	21	1070.4622*	13	1042.0604	10	960.2718	
	21	1069.2947*	14	1041.8900*	11	958.6069	
	22	1071.9036	14	1041.8900*	11	958.4922*	
	22	1070.3068*	15	1041.7013*	12	956.8920	
	23	1073.3239*	15	1041.7013*	12	956.6959	
	23	1071.1956*	16	1041.4913*	13	955.1994	
rR5	5	1052.9239*	16	1041.4988*	13	954.8808	
	6	1054.5354*	17	1041.2599	14	953.5372	
	7	1056.1367*	17	1041.2739	14	953.0431	
	8	1057.7263	18	1041.0057	15	951.9134*	
	9	1059.3049	18	1041.0288	15	951.1774	
	10	1060.8713	19	1040.7239	16	950.3321	
	11	1062.4240	19	1040.7620	16	949.2791	
	12	1063.9636	20	1040.4126	17	948.7994	
	12	1063.9636	20	1040.4768	17	947.3421	
	13	1065.4879	21	1040.0675	18	947.3134	
	13	1065.4879	21	1040.1714	18	945.3613	
	14	1067.0112*	22	1039.8448*	19	945.8664	
	14	1067.0112*	23	1039.2502*	19	943.3313	
	15	1068.4896*	23	1039.4988*	20	944.4455	
	15	1068.4896*	rQ6	7	1049.2726	20	941.2457
	16	1069.9677*	7	1049.2726	21	943.0298*	
	16	1069.9616*	8	1049.1907	21	939.1012	
	17	1071.4260*	8	1049.1907	22	941.5931	
	17	1071.4088*	9	1049.0974	22	936.8755*	
	18	1072.8650	9	1049.0974	23	940.1075	
	18	1072.8457	10	1048.9930	23	934.6179	
	19	1074.2863	10	1048.9930	24	938.5446*	
	19	1074.2516	11	1048.8757	pP5	5	960.8783
	20	1075.6861*	11	1048.8757	5	960.8783	
	20	1075.6301	12	1048.7456	6	959.1505*	
	21	1077.0691	12	1048.7456	6	959.1505*	
	21	1076.9773	13	1048.6023	7	957.4145*	
	22	1078.4318*	13	1048.6023	7	957.4145*	
	22	1078.2888	14	1048.4444	8	955.6703*	
	23	1079.5577	14	1048.4444	8	955.6703*	
	24	1081.1101*	15	1048.2726	9	953.9166*	
	24	1080.7772	15	1048.2726	9	953.9166*	
	25	1081.9363*	16	1048.0851	10	952.1558*	
rR6	6	1061.0380	16	1048.0851	10	952.1558*	
	6	1061.0380	17	1047.8814*	11	950.3875*	
	7	1062.6396	17	1047.8814*	11	950.3875*	
	7	1062.6396	18	1047.6606*	12	948.6166*	
	8	1064.2300*	18	1047.6606*	12	948.6099*	
	8	1064.2300*	19	1047.4220	13	946.8395*	
	9	1065.8098	19	1047.4220	13	946.8262*	
	9	1065.8098	20	1047.1643	14	945.0593	
	10	1067.3781	20	1047.1643	14	945.0298	
	10	1067.3781	21	1046.8878*	15	943.2808	
	11	1068.9348	21	1046.8878*	15	943.2365	
	11	1068.9348	22	1046.5863*	16	941.5041*	
	12	1070.4794	22	1046.5950*	16	941.4301	
	12	1070.4794	23	1046.2623*	17	939.7341*	
	13	1072.0105	23	1046.2773*	17	939.6135	
	13	1072.0105	24	1045.9127*	18	937.9768	
	14	1073.5296	24	1045.9401*	18	937.7859	
	14	1073.5296	rQ7	8	1055.5844*	19	936.2363*
	15	1075.0336*	9	1055.5005	19	935.9466*	
	15	1075.0336*	9	1055.5005	20	934.5220*	
	16	1076.5238*	10	1055.3983	23	928.3993*	
	16	1076.5238*	10	1055.3983	pP6	6	950.8855
	17	1078.9823*	11	1055.2833	6	950.8855	
	17	1078.9823*	11	1055.2833	7	949.1497	
	18	1079.4562*	12	1055.1515*	7	949.1497	
	18	1079.4562*	13	1055.0186	8	947.4049	

Appendix III, continued.

R			Q			P					
Branch	J*		Branch	J*		Branch	J*				
rR6	19	1080.8983*	rQ7	13	1055.0186	pP6	8	947.4049			
	19	1080.8983*		14	1054.8669		9	945.6509			
	20	1082.3227*		14	1054.8669		9	945.6509			
	20	1082.3227*		15	1054.7023		10	943.8883			
	21	1083.7281*		15	1054.7023		10	943.8883			
	21	1083.7281*		16	1054.5236*		11	942.1175			
	22	1085.1118*		17	1054.3329		11	942.1175			
	23	1086.4858*		17	1054.3329		12	940.3385			
	23	1086.4708*		18	1054.1259*		12	940.3385			
	24	1087.8321*		19	1053.9050*		13	938.5518			
	24	1087.8170*		20	1053.6692		13	938.5518			
	25	1089.1610*		20	1053.6692		14	936.7573*			
	25	1089.1333		21	1053.4223*		14	936.7573*			
	26	1090.4248*		21	1053.4223*		15	934.9561*			
	26	1090.3575*		22	1053.1481*		15	934.9561*			
	rR7	7		1069.0363*	rQ8		22	1053.1481*	pP7	18	929.5201*
		7		1069.0363*			9	1061.8161*		18	929.5118*
		8		1070.6266			10	1061.7127*		19	927.6994*
		8		1070.6266			11	1061.5989		19	927.6847*
		9		1072.2067			12	1061.4747		20	925.8776*
		9		1072.2067			12	1061.4747		20	925.8515*
		10		1073.7749			13	1061.3371		21	924.0542*
		10		1073.7749		13	1061.3371	21		924.0132*	
		11		1075.3329		14	1061.1880	22		922.2312*	
		11		1075.3329		14	1061.1880	22		922.1676*	
		12		1076.8785*		15	1061.0259*	7		940.7662	
12		1076.8785*	16	1060.8523*		7	940.7662				
13		1078.4125*	17	1060.6641		8	939.0210				
14		1079.9289*	17	1060.6641		8	939.0210				
15		1081.4438	18	1060.4628*		9	937.2674*				
15		1081.4438	19	1060.2462*		10	935.5052				
16		1082.9402	20	1060.0175		10	935.5052				
16		1082.9402	20	1060.0175		11	933.7342				
17		1084.4232	21	1059.7736		11	933.7342				
17		1084.4232	21	1059.7736		12	931.9544				
18		1085.8867*	22	1059.5139*		12	931.9544				
19		1087.3487	23	1059.2391		13	930.1658				
19		1087.3487	23	1059.2391		13	930.1658				
20		1088.7940*	24	1058.9472*		14	928.3691				
21		1090.2200*	25	1058.6402*		14	928.3691				
21		1090.2200*	26	1058.3147		15	926.5645				
23	1093.0102*	26	1058.3147	15	926.5645						
23	1093.0102*	pQ1	1	1000.9813*	16	924.7520					
24	1094.3885*		2	1001.1124	16	924.7520					
25	1095.7295*		3	1001.3015*	17	922.9322*					
25	1095.7295*		4	1001.5405	17	922.9322*					
rR8	8		1076.9357	5	1001.8174	18	921.1042*				
	8		1076.9357	6	1002.1190*	18	921.1042*				
	9		1078.5143	7	1002.4287	20	917.4283*				
	9		1078.5143	8	1002.7353	20	917.4283*				
	10		1080.0824*	9	1003.0237	21	915.5818*				
	11		1081.6390	10	1003.2853	21	915.5818*				
	11	1081.6390	11	1003.5143	pP8	8	930.5386				
	12	1083.1847	12	1003.7086		8	930.5386				
	12	1083.1847	13	1003.8702		9	928.7860				
	13	1084.7134*	14	1004.0011*		9	928.7860				
	14	1086.2408*	15	1004.1081		10	927.0244				
	15	1087.7500	16	1004.1938		10	927.0244				
	15	1087.7500	17	1004.2634		11	925.2535				
	16	1089.2471	18	1004.3205		11	925.2535				
	16	1089.2471	19	1004.3688		12	923.4737				
	17	1090.7314	20	1004.4104		12	923.4737				
	17	1090.7314	21	1004.4480*	13	921.6856					
	18	1092.2029*	22	1004.4830	13	921.6856					
	19	1093.6596	23	1004.5169	14	919.8884					

Appendix III, continued.

R			Q			P		
Branch	J"		Branch	J"		Branch	J"	
rR8	19	1093.6596	pQ1	24	1004.5503*	pP8	14	919.8884
	20	1095.1036*		25	1004.5828*		15	918.0830
	20	1095.1036*		26	1004.6182*		15	918.0830
	21	1096.5326*		27	1004.6495*		16	916.2684
	22	1097.9470		28	1004.6954*		16	916.2684
	22	1097.9470		29	1004.7359*		17	914.4465
	23	1099.3414*		30	1004.7790*		17	914.4465
	24	1100.7295	pQ2	2	993.4676		18	912.6160
	24	1100.7295		2	993.0378		18	912.6160
	25	1102.0978*		3	992.7770*		19	910.7782
	27	1104.7808*		3	993.6490		19	910.7782
	28	1106.0987*		4	992.4059		20	908.9318
rR9	9	1084.7468		4	993.8895*		20	908.9318
	9	1084.7468		5	991.9070		21	907.0794
	11	1087.8486		5	994.1894		21	907.0794
	11	1087.8486		6	991.2583		22	905.2186*
	13	1090.9030		6	994.5445		23	903.3517*
	13	1090.9030		7	990.4366	pP9	9	920.2284
	14	1092.4124		7	994.9527		9	920.2284
	14	1092.4124		8	989.4200		10	918.4668*
	15	1093.9097		8	995.4107		10	918.4668*
	15	1093.9097		9	988.1900*		11	916.6970
	16	1095.3929*		9	995.9129		11	916.6970
	17	1096.8673*		10	986.7319		12	914.9177
	17	1096.8673*		10	996.4521*		12	914.9177
	18	1098.3274*		11	985.0383		13	913.1299
	19	1099.7738		11	997.0207*		13	913.1299
	19	1099.7738		12	983.1079		14	911.3330
	20	1101.2079		12	997.6071		14	911.3330
	20	1101.2079		13	980.9447		15	909.5262
	21	1102.6284*		13	998.1994		15	909.5262
	21	1102.6284*		14	998.7843*		16	907.7126
	22	1104.0223*		15	999.3473*		16	907.7126
pR1	1	1004.1651		16	999.8737		17	905.8895
	2	1005.6467		17	1000.3537*		17	905.8895
	3	1007.0216		18	1000.7778		18	904.0587*
	4	1008.2766*		19	1001.1414		18	904.0587*
	5	1009.3984		20	1001.4443*		10	909.8565*
	6	1010.3745*		21	1001.6879		10	909.8565*
	8	1011.8422		22	1001.8780		11	908.0866*
	9	1012.3259*		23	1002.0207		12	906.3071
	10	1012.6451		24	1002.1190*		12	906.3071
	11	1012.8126		25	1002.1934*		13	904.5200
	12	1012.8438*		26	1002.2361*		13	904.5200*
	13	1012.7687*		27	1002.2564*		14	902.7215*
	14	1012.6051		28	1002.2851*		14	902.7215*
	15	1012.3836		29	1002.3037*		15	900.9151
	16	1012.1293*	pQ3	3	985.4164		15	900.9151
pR2	2	997.8488*		3	985.4382*		16	899.1004*
	3	999.1911*		4	985.4283*		16	899.1004*
	4	1000.4591		4	985.3671*		17	897.2758*
	5	1001.6371*		5	985.4382*	rPO	2	1005.0696
	6	1006.3518*		5	985.2945		3	1003.5316*
	7	1008.2185*		6	985.4813*		4	1002.0797*
	7	1003.7330		6	985.1924*		5	1000.7299*
	8	1010.0110		7	985.5695		6	999.4985
	8	1004.6495*		7	985.0520*		7	998.4016*
	9	1011.7023		8	985.7177*		8	997.4567*
	9	1005.4748		8	984.8605		9	996.6731
	10	1013.2673		9	985.9377		10	996.0551
	10	1006.2160		9	984.6054		11	995.6010
	11	1014.6849		10	986.2380		12	995.3008
	11	1006.8750*		10	984.2701		13	995.1399*
	12	1015.9388		11	986.6220		14	995.0959
	12	1007.4514		11	983.8347*		15	995.1471*

Appendix III, continued.

R		Q		P						
Branch	J"	Branch	J"	Branch	J"					
pR2	13	1017.0141	pQ3	12	987.0907*	rPO	16	995.2669		
	13	1007.9534		12	983.2784*		17	995.4321		
	14	1017.9005		13	987.6387*		18	995.6203		
	14	1008.3822*		13	982.5775		19	995.8127		
	15	1018.5919		14	988.2622		20	995.9953		
	15	1008.7512*		14	981.7067		21	996.1585*		
	17	1019.3825*		15	988.9500		rP1	4	1008.1281*	
	17	1009.3150*		15	980.6406*			5	1008.3194*	
	18	1019.5032		16	989.6941			5	1006.0794*	
	18	1009.5251		16	979.3608*			6	1007.0793*	
	19	1009.6976*		17	990.4827			7	1005.9205*	
	21	1018.9620*		17	977.8422*			7	1001.9174*	
	22	1018.5698		18	991.3031			8	999.8510*	
	pR3	5		995.5791*	19			992.1436	9	1003.8456
		6		997.3516	20			992.9882	9	997.8300
		6		996.8616*	21			993.8224	10	1002.9319
		7		999.1801*	22			994.6295*	10	995.8851
		7		998.3831*	23			995.3947	11	1002.1016*
		8		1001.0670*	24			996.1022	11	994.0435*
		8		999.8603*	25			996.7844*	12	992.3300*
		9		1001.2852	26			997.4076*	13	1000.6831
		10		1002.6512	28			998.4732*	13	990.7678
11		1007.0793*	pQ4	4	977.4141*	14		1001.0897*		
11		1003.9510		4	977.4141*	14		989.3753		
12		1009.1494		5	977.3718*	15		999.5678*		
12		1005.1782		5	977.3718*	15		988.1679		
13		1006.3285*		6	977.3208*	16		987.1582*		
14		1013.2431		7	977.2778	17		986.3492		
14		1007.3972		7	977.2625	18	985.7379*			
15		1015.2062		8	977.2310*	19	985.3241*			
16		1017.0540*		8	977.1963*	20	985.0787*			
17		1018.8015		9	977.1891*	21	984.9990			
19		1021.7521*		9	977.1199*	rP2	4	1015.9509*		
pR4		7		990.6643	10		977.1609*	5	1014.2566*	
		8		992.2798*	10		977.0319	6	1012.5641*	
	9	994.0085		11	977.1526*		7	1010.8849*		
	10	995.6927		11	976.9286		8	1009.2266		
	10	995.4825		12	977.1707*		9	1007.5971*		
	11	997.4076*		12	976.8040		9	1006.2047*		
	11	997.0645		13	977.2397*		10	1006.0037*		
	12	999.1627*		13	976.6517		10	1004.0011*		
	12	998.6270		14	977.3603*		11	1001.7142		
	13	1000.9692*		14	976.4627		12	1002.9580		
	13	1000.1659*		15	977.5502		12	999.3473*		
	14	1002.8357	15	976.2262	13		1001.5208			
	14	1001.6739	16	977.8212*	13		996.9305			
	15	1003.1454	16	975.9274	14		1000.1527*			
	16	1006.7696*	17	978.1846	14		994.4831*			
	17	1008.8357*	17	975.5511	15		998.8561*			
	17	1006.9491*	18	978.6466	15		992.0420			
	18	1007.1670*	18	975.0783	16		997.6372			
	19	1008.5181*	19	979.2104	16		989.6367			
	20	1009.6976*	19	974.4872	17		996.5003			
	21	1010.8008*	20	979.8744	17		987.3044			
			20	973.7537	18	995.4475*				
		21	980.6335*	18	985.0787*					
		21	972.8532	19	982.9912					
		22	981.4764*	20	993.5984*					
		22	971.7609	20	981.0716					
		23	982.3944*	21	992.8029*					
		23	970.4513	21	979.3436*					
		24	983.3726*	23	976.5387*					
		25	984.3966	24	975.4816*					
		26	985.4507							
		27	986.5186*							

Appendix III, continued.

<u>R</u>		<u>Q</u>	<u>P</u>
	Branch	J*	
	pQ4	28	987.5992*
	pQ5	5	969.2386*
		5	969.2386*
		6	969.1859*
		6	969.1859*
		7	969.1260*
		7	969.1260*
		8	969.0586*
		8	969.0586*
		9	968.9853*
		9	968.9853*
		10	968.9064*
		10	968.9064*
		11	968.8264*
		11	968.8202*
		12	968.7435*
		12	968.7285
		13	968.6588
		13	968.6318
		14	968.5784
		14	968.5291
		15	968.5041
		15	968.4193
		16	968.4421*
		16	968.3020
		17	968.3970*
		17	968.1728
		18	968.3793
		18	968.0280*
		19	968.3970*
		19	967.8656*
		20	968.4421*
		20	967.6744*
		21	968.5614*
	pQ6	6	960.9167
		6	960.9167
		8	960.7837
		8	960.7837
		9	960.7057*
		9	960.7057*
		10	960.6200
		10	960.6200
		11	960.5279
		11	960.5279
		12	960.4291
		12	960.4291
		13	960.3237*
		13	960.3237*
		14	960.2128*
		14	960.2128*
		15	960.0969*
		15	960.0969*
		16	959.9748*
		17	959.8587*
		17	959.8487*
		18	959.7366*
		18	959.7183*
		19	959.5839
		19	959.6133*
		20	959.4937
		20	959.4453*
		21	959.3002*
		21	959.3758*
		22	959.1627*
		23	958.9872*

Appendix III, continued.

<u>R</u>		<u>Q</u>	<u>P</u>
	Branch	J*	
	pQ7	8	952.3931*
		8	952.3931*
		9	952.3136*
		9	952.3136*
		10	952.2261
		10	952.2261
		11	952.1301
		11	952.1301
		12	952.0267
		12	952.0267
		13	952.9134*
		13	952.9134*
		14	951.7966
		14	951.7966
		15	951.6714
		15	951.6714
		16	951.5399
		16	951.5399
		17	951.4016*
		17	951.4016*
		18	951.2580*
		18	951.2580*
		19	951.1094*
		19	951.1094*
		20	950.9490*
	pQ8	8	943.9068
		8	943.9068
		9	943.8256
		9	943.8256
		10	943.7367
		10	943.7367
		11	943.6391
		11	943.6391
		12	943.5336
		12	943.5336
		13	943.4193
		13	943.4193
		14	943.2973
		14	943.2973
		15	943.1668
		15	943.1668
		16	943.0298*
		17	942.8855*
		18	942.7328
		18	942.7328
		19	942.5744
		19	942.5744
		20	942.4087
		20	942.4087
		21	942.2373*
		21	942.2373*
		22	942.0601*
		22	942.0601*
		24	941.6879*
		24	941.6879*
	pQ9	12	934.9675*
		12	934.9675*
		13	934.8515*
		13	934.8515*
		14	934.7237*
		14	934.7237*
		15	934.5948*
		15	934.5948*
		16	934.4536*
		16	934.4536*

Appendix III, continued.

<u>R</u>		<u>Q</u>	<u>P</u>
	Branch	J ^a	
	pQ9	17	934.3056*
		17	934.3056*
		18	934.1575*
		18	934.1575*
		21	933.6237*
		21	933.6237*

^aTransitions in units of cm^{-1} . Blended lines are denoted by an asterisk.

REFERENCES

1. J.T. Hougen, The Calculation of Rotational Energy Levels and Line Intensities in Diatomic Molecules, (National Bureau of Standards Monograph 115, 1970).
2. M.E. Rose, Elementary Theory of Angular Momentum, (John Wiley and Sons, Inc., New York, 1957), Ch. 1.
3. J.H. Van Vleck, Rev. Mod. Phys. **23**, 213 (1951).
4. A. Messiah, Quantum Mechanics, vol. 2, (North-Holland Publishing Co., Amsterdam, 1962), Appendix C.
5. A.R. Edmonds, Angular Momentum in Quantum Mechanics, (Princeton University Press, Princeton, 1960), Ch. 3.
6. A. Messiah, Quantum Mechanics, vol. I, (North-Holland Publishing Co., Amsterdam, 1964), Appendix B.
7. M.E. Rose, ibid, p. 235.
8. A. Messiah, ibid, vol. 1, Ch. 13.
9. M.E. Rose, ibid, Ch. 4.
10. B.L. Silver, Irreducible Tensor Methods, (Academic Press, New York, 1976), Ch. 5.
11. A.R. Edmonds, ibid, Ch. 5.
12. B.L. Silver, ibid, Ch. 2.
13. A.R. Edmonds, ibid, Ch. 4.
14. B.L. Silver, ibid, Ch. 10.
15. D.M. Brink and G.R. Satchler, Angular Momentum, (Clarendon Press, Oxford, 2nd ed., 1968), Ch. 2.
16. B.L. Silver, ibid, Ch. 6.
17. D.M. Brink and G.R. Satchler, ibid, Ch. 4.

REFERENCES (cont.)

18. B.L. Silver, ibid, Ch. 9.
19. B.L. Silver, ibid, Ch. 7.
20. G. Herzberg, Spectra of Diatomic Molecules, 2nd ed., (Van Nostrand, Princeton, 1950), Ch 4.
21. P.W. Atkins, Molecular Quantum Mechanics, 2nd ed., (Oxford University Press, New York, 1983), Ch. 12.
22. Henry Eyring, John Walter and George E. Kimball, Quantum Chemistry, (John Wiley and Sons, Inc., New York, 1944), p.264; G. Herzberg, ibid, p. 240.
23. H. Lefebvre-Brion and R.W. Field, Perturbations in the Spectra of Diatomic Molecules, (Academic Press, New York, 1986), pp. 117-119.
24. G. Herzberg, ibid, Ch 5.
25. A. S-C. Cheung and A.J. Merer, Molec. Phys. **46**, 111-128 (1982).
26. R.A. Frosch and H.M. Foley, Phys. Rev. **88**, 1337 (1952).
27. T.M. Dunn, in Molecular Spectroscopy: Modern Research, Vol. 1, K.N. Rao and C.W. Matthews, eds., (Academic Press, New York, 1972), Ch. 4.4.
28. P.H. Kasai and W. Weltner, Jr., J. Chem. Phys. **43**, 2553 (1965).
29. A. Adams, W. Klemperer and T.M. Dunn, Canad. J. Phys. **46**, 2213 (1968).
30. R. Stringat, C. Athénour, J-L. Féménias, Canad. J. Phys. **50**, 395 (1972).
31. J.M. Brown, I. Kopp, C. Malmberg and B. Rydh, Phys. Scripta **17**, 55 (1978).
32. D.W. Green, Canad. J. Phys. **49**, 2552 (1971).

REFERENCES (cont.)

33. P.W. Atkins, Proc. Roy. Soc. A **300**, 487 (1967).
34. R.F. Barrows, W.J.M. Gissane, D. Richards, Proc. Roy. Soc. A **300**, 469 (1967).
35. K.F. Freed, J. Chem. Phys. **45**, 1714 (1966).
36. H. Lefebvre-Brion and R.W. Field, ibid. p. 89.
37. M. Tinkham, Group Theory and Quantum Mechanics, (McGraw-Hill Book Co., New York, 1964), p. 129.
38. A. Carrington and A.D. McLachlan, Introduction to Magnetic Resonance, (Chapman and Hall, New York, 1967), Ch. 8.
39. K. Kayama and J.C. Baird, J. Chem. Phys. **46**, 2604 (1967).
40. H. Lefebvre-Brion and R.W. Field, ibid. p. 96-101.
41. W.H. Hocking, A.J. Merer, D.J. Milton, W.E. Jones and G. Krishnamurty, Canad. J. Phys. **58**, 516 (1980).
42. A.R. Edmonds, ibid. Ch. 6.
43. B.R. McGarvey, J. Phys. Chem. **71**, 51 (1967).
44. A. Abragam and B. Bleaney, Electron Paramagnetic Resonance of Transition Ions, (Clarendon Press, Oxford, 1970).
45. A.S-C. Cheung, R.C. Hansen and A.J. Merer, J. Molec. Spectrosc. **91**, 165 (1982).
46. P.H. Kasai, J. Chem. Phys. **49**, 4979 (1968).
47. M.E. Rose, ibid. Ch. 5.
48. B.L. Silver, ibid. Ch. 17.
49. A. Messiah, ibid. vol. 2, p. 692.

REFERENCES (cont.)

50. M.R. Spiegel, Mathematical Handbook of Formulas and Tables, (McGraw-Hill Book Co., New York, 1968), p. 19.
51. M.R. Spiegel, ibid, p. 146.
52. A.R. Edmonds, ibid, Ch. 7.
53. M.H. Cohen and F. Reif, Quadrupole Effects in NMR Studies of Solids, in: Solid State Physics, Vol. 5, F. Seitz and D. Turnbull, eds., (Academic Press, Inc., New York, 1957), pp. 327-328.
54. I.C. Bowater, J.M. Brown and A. Carrington, Proc. Roy. Soc. Lond. A **333**, 265 (1973).
55. P.A. Tipler, Modern Physics, (Worth Publishers, Inc., New York, 1978), Ch. 11.
56. Landolt-Börnstein, Zahlenwerte und Funktionen Group I, Vol.3, H. Appel, ed., Numerical Tables of the Wigner 3-j, 6-j and 9-j Coefficients, (Springer-Verlag, New York, 1968), p. 10.
57. J.M. Brown, A.S-C. Cheung and A.J. Merer, J. Molec. Spectrosc. **124**, 464 (1987).
58. A. Messiah, ibid, vol. 2, pp. 718-720.
59. T.A. Miller, Molec. Phys. **16**, 105 (1969).
60. R.S. Mulliken and A.S. Christy, Phys. Rev. **38**, 87 (1931).
61. I. Kopp and J.T. Hougen, Canad. J. Phys. **45**, 2581 (1967).
62. J.M. Brown, J.T. Hougen, K.P. Huber, J.W.C. Johns, I. Kopp, H. Lefebvre-Brion, A.J. Merer, D.A. Ramsey, J. Rostas and R.N. Zare, J. Molec. Spectrosc. **55**, 500 (1975).
63. W. Demotröder, Laser Spectroscopy, (Springer-Verlag, New York, 1982), Ch. 7.
64. J.B. West, R.S. Bradford, J.D. Eversole and C.W. Jones, Rev. Sci. Instrum. **46**, 164 (1975).

REFERENCES (cont.)

65. W. Demtröder, ibid, Ch. 3.
66. W. Demtröder, ibid, Ch. 10.
67. A.J. Merer, Ulf Sassenberg, J-L. Féménias and G. Cheval, J. Chem. Phys. **86**, 1219 (1987).
68. S. Gerstenkorn and P. Luc, Atlas du Spectre d'Absorption de la Molécule d'Iode (CNRS, Paris, France, 1978); S. Gerstenkorn and P. Luc, Rev. Phys. Appl. **14**, 791 (1979).
69. L. Malet and B. Rosen, Bull. Soc. R. Sci. Liège **14**, 382 (1945); B. Rosen, Nature **156**, 570 (1945).
70. T.C. Devore and T.N. Gallaher, J. Chem. Phys. **71**, 474 (1979).
71. D.W. Green, G.T. Reedy and J.G. Kay, J. Molec. Spectrosc. **78**, 257 (1979).
72. R.J. Van Zee, C.M. Brown, K.J. Zeringue, W. Weltner, Acc. Chem. Res. **13**, 237 (1980).
73. W. Weltner, D. McLeod and P.H. Kasai, J. Chem. Phys. **46**, 3172 (1967).
74. G. Herzberg, ibid, pp. 335-337.
75. A.S-C. Cheung, R.M. Gordon, A.J. Merer, J. Molec. Spectrosc. **87**, 289 (1981).
76. M. Krauss and W.J. Stevens, J. Chem. Phys. **82**, 5584 (1985).
77. W. Weltner, Jr., Ber. Bunsenges. Phys. Chem. **82**, 80 (1978).
78. V.I. Srdanov and D.O. Harris, J. Chem. Phys., submitted.
79. M.C.L. Gerry, A.J. Merer, U. Sassenberg and T.C. Steimle, J. Chem Phys. **86**, 4654 (1987).
80. L.J. Thénard, J. Mines **15**, 128 (1805).

REFERENCES (cont.)

81. R.T. Grimely, R.P. Burns and M.G. Inghram, J. Chem. Phys. **45**, 4158 (1966).
82. T.M. Dunn, in Physical Chemistry: An Advanced Treatise, Vol. 5, H. Eyring and W. Jost, eds., (Academic Press, New York, 1970), p. 228.
83. G. Herzberg, ibid., Ch. 3.
84. J.I. Steinfeld, Molecules and Radiation, (Harper and Row, New York, 1974), Ch. 4.
85. O. Appelblad, I. Renhorn, M. Dulick, M.R. Purnell and J.M. Brown, Phys. Scripta **28**, 539 (1983).
86. I. Kopp and J.T. Hougen, Canad. J. Phys. **45**, 2581 (1967).
87. A.S.-C. Cheung, A.M. Lyyra, A.J. Merer and A.W. Taylor, J. Molec. Spectrosc. **102**, 224 (1983).
88. A.S.-C. Cheung, A.W. Taylor and A.J. Merer, J. Molec. Spectrosc. **92**, 391 (1982).
89. W.H. Hocking, M.C.L. Gerry and A.J. Merer, Canad. J. Phys. **57**, 54 (1979).
90. A.S.-C. Cheung, W. Zyrnicki and A.J. Merer, J. Molec. Spectrosc. **104**, 315 (1984).
91. R.M. Gordon and A.J. Merer, Canad. J. Phys. **58**, 642 (1980).
92. O. Appleblad and A. Lagerquist, Phys. Scr. **10**, 307 (1974).
93. O. Appleblad and L. Klynning, USIP Report 81-02, University of Stockholm (1981).
94. T.M. Dunn and K.M. Rao, Nature **222**, 266 (1969).
95. J.-L. Féménias, C. Athénour and T.M. Dunn, J. Chem. Phys. **63**, 286 (1975).

REFERENCES (cont.)

96. B. Chakrabarti, M.Z. Hoffman, N.N. Lichtin and D.A. Sacks, J. Chem. Phys. **58**, 404 (1973).
97. N.N. Kabankova, P.I. Stepanov, E.N. Moskvitina and Yu. Ya. Kuzyakov, Vest. Mosk. Univ., Khim. **15**, 356 (1974).
98. N.N. Kabankova, E.N. Moskvitina and Yu. Ya. Kuzyakov, Vest. Mosk. Univ., Khim. **17**, 492 (1976).
99. E.A. Pazyuk, E.N. Moskvitina and Yu. Ya. Kuzyakov, Vest. Mosk. Univ., Khim. **26**, 418 (1985).
100. E.A. Pazyuk, E.N. Moskvitina and Yu. Ya. Kuzyakov, Spectrosc. Lett. **19**, 627 (1986).
101. N.L. Ranieri, Ph.D. dissertation, Diss. Abst. Int. B. **40**, 772 (1979).
102. J.-L. Féménias, C. Athénour, K.M. Rao and T.M. Dunn, submitted.
103. H. Lefebvre-Brion and R.W. Field, ibid. Sec. 3.4.
104. Ira N. Levine, Quantum Chemistry, 3rd ed., (Allyn and Bacon, Inc., Boston, 1983), Sec. 14.3.
105. D.L. Albritton, A.L. Schmeltpopf and R.N. Zare, in Molecular Spectroscopy: Modern Research, Vol. 2, K. Nakahari Rao, ed., (Academic Press, New York, 1976), Sec. 1.D.
106. R.M. Lees, J. Molec. Spectrosc. **33**, 124-136 (1970).
107. F. Ayres, Jr., Theory and Problems of Matrices, (Schaum Publishing Co., New York, 1962), p.55.
108. B. Higman, Applied Group-Theoretic and Matrix Methods, (Dover Publications, Inc., New York, 1964), p.64.
109. H. Lefebvre-Brion and R.W. Field, ibid., p. 92.
110. J. Raftery, P.R. Scott and W.E. Richards, J. Phys. B **5**, 1293 (1972).

REFERENCES (cont.)

111. T.M. Dunn, L.K. Hanson and K.A. Rubinson, Canad. J. Phys. **48**, 1657 (1970); J.K. Bates, N.L. Ranieri and T.M. Dunn, Canad. J. Phys. **54**, 915 (1976).
112. J.K. Bates and T.M. Dunn, Canad. J. Phys. **54**, 1216 (1976).
113. J.K. Bates and D.M. Gruen, J. Molec. Spectrosc. **78**, 284 (1979).
114. W. Weltner, Jr. and D. McLeod, Jr., J. Phys. Chem. **69**, 3488 (1965).
115. J.M. Brom, Jr. and H.P. Broida, J. of Chem. Phys. **63**, 3718 (1975).
116. L.J. Lauchlan, J.M. Brom and H.P. Broida, J. Chem. Phys. **65**, 2672 (1976).
117. D. McLeod, Jr. and W. Weltner, Jr., J. Phys. Chem. **70**, 3293 (1966).
118. R.F. Barrow, M.W. Bastin, D.L.G. Moore and C.J. Pott, Nature **215**, 1072 (1967).
119. J.K. Bates and D.M. Gruen, J. Chem. Phys. **70**, 4428 (1979).
120. R. Hoffman, J. Chem. Phys. **40**, 2474-2480 (1964).
121. D.R. Armstrong, B.J. Duke and P.G. Perkins, J. Chem. Soc. A, 2566-2572 (1969).
122. O. Gropen and H.M. Seip, Chem. Phys. Lett. **25**, 206-208 (1974).
123. J.D. Dill, P.V.R. Schleyer and J.A. Pople, J. Amer. Chem. Soc. **97**, 3402-3409 (1975).
124. T. Fjeldberg, G. Gundersen, T. Jonvik, H.M. Seip and S. Saebø, Acta Chem. Scand. A **34**, 547-565 (1980).
125. K.W. Boddeker, S.G. Shore and R.K. Bunting, J. Amer. Chem. Soc. **88**, 4396-4401 (1966).

REFERENCES (cont.)

126. P.M. Kuznesof, D.F. Shriver and F.E. Stafford, J. Amer. Chem. Soc. **90**, 2557-2560 (1968).
127. C.I. Kwon and H.A. McGee, Inorg. **9**, 2458-2461 (1970).
128. S.V. Pusatcioglu, H.A. McGee, Jr., A.L. Fricke and J.C. Hassler, J. Appl. Polymer Sci. **21**, 1561 (1977).
129. M. Sugie, H. Takeo and C. Matsumura, Chem. Phys. Lett. **64**, 573-575 (1979).
130. M. Sugie, H. Takeo and C. Matsumura, J. Molec. Spectrosc. **123**, 286 (1987).
131. M.C.L. Gerry, W. Lewis-Bevan, A.J. Merer and N.P.C. Westwood, J. Molec. Spectrosc. **110**, 153 (1985).
132. D. Anderson, Studies in high resolution spectroscopy, Ph.D. thesis, The University of British Columbia, Vancouver, 1986.
133. D. Steunenbergh, The infrared spectrum of gaseous aminoborane: rotational structure of the 8^1 band, B.Sc. thesis, The University of British Columbia, Vancouver, 1986.
134. D. Cramb, The infrared spectrum of gaseous aminoborane: rotational structure of the 10^1 band, B.Sc. thesis, The University of British Columbia, Vancouver, 1985.
135. P.R. Griffiths, Science **222**, 297 (1983).
136. Spectrophotometer System Manual, (Bomem, Inc., Quebec, 1981), Ch. 2.
137. R.J. Bell, Introductory Fourier Transform Spectroscopy, (Academic Press, New York, 1972), Ch. 1.
138. W. Demtröder, ibid, Ch 4.
139. A. Corney, Atomic and Laser Spectroscopy, (Clarendon Press, Oxford, 1977), pp. 19-20.

REFERENCES (cont.)

140. R.J. Bell, ibid. Ch. 3.
141. J.B. Bates, Science **191**, 31 (1976).
142. M.R. Spiegel, ibid., p. 175.
143. R.J. Bell, ibid., pp. 65 and 173.
144. W.D. Perkins, J. Chem. Educ. **63**, A5 (1986).
145. Software User's Guide, Version 3.1, (Bomem, Inc., Quebec, 1984), Ch. 5.
146. R.J. Bell, ibid., Ch. 5.
147. J.K. Kauppinen, D.J. Moffatt, D.G. Cameron, H.H. Mantsch, Applied Optics **20**, 1866 (1981).
148. P.W. Atkins, ibid., p. 307.
149. A.R. Edmonds, ibid., p. 23.
150. H.C. Allen and P.C. Cross, Molecular Vibration-Rotors: The Theory and Interpretation of High Resolution Infrared Spectra, (John Wiley and Sons, Inc., London, 1963), pp. 24-25.
151. W. Gordy and R.L. Cook, Microwave Molecular Spectra, 3rd. ed., (John Wiley and Sons, New York, 1984), p. 60.
152. J.K.G. Watson, in Vibrational Spectra and Structure, (J.R. Durig, ed., vol. 6, Marcel Dekker, New York, 1977), Ch. 1.
153. W. Gordy and R.L. Cook, ibid., Sec 8.3.
154. W. Gordy and R.L. Cook, ibid., Sec 8.4.
155. W. Gordy and R.L. Cook, ibid., Ch. 7.
156. I.M. Mills, Pure and Applied Chemistry **11**, 325 (1965).
157. H.C. Allen and P.C. Cross, ibid. Ch. 4.

REFERENCES (cont.)

158. J. Michael Hollas, High Resolution Spectroscopy, (Butterworth's and Co., Ltd., London, 1982), p. 243.
159. V.A. Job, N.D. Patel, R. D'Chunha, V.B. Kartha, J. Molec. Spectrosc. **101**, 48 (1983).
160. D. Steunenberg, private communication.
161. M.C.L. Gerry, private communication.